INFORMATION TO USERS

This manuscript has been reproduced from the microfilm master. UMI films the text directly from the original or copy submitted. Thus, some thesis and dissertation copies are in typewriter face, while others may be from any type of computer printer.

The quality of this reproduction is dependent upon the quality of the copy submitted. Broken or indistinct print, colored or poor quality illustrations and photographs, print bleedthrough, substandard margins, and improper alignment can adversely affect reproduction.

In the unlikely event that the author did not send UMI a complete manuscript and there are missing pages, these will be noted. Also, if unauthorized copyright material had to be removed, a note will indicate the deletion.

Oversize materials (e.g., maps, drawings, charts) are reproduced by sectioning the original, beginning at the upper left-hand corner and continuing from left to right in equal sections with small overlaps.

ProQuest Information and Learning
300 North Zeeb Road, Ann Arbor, MI 48106-1346 USA
800-521-0600

Static and Modulated Reflectance Measurements on III - V Compounds and Alloys

by

Sreekrishna S. Vishnubhatla

Submitted in partial fulfillment
of the requirements for the degree
of Doctor of Philosophy

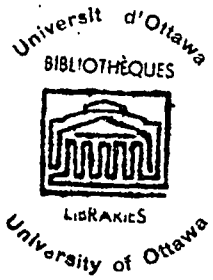

Department of Physics
Faculty of Pure and Applied Science
University of Ottawa
Ottawa, Canada

1970

Approved for the

Department of Physics

Date 15 July 1970

Chairman

STATEMENT OF ORIGINALITY

So far as the author is aware, the following parts of the present work are original:

1. The new structure observed in the reflectance spectra of some III - V compounds in the energy range 3.5 - 7.5 eV.

2. The determination of the thermoreflectance spectra of several III - V compounds in the energy range 1.5 - 6.0 eV.

3. The determination of transition energies versus composition for $Ga_xIn_{1-x}Sb$ alloys from reflectance measurements over the energy range 1.5 - 6.5 eV.

4. The determination of transition energies versus composition for $Ga_xIn_{1-x}Sb$ alloys from thermoreflectance measurements over the energy range 1.5 - 6.0 eV.

5. The determination of transition energies versus composition for $Ga_xIn_{1-x}Sb$, $InAs_{1-x}P_x$ and $InSb_{1-x}As_x$ alloys from electroreflectance measurements over the energy range 1.5 - 6.0 eV.

6. The interpretation of the composition dependence of transition energies beyond the fundamental in III - V alloys.

7. The derivation of a relation to determine the bowing parameters of the spin orbit splitting Δ_1 versus composition curves in III - V alloys.

Other work on the determination of thermoreflectance spectra of III - V compounds by Matatagui et al[140] and the electroreflectance measurements on $InAs_{1-x}P_x$ by Thompson et al[86] were done concurrently with

but independently from the above work. The previous electroreflectance data on $InSb_{1-x}As_x$ were the preliminary results of Thompson and Woolley[84] and the present measurements were made in greater detail. The reflectance spectra of $Ga_xIn_{1-x}Sb$ alloys were determined over a broader energy range on more homogeneous material with results significantly different compared with the previous results of Woolley and Blazey.[81]

Mr. B. Eyglunent collaborated in determining the electroreflectance spectra of $Ga_xIn_{1-x}Sb$ alloy samples.

ABSTRACT

Static and modulated reflectance measurements were made on samples of some III - V compounds and their alloys. Multiplet structures resolved in the reflectance spectra of III - V compounds in the energy range 3.5 - 7.5 eV led to the determination of the spin orbit splittings Δ_0', Δ_2, Δ_1', ΔL_{3V} and ΔL_{3C}. Structure was observed in the thermoreflectance spectra of III - V compounds in the energy range 1.5 - 6.0 eV and it was assigned to interband transitions. Results enabled comparison with previous data obtained using other techniques. Static and modulated reflectance measurements confirmed the nonlinear variation of energy gaps with composition in $Ga_xIn_{1-x}Sb$ alloy. Similar data was obtained for $InAs_{1-x}P_x$ and $InSb_{1-x}As_x$ alloys from electroreflectance measurements. Results on five III - V alloys were analysed, fitting a quadratic equation to the energy gap variation with composition curves. The total bowing parameters determined experimentally were compared with theoretical values. The spin orbit splitting Δ_1 was also found to vary nonlinearly with composition in the five alloy systems investigated and the bowing parameters were related to the atomic spin orbit splittings of the alloying elements.

ACKNOWLEDGEMENTS

I would like to express my sincere gratitude to my supervisor, Professor John C. Woolley for his guidance and encouragement throughout the progress of this work.

I am most grateful to Dr. M. Rubenstein of Westinghouse Research Laboratories for providing me with the $InAs_{1-x}P_x$ samples and Dr. J. H. Simpson of the Research Laboratories of the National Research Council for permitting me to use their vacuum ultraviolet monochromator and to work in their laboratories.

I have benefitted from my association with the faculty and the graduate students of the Physics Department. I am particularly grateful for the discussions I have had with Mr. R. Senechal, Dr. E. Fortin, Dr. K. S. Song and Dr. A. G. Thompson and for their various useful suggestions. I also would like to thank Mr. B. Eyglunent for his collaboration. My sincere thanks are due to the staff members of the machine shop for the assistance I have received from them during the course of this work.

I would like to thank Mrs. A. Martin for typing this thesis.

The financial support received from the Province of Ontario is gratefully acknowledged.

TABLE OF CONTENTS

LIST OF ILLUSTRATIONS

LIST OF TABLES

CHAPTER 1

INTRODUCTION

1.1 Historical Background

In 1952 when most of the investigations on semiconductors were concerned with germanium and silicon, Welker[1] was investigating the properties of III - V compounds. He found them to be semiconductors closely related to the elemental semiconductors and providing a wider selection of the basic parameters of practical interest such as energy gaps and carrier mobilities. Soon after it was realized that continuous alloying of two III - V compounds was possible.[2] This provided a larger selection of materials with continuous ranges of values for basic parameters instead of the descrete values. Investigation of the mixed III - V alloy systems were started in the mid 1950's with active participation of such workers as Goryunova, Ivanov-Omskii and Woolley.

Scientific curiosity and the technological importance of the semiconductor materials led to more intensive experimental and theoretical research. With improved techniques in material preparation, it became increasingly possible to prepare purer material and to grow single crystals from it. Experiments were performed which gave parameters of these materials directly applicable in theoretical calculations. In the theoretical development the energy band concept has been successful in interpreting some of the physical properties of semiconductors. Therefore a theoretical determination of the energy band structure of a

semiconductor from a knowledge of its crystal structure and the chemical nature of the atoms occupying the lattice sites would lead to an understanding of some of its physical properties. Conversely, an experimental determination of some of the physical parameters would give valuable information about its energy band structure. The combination of these two has been responsible for the spectacular growth of semiconductor physics.

The first successful theoretical energy band calculations for a semiconductor were made by Herman[3] in 1952. Since then, improved methods have given more realistic potentials and fast modern computers have solved the complicated numerical problems in band structure determinations. A few active participants in this area have been Herman, Phillips and Cardona.

1.2 Concept of Energy Bands

Soon after the discovery of electrons an electron theory was suggested for metals and insulators by Drude[4] and Lorentz[5]. Under the influence of an electric field, the mobile electrons in metals contribute to conduction current and the bound electrons in insulators give rise to polarization effects. This classical approach met with only partial success in explaining various phenomena. To be able to solve the corresponding wave mechanical problem of electron motion in a solid, a few approximations for the potential which is determined by the electron interaction with the positive atomic nuclei and the other electrons in the material are necessary.

In the Sommerfeld model[6] this potential was assumed to be constant. The wavefunctions of the electron which are solutions of the Schrodinger equation are represented by plane waves of the form $\psi_k = A \exp(ikx)$, where k is the wavevector and A is the normalization constant. The corresponding energy is given by $E(k) = \frac{\hbar^2 k^2}{2m}$, where m is the mass of the electron. The E,k relationship is parabolic in nature. (Fig. 1.1 Broken line) The electron energy spectrum is quasicontinuous. Sommerfeld's free electron model when used along with Fermi-Dirac statistics was successful in explaining many properties of metals. But an explanation for the division of solids into metals and insulators [7,8] depending upon their electronic conduction property had to wait until the concept of energy bands was introduced by Bloch.[9]

In the Bloch model[9] the potential seen by the valence electron was assumed to be periodic with the periodicity of the lattice. The solutions of the Schroedinger equation $\psi_k = U(k,x) \exp(ikx)$ are known as

FIGURE 1.1

PLOT OF ENERGY E VERSUS WAVENUMBER k, FOR A ONE DIMENSIONAL PERIODIC LATTICE.

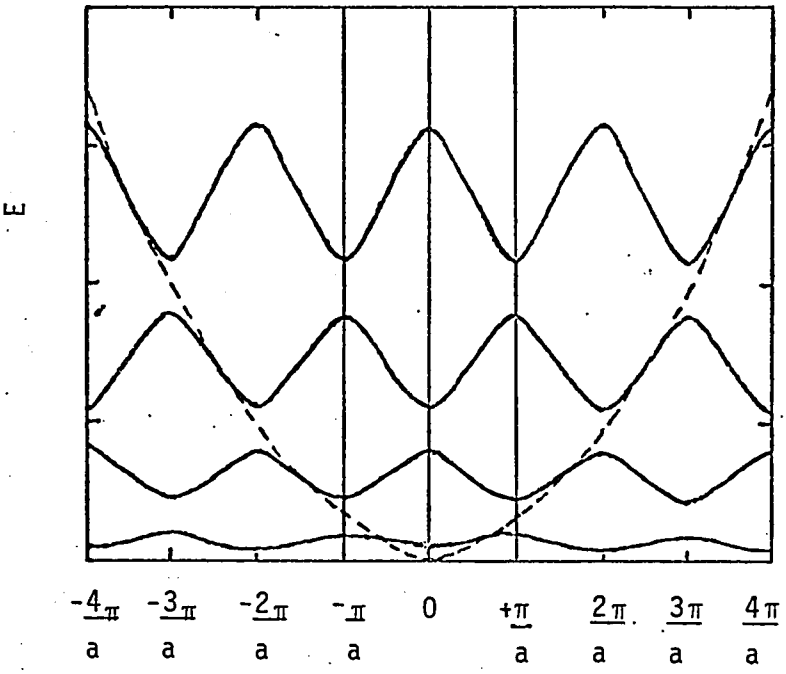

Bloch functions, where $U_k(x)$ is a periodic function with the periodicity of the lattice , $U_k(x + a) = U_k(x)$. The wavefunctions are plane waves, exp(ikx), modulated by the periodic function $U_k(x)$.

In a one dimensional periodic potential problem, the energy spectrum of electrons consists of a number of allowed energy bands separated by forbidden regions. The discontinuous nature of the energy spectrum is shown in Fig. 1.1, where the energy is plotted as a function of the wavevector k. The periodic functions represent the first four energy bands. The dashed parabolic curve represents the energy of a free electron and shows the modification brought about in the behaviour of such an electron by the periodic potential in a crystal lattice.

As is seen in Fig. 1.1, the boundaries of the allowed energy values occur at $k = \pm \frac{n\pi}{a}$ where 'a' is the lattice parameter of the one dimensional crystal and n is an integer. Within any band the energy is a periodic function of k. Hence, it is possible to restrict the k values to a region of extent $\frac{2\pi}{a}$, which is the period of the function E(k). Only those values of k within such a region are distinct. All others can be reduced into one of them by adding or subtracting an integral multiple of the period. The region $-\frac{\pi}{a} < k < \frac{\pi}{a}$ represents the so called first Brillouin zone[10] (BZ) for a one dimensional periodic lattice. The E versus k curve in the first Brillouin zone represents the band structure in the reduced zone scheme.

The above discussion on the one dimensional problem can be extended to three dimensional lattices which are characterized by three primitive translation vectors $\vec{a}_1$, $\vec{a}_2$, and $\vec{a}_3$. By definition the lattice should look identical when viewed from any two points in the lattice

separated by a vector $\vec{R}$,

$$\vec{R} = n_1\vec{a}_1 + n_2\vec{a}_2 + n_3\vec{a}_3$$

where n_1, n_2 and n_3 are integers. The potential in which an electron moves has three dimensional periodicity of the crystal lattice. This leads to energy bands which are periodic in $\vec{k}$ space with the periodicity of a three dimensional Brillouin zone. This may be defined as the smallest volume in $\vec{k}$ space centered at $\vec{k} = 0$ which includes all the nonequivalent values of the vector $\vec{k}$. The number of $\vec{k}$ vectors in each band is equal to the number of primitive unit cells in the crystal and accommodates twice the number of electrons accounting for the spin degeneracy.

1.3 Crystal Structure of III - V Compounds

The materials of interest in this thesis are the III - V compounds which crystallize in the zincblende structure shown in Fig.1.2. This is a less symmetric form of diamond structure. Both diamond and zincblende have the translational symmetry of a face centered cubic space lattice and can be considered to have formed from two interpenetrating face centered cubic sublattices displaced from one another by a quarter of the distance along a body diagonal. In the diamond structure, the lattice sites on the two sublattices are occupied by the same type of atom, for example, Ge in a germanium crystal. Whereas in the zincblende structure each sublattice contains only one of the two kinds of atoms available in III - V compounds, for example, either In or Sb in an InSb crystal. It is obvious that the loss of symmetry from diamond to zincblende is the inversion center that the former has about the midpoint between the two atoms connecting the two sublattices along the body diagonal.

In diamond and zincblende type materials the valence electrons move in a potential field which has the face centered cubic lattice periodicity. Therefore, the electron states are represented by $\vec{k}$ vectors in the corresponding first Brillouin zone which is a truncated octahedron as shown in Fig. 1.3. The letters which identify the various symmetry points and axes of the Brillouin zone are from the group theoretical notation introduced by Bouckaert, Smoluchowski and Wigner.[11]

FIGURE 1.2

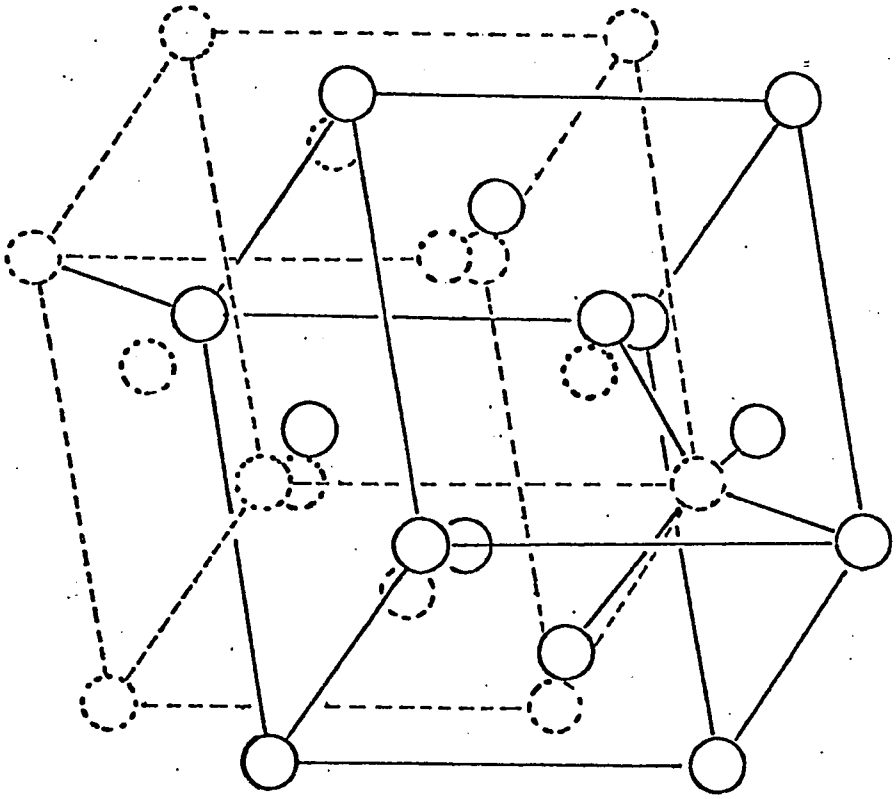

ZINCBLENDE LATTICE

FIGURE 1.3

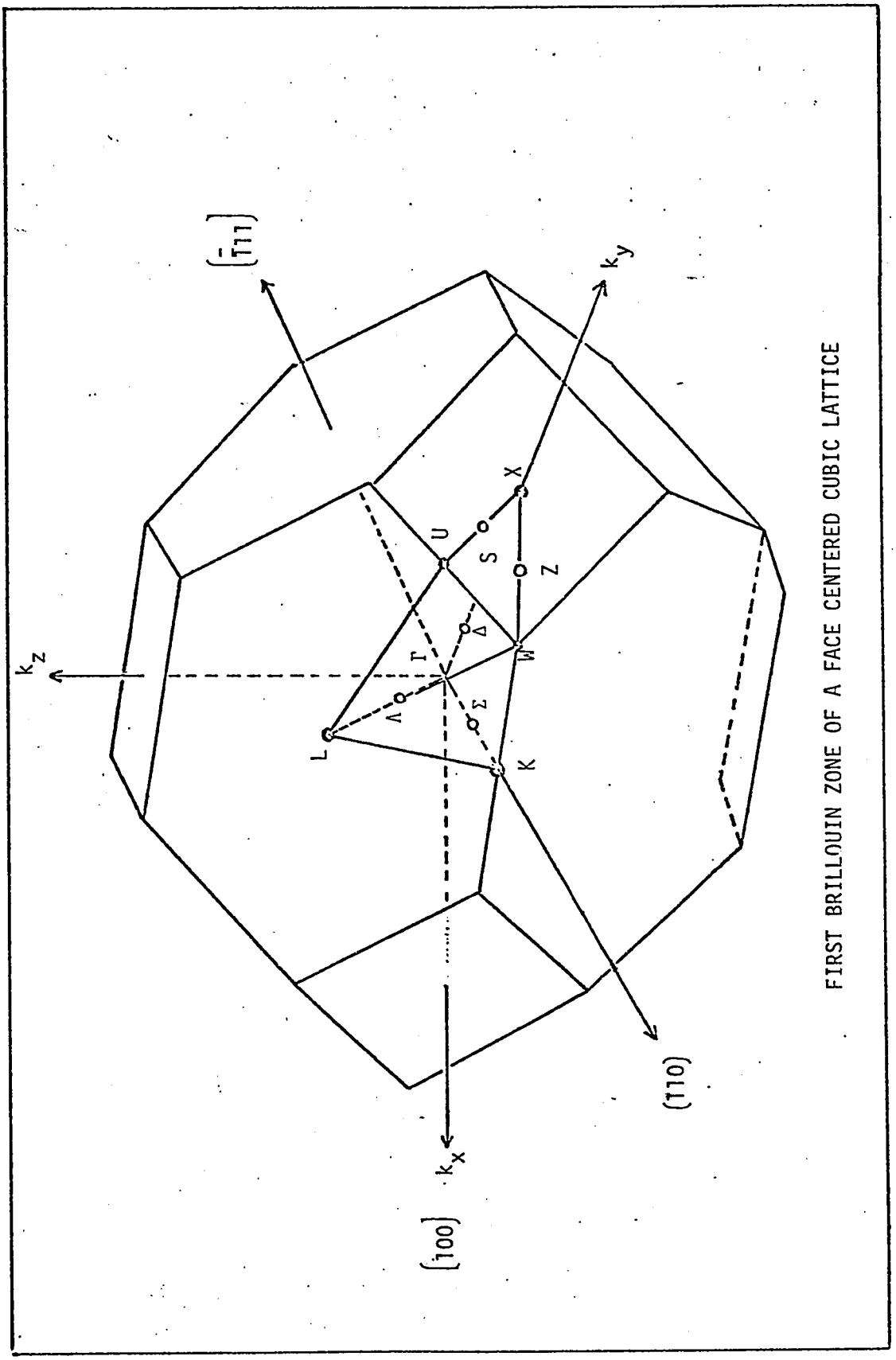

FIRST BRILLOUIN ZONE OF A FACE CENTERED CUBIC LATTICE

1.4 Determination of Band Structure

The aim is to calculate the energy values of all available states in the Brillouin zone over as many bands as possible. Here the symmetry properties of the Brillouin zone, namely the point group symmetry of the crystal lattice reduces the number of $\vec{k}$ vectors which need be considered in this calculation. The variation of energy E as a function of $\vec{k}$ is generally shown along a few specific directions in $\vec{k}$ space in the reduced zone scheme similar to the E versus $\vec{k}$ diagram shown in Fig. 1.1.

The determination of band structure can be approached broadly from two different directions, either from first principles or semi-empirical methods. First principles approach is the most fundamental one which requires only a knowledge of the crystal structure of the material and the chemical nature of the atoms occupying the lattice sites. In this method, the complicated Schroedinger equation is simplified with suitable approximations before solving it for the electronic energies. In the semiempirical schemes either experimental or otherwise well known information about the band structure is included in varying degrees depending upon the method chosen to obtain the remaining part.

Before proceeding with either of the above two methods valuable information can be obtained from an empty lattice band structure calculation where the translational periodicity of the actual lattice is retained but the periodic component of the potential is assumed to be negligible.[12,13,14] Applying group theory arguments the energy levels at the symmetry points and along the symmetry axes in the Brillouin zone are classified and their degeneracies are determined from the symmetry

properties of the crystal lattice. When the periodic potential is treated as a perturbation, some of the empty lattice energy level degeneracies are removed giving a representative band structure for the material.

First Principles Method

The wavemechanical problem describing the motion of an enormous number of electrons and positive ions in a solid is an impossible task to solve unless a number of simplifications are made. The first one is the Born - Oppenheimer approximation which assumes that in a solid the nuclei are at rest. This assumption reduces the problem to a many electron problem which is further simplified by assuming that each electron moves independently of the others. The next simplification generally made is the omission of the spin orbit interaction. The set of one electron wavefunctions may now be written as[15]

$$\left(\left(\frac{-\hbar^2}{2m}\right)\nabla^2 + V_n(\vec{k},\vec{r})\right)\ \psi_n(\vec{k},\vec{r}) = E_n(\vec{k})\ \psi_n(\vec{k},\vec{r}) \qquad (1.1)$$

where $V_n(\vec{k},\vec{r})$ is the potential seen by the electron which is represented by the wavefunction $\psi_n(\vec{k},\vec{r})$ and $E_n(\vec{k})$ is the energy of the state represented by $n,\vec{k}$. The energy band of the solid is defined by the set of energy band functions $E_n(\vec{k})$ and they are determined by solving Eq.(1.1) with a properly chosen potential $V_n(\vec{k},\vec{r})$, wavefunction $\psi_n(\vec{k},\vec{r})$ and a numerical method to solve.

To evaluate the potential, an obvious choice of the first principles approach is the extension of the Hartree, Hartree-Fock, Hartree-Fock Slater self-consistent field scheme developed for atomic

and molecular systems to solve the solid state problem.[14] Herman[16] has been a strong advocate of this procedure. In this scheme, the potential in which an electron moves is calculated from the charge distribution obtained after filling the one electron wavefunctions with the available electrons. When the Schroedinger equation is solved with this potential in the Hamiltonian a set of one electron wavefunctions are obtained from which the potential is again calculated. This process is continued demanding that the resulting final potential be identical with that potential with which the preceeding set of wavefunctions were obtained.

In the covalently bonded materials which are of interest in this thesis, the electron charge distribution varies quite widely from point to point in the unit cell with a similar variation for the resulting potential.[17] The most useful band calculations made on such materials have been by the Orthogonalized Plane Wave (OPW) method developed by Herring.[18] Since the first band structure calculations on Ge by Herman in 1952, the physical realism has been improved by including the relativistic and spin orbit coupling effects into the first principles calculations.[19]

However, accurate band structure calculations from first principles is a long and complicated procedure to perform. Either they do not exist for many semiconductors or the available calculations in several cases agree only qualitatively with the well known experimental results. As it is often possible to determine a few parameters quite accurately from experiments, the semiempirical band calculations incorporating these experimental data should be accurate and useful.

The semiempirical methods so developed are the $\vec{k}.\vec{p}$, the pseudopotential and the dielectric methods.

Semi-empirical Methods

Originally, the $\vec{k}.\vec{p}$ method was used to explore the properties of the energy bands and wavefunctions in the vicinity of some important $\vec{k}$ vector in the Brillouin zone. Dresselhaus[20] extended this method for the empirical determination of band structure. In this method the one electron wave equation is written as[21]

$$\left(\frac{-\hbar^2\nabla^2}{2m} + V(\vec{r}) \right) \psi_n(\vec{k},\vec{r}) = E_n(\vec{k}) \ \psi_n(\vec{k},\vec{r}) \qquad (1.2)$$

where $V(\vec{r})$ is the periodic potential. Substituting Bloch functions for $\psi_n(\vec{k},\vec{r})$,

$$\psi_n(\vec{k},\vec{r}) = U_n(\vec{k},\vec{r}) \ \exp(i\vec{k}.\vec{r}) \qquad (1.3)$$

in Eq.(1.2), the modified wave equation to be satisfied by the cell periodic function $U_n(\vec{k},\vec{r})$ is obtained

$$\left(H_o + \frac{\hbar}{m} \vec{k}.\vec{p} \right) U_n(\vec{k},\vec{r}) = E_n^1(\vec{k}) \ U_n(\vec{k},\vec{r}) \qquad (1.4)$$

where H_o is the Hamiltonian $\left(\frac{-\hbar^2\nabla^2}{2m} + V(\vec{r}) \right)$, originally started with in the one electron wave equation, Eq.(1.2) and

$$E_n^1(\vec{k}) = E_n(\vec{k}) - \frac{\hbar^2k^2}{2m}. \qquad (1.5)$$

At $\vec{k} = 0$, the equation to be satisfied by the cell periodic function Eq.(1.4) reduces to

$$H_o \ U_n(\vec{k},\vec{r}) = E_n(\vec{k}) \ U_n(\vec{k},\vec{r}) \ . \qquad (1.6)$$

Assuming that the above equation is solved a set of wavefunctions and

and their eigenvalues are known at $\vec{k} = 0$. Since the wavefunctions at $\vec{k} = 0$ form a complete set of periodic functions, it is possible to expand the cell periodic part of the wavefunction $U_n(\vec{k},\vec{r})$ at any value of $\vec{k}$ in terms of the Bloch functions at $\vec{k} = 0$. When Eq.(1.4) is evaluated at any point $\vec{k}$, the diagonal elements in the secular determinant are the energy eigenvalues at $\vec{k} = 0$ and the off diagonal elements arise from $(\hbar/m)\vec{k}.\vec{p}$ term connecting states in various bands. The symmetry properties of the wavefunctions reduce the number of these off diagonal elements.

If the diagonal and off diagonal elements are all known, for example, form experiments the secular determinant can be solved to determine the band structure.[22] The required energy levels and matrix elements are obtained from optical and cyclotron resonance experiments whenever available. The data which are not available from experiments are either obtained from other calculations or adjusted continuously until the calculated band structure agrees with the experimental data.

In the above discussion, the spin orbit interaction effects were not included. To take this into account, an extra term

$$H_{s.o} = \frac{\hbar}{4m^2c^2} (\vec{\nabla}V \times \vec{P}) .\vec{\sigma}$$

where $\vec{p}$ and $\vec{\sigma}$ are the momentum and spin operators respectively, is added to the Hamiltonian in Eq.(1.2). The equation satisfied by the cell periodic function Eq.(1.4) contains in addition to the term $H_{s.o}$ another term

$$H_{s.o} = \frac{\hbar}{4m^2c^2} (\vec{\nabla}V \times \vec{k}) .\vec{\sigma}$$

which is generally neglected on the grounds that this contribution is

much smaller compared to the contribution from $H_{s.o}$.

The $\vec{k}.\vec{p}$ method was used by Kane[23,24] to calculate the energy bands in InSb about the Γ point and has been extended by Cardona and co-workers to determine the band structures of Ge and Si[22] and several III - V compounds[25-27] over the entire Brillouin zone.

The empirical pseudopotential method has its foundations in the OPW method. Phillips and Kleinman[28] observed that orthogonalization of plane waves to the core states has the effect of a repulsive potential which is to be added to the actual crystal potential. This net effective potential which is weakly attractive has come to be known as the pseudopotential. The pseudopotential is expanded in reciprocal lattice vectors. The expansion coefficients are called the form factors. Phillips showed that very few form factors are required to calculate the band structures of simple lattices, for example, only three for germanium and silicon.[29] A particular advantage of this method is that from the form factors obtained for simple lattices extrapolations can be made to evaluate the form factors of a more complex lattice.[30] Cohen and Bergstresser[31] calculated the band structures of several diamond and zincblende structure materials obtaining the pseudopotentials empirically from crystalline energy levels from well established optical data.

A more recent method of great interest to calculate band structures is the dielectric method which has been introduced by Phillips and Van Vechten.[32] This method is based on Phillip's theory of electronegativity differences.[33] The dielectric method has been used to determine the band structures of several semiconductors and it has been claimed to be more accurate requiring even fewer number of parameters than the empirical pseudopotential method.[32]

1.5 Band Structures of Some Diamond and Zincblende Materials

At the present time, the band structures of several diamond and zincblende materials are well understood over a large energy range. In diamond structure materials, Si and Ge have been studied extensively both by theoretical and experimental methods. Gray tin is presently understood as a semimetal.[34,35] Diamond itself is an insulator.[36] The III - V compounds which occur in zincblende structure are semiconductor materials.[1]

The energy bands of Si and Ge determined by Herman et al[37] are given in Fig. 1.4. The electronic energy E is plotted as a function of the wave vector $\vec{k}$ starting from the center of the Brillouin zone along the symmetry directions Λ,Δ,Σ and the line between X and U (K). The various energy levels are labelled in the single group notation for diamond symmetry.[38] The valence band is composed of four sub-bands which are sufficient to accommodate the eight valence electrons in the unit cell. When the spin orbit interaction is neglected in the energy band calculations, three of the four bands are degenerate at $\vec{k} = 0$. This energy level is represented by Γ_{25}' symmetry and forms the valence band maximum. The fourth band is not shown in the figure. For $\vec{k}$ values not equal to zero, the three fold degenerate valence band is split into a two fold degenerate band in the (111) and (100) directions. The two fold degenerate band is represented by $\Gamma_{25}' L_3'$ along the Λ direction and by $\Gamma_{25}' X_4$ along the Δ direction. Along the Σ direction, the three fold degeneracy is split into three nondegenerate bands.

FIGURE 1.4

BAND STRUCTURES OF Si AND Ge
SPIN ORBIT INTERACTION NEGLECTED

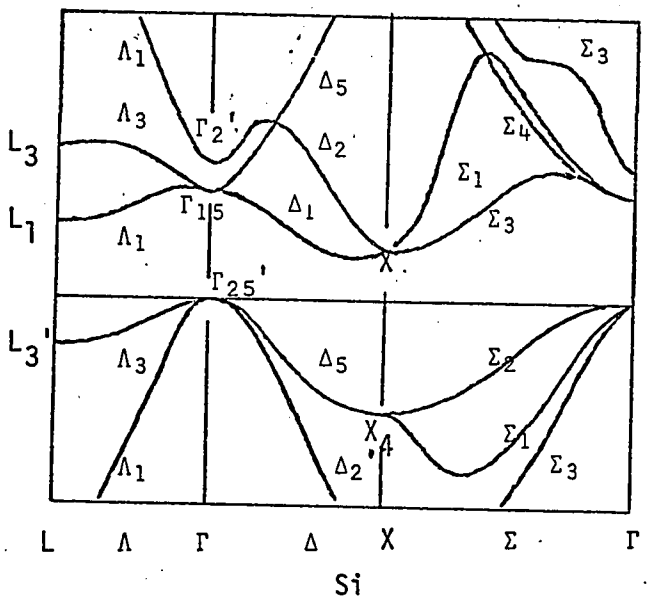

Si

Ge

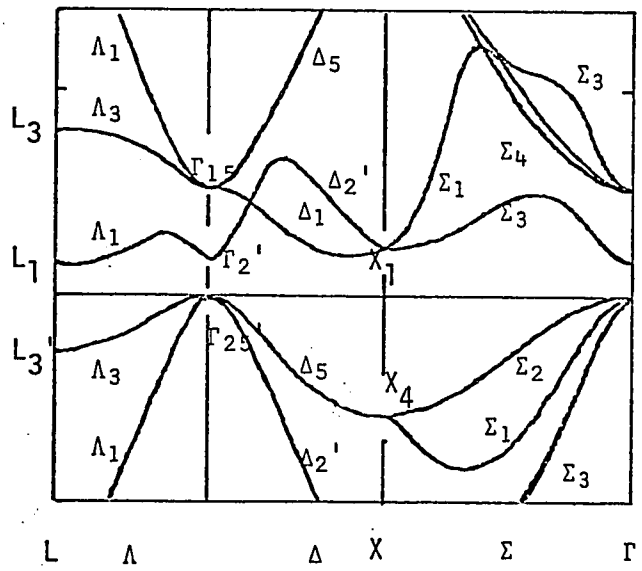

The energy band structure of germanium including the spin orbit interaction is shown in Fig. 1.5. The six fold degenerate Γ_{25}' level is split into two levels, a four fold degenerate Γ_8^+ (double group notation[39]) symmetry level and a two fold degenerate Γ_7^+ level. The magnitude of this splitting is represented by Δ_0. Away from $k = 0$, the Γ_8^+ level splits into two doubly degenerate (Λ_4,Λ_5) and Λ_6 levels along the (111) direction and Δ_7 and Δ_6 levels along the (100) direction. At the zone boundary the L_3' level degeneracy is removed, but the X_4 level degeneracy is unaffected. A general observation of the valence band structures in Ge and Si shows that they are similar.

The conduction bands in Si are represented by Γ_{15} L_1 along Λ, Γ_{15} X_4 along Δ and Γ_{15} K_3 along Σ symmetry directions in Fig. 1.4. In Ge, the conduction bands are Γ_2' L_1, Γ_2' X_1 and Γ_2' K_3 along the three symmetry axes, Λ, Δ, and Σ respectively. It is seen immediately that the form of the conduction bands differ considerably in these two materials. In Si, the conduction band main minimum is situated at a $\vec{k}$ value along the Δ direction inside the BZ.[40,41] In Ge, the minimum is at the L_1 symmetry points on the BZ boundary. In the conduction bands of Si and Ge subsidiary minima occur which have energies larger than the main minima.[41] The movement of the Γ_2' level, which lies above the Γ_{15} level in Si but crosses Γ_{15} level and lies midway between the Γ_{25}' and Γ_{15} levels in Ge is a characteristic feature in the conduction bands of Si and Ge.[42]

When spin orbit interaction is taken into account the conduction band energy levels Γ_2', L_1 and X_1 remain unaffected, Fig. 1.5.

FIGURE 1.5

BAND STRUCTURE OF Ge

SPIN ORBIT INTERACTION INCLUDED

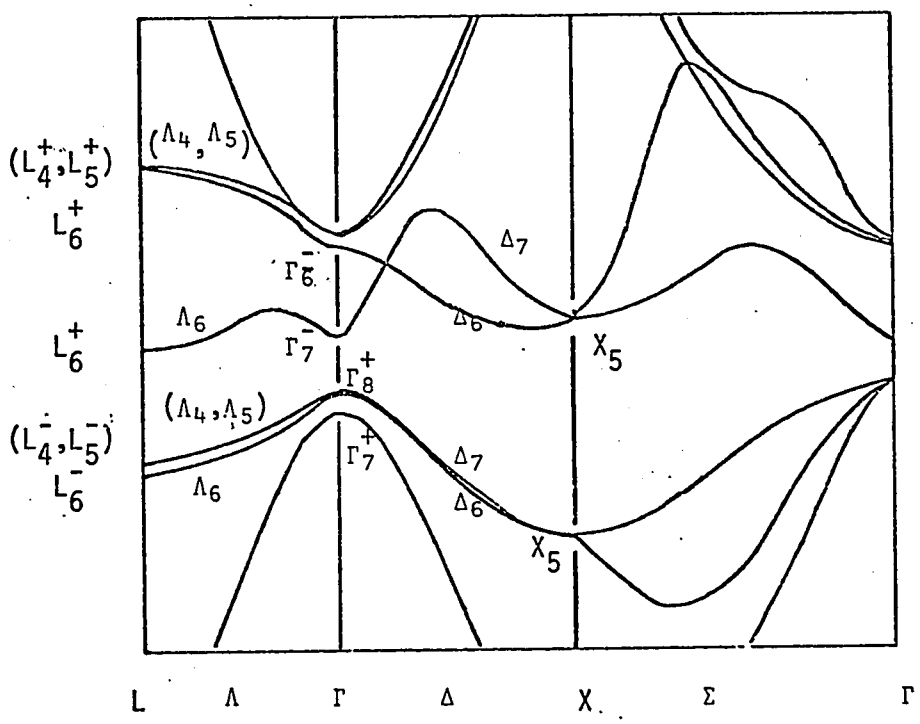

But the Γ_{15} level splits into Γ_6^- and Γ_8^- symmetry levels. The energy level L_3 is split into two components L_6^+ and (L_4^+, L_5^+).

The energy band structures of zincblende materials InSb, GaAs and GaP calculated by Cohen and Bergstresser[31] are shown in Fig. 1.6. The similarity in their structures is apparent. The III - V compounds chosen are the isoelectronic counterparts of gray tin, Ge and a fictitious $Ge_{.5}Si_{.5}$ valence IV material.[1,43] As there are a total of eight valence electrons per unit cell in the III - V compounds, four valence bands are required to accommodate them. As has been seen in the case of the valence bands of Si and Ge when spin orbit interaction is not included three of the four valence bands are degenerate at $\vec{K} = 0$. This three fold degenerate level is represented by Γ_{15} symmetry unlike Γ_{25}' in diamond lattice materials.[44] For $\vec{K} = 0$, the three fold degeneracy of Γ_{15} is removed giving a two fold degenerate and a nondegenerate bands along the Λ and Δ axes and along the Σ direction the three nondegenerate bands are resolved.

When spin orbit interaction is taken into consideration,[44,45] the Γ_{15} valence level is split into Γ_8 and Γ_7 levels shown in Fig. 1.7. At the BZ boundary the L_3 valence level is split into (L_4, L_5) and L_6. The Λ_3 line degeneracy is removed and the split components (Λ_4, Λ_5) and Λ_6 are compatible with (L_4, L_5) and L_6 respectively at the zone boundary and with the Γ_8 level at the zone center. The valence band maximum is no longer situated at $\vec{K} = 0$ but it is shifted to a $\vec{k}$ value by a sufficiently small quantity which is generally always neglected.[44] The X_5 valence level at the X symmetry point is split into two levels X_7 and X_6 which are joined to the Γ_8 level by Δ_5 states along the Δ axis.

FIGURE 1.6

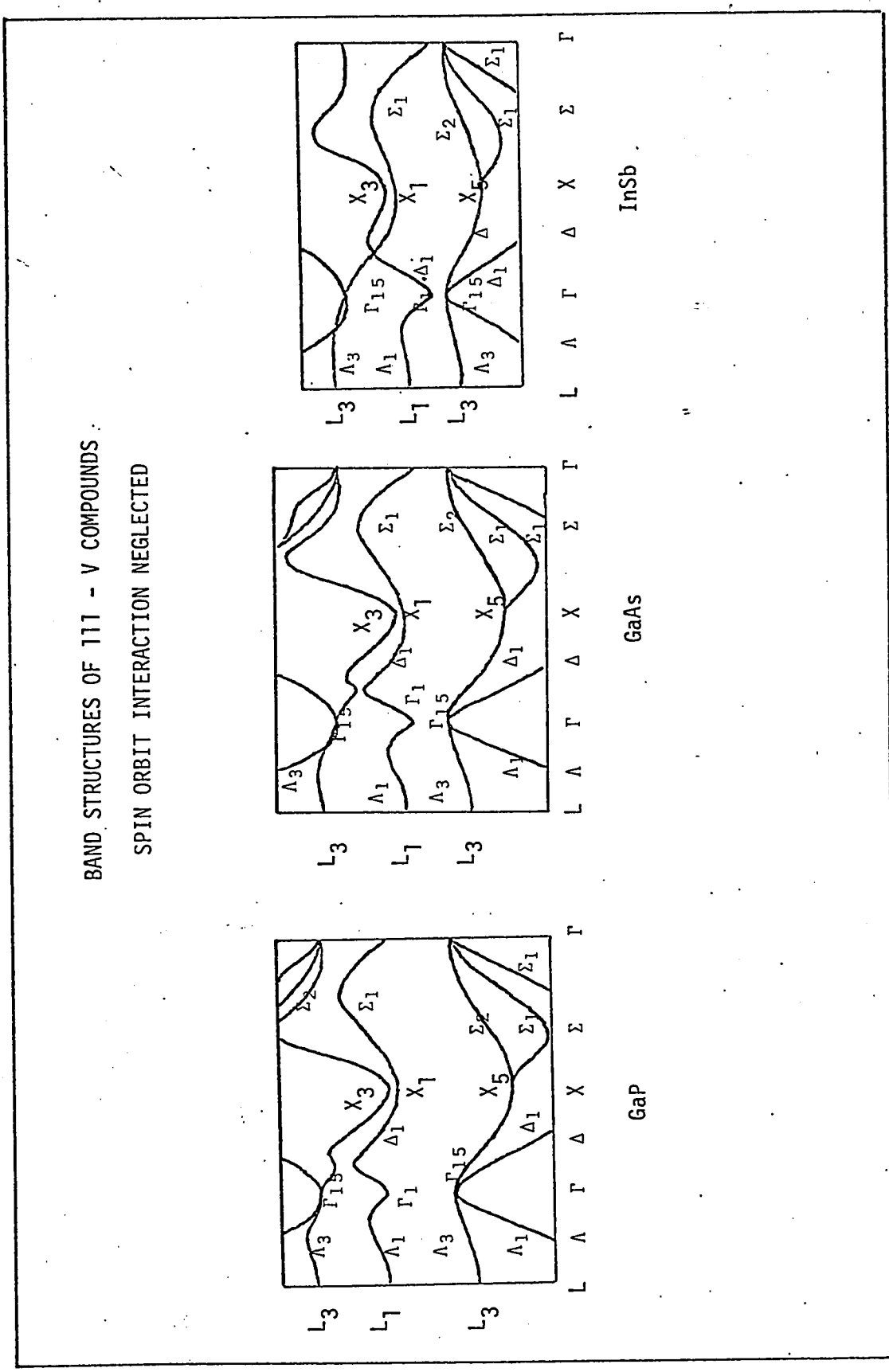
BAND STRUCTURES OF III - V COMPOUNDS
SPIN ORBIT INTERACTION NEGLECTED
GaP
GaAs
InSb
L Λ Γ Δ X Σ Γ
L3 L1 L3
Λ3 Λ1 Λ3
Γ15 Γ1
Δ1
X3 X1 X5
Σ1 Σ2

FIGURE 1.7

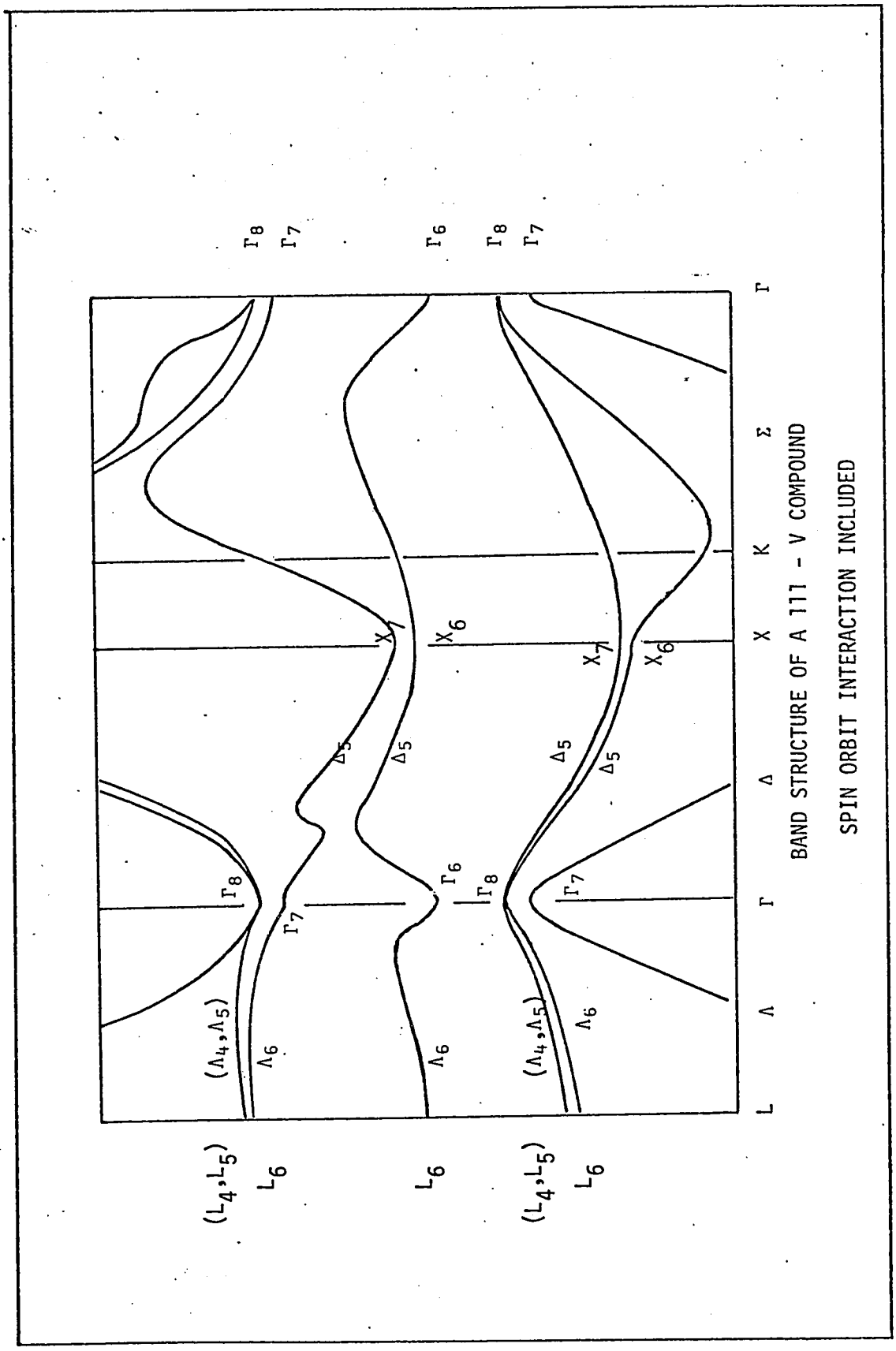

BAND STRUCTURE OF A III - V COMPOUND

SPIN ORBIT INTERACTION INCLUDED

The conduction bands are represented by $\Gamma_1 L_1$, $\Gamma_1 X_1$ and $\Gamma_1 K_1$ along the three directions Λ, Δ and Σ respectively as shown in Fig. 1.6. These bands are unaffected by the inclusion of spin orbit interaction but the Γ_{15} and L_3 conduction band energy level degeneracies are lifted and their components are shown in Fig. 1.7.

A comparison between the band structures of the diamond and zincblende materials shown in Fig. 1.5 and Fig. 1.7 shows that the X_5 energy levels of diamond symmetry are split in zincblende structure. The zincblende energy level with X_5 symmetry is split into X_6 and X_7 under spin orbit interaction. The lack of inversion center in zincblende is responsible for the removal of X_1 , X_3 degeneracy present in diamond structure. The energy difference between the two levels X_1 and X_3 is a measure of the heteropolar nature of the bond between valence III and valence V atoms.[46]

In the III - V compounds, InSb,[46] InAs, InP, GaSb and GaAs the valence band maximum $\Gamma_{15}(\Gamma_8)$ is directly below the conduction band minimum $\Gamma_1(\Gamma_6)$ at the center of the BZ. They are known as the direct gap materials.[41,43] But in GaP and AlSb the conduction band main minimum is at a k value along the Δ direction and the valence band maximum is at Γ_{15} (Γ_8) for which reason they are known as the indirect gap materials.[41,43]

Experiments generally conducted to obtain information on energy band structure are optical transmission and reflection measurements which measure the interband energy separations and experiments like electrical conductivity, Hall Effect, magnetoresistance, piezoresistance, cyclotron resonance absorption, etc., which lead to an understanding of band structure around the extrema.

1.6 Semiconductor Alloys

A disordered substitutional solid solution represented by $A_{1-x}B_x$ contains x molepercent of B atoms replacing the A atoms on their lattice sites at random. The occurence of such a binary system with continuous solid solubility for all compositions is possible when the atomic radii of the solvent and the solute atoms do not differ by more than 15 percent and when the valence and chemical nature of the alloying atoms do not promote formation of intermediate compounds.[47]

An alloy of two valence IV elements is a binary system where solid solubility is controlled by the sizes of the alloying atoms. Continuous solid solubility exists between Si and Ge;[48,49] Ge and α-Sn are only weakly soluble in one another and a mixed crystal between C and Si is obtained at only one composition, SiC.[43]

An alloy of two III - V compound materials which have one of either valence III or V element in common is strictly a ternary system. But it can be assumed that the three elements involved in each alloy would combine to form two stochiometric III - V compounds which act as the components of a binary system. This pseudobinary character of the alloy system is demonstrated by annealing a number of samples of different composition within the solidus - liquidus field at the same temperature. In the quenched samples, the equilibrium phases must have the same composition if the system is pseudobinary.[50]

In the alloy lattice of two zincblende materials alloying takes place by substitution at random in either one of the two face centered cubic sublattices depending upon the valence of the alloying element. An important factor in achieving continuous solid solubility is the

heteropolar nature of the chemical bond between the valence III and V atoms in addition to their geometrical sizes.[51,52] A miscibility gap is predicted by Müller and Richards in alloys with a radius mismatch of 17 percent between the alloying atoms.[52] This leads to complete miscibility between those III - V compounds which have valence V elements in common. The radius mismatch for Ga and In is 12 percent and the radii of Al and Ga are almost equal. For alloys with valence III element in common, the radius mismatch for P and As is 7 percent; for As and Sb 17 percent and for P and Sb 24 percent. Therefore a miscibility gap is expected when P is substituted for Sb or vice versa. In alloys where the substitution is between As and Sb complete miscibility has been found.[50] With respect to the ionic nature of the bond between valence III and V atoms, Folberth has arranged the most common III - V compounds in the order of increasing ionicity: AlSb, (GaSb, GaP, GaAs), InSb, (InP, InAs).[51] Taking the size factor into consideration those two compounds adjacent to each other in the above sequence form alloys readily.

The preparation of binary and pseudobinary alloys and a study of their physical properties adds to the understanding of the terminal materials and provides information on the composition dependence of the physical properties under investigation. A large number of semiconductor alloy systems have been measured experimentally. But not many theoretical band structure calculations have been attempted for alloy semiconductors from first principles methods as in the case of elemental or compound semiconductors. However, there exist some semiempirical calculations using the pseudopotential[53,54] and dielectric methods.[55] The obvious complexity of the alloy problem is in the choice of a potential. The

periodic nature of the lattice still exists giving rise to energy bands but the magnitude of the potential in which an electron moves changes from one lattice site to the other depending upon the atom occupying the site. The concept of a virtual crystal introduced by Nordheim[56] and later developed by Muto[57] and Parmenter[58-60] is valuable in alloy studies.

1.7 Virtual Crystal Model

In a disordered alloy lattice the potential in which an electron moves can be divided into two parts

$$V_{alloy}(r) = V_{per}(r) + V_{aper}(r)$$

where V_{per} and V_{aper} are the periodic and the aperiodic parts of the crystal potential. In the virtual crystal analysis it is assumed that V_{per} may be obtained as the average potential of all the possible allowed random configurations of the alloyed atoms. Then V_{aper} is the difference between the actual value V and V_{per}. The function V_{per} will then give a band structure corresponding to a virtual crystal. The effect of V_{aper} on this virtual crystal band structure may in principle be calculated by perturbation theory provided V_{aper} is sufficiently small. For any case where the effect of disorder produces a free energy term sufficiently small for the single phase alloy to exist V_{aper} is likely to satisfy the above conditions.

In a one dimensional model Muto[57] showed that the first order perturbation has no effect on the virtual crystal band structure. Parmenter[58] calculated the higher order effects and his results show that the influence of perturbation is large at the band edges smearing them into the gaps by a finite extent. When the second and higher order effects are assumed to be negligible the general result of a virtual crystal model is expected to give a smooth variation of band structure from one compound to the other. This should be observable in the experimental results of the variation of energy gaps, effective masses, scattering parameters and lattice parameters as a function of alloy composition. A linear variation of lattice parameter, known as Vegards

law[172] has been well established with only minor deviations.[50] In the spirit of the virtual crystal model a linear variation of potential was assumed in the pseudopotential band calculations of Bassani and Brust[53] and Jones and Lettington.[54] Similarly, in the dielectric method the homopolar and the ionic energy gap parameters were assumed to vary linearly as a function of composition by Van Vechten and Bergstresser.[55] Results of these calculations will be discussed along with experimental data.

1.8 The $Ge_{1-x}Si_x$ Alloy System

This alloy system was first prepared by Stohr and Klemm[48] by annealing compressed powders over long periods of time. Later, Johnson and Christian[49] prepared $Ge_{1-x}Si_x$ alloy samples by homogenization at high temperatures. They determined various parameters including the forbidden gap of those samples. An abrupt change of slope was observed in the band gap versus composition curve.

In the same year, Herman[42] published his "Speculations on the energy band structure of Ge-Si alloys". Theoretical energy band calculations for Ge were available.[61] The conduction and valence band structures of silicon were known from piezoresistance measurements of Smith,[62] magnetoresistance data of Pearson[63] and cyclotron resonance absorption measurements of Lax and Dexter.[64] To interpret the available energy gap variation as a function of composition, Herman made the assumptions that alloying produced more radical changes in the conduction bands. As the silicon content is increased the <111> conduction band minima in Ge moved up at a faster rate than the <100> minima. At one particular composition the two sets of minima will be situated at the same energy. Further increase in Si composition raises the <111> minima in energy beyond the <100> minima, which would lead to the silicon band structure with <100> conduction bands. In this argument the valence band maximum was assumed to remain at the center of the BZ in both Ge and Si and in the $Ge_{1-x}Si_x$ alloy specimens as well. On this alloy system further optical work includes the reflectance measurements by Tauc and Abraham[65,66] which gave information on several high energy band gaps. More recently electroreflectance measurements were made by Klein et al.[67]

The composition dependence of various band gaps is observed to be linear in their results. The calculated energy levels by Brust and Bassani[53] agreed approximately with a linear variation as a function of composition. The variation of E_o gap as a function of composition determined by the dielectric method by Van Vechten and Bergstresser[55] is in good agreement with the electroreflectance results of Klein et al.[67]

1.9 The Mixed III - V Alloys

Since the preparation of the $Ge_{1-x}Si_x$ alloy material and the determination of its semiconductor properties the most logical step was to investigate the solid solubility of III - V compounds. The initial work was concentrated on pairs of III - V compounds which have one element in common to simplify the problem but not with very encouraging results. The first successful work was reported by Folberth[2] and Weiss[68] on the $InAs_{1-x}P_x$ and $GaAs_{1-x}P_x$ alloys. They showed that in these alloys solid solution was obtained throughout the whole range of composition. Goryunova and Federova [69] investigated the $Ga_xIn_{1-x}Sb$ and $Ga_xIn_{1-x}As$ alloys and found that the antimonides reached single phase condition after long annealing times and the arsenide alloys were still in two phase condition. Woolley and co-workers,[70-72,50] annealing compressed powders over long periods of time, showed that solid solution occurred at all compositions in the $Ga_xIn_{1-x}Sb$, $Ga_xIn_{1-x}As$ and $InSb_{1-x}As_x$ alloy systems and possible at all compositions in $Al_xIn_{1-x}Sb$ and $Ga_xSb_{1-x}As_x$ alloys. The work of many active researchers in this area has been described in the review article on solid solution of III - V compounds by Woolley[50] and recently in the book on III - V compounds by Madelung.[43]

While the alloy samples obtained from annealing powders were sufficient to determine the solid solubility and the solidus line in the T - X phase diagram, they were not suitable for measuring either the optical or the electrical properties which require good single phase solid material. Two methods which involve melting compounds mixed in stochiometric proportion to give reasonably solid material are zone

recrystallization and directional freezing.[70,73,74] To overcome some of the disadvantages of directional freezing a third method, horizontal Bridgman was later developed.[75]

In zone recrystallization a small portion of the ingot is melted and the molten zone is swept through the entire ingot by either moving the ingot or the furnace relative to one another. At the leading edge of the molten zone material is melted and at the trailing edge recrystallization takes place. For a narrow enough zone and slow enough rate of zone travel the alloy composition within the molten zone comes quickly to its equilibrium value. This should give an ingot with one composition value along its ingot length except at the two ends.

In directional freezing, a temperature gradient is maintained along the length of the ingot. To start with, the ingot is in the molten state. The temperature along the whole length of the ingot is lowered at a constant rate maintaining the gradient. This causes the ingot to solidify from one end to the other gradually as the freezing surface moves along the ingot. With this method a continuous variation of composition is obtained along the length of the ingot with homogeneous cross sectional slices. In this method, a steep temperature gradient is required to prevent inhomogeneous solidification at the freezing interface. For materials with high melting temperatures obtaining a steep temperature gradient creates serious experimental problems, which have been overcome in the horizontal Bridgman method described next.

In the horizontal Bridgman method a molten ingot is pulled through a steep temperature gradient from a hot zone into the adjacent cold zone. Recrystallization takes place as the freezing interface

moves along the length of the ingot. This method requires a furnace with two flat temperature profile sections, one maintained at a temperature higher than the melting temperature of the two alloying compounds and the other maintained below the freezing temperatures of the alloying compounds. The temperature gradient between the two temperature zones is made as steep as possible. As this technique has been used to prepare alloy material in the present work, a more detailed description of the method is given in Chapter 3. Next, a brief summary of previous work carried out on III - V alloys which is directly related to the present work is given.

$Ga_xIn_{1-x}Sb$ alloy

In this alloy system, the optical energy gap was investigated by Ivanov-Omskii and Kolomiets;[73] Woolley, Evans and Gillett,[76] and Woolley and Evans.[77] The band gaps determined by Woolley and Gillett[78] from electrical data did not agree with the optical data in GaSb and in GaSb rich alloy samples. This anomaly was attributed to the presence of subsidiary minima in proximity to the main minimum in the conduction bands of GaSb[79] and GaSb rich alloy samples.[80] To investigate further this anomaly highly homogeneous material was prepared by Coderre[75] using the horizontal Bridgman method. In the present work, reflectance, electroreflectance and thermoreflectance measurements were made on this alloy system. Earlier reflectance measurements were made by Woolley and Blazey[81] in order to investigate the composition dependence of the high energy band gaps beyond the fundamental. A linear variation was reported for various band gaps.

$InSb_{1-x}As_x$ alloy

First, it should be mentioned that the preparation of this material is relatively more difficult except perhaps when compared with the preparation of $GaSb_{1-x}As_x$ alloy.[50] The atomic size factor is not exactly in favour of alloy formation and therefore a high degree of strain is expected in the alloy lattice.[52] First solid samples of $InSb_{1-x}As_x$ were prepared by Woolley and Warner[82] by using the gradient freeze and zone levelling techniques. Homogeneous material was obtained near the InSb and InAs ends leaving a wide range of composition in the middle of the ingot. From the energy gap measurements made on these samples, the composition dependence was investigated. The energy gap variation was particularly interesting because it decreases as the As mole fraction increases in the alloy and goes through a minimum. This minimum represents the smallest direct gap obtainable in the III - V alloy materials. To further investigate the properties of this material, it was necessary to improve the quality of the material. Using the horizontal Bridgman method[75] single phase material has been prepared and its optical and electrical properties have been determined. The minimum in the energy gap versus composition has been observed and the results have been found to be in good agreement with previous data. Further, above a transition temperature which is below the solidus temperature for alloy specimens, over a considerable range of alloy composition a normal to inverted band transition has been observed by Coderre and Woolley.[83] Initial investigations of the electroreflectance spectra of the alloy samples were started by Thompson and Woolley.[84] In the present work, this alloy system has been measured in detail and the results are given in Chapter 4.

$InAs_{1-x}P_x$ alloy

This was one of the first alloy systems to be prepared successfully.[2] Alloys of all compositions solidify immediately as reasonably homogeneous single phase specimens without requiring time-consuming homogenization processes. The linear variation of the lattice parameter as a function of composition was reported by Folberth[2] and Koster and Ulrich.[85] In a recent determination of the lattice parameter by Thompson et al[86] a slight deviation from linearity has been observed. The fundamental gap energy was determined by Oswald[87] from optical absorption measurements and by Weiss[68] from electrical data. The gap width versus composition curve is shown to be linear. Earlier work by Krioturu et al[88] giving reflectance data on the $InAs_{1-x}P_x$ alloys indicated that for all transitions observed the energy varied linearly with alloy composition within the limits of the experimental error. Recent interest in this alloy material arises because of its possible use for injection lasers.[89] The emitted radiation will be in the infrared as the direct gap width in InP is 1.34 eV and decreases as the InAs molefraction increases in the alloy specimens. Homogeneous polycrystalline $InAs_{1-x}P_x$ alloys were grown by a halogen vapour transport technique by Rubenstein[86] and their optical properties were measured by Thompson et al[86] using the electroreflectance and the wavelength modulated reflectance techniques. Their results are in good agreement with the electroreflectance results obtained concurrently in the present work. These results are given in Chapter 4.

$Ga_xIn_{1-x}As$ alloy

The solid solubility of the $Ga_xIn_{1-x}As$ alloy system and the variation of lattice parameter as a function of composition was investigated by Woolley and Smith.[70,71] The composition dependence of the lattice parameter is shown to be linear. The solid samples required for optical and electrical measurements were grown by gradient freeze and zone recrystallization methods. The optical energy gap measurements were made by Abrahams et al,[74] Woolley et al[90] and Hockings et al.[91] There has been quantitative disagreement between the three sets of results. In order to resolve the ambiguity Woolley et al[92] again measured the optical energy gaps in highly homogeneous specimens grown from horizontal Bridgman method. Corrections were made for the Burstein shift in the analysis to determine band gaps. The energy gap versus composition curve obtained from their results is nonlinear. Coderre and Woolley[93] determined the energy gaps in alloy specimens by means of high temperature Hall effect measurements and the results are in good agreement with the earlier optical work. Reflectance measurements were made on this system by Woolley and Blazey[81] and Conrad et al.[94] The higher energy gaps beyond the fundamental were found to vary linearly as a function of composition within the limits of experimental uncertainty. Electroreflectance measurements were made by Thompson and Woolley[95] and Williams and Rehn.[96] The fundamental gap variation found from the electroreflectance results of Williams and Rehn[96] is in agreement with previous results. Two higher energy gaps were found to vary nonlinearly as a function of alloy composition. The electroreflectance data of Thompson and Woolley[95] are included in the discussion along with the

the results on several other III - V compounds in Chapter 4.

$GaAs_{1-x}P_x$ alloy

The existence of the complete mixed crystal system of $GaAs_{1-x}P_x$ was shown by Folberth.[2] Preparation of alloy material is expected to be no more difficult than the preparation of GaAs and GaP materials. This is a particularly interesting alloy material from both scientific and technological aspects. Scientifically, the conduction band structures are different in GaAs and GaP. GaAs is a direct gap material whereas the gap in Gap is indirect. In the fundamental gap versus composition curve a kink is expected at the composition value where the (000) minimum and the minima along the <100> directions cross each other. Technologically, the energy gap values in the direct gap composition range of the alloy material is valuable for light emitting devices. First optical absorption measurements were made by Folberth.[2] Rubenstein[97] prepared alloy samples with good homogeneity by a sealed tube iodine transport method and measured the optical energy gap. Absorption measurements were also made by Tietjen and Amick[98] on alloys grown by vapour deposition technique. The existence of a kink is well established experimentally in the energy gap versus composition curve. Reflectance measurements on this alloy system were made by Abagyan et al,[99] Bergstresser et al,[100] Thompson et al,[101] Woolley et al,[102] and Williams and Jones.[103] By following the reflectance structure through the alloy composition range, the reflectance data for GaAs was correlated to that for GaP. Electroreflectance measurements were made by Thompson et al.[104] The direct energy gap was determined over the whole composition range. A parabolic

variation of direct gap as a function of composition was found to fit the results of this alloy system as well as in several other III - V alloys.[105] The reflectance and electroreflectance measurements of Thompson et al[101,104] are included in the discussion in Chapter 4, along with the data on several other III - V compounds.

CHAPTER 2

OPTICAL PROPERTIES

2.1 Introduction

In the present work, the optical properties measured were the static and the modulated reflectance in order to obtain information about the energy band structure. It is therefore necessary to first relate the optical properties of a solid with its band structure. This is usually done through the macroscopic optical parameters ε_1 and ε_2, the real and imaginary components of the complex dielectric function, respectively. An expression for ε_2 is obtained by treating the electromagnetic wave interacting with the solid as a time dependent perturbation which induces interband electron transitions. The structure found in a reflectance spectrum can be transformed into structure in ε_2 which is correlated with the critical point band gaps. To understand modulated reflectance spectra, first the effect of modulating parameter on ε_1 and ε_2 should be known. A phenomenological description of this is given which shows that structure should be present at the critical point energy positions in a modulated reflectance spectrum. This is followed by the theory of two modulation methods, thermoreflectance and electroreflectance. Finally, a review of reflectance and modulated reflectance results is given.

2.2 Definition of Optical Parameters

The response of an isotropic material under the influence of an electromagnetic field is governed by Maxwells' equations[106] and described equivalently by either the complex index of refraction $\tilde{n} = n + ik$, where n and k are the indices of refraction and absorption respectively or by the complex dielectric function, $\tilde{\varepsilon} = \varepsilon_1 + i\varepsilon_2$, where ε_1 and ε_2 are its real and imaginary components.[107] The relationship between $\tilde{\varepsilon}$ and $\tilde{n}$ being $\tilde{\varepsilon} = |\tilde{n}|^2$ gives for ε_1 and ε_2 in terms of n and k

$$\varepsilon_1 = n^2 - k^2 \qquad \text{and} \qquad \varepsilon_2 = 2nk.$$

The optical properties of a material are determined when the parameters ε_1 and ε_2 are known as a function of frequency ω or photon energy $\hbar\omega$ of the electromagnetic wave. The imaginary component ε_2 is a measure of the energy absorbed by the material from the electromagnetic wave and its determination over a broad energy range represents the absorption spectrum of the material. An absorption coefficient α may be defined as the relative decrease of energy flow per unit distance of travel in the direction of the propagation of the electromagnetic wave. The coefficient α can be expressed in terms of either ε_2 or k

$$\alpha = \frac{\omega}{nc}\,\varepsilon_2 = \frac{4\pi k}{\lambda},$$

where ω is the angular frequency, λ is the wavelength and c is the velocity of light.

2.3 The Optical Absorption Process in a Solid

In the energy band model of solids discussed in Chapter 1, the electron states of a periodic lattice form a set of quasicontinuous bands in momentum space. Each band extends over the entire first BZ in the reduced zone representation, Fig. 1.1. Under the influence of an electromagnetic field, an electron absorbs a photon and is lifted into a higher energy state. Therefore, the absorption spectrum of a solid should show the characteristic profile of its energy band structure.

An expression for ε_2, which is a measure of the energy absorbed by the solid can be derived in terms of its energy band parameters by treating the electromagnetic field as a perturbation on the electron motion. The total Hamiltonian can be written as[108]

$$H = \frac{1}{2m}\left(\vec{p} + \frac{e}{c}\vec{A}\right)^2 + V(\vec{r}) \qquad (2.1)$$

where $\vec{p}$ is the momentum, $\vec{A}$ the vector potential of the electromagnetic wave, $V(\vec{r})$ the periodic potential of the crystal, e the charge and m the mass of an electron and c is the velocity of light. Expanding Eq.(2.1) and neglecting the term $\frac{e^2A^2}{2mc^2}$, the Hamiltonian becomes $H = H_o + H_I$ where $H_o = \left(\frac{p^2}{2m} + V(\vec{r})\right)$ and

$$H_I = \frac{e}{mc}\vec{A}.\vec{p} \qquad (2.2)$$

The term H_o represents the Hamiltonian before light is incident on the solid. Therefore, H_I gives the interaction of radiation with the solid. Taking a plane wave solution of the wave equation for the vector potential $\vec{A}$, with propagation vector $\vec{\ell}$ and angular frequency ω

$$\vec{A}(\vec{r}, t) = \vec{A}_o \{\exp(i\vec{\ell}.\vec{r} - i\omega t) + c.c\}, \qquad (2.3)$$

where c.c. represents the complex conjugate of the term preceding it. Substitution of Eq.(2.3) in Eq.(2.2) gives for the interaction term

$$H_I = \frac{e}{mc} \vec{p}.\vec{A}_o \{\exp(i\vec{\ell}.\vec{r} - i\omega t) + c.c\} . \qquad (2.4)$$

Treating H_I as a time dependent perturbation, the transition probability of an electron between two of its stationary states can be calculated. One of the two terms in H_I Eq.(2.4), will induce upward transitions resulting absorption and the other will induce downward transitions resulting emission at the same rate.[108]

The transition probability per unit time per unit volume for a pair of bands with one fully occupied and the other empty is[108,109]

$$W = \frac{2\pi e^2}{m^2c^2\hbar} A_o^2 \int \frac{2}{(2\pi)^3} d^3k \ |\vec{n}_o.p_{if}|^2 \times \delta (E_F - E_i - \hbar\omega) \qquad (2.5)$$

where n_o is a unit vector in the direction of polarization of the electromagnetic wave and p_{if} the momentum matrix element

$$p_{if} = \int \psi_f^* \vec{p} \exp(i\vec{\ell}.\vec{r}) \psi_i \, d\tau \qquad (2.6)$$

with ψ_i and ψ_f representing the initial and final states. The δ function, $\delta(E_F - E_i - \hbar\omega)$ imposes the restriction that no transitions occur unless the photon energy $\hbar\omega$ matches the energy difference $(E_F - E_i)$ between the final and the initial states.

In a solid, the initial and final states of an electron are represented by Bloch functions

$$\psi_i = U_{k_i} \exp(i\vec{k}_i.\vec{r}) \ , \text{ and}$$

$$\psi_f = U_{k_f} \exp(i\vec{k}_f.\vec{r}) \ . \qquad (2.7)$$

Introducing the Bloch functions, Eq.(2.7) for ψ_f and ψ_i, in Eq.(2.6)

$$p_{if} = \int U_{k_f}^{*} \exp(-i\,\vec{k}_f.\vec{r})\ (-i\,\hbar\,\nabla)\ \exp(i\,\vec{\ell}.\vec{r})\ U_{k_i}\ \exp(i\vec{k}_i.\vec{r})\ d\tau \tag{2.8}$$

which vanishes unless

$$\vec{k}_f - \vec{k}_i - \vec{\ell} = \vec{K} \tag{2.9}$$

where $\vec{K}$ is a reciprocal lattice vector, is satisfied. This is a consequence of the exponential term, $\exp[i\vec{k}_i + \vec{\ell} - k_f).\vec{r}]$ in p_{if}. (Eq. (2.8)). The wavelength of a photon is large when compared with the wavelengths of an electron of comparable energy. Therefore $\vec{\ell}$ is much smaller than $\vec{k}_f$ or $\vec{k}_i$ and hence may be neglected, giving

$$\vec{k}_f - \vec{k}_i = \vec{K}. \tag{2.10}$$

This requires that the electron transition be vertical in the reduced zone scheme. This condition is represented by the δ function, $\delta(\vec{k}_f - \vec{k}_i - \vec{K})$.

The presence of the polarization vector $\vec{n}_o$ in Eq.(2.5) imposes selection rules on the transition whether it is allowed or not depending upon the symmetry properties of the initial and final state wavefunctions.

The rate at which energy is absorbed by the solid from the electromagnetic field is given by $W.\hbar\omega$, which is equal to $({}^{\omega E_o{}^2}/_{8\pi})\varepsilon_2$ where $E_o{}^2 = \dfrac{2\omega^2 A_o{}^2}{c^2}$. This gives for ε_2

$$\varepsilon_2 = \frac{8\pi^2 e^2}{m^2\omega^2} \int \frac{2}{(2\pi)^3} d^3k\ \ |\vec{n}_o.p_{if}|^2\ \ \delta(E_F - E_i - \hbar\omega)\ \delta(\vec{k}_f - \vec{k}_i - \vec{K}), \tag{2.11}$$

when Eq.(2.5) is substituted for W.

The expression for ε_2, Eq.(2.11) essentially forms the link between the theory and the experiment. It relates the optical absorption

process to the band structure simply in terms of allowed and forbidden transitions and when the transitions are allowed the energy separation between the final states which are directly above the initial states in the reduced zone scheme representation, matches the photon energy of the incident radiation.

The expression for ε_2, Eq.(2.11) may be simplified further by assuming that the orientation of the polarization vector $\vec{n}_o$ is random and the matrix element p_{if} remains constant for a pair of bands over the entire BZ. With these assumptions, ε_2 becomes

$$\varepsilon_2 = \frac{8\pi^2 e^2}{3m^2\omega^2} (p_{if})^2 \left[\int_{BZ} \frac{2}{(2\pi)^3} d^3k \times \delta(E_F - E_i - \hbar\omega) \times \delta(\vec{k}_f - \vec{k}_i - \vec{K}) \right] \tag{2.12}$$

The expression in parentheses of Eq.(2.12) gives the number of pairs of states separated by energy $\hbar\omega$, which is defined as the joint density of states function $\rho(\hbar\omega)$,

$$\rho(\hbar\omega) = \int \frac{2}{(2\pi)^3} d^3k \times \delta(E_F - E_i - \hbar\omega) \times \delta(\vec{k}_f - \vec{k}_i - \vec{K}) \tag{2.13}$$

and

$$\varepsilon_2 = \frac{8\pi^2 e^2}{3m^2\omega^2} (p_{if})^2 \rho(\hbar\omega) \tag{2.14}$$

from Eqs.(2.13) and (2.12). A transformation of the volume integral in $\rho(\hbar\omega)$ into a surface integral over a constant energy surface gives,

$$\rho(\hbar\omega) = \int \frac{2}{(2\pi)^3} \frac{ds_k}{\nabla_k (E_F - E_i)} \tag{2.15}$$

It is seen from the above equation that the density of states function is singular at places in the BZ whenever $\nabla_k (E_F - E_i) = 0$. This condition is satisfied when[111]

$$\nabla_k E_f = \nabla_k E_i = 0$$

and

$$\nabla_k E_f = \nabla_k E_i \neq 0 .$$

Such critical points occur in E versus K curves at high symmetry points and along symmetry axes in the BZ. The critical point concept was originally introduced by van Hove[112] and its application to optical absorption process was extended by Phillips.[111,113]

The analytic behaviour of the density of states function near a van Hove singularity is obtained by expanding $(E_f - E_i)$ in a Taylor series about $k = k_o$,

$$E_f(k) - E_i(k) = \hbar\omega_o(k_o) + \sum_{j=1}^{3} a_j (k_j - k_{oj})^2 \qquad (2.16)$$

and solving the integral for $\rho(\hbar\omega)$, Eq.(2.5). Four types of critical points are defined depending upon the sign of the coefficients a_1, a_2 and a_3 in Eq.(2.16). Table (2.1) gives the classification of the critical points and Fig. 2.1 shows the density of states function near the critical points.

The critical points introduce distinct structure in the density of states function, Fig. 2.1, and this structure is carried over into ε_2 through Eq.(2.14). Therefore, the energy positions where structure is observed in an ε_2 spectrum should give the energy separations between the two bands (E_f,k) and (E_i,k) where the condition $\nabla_k(E_f - E_i) = 0$, is satisfied. The ε_2 line shape should reveal the type of critical point responsible. This forms the working hypothesis of the band structure analysis.

TABLE 2.1

Joint Density of States Function near the four types of critical points

Type of Critical Point	Notation	a_1	a_2	a_3	$\rho(\hbar\omega)$ $\hbar\omega < E_0$	$\rho(\hbar\omega)$ $\hbar\omega > E_0$
Minimum	M_0	+	+	+	0	$c_0(E-E_0)^{\frac{1}{2}}$
Saddle Point	M_1	+	$\pm$	-	$c_1-c_1'(E_0-E)^{\frac{1}{2}}$	c_1
Saddle Point	M_2	+	-	-	c_2	$c_2-c_2'(E-E_0)^{\frac{1}{2}}$
Maximum	M_3	-	-	-	$c_3(E_0-E)^{\frac{1}{2}}$	0

FIGURE 2.1

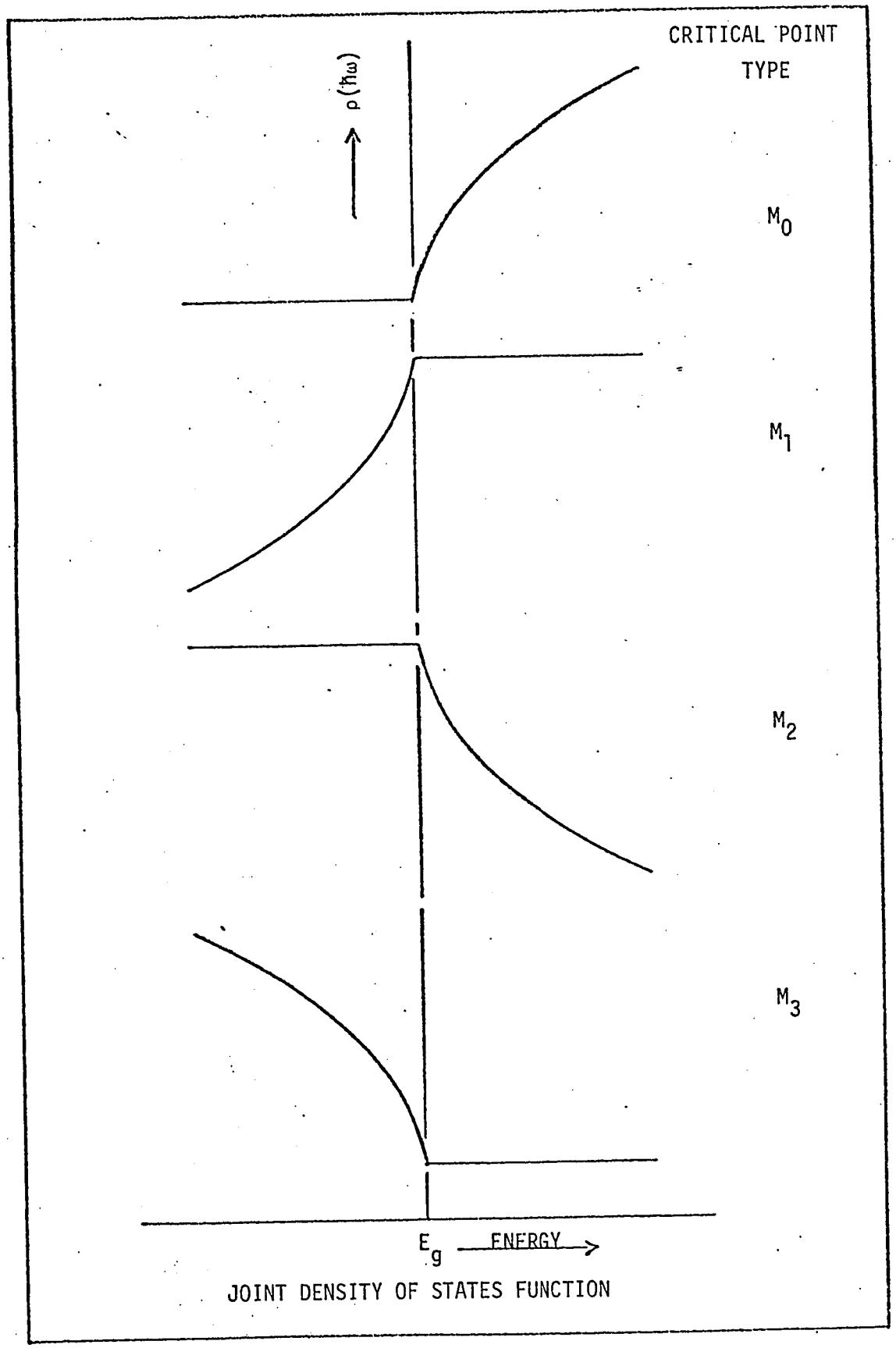

JOINT DENSITY OF STATES FUNCTION

2.4 Experimental Determination of Absorption Spectrum

According to the discussion in the previous section, the optical parameter of great significance is ε_2, the imaginary part of the complex dielectric function. A theoretical computation of ε_2 is possible when the function $E_j(k)$ is known over as many bands as possible for the material.[114-118] However, to determine ε_2 from experiments, optical absorption measurements are the most direct way. The absorption coefficient α is simply related to ε_2,

$$\alpha = \frac{\omega}{nc}\ \varepsilon_2 \ . \tag{2.17}$$

But in the wavelength regions where the absorption coefficient is large, transmission measurements become impractical to measure α. Generally in semiconductors α is quite large beyond the fundamental gap energy.[119] In this region, reflectance measurements are more practical to determine ε_2.

The normal incidence reflectance R is related to both components ε_1 and ε_2 of the complex dielectric function by the Fresnel equation

$$R = \frac{(\varepsilon_1^2 + \varepsilon_2^2)^{\frac{1}{2}} - \left(2\varepsilon_1 + 2(\varepsilon_1^2 + \varepsilon_2^2)^{\frac{1}{2}}\right)^{\frac{1}{2}} + 1}{(\varepsilon_1^2 + \varepsilon_2^2)^{\frac{1}{2}} + \left(2\varepsilon_1 + 2(\varepsilon_1^2 + \varepsilon_2^2)^{\frac{1}{2}}\right)^{\frac{1}{2}} + 1} \ . \tag{2.18}$$

From the above equation it is seen that it is not possible to separate ε_1 and ε_2 from a single reflectance measurement at near normal incidence. But the Kramers - Kronig general dispersion relations[107] which relate the real and imaginary components of a complex function can be applied to the amplitude reflectance $\tilde{r}$,

$$\tilde{r} = |r| \ \exp(-i\phi) \ , \tag{2.19}$$

to determine the phase ϕ,

$$\phi(E_o) = \frac{-E_o}{\pi} P \int_0^\infty \frac{\ell n\, R(E)}{E^2 - E_o^2}\, dE \qquad (2.20)$$

where the reflectance $R = \tilde{r} * \tilde{r} = |r|^2$. Knowing R and ϕ, ε_1 and ε_2 are calculated from the equations

$$\varepsilon_1 = \frac{(1 - R)^2 - 4R \sin^2\phi}{(1 + R - 2\sqrt{R} \cos \phi)^2} \qquad (2.21)$$

and

$$\varepsilon_2 = \frac{4\sqrt{R}\,(1 - R) \sin \phi}{(1 + R - 2\sqrt{R} \cos \phi)^2} \,. \qquad (2.22)$$

In order to apply the dispersion relations to calculate ϕ, R should be known over an infinite energy range, Eq.(2.20). As this is not possible, proper extrapolation procedures should be applied beyond the range of measurement.[120-122]

In practice, when ε_2 is evaluated by the above integral transforms, the fine structure in R is smoothed out in ε_2. While the ε_2 spectrum is necessary for the absorption line shape analysis in order to find out the type of critical point, the reflectance spectrum itself is more useful for the observation of fine structure.

2.5 Relating Reflectance Spectrum to Band Structure

The structural features observed in a reflectance spectrum appear as peaks, dips and shoulders as seen in the spectra of Ge and GaAs shown in Figs. 2.2 and 2.3. These features are to be identified with a set of critical points in the joint density of states function. The information required about the critical points is the energies where they occur, $\nabla_k(\hbar\omega) = 0$, the type M_0, M_1, M_2, and M_3 and their k location of the Brillouin zone.

An unambiguous assignment of the structure is possible only when an accurate theoretical ε_2 spectrum is also available for the material to compare it with the experimental data. The (ε_2, E) spectrum of Ge was calculated by Brust[114,116] using the empirical pseudopotential method. The input data required for the empirical calculation were the critical point band gaps identified by Phillips[113] in the experimental reflectance spectrum of Ge determined by Philipp and Taft.[121] The results of his calculations are shown in Fig. 2.4, along with the experimental (ε_2, E) curve obtained from a Kramers - Kronig transformation of the reflectance data. The first peak, E_1 in the reflectance spectrum at 2.2eV in Fig. 2.2, was originally assigned to the $L_3' - L_1$ transitions by Phillips[113] is seen closer to the $\Lambda_3 - \Lambda_1$ critical point transitions with an ε_2 line shape characteristic of an M_1 type critical point. The transition corresponding to $L_3' - L_1$ is shown to be too weak to be noticed. The prominent peak in the reflectance spectrum E_2 at 4.4eV was assigned to the $X_4 - X_1$ transition. In Fig.2.4, it is seen that this peak is as a result of the accidental degeneracy of the M_1 and M_2 type critical points at $X_4 - X_1$ and $\Sigma_3 - \Sigma_2$ band edges in agreement with

FIGURE 2.2

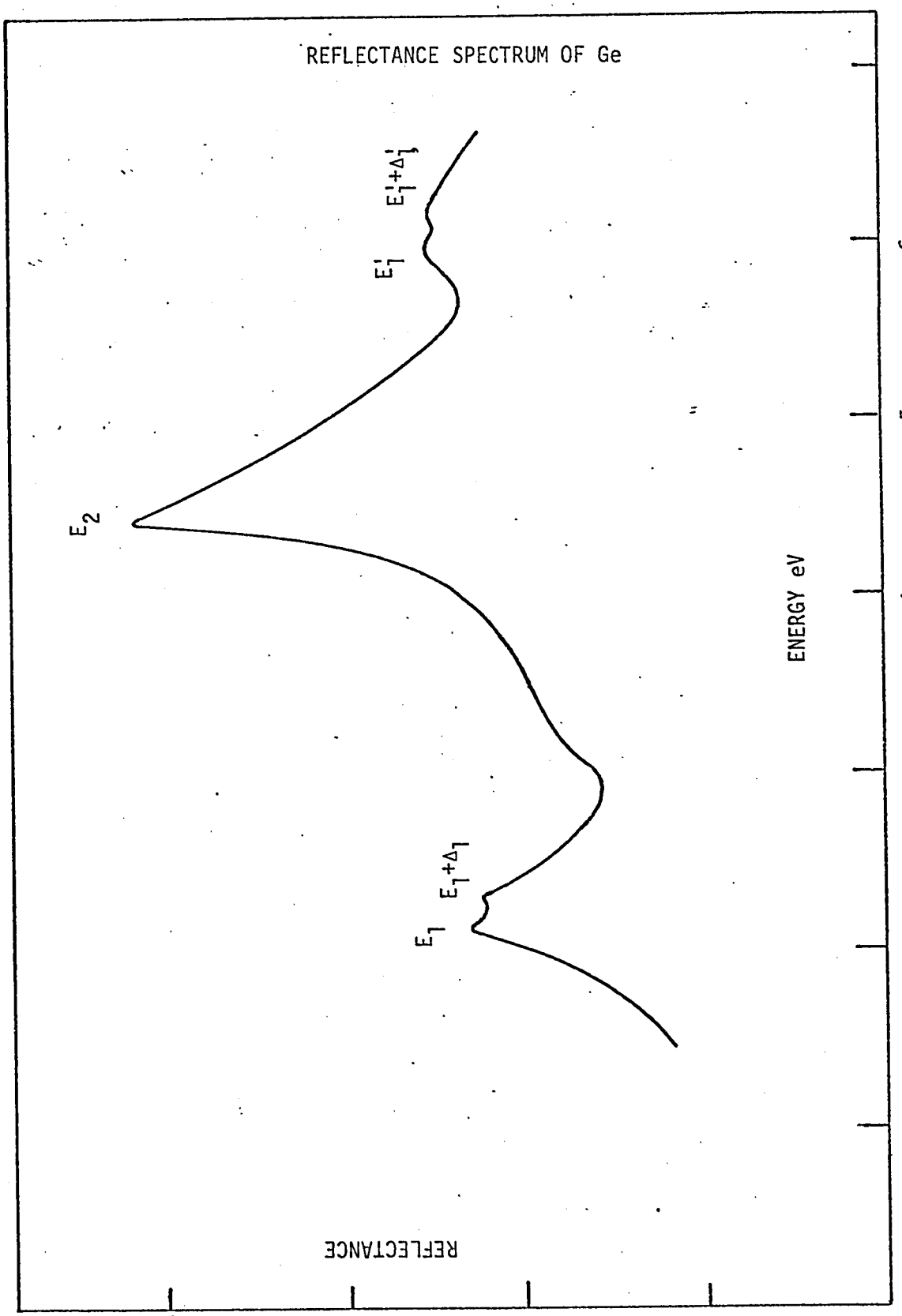
REFLECTANCE SPECTRUM OF Ge
$E_1'+\Delta_1'$
E_1'
E_2
$E_1+\Delta_1$
E_1
ENERGY eV
1
2
3
4
5
6
REFLECTANCE

FIGURE 2.3

REFLECTANCE SPECTRUM OF GaAs

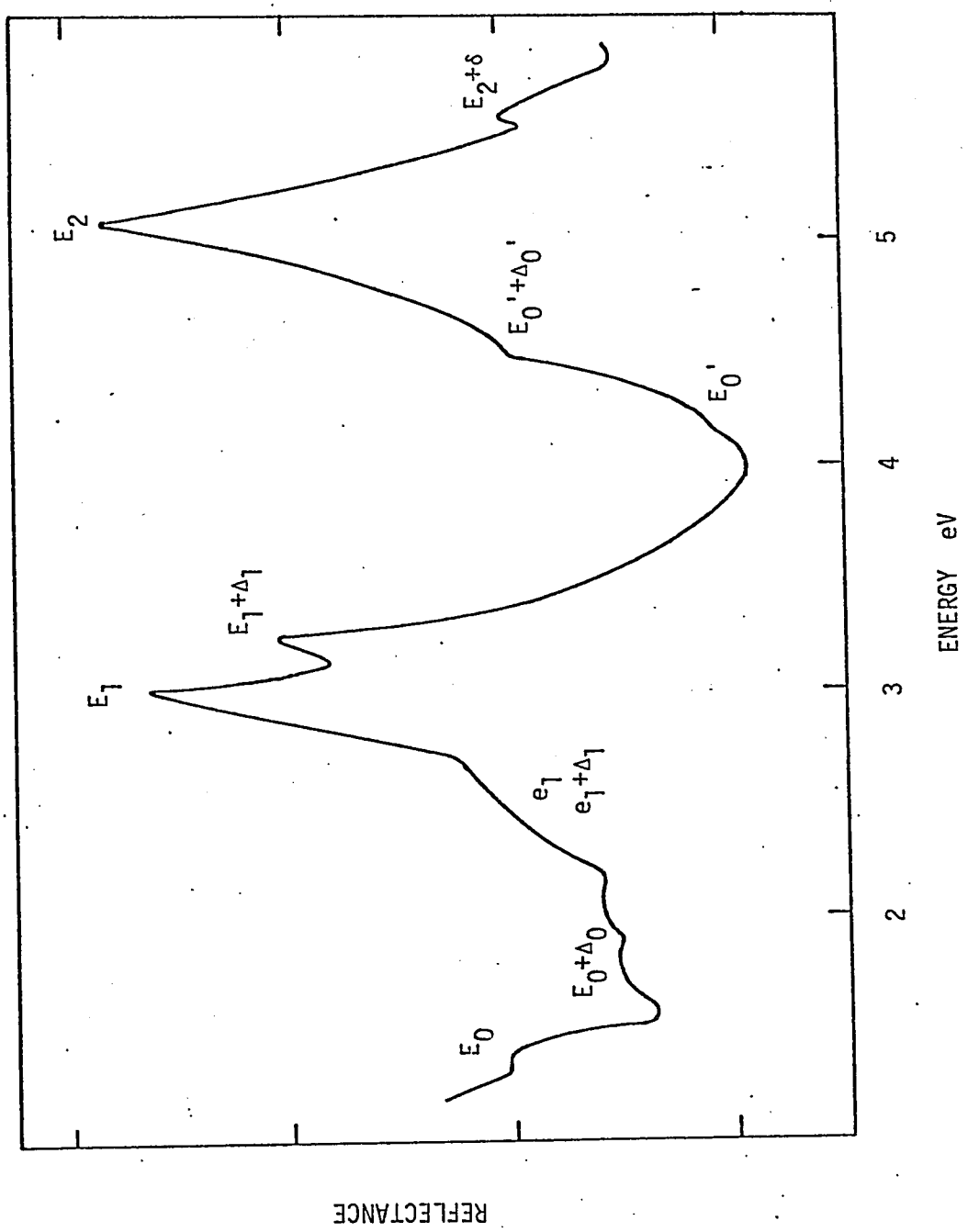

FIGURE 2.4

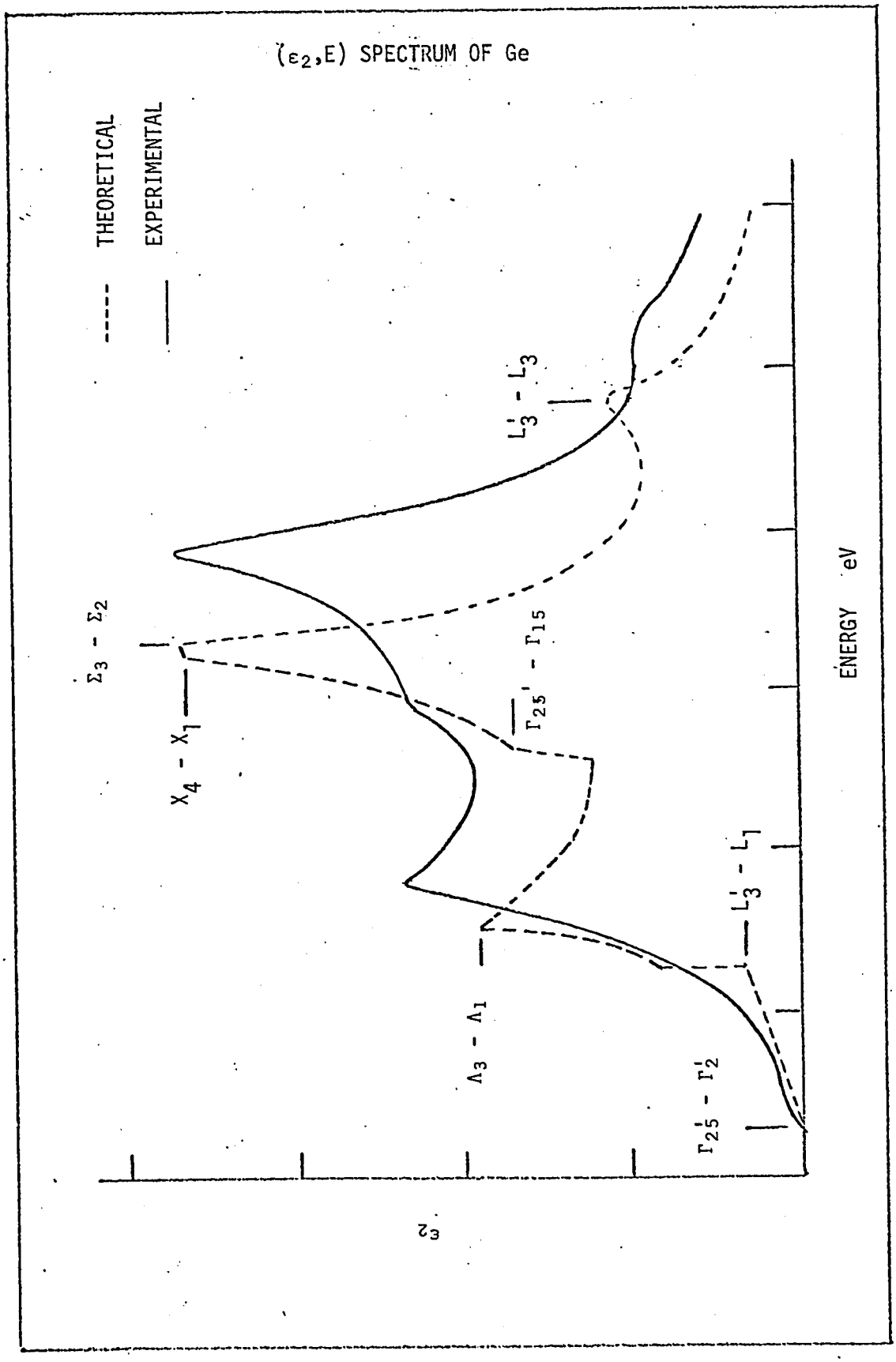
(ε_2, E) SPECTRUM OF Ge
THEORETICAL
EXPERIMENTAL
$L_3' - L_3$
$\Sigma_3 - \Sigma_2$
$X_4 - X_1$
$\Gamma_{25}' - \Gamma_{15}$
$L_3' - L_1$
$\Lambda_3 - \Lambda_1$
$\Gamma_{25}' - \Gamma_2'$
ENERGY eV
ε_2

Phillips' suggestion that a single critical point can only produce an edge like structure in ε_2, where as to form a peak a degeneracy of an M_1 and M_2 type critical points is necessary.[111] The high energy structure E_1' at 6 eV is shown from Brust's calculations to come from the interband transitions $L_3' - L_3$ at the L symmetry point on the BZ boundary. Therefore, it is seen from Fig. 2.4, that there exists a qualitative agreement between theory and experiment. The importance of the critical point concept, its connection with the structure in a reflectance spectrum and the usefulness of the critical point band gaps as empirical parameters in pseudopotential band calculations is well brought out by Brust's work.

However, from recent studies on silicon band structure with a slightly different pseudopotential scheme, Kane[117] showed that a peak in reflectance may be produced by a set of interband transitions whose high density is not due to a specific critical point but due to an extended region of the BZ. In fact, Kane showed from his calculations that only 5 percent of the total contribution to ε_2 at 4.3 eV came from the $X_4 - X_1$ transition to which the peak was originally assigned. A more detailed study of the silicon band structure was made by Herman[37] with his "slightly adjusted first principles" method. His results are in good agreement with Kane's calculations.

The energy band structure of GaAs calculated by Pollak et al[26] using the k.p method is shown in Fig. 2.5. The location of the critical points and the transitions responsible for the structure in the reflectance spectrum of GaAs are indicated in it.

When accurate band structure calculations are not available for

FIGURE 2.5

BAND STRUCTURE OF GaAs

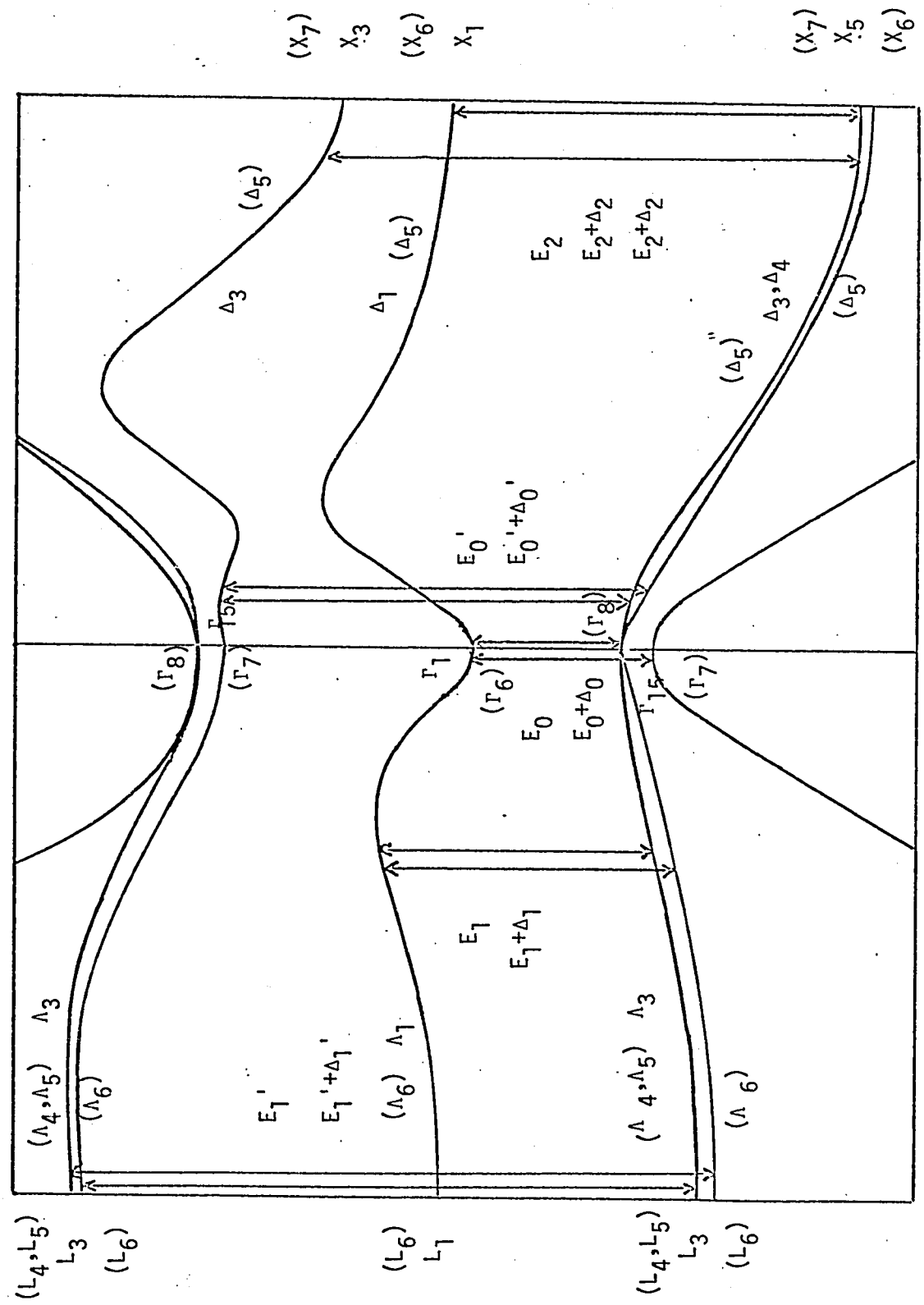

the material under investigation, a great deal of assistance to the assignment of structure to critical points comes from such sources as the well-interpreted results of those materials which are in the same crystal class, division of materials into isoelectronic sequences, spin orbit interaction effects and alloying of two materials and following the shift of the structure in the known material continuously as a function of composition to the unknown material.

In the method of isoelectronic sequences suggested by Herman[46] the crystal potential is divided into homopolar and heteropolar components. The homopolar part for a zincblende material is taken to be the potential of its isoelectronic group lV material. For example, for zincblende GaAs, Ge is its isoelectronic counterpart. The heteropolar or ionic potential is treated as a perturbation on diamond structure band scheme which shifts the energy levels and therefore changes the interband energy gaps. This method predicts the behaviour of energy gaps in an isoelectronic sequence by means of which it can be used effectively to identify interband trnasitions as shown by Cardona and Greenaway.[123]

When spin orbit interaction effects are considered the critical point band edges may be split, which would therefore provide extra structure in the reflectance peaks in the form of multiplets. Observation of this structure is significant to the assignment procedure. When spin orbit interaction is not included the Γ_{25}' valence level of Ge is threefold degenerate. The inclusion of spin orbit interaction removes this degeneracy and splits the energy levels into a four fold and a doubly degenerate levels. The magnitude of this splitting, Δ_0 is

closely related to the corresponding spin orbit splitting Δ_{at} of the free atom and is shown to be $\Delta_o = A.\ \Delta_{at}$, where A is 1.4 for Ge and Si.[124] In III - V compounds where there are two constituent atoms, the spin orbit splitting Δ_o is given in terms Δ_{at}^{III} and Δ_{at}^{V} of the valence III and V atoms

$$\Delta_o = A\ (t^{III}\ \Delta_{at}^{III} + t^{V}\ \Delta_{at}^{V})$$

with values of 0.35 and 0.65 for t^{III} and t^{V} respectively.[124] A similar relationship for Δ_o is shown to exist for II - VI compounds by Cardona,[125]

$$\Delta_o = A\ (t^{II}\ \Delta_{at}^{II} + t^{VI}\ \Delta_{at}^{VI})$$

with values of 0.2 and 0.8 for t^{II} and t^{VI} respectively. Δ_{at}^{II} and Δ_{at}^{VI} are the respective atomic spin orbit splittings. Therefore, a knowledge of the atomic splittings derived either from spectroscopic data or from theoretical calculations will lead to the determination of Δ_o, identification of which in an optical spectrum is a strong characteristic of the energy levels involved in the transition.

Another assignment feature of great value has been the two thirds rule which states that the spin orbit splitting of the two fold degenerate L_3' valence state should be equal to two thirds the splitting of the three fold degenerate Γ_{25}' state.[111] This argument was responsible for checking the correctness of the assignment of the 2.2 eV peak of Ge to the $L_3' - L_1$ transitions by Phillips because this peak was shown to split into two components at 2.1 / 2.3 eV in Tauc's[126] measurements. However, spin orbit interaction does not remove the degeneracy of the X_4 valence level of diamond structure but the X_5 valence level of

zincblende symmetry is split into two components. This spin orbit splitting Δ_2 was related to the spin orbit split values of the Γ_{15_V} and Γ_{15_C} levels by Cardona.[127]

The classic experiments in the alloy studies are the Ge-Si and GaAs-GaP mixed crystal systems. The reflectance spectra of the $Ge_{1-x}Si_x$ alloy samples were determined by Tauc and Abraham.[65,66] In the plot of the energy of the first peak observed in the reflectance spectra as a function of composition a discontinuous slope change was observed at about 79 percent silicon content. They interpreted that the nature of the transitions corresponding to the first peak in silicon is different from the one in Ge. From the $GaAs_{1-x}P_x$ alloy studies[100-102,104] the peak at 3.7 eV in the reflectance spectrum of GaP was correctly assigned to the $\Lambda_3 - \Lambda_1$ transition instead of the $\Gamma_{15V} - \Gamma_{15C}$ transition as in the case of Si. The recent k.p calculations of Pollak et al[26] are also in favour of this assignment and further show that the E_0' and E_2 transitions are almost degenerate, at 4.8 eV in GaP.

However, the assignment of structure found in their reflectance spectra is not straight forward for little known materials. From a knowledge of its crystal structure, applying group theory energy levels and their symmetry properties can be determined at high symmetry points in its BZ. But this does not provide the details about the ordering of the energy levels at the symmetry points. The fundamental gap is determined from optical absorption measurements. The band structure in the vicinity of the valence band maximum and the conduction band minimum is determined by measuring electrical conductivity, Hall effect, cyclotron resonance absorption, magnetoresistance and piezoresistance

measurements. With this limited knowledge a coarse theoretical band structure is determined. With constant interaction between theory and experiment, any discrepancies present in the earlier assignment are removed and refinements are made.

It is seen from the above discussion that neither the reflectance measurements nor the absorption spectrum obtained from them alone can provide a full account of the critical points. The reason as shown by Kane[117] is that the ε_2 spectrum obtained from the reflectance data is a sum of two components. One arising from the transitions between the initial and final states which meet the general requirement that they be separated by energy $\hbar\omega$. These states are likely to be distributed over the entire BZ. Therefore the absorption spectrum arising from this contribution should be lacking the sharp structure expected from a localized critical point with its characteristic line shape, Fig. 2.1. Often this latter component may disappear in the large characterless background of the former.

At this stage, the recent modulation techniques employed in reflectance are found to be extremely useful because they apparently separate the critical point contribution to the absorption coefficient from the noncritical background.[128,129] This topic will be discussed in the next section.

2.6 Modulated Reflectance

In modulated reflectance methods, the modulation is produced through the changes induced in the real and imaginary components of the complex dielectric function by the modulating parameters. A phenomenological description of modulated reflectance is given by Seraphin and Botka[129-131] by taking the total differential of the Fresnel equation, Eq.(2.18),

$$\frac{\Delta R}{R} = \alpha(\varepsilon_1, \varepsilon_2)\,\Delta\varepsilon_1 + \beta(\varepsilon_1, \varepsilon_2)\,\Delta\varepsilon_2 \tag{2.23}$$

where

$$\alpha = C_1 \left((\varepsilon_1 - 1) A_+ + \varepsilon_2 A_- \right) \tag{2.24}$$

and

$$\beta = C_2 \left(\frac{(\varepsilon_1 - 1)}{A_+} - \frac{\varepsilon_2}{A_-} \right) \tag{2.25}$$

with

$$A_+ = \frac{\left(2(\varepsilon_1^2 + \varepsilon_2^2)^{\frac{1}{2}} + 2\varepsilon_1 \right)^{\frac{1}{2}}}{(\varepsilon_1^2 + \varepsilon_2^2)^{\frac{1}{2}}} ,$$

$$A_- = - \frac{\left(2(\varepsilon_1^2 + \varepsilon_2^2)^{\frac{1}{2}} - 2\varepsilon_1 \right)^{\frac{1}{2}}}{(\varepsilon_1^2 + \varepsilon_2^2)^{\frac{1}{2}}} ,$$

$$C_1 = \frac{1}{(\varepsilon_1 - 1)^2 + \varepsilon_2^2} ,$$

and

$$C_2 = \frac{2\varepsilon_2}{\left((\varepsilon_1 - 1)^2 + \varepsilon_2^2\right)(\varepsilon_1^2 + \varepsilon_2^2)} .$$

In a modulated reflectance spectrum, which is a graph of $\frac{\Delta R}{R}$ versus $\hbar\omega$, the components $\Delta\varepsilon_1$ and $\Delta\varepsilon_2$ are the changes produced in ε_1 and ε_2 by a modulation parameter. The characteristic nature of modulation parameters appears through these components.

The coefficients α and β determine the fractions of $\Delta\varepsilon_1$ and $\Delta\varepsilon_2$ contributing to $\Delta R/R$ at a photon energy $\hbar\omega$. The fractional coefficients α and β are functions of ε_1 and ε_2 and therefore exhibit spectral dependence. These coefficients have been determined for Ge, Si and GaAs[131] from values of ε_1 and ε_2 available from Kramers - Kronig analysis of the experimental reflectance data.[132,133] In Fig. 2.6, α and β calculated by Seraphin and Botka[131] for GaAs are shown. The curves obtained for Ge and Si are similar to the one shown for GaAs and similar nature is expected for the other III - V compound materials.[131]

It is seen from Fig. 2.6 that in the low energy region, the fractional coefficient α is much larger than β. In this region containing the fundamental absorption edge E_0, the contribution of $\Delta\varepsilon_1$ to $\Delta R/R$ is considerable. As the photon energy is increased, α decreases and β increases. In the vicinity of 2.5 eV, where structure is observed due to E_1 transitions α and β can be assumed to contribute equally to $\Delta R/R$. Beyond this energy range β is larger than α and goes through a maximum at about 4 eV where the energies of the E_0' transitions occur. The contribution of $\Delta\varepsilon_2$ to $\Delta R/R$ is more important. Further increase in energy changes the sign of both coefficients and α increases quite rapidly. In this energy region, the whole complex of E_2 transitions occur. The Fresnel equation and the coefficients α and β determined from it are valid when normal incidence reflectance measurements are made at air-sample interface. In experimental arrangements where the sample is surrounded by a medium other than air, the dielectric constant of the medium should be included in the Fresnel equation.[127]

FIGURE 2.6

FRACTIONAL COEFFICIENTS α AND β AS A FUNCTION OF ENERGY

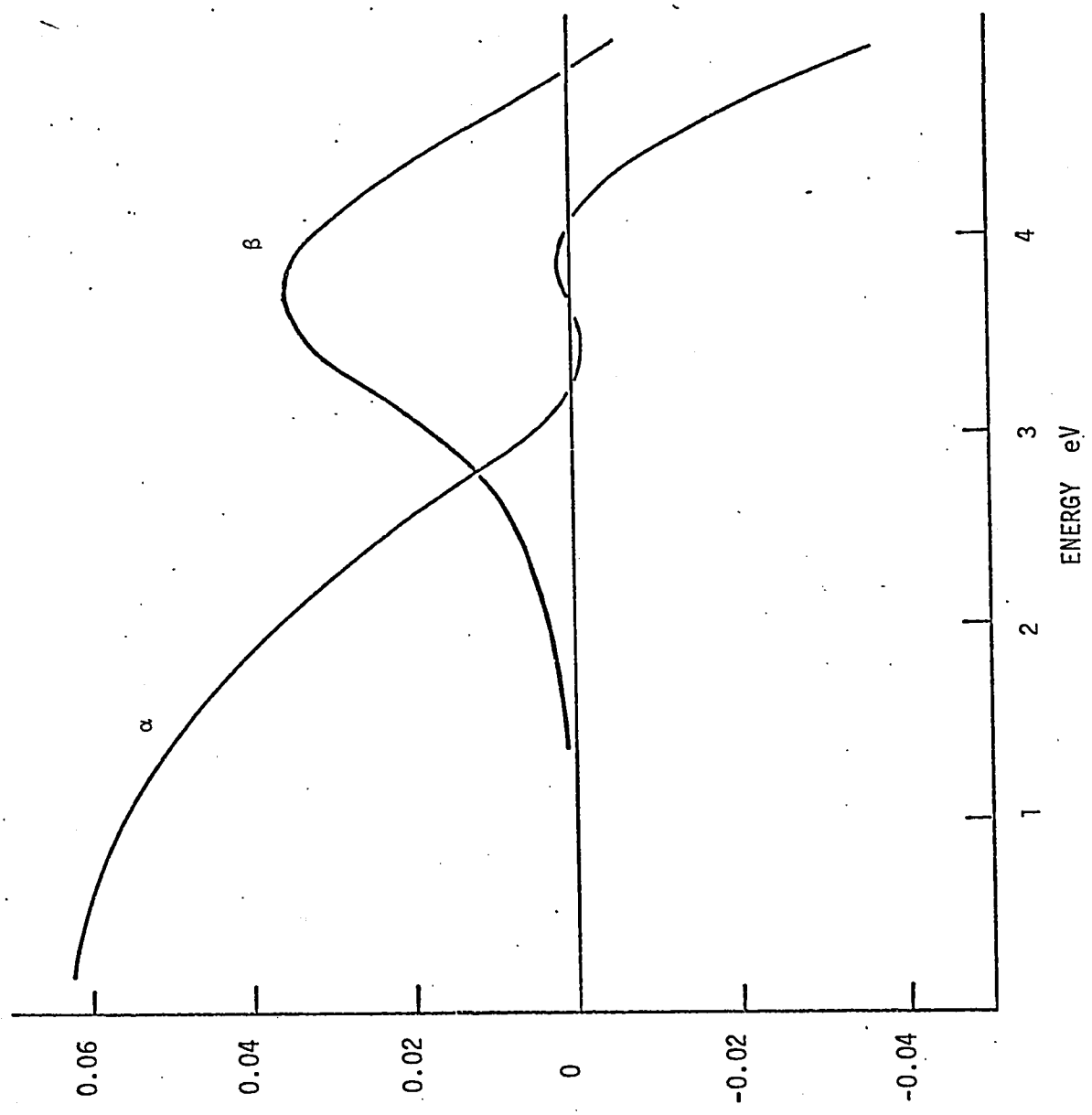

The imaginary component of the dielectric function at an M_o type critical point can be written as

$$\varepsilon_2(\hbar\omega) = \frac{C}{(\hbar\omega)^2} (\hbar\omega - Eg)^{\frac{1}{2}} \qquad (2.26)$$

where C is a constant, from Eq.(2.14) and Table 2.1. A change in ε_2 can be produced thereby modulating it when either the photon energy ($\hbar\omega$) or the energy gap E_g characteristic of the material is varied periodically. The first technique leads to the principle of the wavelength modulation and in the second case modulation is obtained through the variation of the energy gap. Physical parameters like hydrostatic pressure and uniaxial stress[134-136] produce the required energy gap change directly. Temperature[137] and electric field[138,139] are also being used as modulation parameters but the mechanism of modulation is not a strict energy gap shift.[128]

In the energy gap modulation method, the change in ε_2 produced by the modulation parameter is obtained from Eq.(2.26)

$$\Delta\varepsilon_2 = \frac{C}{(\hbar\omega)^2} \frac{d}{dE_g} (\hbar\omega - E_g)^{\frac{1}{2}} \Delta E_g$$

$$= \frac{C}{(\hbar\omega)^2} \frac{1}{2(\hbar\omega - E_g)^{\frac{1}{2}}} \Delta E_g$$

which is singular at the critical points, $\hbar\omega = E_g$. The magnitude of $\Delta\varepsilon_2$ is large at the critical point and decreases as the spectral distance from the critical point increases. This sensitive behaviour of $\Delta\varepsilon_2$ at the critical point is responsible for the importance of modulation experiments. The structure in a modulated reflectance spectrum is therefore limited to the energy positions of the critical points. Any constant contributions to ε_2 which appear in reflectance spectra are

eliminated in modulated reflectance spectra because their derivative with respect to E_g gives zero contribution to $\Delta\varepsilon_2$.

For all four types of critical points, $\Delta\varepsilon_2$ is given by

$$\Delta\varepsilon_2 = \frac{C^1}{(\hbar\omega)^2} \frac{d}{dE_g} \{ \rho(\hbar\omega) \} \Delta E_g \qquad (2.27)$$

which is singular at critical point band gap energies because the density of states function $\rho(\hbar\omega)$ varies as the square root of the spectral distance from the critical point.

The components $\Delta\varepsilon_1$ and $\Delta\varepsilon_2$ are coupled to each other by Kramers - Kronig dispersion relations and from a knowledge of one the other can be determined. Knowing $\Delta\varepsilon_2$ from Eq.(2.27)

$$\Delta\varepsilon_1 = \frac{2}{\pi} P \int_0^\infty \frac{\omega\Delta\varepsilon_2}{\omega_0^2 - \omega^2} d\omega \,. \qquad (2.28)$$

2.7 Thermoreflectance

In a thermoreflectance experiment, a periodic change of temperature of a sample produces a corresponding modulation in its reflectance. The effect of an increase of temperature is to shift the interband energy gaps and to broaden the critical point transitions. The energy gap shift is produced by the thermal expansion of the lattice and by the electron phonon interaction. The critical point broadening is due to the electron phonon interaction. Therefore, the two modulation mechanisms, namely, the energy gap shift modulation and the broadening parameter modulation are expected to contribute to thermoreflectance. The individual contributions are determined from the dielectric function in the vicinity of a critical point which is given by[140]

$$\tilde{\varepsilon} \propto b\ (\hbar\omega - E_g)^{\frac{1}{2}} \tag{2.29}$$

where $b = i^{r+1}$ for an M_r type critical point. The effects of Lorentzian broadening are introduced in $\tilde{\varepsilon}$ phenomenologically by replacing the frequency ω by $\omega + i\Gamma$, where Γ represents the broadening parameter,

$$\tilde{\varepsilon} \propto b\ (\hbar(\omega + i\Gamma) - E_g)^{\frac{1}{2}} \quad . \tag{2.30}$$

Separating the real and imaginary components and rewriting Eq.(2.30) in the form

$$\tilde{\varepsilon} \propto b(\hbar\Gamma)^{\frac{1}{2}}\ (\ \phi(x) + i\ \phi(-x)\ ), \tag{2.31}$$

where

$$\phi(\pm x) = (\ \pm x + (x^2 + 1)^{\frac{1}{2}}\ )^{\frac{1}{2}} \quad ,$$

with the reduced variable $x = (\hbar\omega - E_g)\ /\hbar\Gamma$.

Next the components $\Delta\varepsilon_1$ and $\Delta\varepsilon_2$ are determined from Eq.(2.31) for the gap shift (E_g) and broadening parameter ($\hbar\Gamma$) modulation

mechanisms

$$\Delta\tilde{\varepsilon}\ (E_g\ \text{Mod.}) \propto -\frac{b}{2}(\hbar\Gamma)^{-\frac{1}{2}}\ \{F(x) - i\ F(-x)\}\ \Delta E_g\ , \qquad (2.32)$$

and

$$\Delta\tilde{\varepsilon}\ (\hbar\Gamma\ \text{Mod.}) \propto \frac{b}{2}(\hbar\Gamma)^{-\frac{1}{2}}\ \{F(-x) + i\ F(x)\}\ \Delta(\hbar\Gamma)\ , \qquad (2.33)$$

where

$$F(x) = 2\frac{d\,\phi(x)}{dx} = \{(x^2+1)^{\frac{1}{2}} + x\}^{\frac{1}{2}}\ (x^2+1)^{-\frac{1}{2}} \qquad (2.34)$$

Explicitly, at an M_o critical point, from Eq.(2.32)

$$\Delta\tilde{\varepsilon}\ (E_g\ \text{Mod.}) = \Delta\varepsilon_1 + i\ \Delta\varepsilon_2 \propto -\frac{1}{2}(\hbar\Gamma)^{-\frac{1}{2}}\ \{F(x) - i\ F(-x)\}\ \Delta E_g \qquad (2.35)$$

and from Eq.(2.33)

$$\Delta\tilde{\varepsilon}\ (\hbar\Gamma\ \text{Mod.}) = \Delta\varepsilon_1 + i\ \Delta\varepsilon_2 \propto \frac{1}{2}(\hbar\Gamma)^{-\frac{1}{2}}\ \{F(-x) + i\ F(x)\}\ \Delta(\hbar\Gamma) \qquad (2.36)$$

The real and imaginary components, $\Delta\varepsilon_1$ and $\Delta\varepsilon_2$ are separated from Eqs.(2.35) and (2.36) giving for the gap shift modulation,

$$\Delta\varepsilon_1\ (E_g\ \text{Mod.}) \propto \frac{-(\hbar\Gamma)^{-\frac{1}{2}}}{2}\ F(-x)\ \left(\frac{dE_g}{dT}\right)\ \Delta T \qquad (2.37)$$

and

$$\Delta\varepsilon_2\ (E_g\ \text{Mod.}) \propto \frac{-(\hbar\Gamma)^{-\frac{1}{2}}}{2}\ F(x)\ \left(\frac{dE_g}{dT}\right)\ \Delta T \qquad (2.38)$$

with $\Delta E_g = \left(\frac{dE_g}{dT}\right)\ \Delta T$

For the broadening parameter modulation

$$\Delta\varepsilon_1\ (\hbar\Gamma\ \text{Mod.}) \propto \frac{-(\hbar\Gamma)^{-\frac{1}{2}}}{2}\ F(x)\ \frac{d(\hbar\Gamma)}{dT}\ \Delta T \qquad (2.39)$$

and

$$\Delta\varepsilon_2\ (\hbar\Gamma\ \text{Mod.}) \propto \frac{(\hbar\Gamma)^{-\frac{1}{2}}}{2}\ F(-x)\ \frac{d(\hbar\Gamma)}{dT}\ \Delta T \qquad (2.40)$$

with $\Delta(\hbar\Gamma) = \frac{d(\hbar\Gamma)}{dT}\ \Delta T$.

Similar calculations can be made at M_1, M_2 and M_3 critical points to evaluate the changes produced in ε_1 and ε_2 by modulating with temperature. The results are given in Table 2.2. The line shapes of $\Delta\varepsilon_1$ and $\Delta\varepsilon_2$ are determined by the function F(x), Eq.(2.34), which is shown in Fig. 2.7.

It is known experimentally that the temperature coefficient of the energy gaps, $\frac{dE_g}{dT}$, is of the order of -4×10^{-4}eV/^{o}C which is several times larger than the temperature coefficient of the broadening parameter $\frac{d(\hbar\Gamma)}{dT}$ which is approximately 10^{-4}ev/^{o}C. Therefore it is expected that the gap shift modulation would contribute more to the thermoreflectance spectra and further should resemble other modulation spectra where modulation is obtained through gap shift.

Knowing the magnitudes of $\Delta\varepsilon_1$ and $\Delta\varepsilon_2$ at a critical point, the $\frac{\Delta R}{R}$ spectrum around the critical point can be synthesized from Eq.(2.23) if the fractional coefficients α and β are known. At an M_0 critical point, from Eqs.(2.37) and (2.38)

$$\frac{\Delta R}{R} \propto \frac{(\hbar\Gamma)^{-\frac{1}{2}}}{2} \left(-\alpha F(-x) - \beta F(x) \right) \frac{dE_g}{dT} \Delta T \quad . \tag{2.41}$$

Similarly, $\frac{\Delta R}{R}$ can be obtained at the other critical points (Batz)[141]

$$\frac{\Delta R}{R} \propto \frac{(\hbar\Gamma)^{-\frac{1}{2}}}{2} \left(\alpha F(x) - \beta F(-x) \right) \frac{dE_g}{dT} \Delta T \tag{2.42}$$

at an M_1 critical point,

$$\frac{\Delta R}{R} \propto \frac{(\hbar\Gamma)^{-\frac{1}{2}}}{2} \left(\alpha F(-x) + \beta F(x) \right) \frac{dE_g}{dT} \Delta T \tag{2.43}$$

at an M_2 critical point,

$$\frac{\Delta R}{R} \propto \frac{(\hbar\Gamma)^{-\frac{1}{2}}}{2} \left(-\alpha F(x) + \beta F(-x) \right) \frac{dE_g}{dT} \Delta T \tag{2.44}$$

at an M_3 critical point.

TABLE 2.2

The changes produced in ε_1 and ε_2 due to gap shift and broadening parameters by modulating with temperature.

Critical Point	Gap Shift Modulation		Broadening Parameter Modulation	
	$\frac{d\varepsilon_1}{dE_g}$	$\frac{d\varepsilon_2}{dE_g}$	$\frac{d\varepsilon_1}{dh\Gamma}$	$\frac{d\varepsilon_2}{dh\Gamma}$
M_0	$-F(-x)$	$-F(x)$	$-F(x)$	$F(-x)$
M_1	$+F(x)$	$-F(-x)$	$-F(-x)$	$-F(x)$
M_2	$+F(-x)$	$+F(x)$	$F(x)$	$-F(-x)$
M_3	$+F(x)$	$+F(-x)$	$F(-x)$	$F(x)$

FIGURE 2.7

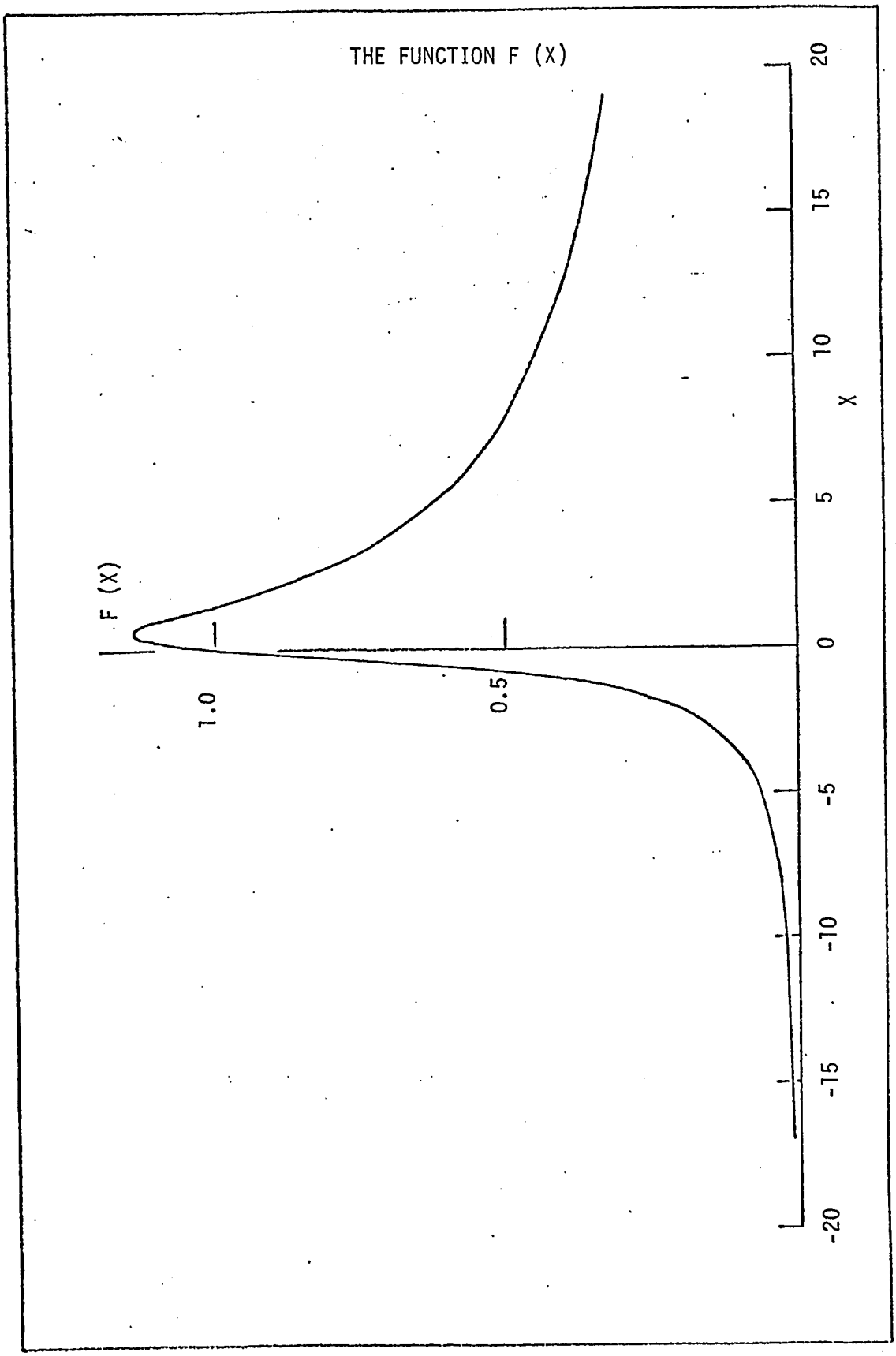

Batz[137] introduced temperature as a modulation parameter and investigated the thermoreflectance spectrum of Ge which is shown in Fig. 2.8. A comparison of this spectrum with the reflectance spectrum of Ge, Fig. 2.2, shows the sharpness of structure in the modulated reflectance spectrum with characteristic line shapes. The E_1 and $E_1 + \Delta_1$ doublet is well resolved at 2.1 / 2.3 eV. The large peak at 4.4 eV corresponds to the E_2 transition. Knowing that the E_1 and $E_1 + \Delta_1$ transitions occur at M_1 interband edges, Batz synthesized the spectrum in this energy region which is shown in Fig. 2.9. The agreement between the experimental and theoretical line shapes is in favour of the gap shift modulation mechanism for thermoreflectance. However, an unambiguous line shape assignment and hence the identification of the critical point involved at the 4.4 eV transition has not become possible so far. Cardona favours an M_2 critical point assignment which is mixed with exciton interaction to this structure at 4.4 eV assuming that the gap shift modulation is more dominant in thermoreflectance.[140]

FIGURE 2.8

THERMOREFLECTANCE SPECTRUM OF Ge

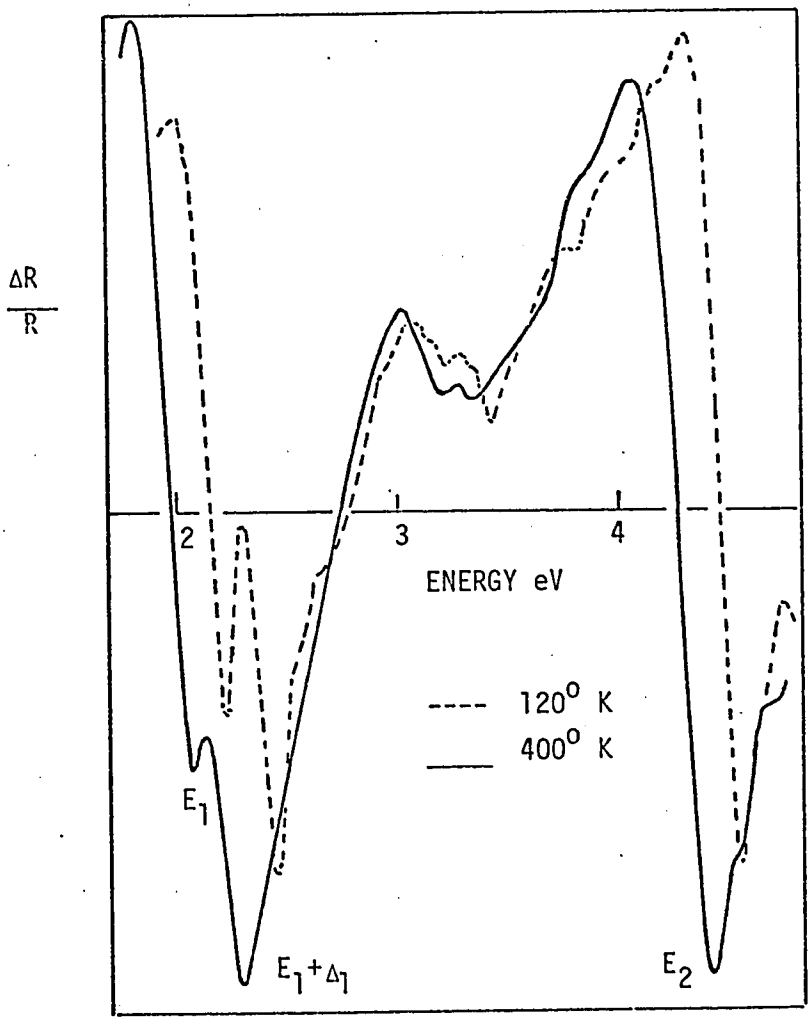

FIGURE 2.9

SYNTHESIZED THERMOREFLECTANCE SPECTRUM OF Ge

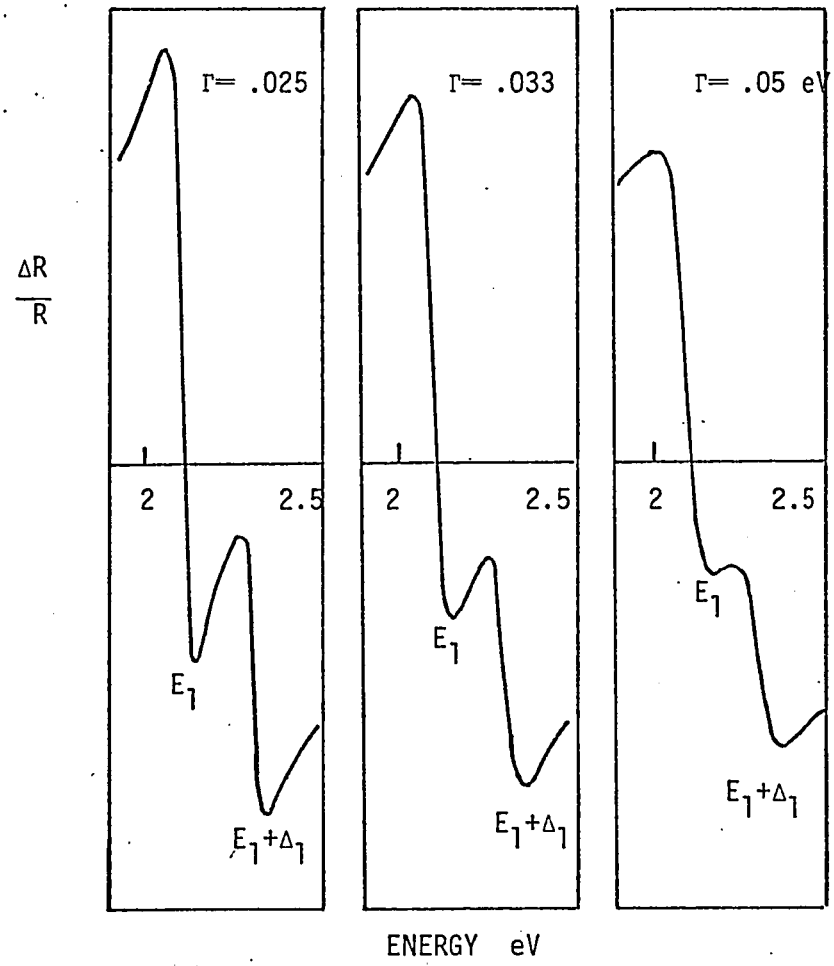

2.8 Electroreflectance

In electroreflectance, the reflectance is modulated by a periodic electric field at the reflecting surface. Modulation enters into reflectance through the field induced changes in the real and imaginary components of the complex dielectric function of the material.

The early investigations of the effect of an electric field on the absorption coefficient at a parabolic band gap were made by Franz[142] and Keldysh.[143] According to their results, electrons and holes tunnel into the band gap from the conduction and valence band edges respectively thereby narrowing the gap and producing an exponential tail in the absorption coefficient below the band gap energy. Henceforth the effect of an electric field on interband optical transitions has come to be known as Franz-Keldysh effect. Experimentally, this effect was observed by Moss.[144]

Using two different but equivalent techniques, Callaway[145] and Tharmalingam[146] calculated the effect of an electric field on a parabolic band gap both below and above the gap energy. From Tharmalingam's results the absorption coefficient $\alpha(\omega,F)$ in the presence of an electric field

$$\alpha(\omega,F) = \frac{C\theta_F^{\frac{1}{2}}}{\omega}\left[\left|\frac{d}{d\beta}\,Ai(\beta)\right|^2 - \beta\,|Ai(\beta)|^2\right], \qquad (2.45)$$

where $\theta_F^3 = \frac{e^2F^2}{2\mu h}$, $\beta = \frac{\omega_1-\omega}{\theta_f}$ and $Ai(\beta)$ is the Airy function defined by

$$Ai(\beta) = \frac{1}{\sqrt{\pi}}\int_0^\infty \cos\left(\frac{1}{3}u^2 + u\beta\right)\,du\ . \qquad (2.46)$$

e is the electron charge. h is the planck's constant. $\hbar\omega_1$ is the band gap energy. μ is the reduced mass of the electron hole pair. C is a

constant containing the matrix elements between the periodic parts of the Bloch functions at the band edges and fundamental constants.

The field induced change in the absorption coefficient $\Delta\alpha(\omega,F)$ above and below ω_1 can be obtained by subtracting the absorption due to direct allowed transitions, $\alpha(\omega,0)$ (Bardeen et al)[147]

$$\alpha(\omega,0) = 0.3187 \frac{C}{\omega} (\omega - \omega_1)^{\frac{1}{2}} , \omega > \omega_1 \qquad (2.47)$$

$$= 0 \qquad \omega < \omega_1$$

from $\alpha(\omega,F)$. Seraphin and Botka[130] calculated $\Delta\alpha(\omega,F)$ for Ge and GaAs for a number of electric field intensities. The results obtained are similar for both materials. An exponential tail is observed for energies below the band gap, $\omega < \omega_1$, followed by damped oscillations for energies above the gap, $\omega > \omega_1$. These oscillations reflect the nature of the Airy function. The amplitude and the period of oscillations increase with an increase in field strength.

While the above theory is sufficient to explain the effect of an electric field on optical transmission through a sample, to explain the field effects on reflectance $\Delta\varepsilon_1$ should also be known. This can be obtained at a parabolic edge by a Kramers - Kronig transformation of $\Delta\varepsilon_2$, Eq.(2.28). Electroreflectance of Ge at the fundamental gap was explained by Seraphin in the above manner.[139] Observation of Franz-Keldysh effect in reflectance encouraged the investigation of electroreflectance at higher band gaps where structure is observed in reflectance spectra. The nature of these band gaps are both parabolic and saddle point type. The effect of an electric field on a saddle point transition is necessary to be known before an explanation of the reflectance change at higher energy band gaps could be interpreted

successfully.

First predictions on the nature of the change in ε_2 at a saddle point edge were given by Phillips[148] in a duality theorem which states that the change in ε_2 at a saddle point edge is obtained from the corresponding change at the parabolic edge by reversing the signs of $(\omega - \omega_1)$ and $\Delta\varepsilon_2$ in it. This transforms $\Delta\varepsilon_2$ at a parabolic edge with oscillations following the energy gap to $\Delta\varepsilon_2$ at a saddle point edge with oscillations preceeding the band gap energy. The difference in line shapes of $\Delta\varepsilon_2$ at a parabolic and saddle point edges is significant in the identification of critical points. Seraphin computed the components $\Delta\varepsilon_1$ and $\Delta\varepsilon_2$ at a saddle point using Phillips duality theorem in his analysis of electroreflectance studies on Ge, Si and GaAs.[131]

A generalized theory of the Franz-Keldysh effect at the four kinds of critical points was developed by Aspnes[149,150] and Aspnes, Handler and Blossey.[151] Aspnes et al[151] derived a general expression for the imaginary component of the one electron interband dielectric function of a solid in the presence of an electric field on the lines originally developed by Callaway.[145,128] The wavefunctions of a band in the presence of an electric field are expressed in terms of a linear combination of Bloch functions of that band. To preserve the translational symmetry of the solid perpendicular to the field direction, only those wavefunctions whose $k_\perp$ is the same are mixed by the electric field. The optical matrix element is solved with these wavefunctions in the expression for ε_2. In the weak field approximation, for a pair of bands the imaginary component of the dielectric function, ε_2 in the presence

of an electric field is shown to be[151]

$$\varepsilon_2(\omega,F) = \frac{4\pi^2e^2}{m^2\omega^2}\int \frac{2}{(2\pi)^3}\, d^3k\, |\vec{n}_o\cdot P_{if}|^2 \left\{\frac{1}{\hbar\Omega}\, Ai\left(\frac{E_F - E_i - \hbar\omega}{\hbar\Omega}\right)\right\} \tag{2.48}$$

where

$$\hbar\Omega = \left(\frac{e^2F^2\hbar^2}{8\mu_{11}}\right)^{\frac{1}{3}} ,$$

and

$$\frac{1}{\mu_{11}} = \frac{1}{\hbar^2}\frac{\partial^2}{\partial k_{11}^2}(E_F - E_i) .$$

The zero field expression for ε_2 is given by

$$\varepsilon_2(\omega,0) = \frac{4\pi^2e^2}{m^2\omega^2}\int \frac{2}{(2\pi)^3}\, d^3k\, |\vec{n}_o\cdot P_{if}| \times \delta(E_F - E_i - \hbar\omega) \tag{2.49}$$

Aspnes et al[151] showed that in the weak field approximation the finite electric field dielectric function $\varepsilon_2(\omega,F)$ can be obtained by convoluting the zero field dielectric function $\varepsilon_2(\omega,0)$ with an Airy function. From Eqs.(2.48) and (2.49) it is seen that the effect of electric field is therefore simply to replace the δ function by the Airy function with the appropriate prefactor. For finite values of field, at any point k, the electric field mixes contributions from other points in the neighbourhood of k and this mixing should vanish as the field is removed.

Seraphin[129] explains that this mixing in the presence of an electric field extending over a slope discontinuity in the density of states function is responsible for the large changes observed in $\tilde{\varepsilon}$ at the critical points while the effects are small in the smoother regions.

The nature of the Airy function depends upon the sign of its argument. It decays exponentially for positive arguments and extends in

a progressively damped oscillatory pattern for negative arguments. In the expression for $\varepsilon_2(\omega,F)$ the sign of the argument of the Airy function depends upon the sign of the reduced mass μ_{11} along the electric field direction, which leads to significant information on the saddle points, whether the electric field is along the positive or negative reduced mass axis.

Aspnes[150] derived expressions for $\Delta\varepsilon_2(\omega,F)$ at the four types of critical points in terms of two electro-optic functions $F(\eta)$ and $G(\eta)$,

$$F(\eta) = \frac{1}{\pi}\left[\mathrm{Ai}'^2(\eta) - \eta\,\mathrm{Ai}^2(\eta)\right] - (-\eta)^{\frac{1}{2}}\,U(\eta) \qquad (2.50)$$

and

$$G(\eta) = \frac{1}{\pi}\left[\mathrm{Ai}'(\eta)\,\mathrm{Bi}'(\eta) - \eta\,\mathrm{Ai}(\eta)\,\mathrm{Bi}(\eta)\right] + (\eta)^{\frac{1}{2}}\,U(\eta)\,,$$

where $\mathrm{Ai}(\eta)$, $\mathrm{Bi}(\eta)$ and $\mathrm{Ai}'(\eta)$, $\mathrm{Bi}'(\eta)$ are the Airy functions and their derivatives respectively. $U(\eta)$ is the unit step function. The argument η is the dimensionless variable $(E_F - E_i - \hbar\omega/\hbar\Omega)$. Through Kramers - Kronig transformation, $\Delta\varepsilon_1$ is determined from $\Delta\varepsilon_2$. Six distinct line shapes which are combinations of the two electro-optic functions and unique were obtained for both $\Delta\varepsilon_1$ and $\Delta\varepsilon_2$ at the four types of critical points, shown in Fig. 2.10. Recognition of these line shapes in $\frac{\Delta R}{R}$ spectra would lead to an identification of the critical point.

However, in practice the symmetry nature of the critical point[152] and life time broadening of the states[131,150] modify the line shapes quite drastically. Line shape analysis is further complicated by non-uniform field intensity over the penetration depth of the electromagnetic wave into the sample[129] and exciton effects.[153,154] But the energies of

FIGURE 2.10

THEORETICAL LINE SHAPES FOR $\Delta\varepsilon_1$ $(\hbar\omega,F)$ AND $\Delta\varepsilon_2$ $(\hbar\omega,F)$ AT THE FOUR TYPES OF CRITICAL POINTS

CRITICAL POINT	$\Delta\varepsilon_1$ $(\hbar\omega,F)$	$\Delta\varepsilon_2$ $(\hbar\omega,F)$
M_0	+A.G(−η)	+A.F(−η)
M_1	+A.G(+η)	−A.F(+η)
	−A.F(−η)	+A.G(−η)
M_2	−A.G(−η)	−A.F(−η)
	+A.F(+η)	+A.G(+η)
M_3	−A.G(+η) $(\hbar\omega - E_g)$	+A.F(+η) $(\hbar\omega - E_g)$

the critical point band gaps can be determined from electroreflectance spectra without a detailed line shape analysis.

The electroreflectance spectrum of Ge obtained by Cardona is shown in Fig. 2.11 which may be compared with its reflectance, Fig. 2.2 and thermoreflectance, Fig. 2.8, spectra. The structure is sharp and well resolved. The E_1 and $E_1 + \Delta_1$ transitions represented by the doublet at 2.1 / 2.3 eV are clear. The E_2 structure is seen at 4.4 eV. The E_0' and $E_0' + \Delta_0'$ transitions are weak but clearly observed.

The first electroreflectance measurements were reported by Seraphin[138] by a technique usually known as the field effect electroreflectance.[129] The electric field applied to the reflecting surface was obtained by a capacitor like system. The dc bias and the ac modulating voltages were applied between the sample surface and a transparent conducting field electrode separated by a thin "Mylar" or "Saran" dielectric material, matching the interfaces optically with suitable liquids. Precautions should be taken in this experimental arrangement to eliminate unwanted reflectance variations due to changes in the electrode sample separation caused by Coulomb forces. Recent improvements in this technique are the use of thin films of dielectric materials between the reflecting surface and the field electrode which is either a conducting SnO_2 film or a thin metal film. This technique allowed measurements over a wide range of temperatures and surface potentials.[156] The spectral transmission properties of the dielectric film and the field electrode determine the useful range of the system.

The electrolytic electroreflectance technique was developed by Shaklee et al.[139] In this method an electric field is obtained at

FIGURE 2.11

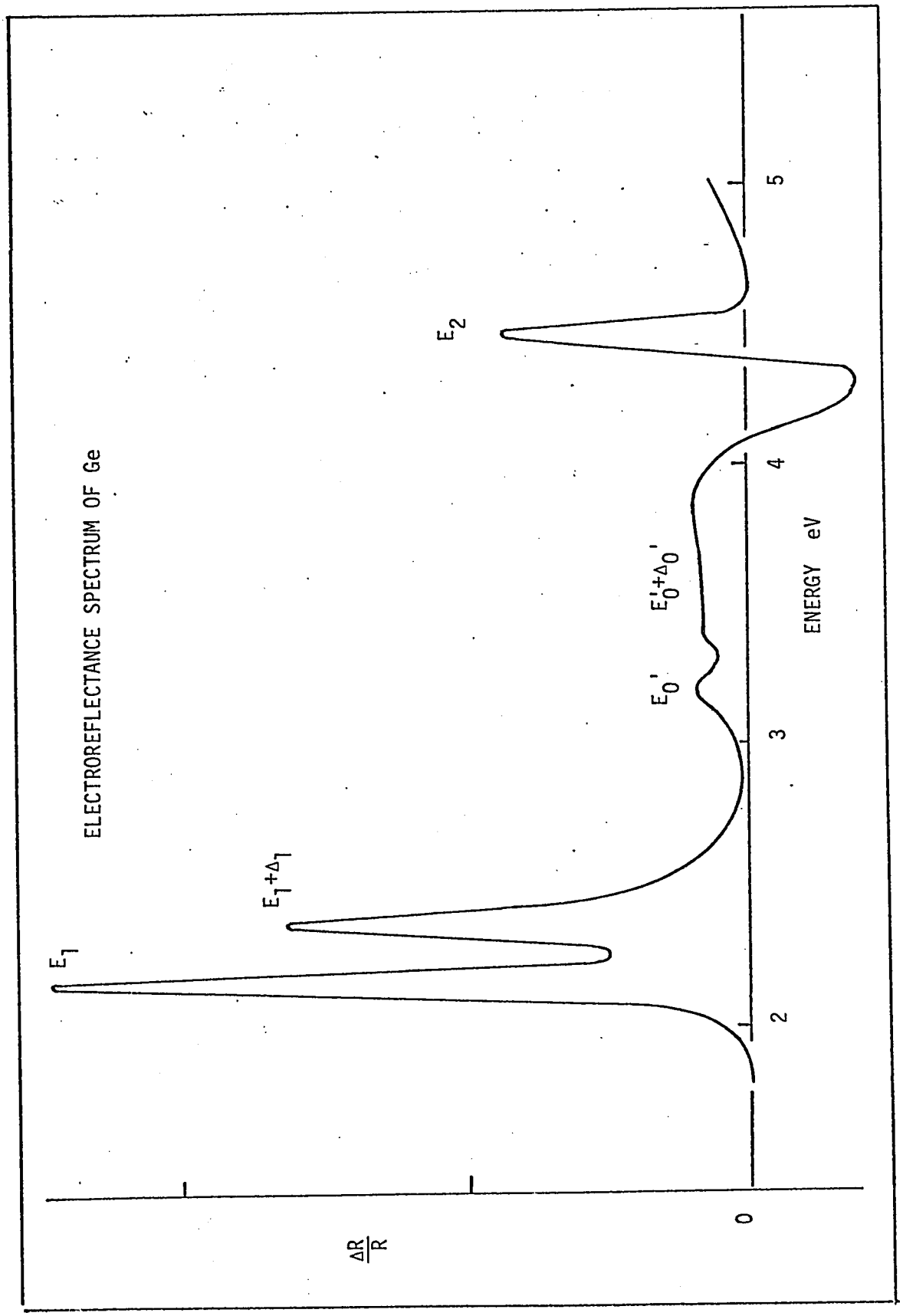
ELECTROREFLECTANCE SPECTRUM OF Ge
E_1
$E_1+\Delta_1$
E_0'
$E_0'+\Delta_0'$
E_2
$\frac{\Delta R}{R}$
0
2
3
4
5
ENERGY eV

the sample surface by immersing the sample in an electrolyte and biasing it in the proper direction with respect to a platinum reference electrode so as to form a blocking contact. An ac voltage is added to the dc bias in order to obtain modulation in reflectance. A characteristic advantage of the electrolytic technique is that large field strengths and large reflectance changes are caused by relatively small voltages along with the associated disadvantage that a small bias change will also lead to a large change in the surface potential. The spectral range of measurement is limited by the transmission of the electrolyte. The temperature range over which measurements can be made is determined by the freezing and boiling points of the electrolyte.

2.9 Review of Reflectance and Modulated Reflectance Results

Reflectance Results

The first reflectance measurements on semiconductors over a sufficiently wide range were made by Philipp and Taft on Ge[121] and Si.[132] Two peaks observed in the reflectance spectrum of Ge were tentatively assigned by Phillips[113] to the interband transitions $L_3' - L_1$ and $X_4 - X_1$. Spin orbit splitting of the L_3' level was observed by Tauc and Antoncik.[126] Their studies on Ge-Si alloy[65,66] and Phillips[157] classification of the energy levels at the Γ, X and L symmetry points led to the correct assignment of the first peak in Si to $\Gamma_{25'} - \Gamma_{15}$ gap. The pseudopotential band structure calculations of Ge and Si by Brust et al[114 - 116] corrected the earlier assignments and predicted extra structure. The first peak, E_1 in Ge was reassigned to $\Lambda_3 - \Lambda_1$ transition. The doublet nature of the peak was shown to be from spin orbit split Λ_3 levels. The accidental degeneracy of the two critical points M_1 at $X_4 - X_1$ and M_2 at $\Sigma_3 - \Sigma_2$ was responsible for the E_2 peak. The E_1' transitions at $L_3' - L_3$ predicted from Brust's band calculations were observed by Ehrenreich, Philipp and Phillips.[158,159]

First reflectance measurements on the III - V compounds GaAs, GaSb, InAs and InSb were reported by Tauc and Abraham[65] in 1960 immediately after the measurements on Ge and Si by Philipp and Taft. The similarity between the reflectance spectra of diamond and zincblende lattice materials was shown clearly in their results. Cardona determined the reflectance spectra of GaSb,[160] InP,[161] GaP, and AlSb[125] and his results include the temperature coefficients and the spin orbit

splittings of the E_1 transition. The 3.7 eV peak in GaP was assigned to the $L_3' - L_1$ transition. The doublet nature of the peak was not observed because of the small spin orbit value for L_3'. The reassignment of peaks for Ge and Si after Brust's band calculations was extended to the zincblende materials. Extra structure due to lowering of diamond symmetry to zincblende was observed by Greenaway and Cardona[162,163] and Zallen and Paul.[164] The $X_3 - X_1$ splitting was found to be nearly constant in all III - V compounds. The higher energy transitions between $L_3' - L_3$ levels were observed by Ehrenreich and Philipp.[158]

Recent band structure calculations by Herman et al[37] placed the E_0' transition energies in Si, Ge and α-Sn at a lower value from the experimental structure observed. The origin of the E_2 peak was suggested due to interband transitions over an extended region of the Brillouin zone, which is in agreement with the results of Kane.[117] Cardona et al determined the band structures of several III - V compounds using the k.p method.[26,22,27] Their results indicate that $\Sigma_2 - \Sigma_1$ transition energy is closer to the observed E_2 peak than the $X_4 - X_1$ transition energy.

Reflectance spectra of mixed III - V alloys were obtained for InSb-GaSb and InAs-GaAs by Woolley and Blazey[81] and GaAs-GaP by Thompson and Woolley.[101] A linear variation for the band gaps as a function of alloy composition was observed from their results.

Thermoreflectance Results

The thermoreflectance spectrum of Ge was determined by Batz[137,141] at two temperatures, 120° and 400°K, over a spectral range 0.6 to 5.0 eV. He observed structure corresponding to the fundamental gap and its spin orbit split component at 0.76 eV and 1.06 eV respectively giving 0.3 eV for Δ_0. The twin structure at 2.1 / 2.3 eV represented the E_1 and $E_1 + \Delta_1$ transitions. The E_2 peak occurred at 4.4 eV. More structure was observed in the energy range of 3.0 to 3.5 eV associated with the E_0' transitions. The structure found at 1.97 eV before the E_1 transitions was assigned to the $L_3' - L_1$ transitions generally labelled e_1.[128] This energy value is smaller than the energy reported by Ghosh,[165] (2.15 eV), and higher than the energy value given by Potter.[166](1.84 eV). The spin orbit split component $e_1 + \Delta_1$ was not observed by Batz.

Matatagui et al[140] determined the thermoreflectance spectra of several diamond, zincblende and wurtzite structure materials both at room temperature and liquid nitrogen temperature. The structure observed in their spectra was correlated with known electroreflectance measurements. The line shapes were discussed in terms of the nature of the critical points.

Electroreflectance Results

The electroreflectance spectra of Ge, Si and GaAs were determined by Seraphin using the field effect electroreflectance technique.[138] In the spectrum of Ge sharp structure corresponding to E_0, $E_0 + \Delta_0$, E_1, $E_1 + \Delta_1$, E_0' complex and E_2 were well resolved.[167,168] The $E_0 + \Delta_0$ transition was not observed in reflectance spectra. In the electroreflectance spectrum of Si[156] three peaks were observed in the energy range 3.3 to 3.5 eV. The second and third peaks changed sign in p and n type materials and also were found to be having a large temperature coefficient. At room temperature, the second peak almost disappeared. On these grounds Seraphin suggested that the low and high energy peaks at 3.34 and 3.45 eV represent the $\Gamma_{25}' - \Gamma_{15}$ and $\Lambda_3 - \Lambda_1$ transitions, respectively, with an excitonic peak at 3.4 eV in between. Structure found in the electroreflectance spectrum of GaAs[169] was in good agreement with the reflectance data. The field shift of the M_0 type E_0 and $E_0 + \Delta_0$ and M_1 type E_1 and $E_1 + \Delta_1$ transitions was measured in GaAs. Utilizing one of the advantages of this technique the $\frac{\Delta R}{R}$ line shapes were determined as a function of surface potential by varying the values of dc bias from -600 to 600 V.[170] It was observed that at the flat band condition the $\frac{\Delta R}{R}$ signal was minimum at the fundamental frequency. This technique was improved by Pidgeon et al[171] to determine the electroreflectance spectra of InSb and InAs at helium temperatures in a magnetic field.

Because of its simplicity the electrolytic electroreflectance technique[139] has been in extensive use to obtain the electroreflectance spectra of semiconductors in order to determine the energies of the

critical band gaps which contribute to optical absorption in the spectral range 0.6 to 6.0 eV.[128] Cardona et al applied this technique to several semiconductors with diamond (Si, Ge, α-Sn)[127] zincblende (AlSb, GaP, GaAs, GaSb, InP, InAs, InSb, ZnTe, CdTe, CdS, HgSe, HgTe)[127] wurtzite (CdSe, CdS, ZnO)[127] rock salt (PbS, PbSe, PbTe, SnTe, GeTe)[173] structures and materials with antifluorite structure (Mg_2Si, Mg_2Ge, Mg_2Sn).[174] The direct interband energy gaps and spin orbit splittings obtained from the results have been useful as parameters in semiempirical band calculations.

The structure observed in an electrolytic electroreflectance spectrum is sharp and well resolved. The spin orbit split components E_0 and $E_0 + \Delta_0$ separated by about 0.1 eV in GaP were resolved as shown from the results of Thompson et al.[104] In InP the E_1 and $E_1 + \Delta_1$ doublet which was not observed in reflectance was observed in its electroreflectance spectrum.[127] In the electroreflectance spectrum of Ge, Ghosh[165] observed more structure, some of which was assigned to the e_1 and $e_1 + \Delta_1$ transitions. This assignment, while in good agreement with Herman's band structure calculations disagrees with Potter's results.[166] Line shape analysis of the electroreflectance spectrum of Ge was attempted by Hamakawa et al.[153] They determined the $\Delta\varepsilon_1$ and $\Delta\varepsilon_2$ line shapes from the $\frac{\Delta R}{R}$ spectrum in order to compare them with the theoretical line shapes to find out the type of critical point transition involved. For InP, InAs, and CdTe the $\Delta\varepsilon_1$ and $\Delta\varepsilon_2$ line shapes were discussed by Cardona.[128]

The electrolytic electroreflectance technique has been extended to alloy studies to determine more accurately the band gap energies as a function of composition.[104] The Ge-Si alloy system was measured by

Klein et al.[128]. A linear variation for the energy gaps as a function of composition was shown from their results. In Si around 3.4 eV, the E_1, $E_1 + \Delta_1$, E_0' and $E_0' + \Delta_0'$ were all found to be superimposed. From the electroreflectance studies on GaAs-GaP[104] and InAs-GaAs[95, 96, 188, 191] the first peak observed in the reflectance spectrum of GaP was assigned to $\Lambda_3 - \Lambda_1$, transitions and a non-linear composition dependence of the $\Lambda_3 - \Lambda_1$ gap in InAs-GaAs alloy system was clearly observed.

2.10 Scope of the Present Work

Optical techniques which measure static and modulated reflectance have been used widely to obtain information necessary either to check the computed band structure or to provide parameters required for empirical calculations. For this purpose, modulation techniques have been found to be superior to static reflectance measurements. The most used of the modulation techniques is electroreflectance. In general, this technique can be used over a broad energy range if strong light sources, sensitive detectors and suitable electronics are available. However, a preliminary reflectance measurement is still of considerable value because the experiment is relatively simple to perform compared with modulation experiments. A direct correlation is obtained between the structure of the reflectance spectrum and the band structure.

In the present work, in order to obtain information about the higher energy transitions and the spin orbit split values of the energy levels at the X and L symmetry points, absolute reflectance measurements at near normal incidence have been made on some III - V compounds in the vacuum ultraviolet region. Thermoreflectance measurements were made in the energy range 1.0 - 6.0 eV. The structure found in the reflectance and thermoreflectance spectra is correlated to interband transitions with the help of previous work.

The study of energy gap variation in III - V alloys by determining the reflectance spectra was initiated by Woolley and Blazey.[81] The electroreflectance technique was applied to alloy studies by Thompson and Woolley[104] with improved accuracy in the determination of band gaps. By extending these measurements to three more alloy systems the nonlinear

variation of energy gaps as a function of composition has been found to be in part due to the effect of lattice disorder. The bowing parameter has been determined for various band gaps and for one spin orbit splitting. In the latter case, the bowing parameter is shown to be related to the atomic spin orbit split values of the alloying atoms.

In the III - V alloy studies, the preparation of alloy material is the first requirement. Intensive growth studies by Woolley and co-workers showed that the horizontal Bridgman method is suitable for the preparation of homogeneous polycrystalline samples of some III - V alloys. Two alloy systems measured presently were grown by this technique. A third alloy system was prepared by vapour transport technique at the Westinghouse Research Laboratories.

In the following chapter, the experimental techniques and the method used to prepare III - V alloys are described. Results and Discussion are given in Chapter Four which is followed by conclusions as Chapter Five. Further organization of material in each chapter is indicated in its introductory section.

CHAPTER 3

EXPERIMENT

3.1 Introduction

The physical properties measured in this research were the values of reflectance and modulated reflectance for some III - V compound semiconductors and their alloys. The following section is concerned with the measurement of reflectance. The principle of the method, the apparatus and the experimental details are described. The third section is devoted to modulated reflectance. Details of the two modulation experiments, namely, electroreflectance and thermoreflectance, which were set up in our laboratories are given. Preparation of III - V alloys is treated in the fourth section. The III - V compound semiconductor materials used in this work were purchased from industrial organizations. Of the III - V alloys which were measured, the $Ga_xIn_{1-x}Sb$ and $InSb_{1-x}As_x$ systems were grown in our laboratories. The $InAs_{1-x}P_x$ alloy samples were kindly provided by Dr. M. Rubenstein of the Westinghouse Research Laboratories. The method used for the preparation of the former two alloys is described.

3.2 Measurement of Reflectance

The reflectance of a material is defined as the ratio of the reflected to the incident light intensities. It is a function of the wavelength of the incident radiation and the angle of incidence. Another factor which influences the reflectance of a sample to a considerable degree is how the surface itself has been prepared. The object of this experiment is to measure the values of reflectance as a function of wavelength or photon energy over an extended range for a semiconductor whose reflecting surface has been prepared with care. The angle of incidence is chosen to be near normal as this permits application of the simple Fresnel equation in the analysis of reflectance data. Furthermore, for this angle of incidence, the reflectance is independent of the state of polarization of the radiation.[175]

The equipment required to perform such an experiment are the following: a lamp, a monochromator which disperses the radiation from the lamp into a spectrum and a detector to measure the intensity of the radiation. A selection of these components depends upon the wavelength range of the experiment.

The lamp is usually chosen on the basis that it be intense and stable. In the infrared and near infrared regions either a Globar or a Nernst filament which gives a continuous spectrum is almost always used. A tungsten filament lamp with either a glass or quartz envelope covers the wavelengths in the near infrared and the visible regions. This is also a source of continuous spectrum. For more intense visible radiation high pressure xenon arc lamps are generally used. A high pressure xenon arc lamp with quartz envelope provides radiation down

to 1600Å in the vacuum ultraviolet region. Lamps which give radiation below 1600Å are usually gas discharge lamps. Electrical discharge in rare gases have been used as sources of continuous spectra from 1000 to 2000Å.[176,177] A most commonly used source in the vacuum ultraviolet region is the hydrogen discharge lamp.[178]

In monochromators, the dispersing element used is either a prism or a grating. The wavelength range of a prism monochromator depends upon the optical properties of the material of the prism. Quartz is used in the wavelength range from near infrared to near ultraviolet. The resolution of prism monochromator varies over its wavelength range. Higher resolution and lower scattered light intensity are achieved in double pass monochromators which are incorporated with a chopper. In principle, a grating monochromator can be used in any region of the spectrum. Over its wavelength range the resolution of the instrument remains approximately constant. When grating monochromators are used it is necessary to remove the overlapping higher order spectra by using suitable filters.

In the infrared and near infrared regions, thermocouples and lead sulphide and lead selenide cells are usually chosen as detectors. Photomultiplier tubes are commonly used in the visible and ultraviolet regions. In the vacuum ultraviolet, the short wavelength radiation is first converted into visible radiation by using a phosphor which is then detected by a photomultiplier tube.[179]

A schematic arrangement of the apparatus for measuring reflectance is shown in Fig. 3.1. This particular set-up which was used to measure reflectance in the 3.5 - 7.5 eV range is described later in

FIGURE 3.1

SCHEMATIC ARRANGEMENT OF A REFLECTANCE EXPERIMENT

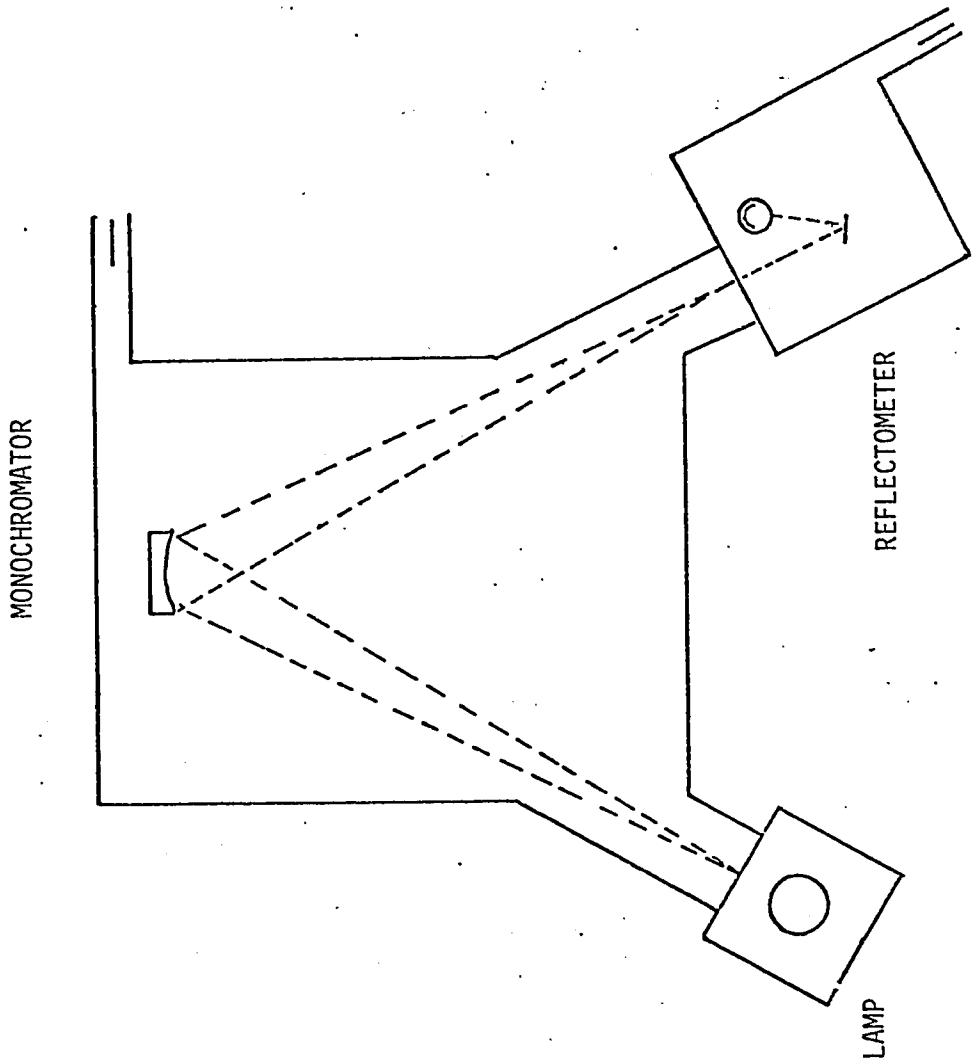

this section. The apparatus consists of a monochromator with a lamp at its entrance slit and a reflectometer at the exit slit. Radiation from the lamp is dispersed by the monochromator and the monochromator radiation enters the reflectometer through the exit slit. The reflectometer unit contains a sample in a holder and a detector. In two measurements, the intensities of the monochromatic light reflected from and incident on the sample are measured with the same detector. The ratio of the reflected to the incident light intensities gives the reflectance of the sample.

During the course of this research reflectance measurements were made in two wavelength regions extending from 1.0 to 4.5 eV and 3.5 to 7.5 eV which will be identified as the low and high energy experiments. In these two experiments the reflectometer used was the same unit. Therefore, this unit will be described first followed by the details of sample surface preparation and the measurement of reflectance in the low and the high energy regions.

Reflectometer

The reflectometer unit is shown in Fig. 3.2. This unit was originally constructed for mounting it on the exit slit arm of a Jarrel Ash halfmeter grating monochromator, shown schematically in Fig. 3.1, to measure reflectance in the vacuum ultraviolet region. It contains a sample holder which can be raised or lowered either to take the sample out of the path of the light beam or to receive it. The sample holder can also be rotated about a vertical axis allowing any desired angle of incidence of the light beam on the sample surface. The axis of rotation is in the plane of the sample surface. A photomultiplier tube equipped with a side window is mounted on a radial arm which could be rotated about the same vertical axis around which the sample holder rotates. To measure the reflected light intensity the sample is lowered into the optical path. The angle of incidence is adjusted to the desired value by rotating the sample holder. The detector is rotated into its position to receive the reflected light from the sample. The incident light intensity is measured by taking the sample out of the optical path and rotating the detector to face the direct beam.

Light entering the reflectrometer is stopped by a diaphragm placed in front of the LiF lens which focussed the light on the sample at an effective aperture ratio of f/12.5. The minimum average angle of incidence obtained with this unit is 7^{o}. As the length of the radial arm from the sample surface to the detector is fixed, the dimensions of the light beam on the detector remain constant when the detector receives either the reflected light beam from the sample for any angle of incidence or the direct beam. To be able to select the same sensitive area, stops can be arranged on the radial arm travel.

FIGURE 3.2

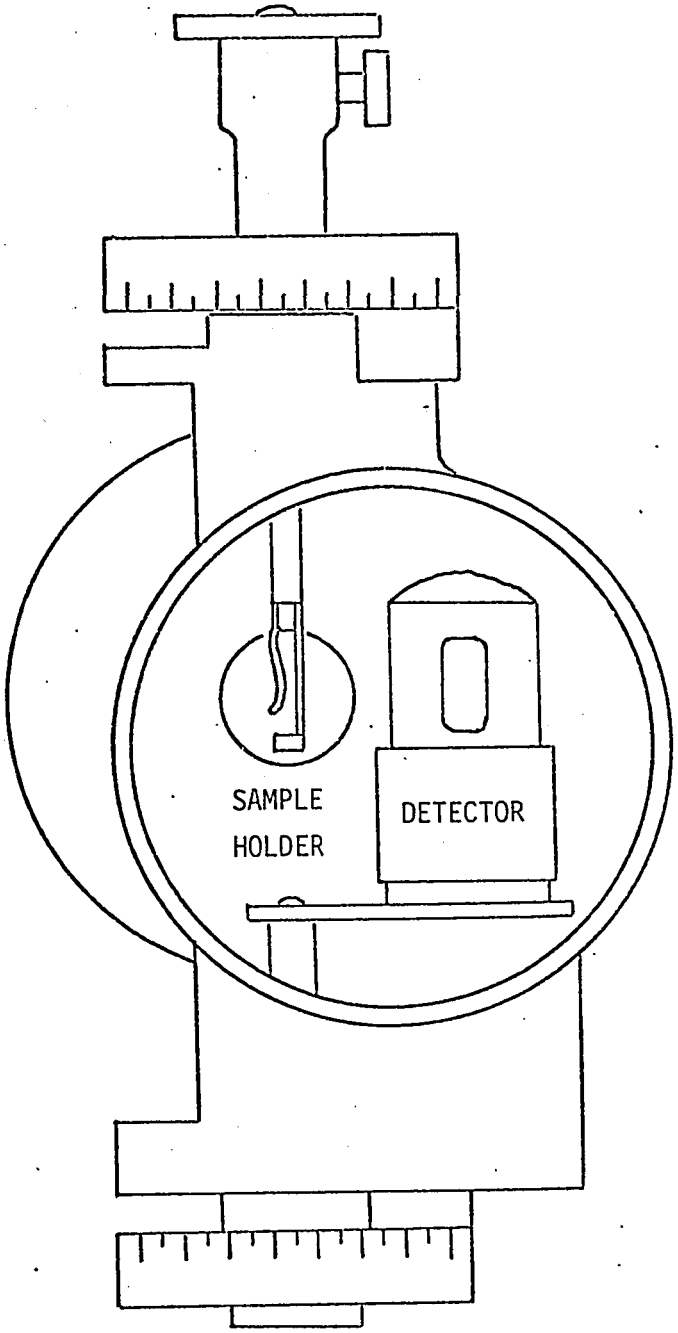

REFLECTOMETER

Similarly the sample holder motion can be stopped mechanically to expose the same sample surface repeatedly and to maintain the same angle of incidence. Resetting errors associated with the sample and detector positioning are negligible. The reflectance measured is an absolute value.

The reflectance value at a given wavelength was determined from consecutive readings with the sample in and then with the sample out. This technique although more time-consuming than that of running through the spectrum first with the sample in and then with the sample out of the incident beam, reduces effects due to fluctuations in the electronics and the lamp intensity. These point by point measurements were made at wavelength intervals suitable for the particular region of the spectrum being investigated.

Sample Surface Preparation

Sample surface preparation plays an important role in reflectance measurements. Light incident on the surface interacts with the sample material within the penetration depth of the radiation which depends upon the absorption coefficient of the material. The penetration depth is large for long wavelength radiation and decreases as the wavelength decreases for a semiconductor. Reflectance measurements therefore represent the properties of the material in the surface layer whose thickness varies from a few thousand to a few hundred Angstroms. Ideally, when the surface is atomically clean and free from lattice distortion effects, the material in the surface is a true representative of the bulk material.

Experimentally, it is not possible to prepare ideal surfaces. The closest to an ideal surface is a surface cleaved in high vacuum. Reflectance measurements on such a surface should also be conducted under high vacuum conditions. When the sample is exposed to atmosphere the surface gets oxidised rapidly. The oxide layer thickness is an important parameter when the penetration depth of the radiation is of the same order of magnitude. For materials which cannot be cleaved, surfaces are prepared by cutting and mechanical polishing which distort the surface layers. Chemical etching is necessary to dissolve the distorted material away from the surface before proceeding with the experiment.

Samples for reflectance experiment were cut from these materials in the shape of thin plates of approximate dimensions 8 x 5 x 2 mm. They were held in Glyptol cement on polishing rods to be mechanically polished

in steps on grinding and polishing wheels using various grain sizes of alumina powder suspended in distilled water. The final polishing was done with .05 micron grain size alumina. The surface layers strained by mechanical polishing were removed by etching just before making the reflectance measurements. The etchants used were mainly mixtures of nitric and hydrochloric acids in various proportions. After etching each sample was washed successively in distilled water, ethyl alcohol and acetone in that order, dried and mounted in the sample holder of the reflectometer. The initial positioning of the sample was carried out so that the reflected beam for the sample in position and the incident beam in the sample out position both fell on the same part of the detector window. With the sample positioned properly in its holder, the reflectometer was ready to be used either with the low or the high energy reflectance experiment.

Measurement of Reflectance in the Low Energy Region

A Zeiss M4Q 111 prism monochromator was used with a low voltage tungsten filament lamp. Monochromatic radiation over the energy range 1.0 to 4.5 eV, chopped at 120 Hz was obtained with this combination. The monochromatic radiation was focussed on the sample by a quartz lens. The incident and the reflected light intensities were measured by an RCA 1P28 photomultiplier tube operated at a stabilized voltage of the order of 400 V supplied by a Zeiss Amplifier / Indicator unit. The 120 Hz output signal from the detector was amplified and converted to dc with a phase sensitive detector in the Amplifier / Indicator unit, and was displayed as a galvanometer deflection on a scale which had 110 divisions.

Reflectance measurements were made by measuring the reflected and the incident light intensities with the sample in and sample out technique. At each wavelength selected, first the incident light was brought to read close to the full scale deflection of 110 divisions by adjusting the amplifier gain. This reading gave the incident light intensity I_o. For the same gain setting, the reflected light intensity I_R was measured. The reflectance value R at the wavelength λ is determined from the ratio of I_R to I_o. This procedure was repeated at 50$\mathring{A}$ intervals over the wavelength range.

Measurement of Reflectance in the High Energy Region

The equipment used in this experiment consisted of a Jarrel-Ash half meter concave grating monochromator, a Sylvania DE 350 deuterium lamp and the reflectometer. The lamp was run by a stabilized power supply. Monochromatic radiation in the energy range 3.5 to 7.5 eV was available at the exit slit of the monochromator. The monochromatic radiation was focussed on the sample by a LiF lens. The incident and the reflected light intensities were measured by an RCA 1P21 photomultiplier tube. The window of the photomultiplier tube was coated with sodium salicilate phosphor. The detector was operated at 500 V supplied by a Keithley model 240 stabilized voltage source. The signal output from the detector was fed to a Keithley model 409 picoammeter whose proportional output was read on a Cimron digital multimeter.

To proceed with the experiment the reflectometer was mounted on the exit slit arm of the monochromator with an O - ring vacuum seal. At the entrance slit of the monochromator a suprasil window was attached. The monochromator and the reflectometer were evacuated. The reflectance values were determined from consecutive readings with the sample in and sample out technique, as discussed before. These point by point measurements were made at wavelength intervals suitable for the particular region of the spectrum being investigated. The resolution of the monochromator permitted 10 $\mathring{A}$ intervals. The correction for the scattered light was made by measuring the detector output by setting the monochromator at a wavelength below the transmission limit of suprasil. This value was assumed to remain constant over the entire wavelength range of the experiment.

3.3 Measurement of Modulated Reflectance

The underlying principle of modulation techniques is that by applying a periodic perturbation to a sample, periodic changes with the same period can be introduced into its physical properties which can be retrieved later by using conventional phase sensitive detection techniques. When the physical property observed is reflectance, modulated reflectance is the result. The external agents which can be used to modulate reflectance are for example, temperature, electric field, uniaxial stress, etc.[129,128] The mechanism of modulation differs from one modulating parameter to the other. But a simple shift of the energy of the critical point in the joint density of states function by the modulation parameter accounts for the observation of structure in the modulated reflectance spectra. As the line shapes in these spectra do change for different external perturbation agents, additional information is available in their examination.

One consideration which speaks highly in favour of the modulated reflectance experiments is that the structure in their spectra is limited to few energy positions with either very little or no background as otherwise found in ordinary reflectance spectra. Usually, the changes in reflectance, $\Delta R/R$ produced by the modulating parameters are quite small. They are of the order of 10^{-4} to 10^{-6} and require special apparatus: strong light sources, sensitive detectors and suitable electronics to provide a good final result for $\Delta R/R$ as a function of wavelength in such an experiment. Since in the present work, the same setup was used with different modulating parameters, namely temperature and electric field, the common setup is described first. Further details

of how this setup was used to obtain electroreflectance and thermoreflectance are described in their respective subsections.

A schematic layout of the common setup is shown in Fig. 3.3. A Bausch and Lomb half meter grating monochromator was used to disperse the light from a Hanovia 907 C 1, 600 W high pressure xenon arc lamp. The resulting radiation at the exit slit of the monochromator was passed through a suitable filter to remove the wavelengths of the overlapping orders. The filters used were Wratten 29, Wratten 2A and Glass. The filtered monochromatic radiation was focussed on the sample by a quartz lens at near normal incidence. The reflected light was gathered by a front silvered concave mirror and redirected to a detector. This was a photomultiplier tube which was either a Du Mont 6911 for the infrared and the visible regions or an EMI 6255 S for the visible and ultraviolet regions. The detectors were operated by Keithley Model 240 and NJE Corporation Model S - 326 regulated power supplies.

During a modulated reflectance experiment the output current from the detector contained a dc component proportional to the intensity of the light reflected from the sample (α R) and an ac component proportional to the change in reflectance ($\alpha \Delta$ R) caused by the periodic perturbation of the modulating parameter. The dc signal was maintained at a constant value of the order of 1V by adjusting the voltage applied to the photomultiplier tube by a servo (Heathkit Recorder) continuously. The ac signal output from the detector which was proportional to $\frac{\Delta R}{R}$ was detected by either a PAR JB6 or PAR Model 122 Lock In Amplifier. The output from the lock in amplifier was recorded on a Heathkit chart recorder. The wavelength control of the monochromator was driven by a

FIGURE 3.3

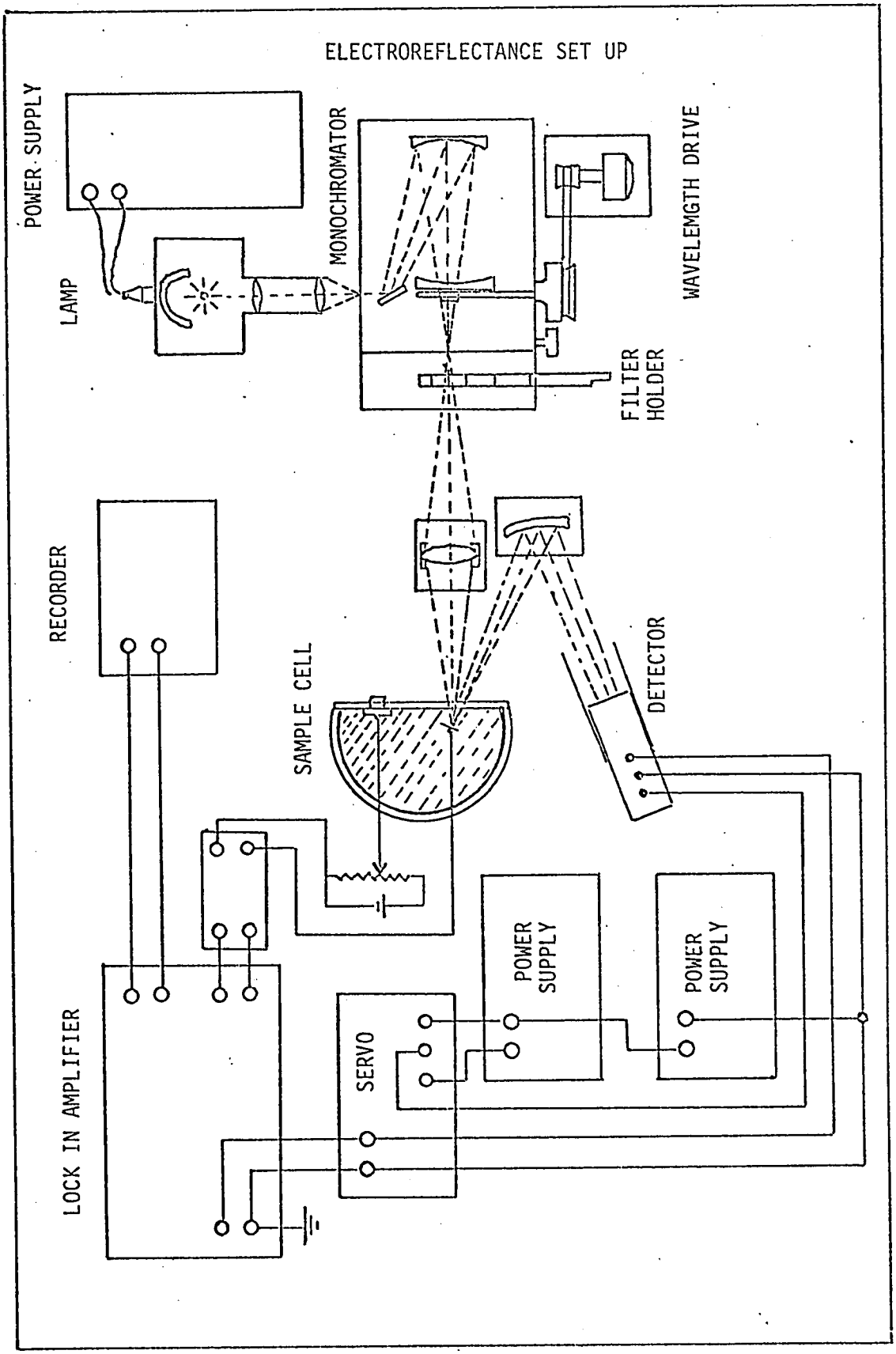
ELECTROREFLECTANCE SET UP
POWER SUPPLY
LAMP
MONOCHROMATOR
WAVELEMGTH DRIVE
FILTER HOLDER
RECORDER
SAMPLE CELL
DETECTOR
POWER SUPPLY
POWER SUPPLY
SERVO
LOCK IN AMPLIFIER

motor and the wavelengths were marked manually at every 50 Å intervals on the spectrum.

Electroreflectance

The electrolytic electroreflectance technique was used in the present work. This experiment was first set up in our laboratories by Dr. A. G. Thompson.[180] The same equipment was used with a few modifications in setting up the present experiment.

An electric field was applied to the reflecting surface of a semiconductor sample by immersing it in an electrolyte and biasing it in the blocking direction with respect to a platinum reference electrode. The modulation in reflectance was obtained by adding an ac voltage to the dc bias. The dc bias was obtained from a 9V Mallory battery and it could be adjusted by a potentiometric control. The ac modulation voltage was derived from the reference output of the lock in amplifier when the unit was operating in the internal reference mode. The reference output was applied between the sample and the reference electrode through an impedence matching circuit. The modulation voltage could be adjusted continuously from 0 to 3V.

The sample cell was made out of a Pyrex beaker with a quartz window. In the early investigations a 0.3 N solution of KCl in distilled water was used as the electrolyte. To obtain a blocking contact, the sample was made negative with respect to the reference electrode. To avoid excessive current flow through the sample, the bias and modulation voltages were maintained at lower values. During this work, another electrolyte, glycerol in distilled water, was found to be more suitable for work with the III - V compounds and their alloys. With this electrolyte, it became possible to change the bias over a considerable range of voltages without drawing excessive currents and even to make the

polarity of the sample positive with respect to the reference electrode. The bias variation was particularly important for InAs and InAs rich alloys. This will be discussed further in the chapter on Results and Discussion.

The samples for the electroreflectance experiment were cut from alloy ingots. They were elliptic in shape with approximate dimensions 6 x 3 x 1 mm. One face of each sample was mechanically polished with alumina powder, the last stage being with 0.05 micron grain size. The sample was mounted on a brass rod using silver paint (GC #21 - 1) for good electrical contact between the rod and the sample and insulated from the electrolyte except for the reflecting surface of the sample with an insulating liquid tape (GC #176 - 2). Just before starting with the experiment, the samples were etched in mixtures of nitric and hydrochloric acids.

To proceed with the experiment, the sample was positioned in the optical path to reflect the light from the monochromator into the detector at near normal incidence. The bias and modulation voltages were chosen and applied to the sample. The best operating values were known after a few trial experiments. With a rapid scan over the wavelength range of the experiment suitably selecting the filters, first the location of structure in the $\Delta R/R$ spectrum was found. Later, a slow scanning speed of 50 Å / min at a chart speed of 2" / min and a time constant of either 1 or 3 sec provided spectra with ample resolution and good signal to noise ratio.

Thermoreflectance

In the thermoreflectance experiment the reflectance of a sample was modulated by a periodic variation of the temperature of the sample. The temperature variation was obtained for low resistance samples by passing a periodic current through them. High resistance samples were mounted on a heater and heated indirectly by passing the periodic current through the heater. A Hewlett-Packard audiosignal generator followed by an amplifier, Fig. 3.4, supplied power to heat the sample either directly or indirectly. The frequency selected was between 7 and 19 Hz.

Samples for thermoreflectance measurements were cut as rectangular plates of approximate dimensions 6 x 3 mm. and a few hundred microns thick. The reflecting surface of the sample was mechanically polished (with alumina powder) and etched just before mounting it on the sample holder shown in Fig. 3.5. The sample was electrically insulated from the water cooled copper block by a thin sapphire disc and it was attached to the sapphire disc with silver paint. The electrical contacts were made either to the sample or to the heater strip depending upon the resistance of the sample.

A PAR model 122 lock in amplifier was used to pick up the modulated component from the detector output. The reference signal for the lock in amplifier was derived from the signal generator. A thermoreflectance spectrum was recorded from the output of the lock in amplifier as described in the preceeding sections.

FIGURE 3.4

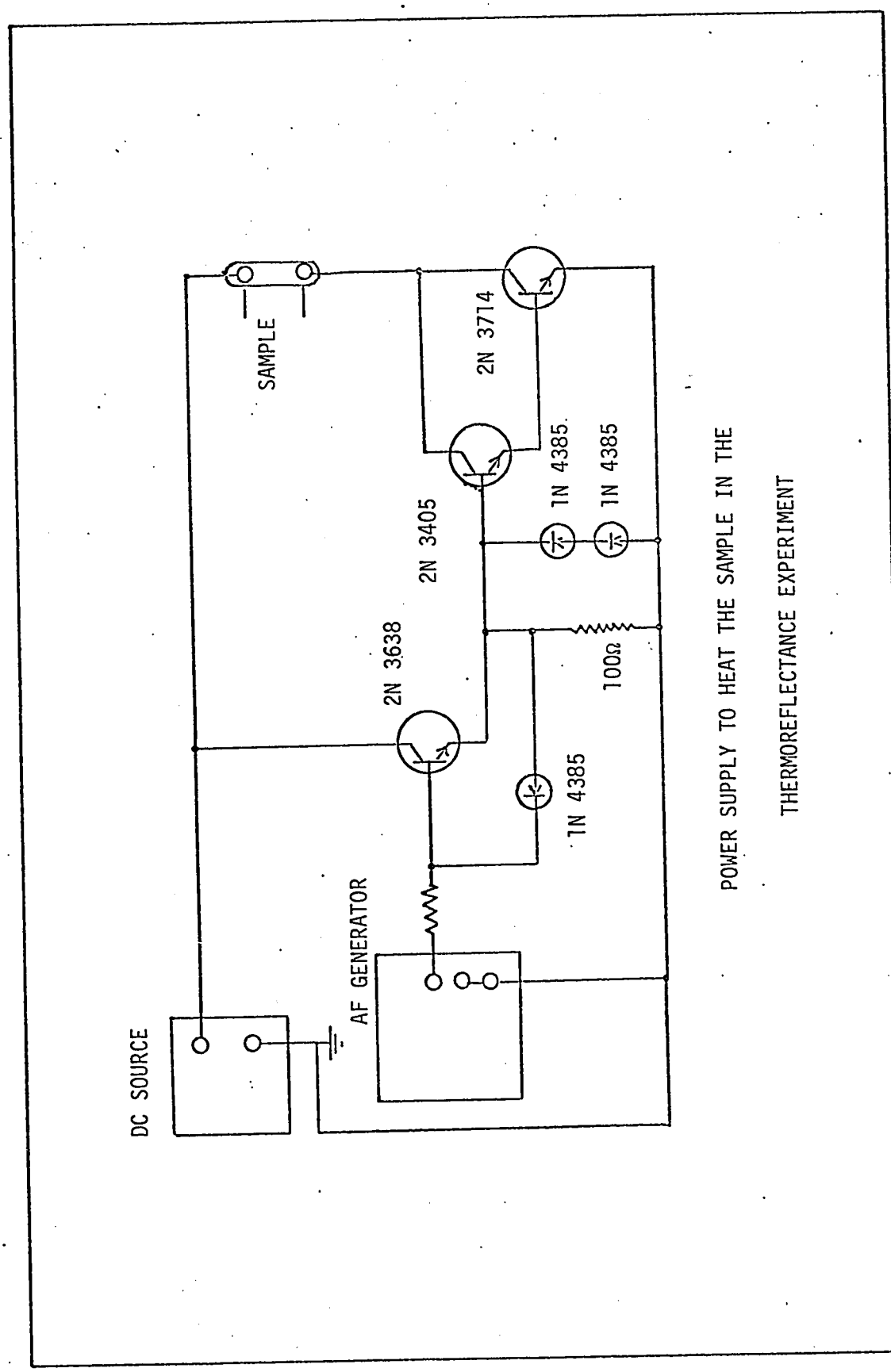

POWER SUPPLY TO HEAT THE SAMPLE IN THE THERMOREFLECTANCE EXPERIMENT

FIGURE 3.5

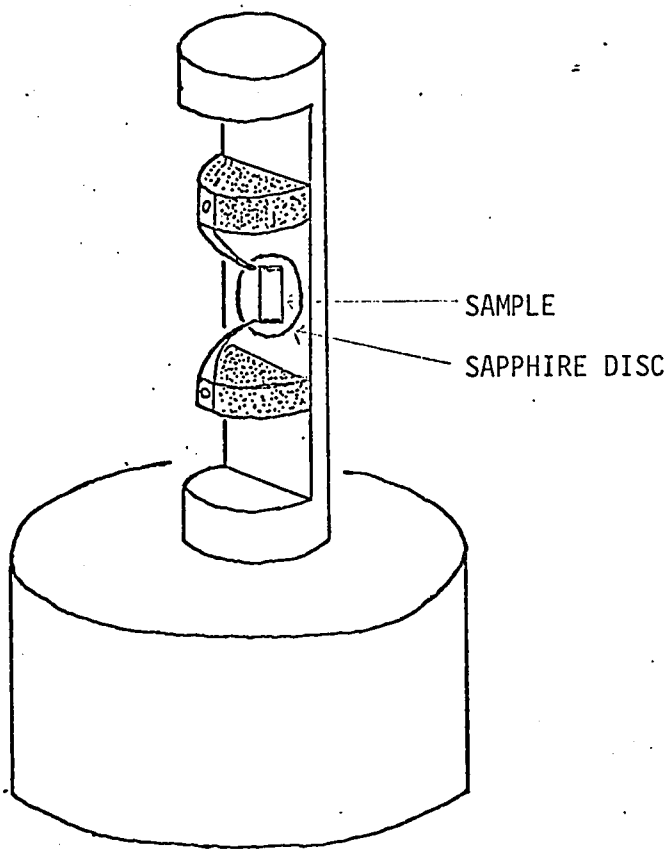

THERMOREFLECTANCE SAMPLE HOLDER

3.4 Preparation of III - V Alloys

Through a careful study of the material growth techniques by Woolley and co-workers, the horizontal Bridgman method has been found to be suitable for the preparation of mixed III - V alloys.[75] In this technique, an alloy material in the molten state is pulled through a steep temperature gradient solidifying as it passes into the cold zone. This method produces coarsely polycrystalline ingots in which there is a gradient of composition along the length of the ingot with homogeneous cross sectional slices. Therefore, slices cut from various positions along the length of an ingot give specimens of different alloy compositions.

The furnace design used in horizontal Bridgman method is shown in Fig. 3.6. It consisted of two sections, one maintained at a higher temperature than the other. These two sections were separated by water cooled brass discs to make the temperature gradient as steep as possible. The selected temperatures for the high and low temperature zones were monitored by Pt-Pt Rh thermocouples and maintained by an "Ether Transitrol" proportional controller and a "Phillips on-off" controller, respectively. The temperature profile of the furnace is also shown in Fig. 3.6.

The drive mechanism used to pull the ingot through the temperature gradient consisted of a "Meccano" worm and gear assembly and a Barber-Coleman motor.

To prepare an alloy material, appropriate amounts of the two III - V compounds to be alloyed were weighed and vacuum sealed in quartz capsules. The mixture was melted first in a high temperature furnace. After a thorough mixing of the contents, the mixture was allowed to

FIGURE 3.6

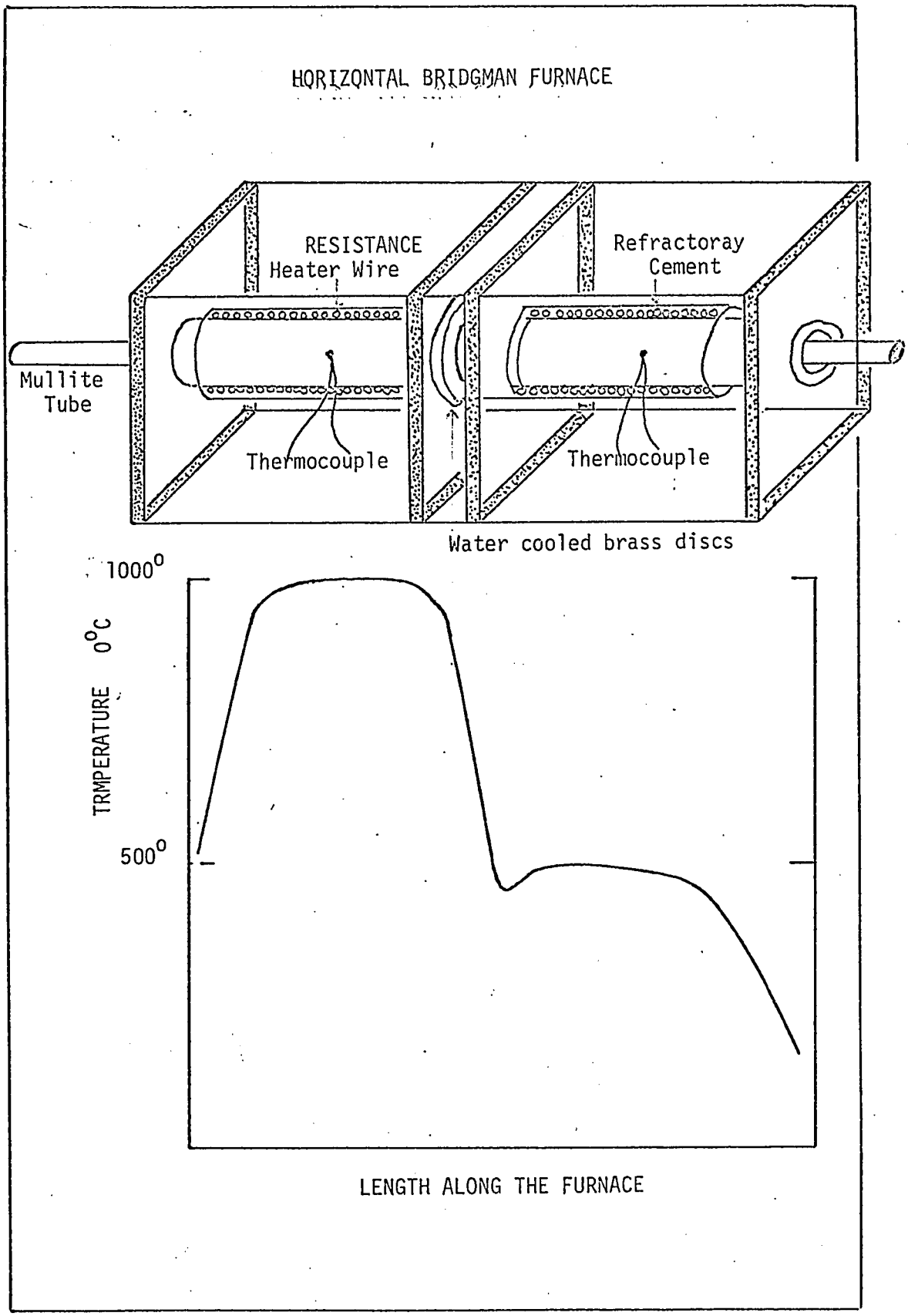
HORIZONTAL BRIDGMAN FURNACE
RESISTANCE
Heater Wire
Refractoray
Cement
Mullite
Tube
Thermocouple
Thermocouple
Water cooled brass discs
1000°
500°
TEMPERATURE °C
LENGTH ALONG THE FURNACE

solidify. The solid ingot thus obtained will be in general inhomogeneous. The ingot was then placed in the hot zone of the horizontal Bridgman furnace, the temperature of which was selected to be higher than the melting point of the alloy ingot. It was slowly pulled through the temperature gradient into the cold zone whose temperature was generally maintained below the melting point of either compound but sufficiently high in order to prevent the condensation of high vapour pressure constituents of the alloy on the cooler parts of the capsule. The rate of travel was selected depending upon the alloy system and in general varied between 2 to 8 weeks for an ingot of 15 cms. in length.

The $Ga_xIn_{1-x}Sb$ and $InSb_{1-x}As_x$ alloy materials were grown by horizontal Bridgman technique. Ingots grown by this method have composition gradient along their length. To determine the composition of the alloy material as a function of length along the ingot cross sectional slices were cut from the ingot at different positions. From x-ray powder photographs the lattice parameters of the material from these cross sectional slices were determined. The compositions were then obtained from the lattice parameters by comparing them with the lattice parameter versus composition curves determined before for III - V alloys by Woolley and co-workers.[50,75] For $Ga_xIn_{1-x}Sb$ and $InSb_{1-x}As_x$, the variation of composition as a function of length along the ingots are shown in Figs. 3.7 and 3.8. A comparison of the two figures shows the particularly steep variation of composition in the mid composition range for the $InSb_{1-x}As_x$ ingot along its length.

FIGURE 3.7

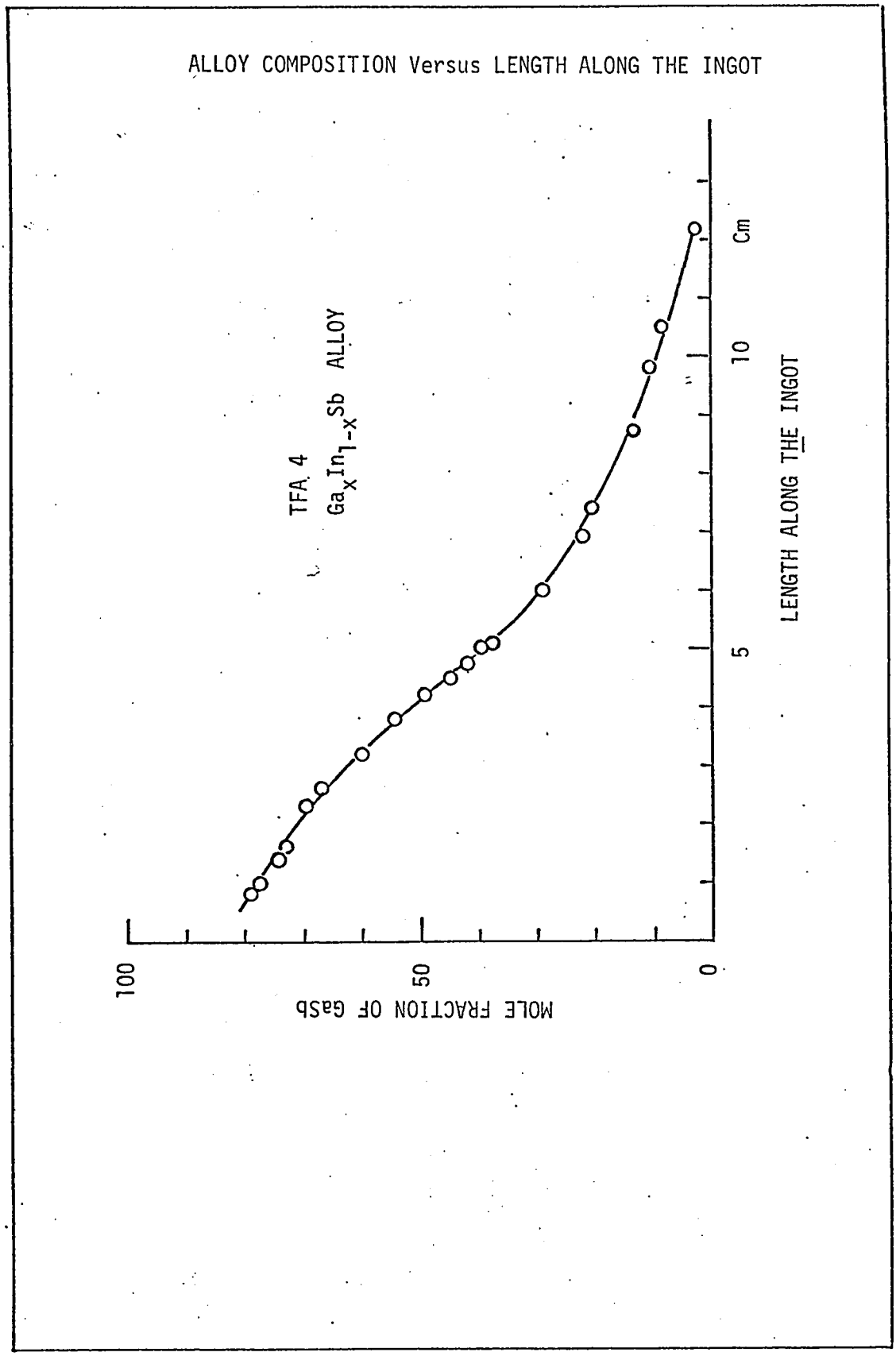
ALLOY COMPOSITION Versus LENGTH ALONG THE INGOT
TFA 4
$Ga_xIn_{1-x}Sb$ ALLOY
MOLE FRACTION OF GaSb
100
50
0
5
10
Cm
LENGTH ALONG THE INGOT

FIGURE 3.8

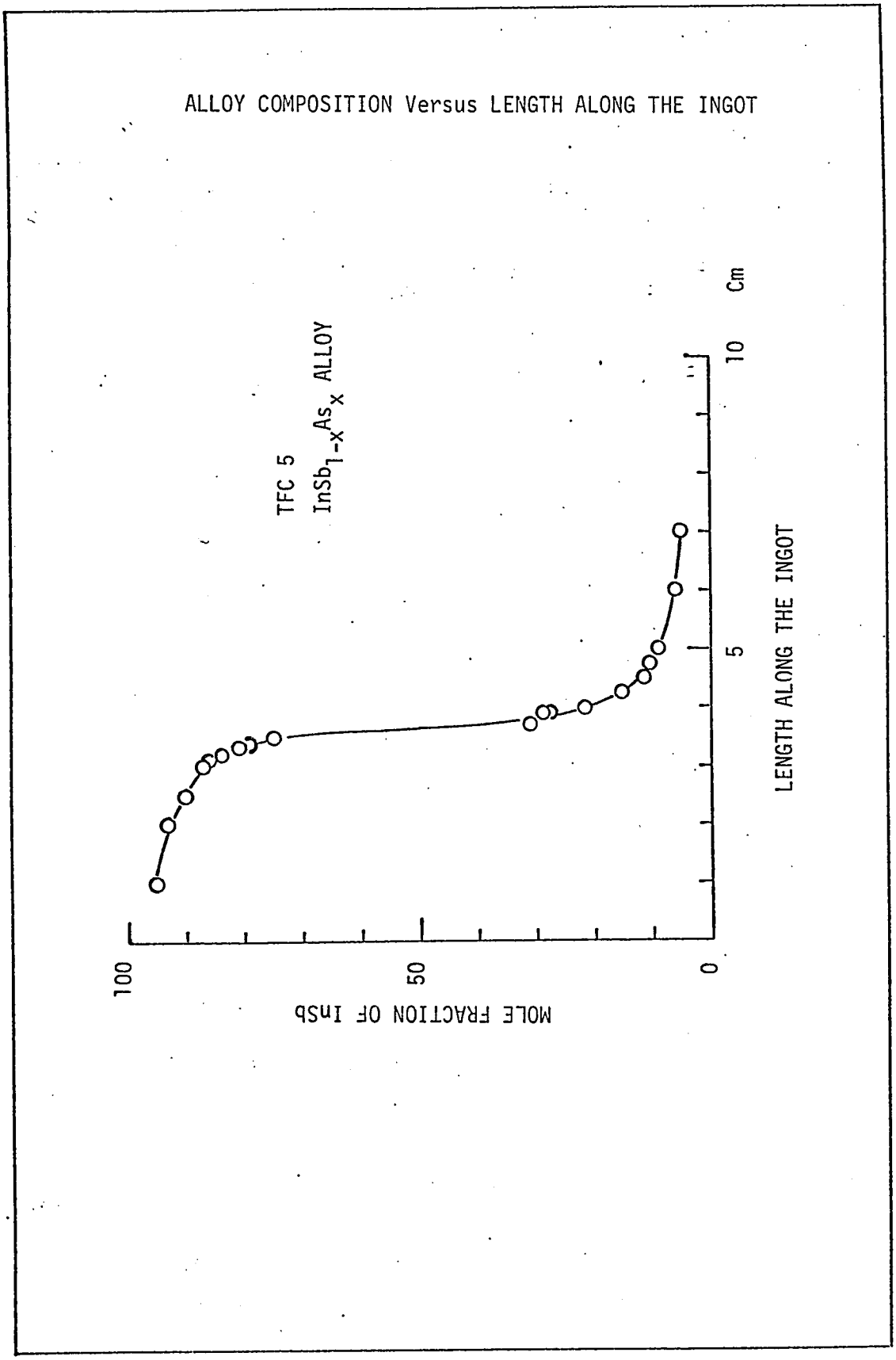
ALLOY COMPOSITION Versus LENGTH ALONG THE INGOT
TFC 5
$InSb_{1-x}As_x$ ALLOY
MOLE FRACTION OF InSb
100
50
0
LENGTH ALONG THE INGOT
5
10
Cm

CHAPTER 4

RESULTS AND DISCUSSION

4.1 Introduction

This chapter is broadly divided into two sections. In the first section, results obtained from the reflectance and thermoreflectance experiments on III - V compounds are presented and they are discussed in terms of interband electronic transitions. In the second section, results on mixed III - V alloys $Ga_xIn_{1-x}Sb$, $InAs_{1-x}P_x$ and $InSb_{1-x}As_x$ are given in that order. Of these three, the $Ga_xIn_{1-x}Sb$ alloy system has been studied extensively using the reflectance, thermoreflectance and electroreflectance techniques. Only electroreflectance measurements were carried out on $InAs_{1-x}P_x$ and $InSb_{1-x}As_x$ alloy systems. Results obtained for the three alloy systems together with the results from previous work in $GaAs_{1-x}P_x$ and $Ga_xIn_{1-x}As$ alloys are analysed using the modified virtual crystal model.

4.2 Results and Discussion of Reflectance Measurements on III - V Compounds

Reflectance values were determined in the energy range 3.5 to 7.5 eV for samples of GaP, InP, GaAs, InAs, AlSb, GaSb and InSb. Samples which were cut from polycrystalline ingots were polished and etched just before proceeding with the measurements. The experimental procedure adopted to measure reflectance in this energy range has been described in Section 3.2. The reflectance spectra which are values of reflectance plotted as a function of photon energy $\hbar\omega$, are shown in Figs. 4.1 and 4.2.

Each curve in Figs. 4.1 and 4.2 represents a single set of measurements made on a sample. As it was not found possible to reproduce the same quality sample surface repeatedly the reflectance values determined in repeated trials at the same wavelength were different. This change in reflectance in repeated trials was found to be sufficient to smoothen the fine structure in an averaged reflectance spectrum. Therefore, the structure which was observed repeatedly in individual trials has only been included for further discussion.

The two sets of peaks marked (1, 2, 3) and (4, 5, 6, 7) in the reflectance spectra shown in Figs. 4.1 and 4.2 have been identified as the components of the E_2 and E_1' structure complexes from previous work.[127,158,181] The energies of the E_2 (Peak 1), $E_2 + \delta$ (Peak 3) and in a few cases the E_1' (Peak 4) and the $E_1' + \Delta_1'$ (Peak 7) transitions have been determined previously. These values are used to compare the energies obtained in the present work and to identify the extra structure found in the spectra, for example, the $E_2 + \Delta_2$ (Peak 2) and the components of the E_1' (Peaks 5 and 6) transitions. The structure observed on the low energy side of

REFLECTANCE SPECTRA FIGURE 4.1

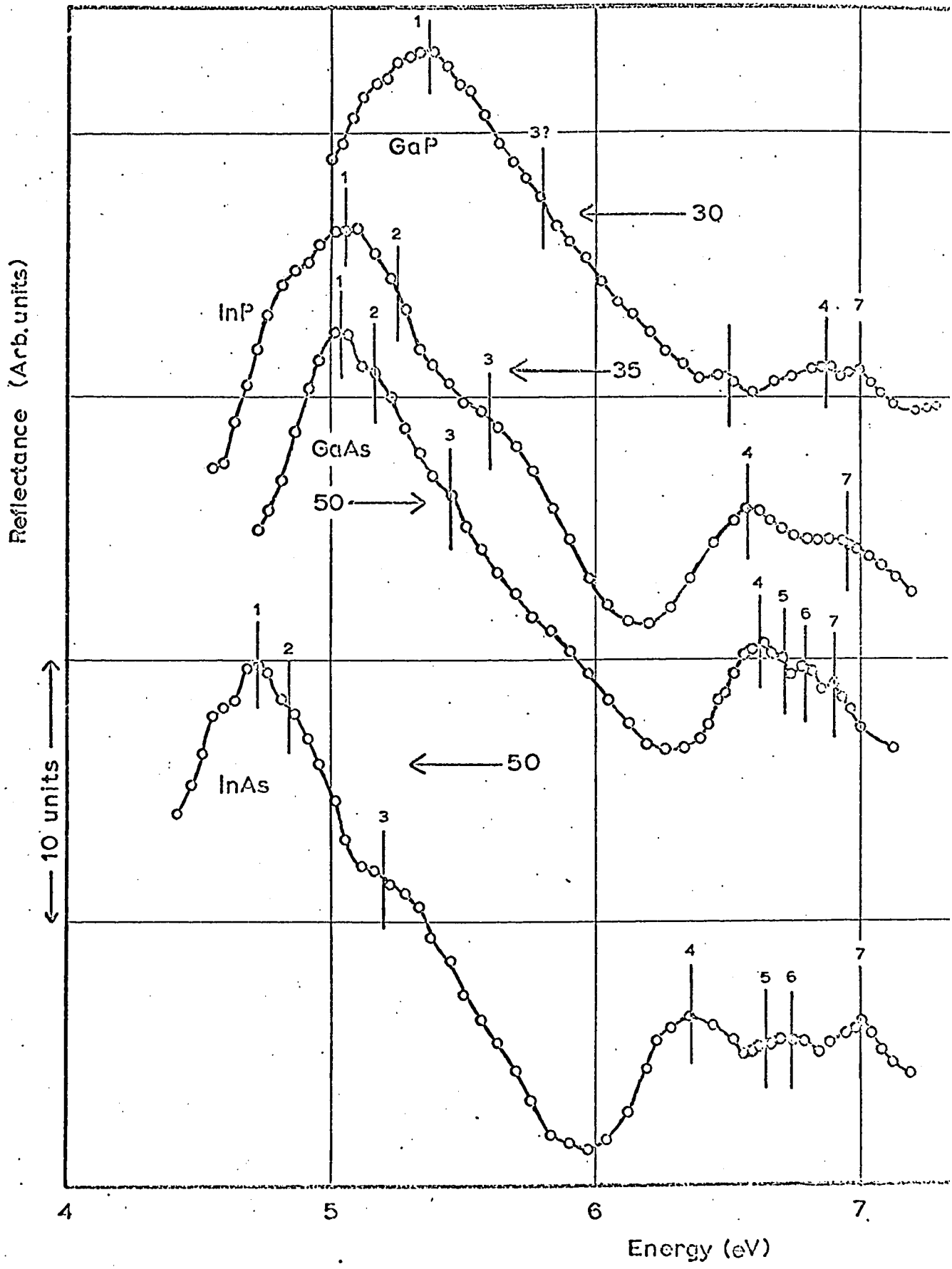

REFLECTANCE SPECTRA FIGURE 4.2

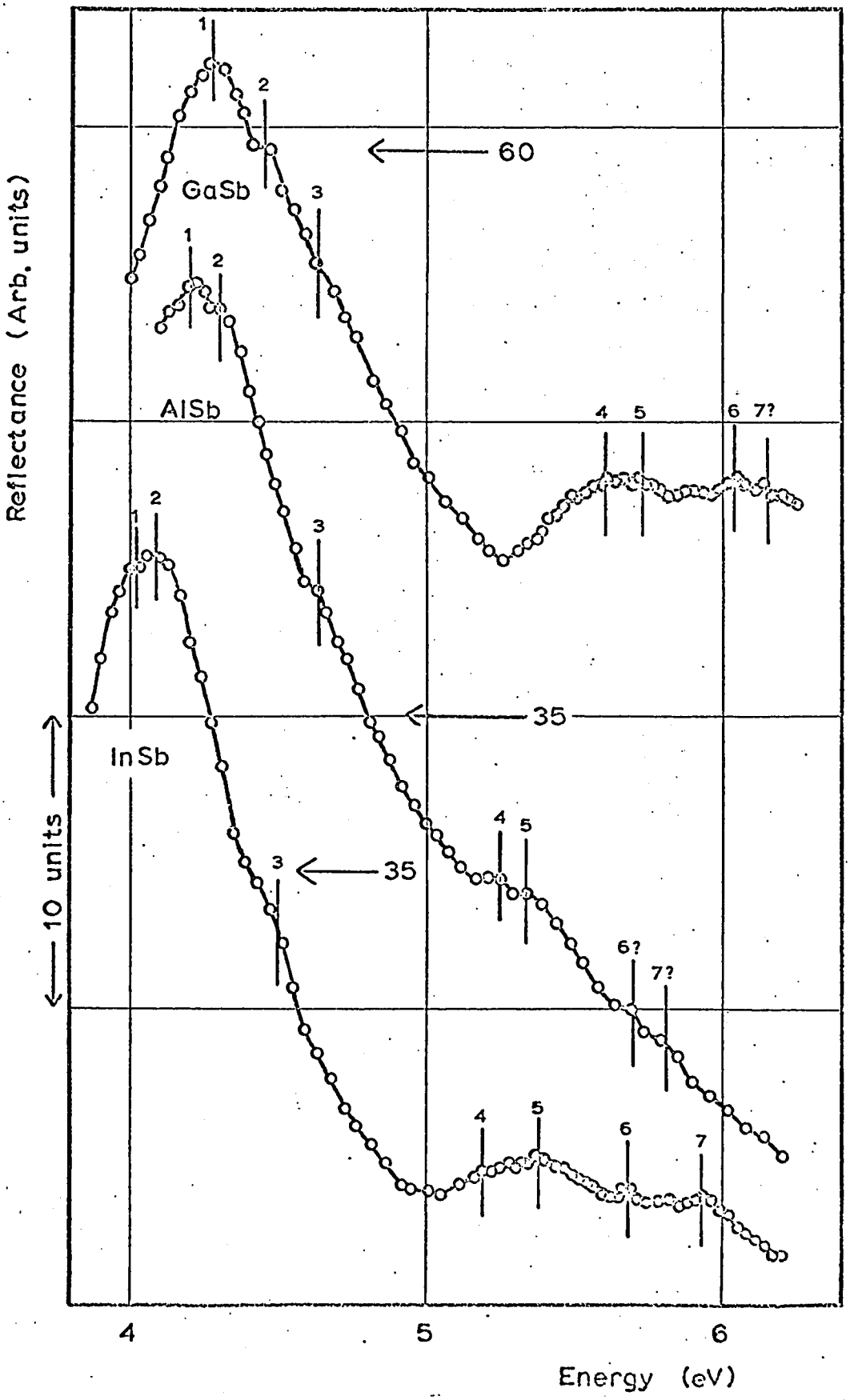

Peak 1 corresponds to E_0' and $E_0' + \Delta_0'$ transitions. While E_0' is a well investigated transition, data is not available for $E_0' + \Delta_0'$ in all III - V compounds. The $E_0' + \Delta_0'$ transition energies are determined for some III - V compounds in the present work.

The assignment of structure found as peaks and shoulders in the reflectance spectrum of a material to its band structure has been discussed in Section 2.5. It is seen that the assignment of E_2 peak particularly is not unambiguous. Contributions to this structure are shown to come from several critical interband transitions.[117,182,22,26,37] One of them which was originally suggested by Phillips[113] is the transitions between the X_5 valence and the X_1 conduction levels, shown in Fig. 2.5. The other transition responsible for the E_2 structure is $\Sigma_2 - \Sigma_1$ at a critical point along (110) direction.[26] The $X_5 - X_1$ assignment was strongly supported by the observation of the $E_2 + \delta$ peak corresponding to the transition $X_5 - X_3$.[162] The value of δ was estimated to be of the order of 0.4 ± 0.1 eV in all III - V compounds.[111] On this basis the E_2 and $E_2 + \Delta_2$ doublet structure which is shown in Figs. 4.1 and 4.2 by 1 and 2 are assigned to transitions between the spin orbit split X_{5V} and X_{1C} states. The value of Δ_2 obtained from experiment gives the spin orbit splitting of the X_5 valence level.

The E_1'structure is assigned to the transitions between the $L_{3V} - L_{3C}$ levels, shown in Fig. 2.5. Its observation in Ge and Si was significant in Brust's energy band calculations.[116] The experimental observation of E_1' is useful because this gap is found to be relatively insensitive to the choice of the core potential in the energy band calculations and therefore the observed peaks should agree with the

calculated values.[157] The doubly degenerate L_{3v} and L_{3c} states split under spin orbit interaction (Fig.2.5) and the E_1' complex should therefore contain four peaks. Instead a doublet was observed by Ehrenreich et al[158] in the reflectance spectra of GaAs, InAs and InSb which was interpreted in terms of the L_{3V} level splitting only assuming that the L_{3C} level splitting to be negligible.[183] In this case it is expected that Δ_1' which is equal to the spin orbit splitting of the L_{3V} level only should be of the same order of magnitude as Δ_1 which is the spin orbit splitting of the Λ_{3V} level. But the experimental values of Δ_1' are considerably larger than the values of Δ_1. Further, additional structure due to the L_{3C} level splitting was observed in the E_1' complex in the low temperature reflectance spectra of HgSe and HgTe.[184,181] In the electroreflectance spectrum of α-Sn, a triplet was observed in E_1' by Cardona et al.[35] In the reflectance spectra presently obtained for the III - V compounds, (Figs. 4.1 and 4.2) multiplet structure is clearly seen in the E_1' complex, and this should be assigned to the transitions between the spin orbit split L_3 valence and conduction levels.

The E_0' and $E_0' + \Delta_0'$ structures are due to transitions between the spin orbit split $\Delta_{5V} - \Delta_{1C}$ states, shown in Fig. 2.5. This inter-band critical point is located near the Brillouin zone center. The value of Δ_0' is the spin orbit splitting of the Δ_{5V} level close to the Γ point.

In the reflectance spectra shown in Figs. 4.1 and 4.2, the E_2 peak identified by 1 is a clear maximum which can be determined accurately. But the $E_2 + \Delta_2$ and $E_2 + \delta$ structures represented by 2 and 3 appear as shoulders on the high energy side of the main peak. In most

cases they can be clearly observed but their exact energy positions can be less easily determined. The accuracy of the $E_2 + \Delta_2$ and $E_2 + \delta$ energy values is 0.05 eV at best. The E_1' complex is broad in which two, three or four maxima can be detected. The value of Δ_1' which is the sum of the spin orbit split values of the L_{3V} and L_{3C} levels has been taken as the energy separation between the peaks 4 and 7. The individual values of L_{3V} and L_{3C} are determined whenever three or four peaks could be resolved in the E_1' complex. When four peaks are resolved the extreme peaks 4 and 7 represent the energy gaps E_1' and $E_1' + \Delta L_{3V} + \Delta L_{3C}$ ($= E_1' + \Delta_1'$) respectively. The assignment of peaks 5 and 6 between $E_1' + \Delta L_{3V}$ and $E_1' + \Delta L_{3C}$ transitions is guided by the available computed values for L_{3V} and L_{3C}.[127] When the spin orbit split values L_{3V} and L_{3C} are equal peaks 5 and 6 merge into one another resulting in only three peaks in the E_1' complex.[157] The energy values of the various peaks and the spin orbit splittings determined from Figs. 4.1 and 4.2 are listed in Table 4.1. The values determined only approximately are followed by a question mark. The experimental values of Cardona et al,[127] Ehrenreich et al[158] and also the theoretically computed values of various spin orbit splittings by Cardona et al[127] are included in the table for comparison. Below, results are discussed for each material.

GaP

The reflectance spectrum of GaP is shown in Fig. 4.1. In the E_2 complex, the E_2 peak is observed at 5.37 eV with the associated high energy shoulder due to $E_2 + \delta$ transition which is vaguely present at

TABLE 4.1

Peak energies and spin orbit splitting values.

( ) previous experimental values (Cardona et al[127] Ehrenreich et al[158])

( ) theoretically predicted values (Cardona et al[127])

Compound	E_2	$E_2+\Delta_2$	Δ_2	$E_2+\delta$	δ ---------- E_1' etc. ----------→				Δ_1'	ΔL_{3_V}	ΔL_{3_C}
GaP	5.37 (5.27)		 (0.01)	5.80? (5.74)	0.43 (0.47)	6.87			7.00	0.13 (0.16)	
InP	5.05 (5.04)	5.25 (5.24)	0.20 (0.21)	5.60 (5.60)	0.55 (0.56)	6.57			6.95	0.38 (0.38)	
GaAs	5.03 (4.99)	5.16	0.13 (0.07)	5.45 (5.33)	0.42 (0.34)	6.62 (6.6)	6.71	6.79	6.90 (6.9)	0.28 (0.29)	0.18 (0.18)	0.10 (0.11)
InAs	4.72 (4.70)	4.84	0.12 (0.03)	5.20 (5.18)	0.48 (0.48)	6.36 (6.4)	6.65	6.74	7.00 (7.0)	0.64 (0.53)	0.37 (0.28)	0.27 (0.25)
AlSb	4.20 (4.20)	4.30	0.10 (0.28)	4.64 (4.60)	0.44 (0.40)	5.25	5.34	5.70?	5.81?	0.56? (0.43)	0.46? (0.34)	0.10 (0.09)
GaSb	4.28 (4.20)	4.45	0.17 (0.29)	4.62 (4.57)	0.34 (0.37)	5.60 (5.50)	5.73	6.04	6.16?	0.56 (0.55)	0.43 (0.39)	0.13 (0.16)
InSb	4.02 (4.08)	4.09	0.07 (0.09)	4.50 (4.66)	0.48 (0.58)	5.19? (5.25)	5.38	5.68	5.93 (6.0)	0.74 (0.83)	0.55 (0.50)	0.27 (0.33)

5.80 eV. The second component of the complex, $E_2 + \Delta_2$ is not resolved perhaps because the estimated value of Δ_2 is only .007 eV.[127] In the E_1' complex, the two peaks located at 6.87 / 7.00 eV correspond to the E_1' and $E_1' + \Delta_1'$ transitions. The value of Δ_1' is 0.13 eV which is in good agreement with the calculated value, 0.16 eV.[127] The E_2 and $E_2 + \delta$ gaps determined presently are in good agreement with the published data.[101] The single peak observed for E_1' at 6.90 eV by Ehrenreich et al was resolved into a doublet at 6.67 / 6.90 eV in the reflectance spectrum determined by Thompson and Woolley[101] giving a value of 0.23 eV for Δ_1' which is larger than the present value (0.13 eV) and the estimated value, (0.16 eV).

InP

In the reflectance spectrum of InP, shown in Fig. 4.1, the E_2 $E_2 + \Delta_2$ and $E_2 + \delta$ transitions are assigned to the structures seen at 5.05, 5.25 and 5.60 eV respectively. The value of Δ_2 is 0.2 eV which agrees well with thermoreflectance results (0.25 eV, Table 4.2) and the computed value (0.21 eV).[127] Two peaks are observed in the E_1' complex at 6.57 / 6.95 eV corresponding to the E_1' and $E_1' + \Delta_1'$ transitions. This doublet was not resolved in previous experiments.[181] The energy of Δ_1' splitting is 0.38 eV which is also the computed value.[127] Because Δ_1' is considerably larger than the spin orbit splitting Δ_1 (0.14 eV, Tables 4.2 and 4.3), additional structure should be present in the E_1' complex due to the L_{3c} level splitting which should be of the order of 0.24 eV but this could not be resolved here. A shoulder is found at 4.90 eV on the low energy side of the E_2 peak which is assigned

to $E_0' + \Delta_0'$ transition. This assignment is in good agreement with the present thermoreflectance results for $E_0' + \Delta_0'$ (4.86 eV) given in Table 4.2. Taking the value of E_0' as 4.80 eV (thermoreflectance data from Table 4.2) the value of Δ_0' is 0.1 eV which compares well with the estimated value 0.09 eV and the value determined from electroreflectance measurements, 0.07 eV.[127]

GaAs

Both E_2 and E_1' complexes are well resolved in the reflectance spectrum of GaAs shown in Fig. 4.1. The E_2 transition energy agrees well with previous data. From the energy of the $E_2 + \Delta_2$ structure observed at 5.16 eV the Δ_2 splitting is determined as 0.13 eV which should be compared with the computed value 0.07 eV.[127] The E_1' and $E_1' + \Delta_1'$ doublet observed by Ehrenreich et al[158] and Thompson and Woolley[101] are in good agreement with the extreme peaks 4 and 7 at 6.62 / 6.90 eV giving a value of 0.28 eV for Δ_1'. The individual components of Δ_1', ΔL_{3_V} and ΔL_{3_C} are determined as 0.18 and 0.10 eV which agree with the corresponding estimated values 0.18 and 0.11 eV.[127]

InAs

In the reflectance spectrum of InAs shown in Fig. 4.1, the E_2, $E_2 + \Delta_2$ and $E_2 + \delta$ structures are clearly observed at 4.72, 4.84 and 5.20, respectively. The experimental value of Δ_2 (0.12 eV) which is very much larger than the estimated value (0.03 eV)[127] is in good agreement with the thermoreflectance data (0.13 eV, Table 4.2). The values of Δ_2 found in two other indium compounds are 0.2 eV in InP and 0.07 in InSb.

Therefore, the splitting of 0.12 eV which is somewhere in between the values obtained for InP and InSb seems to be a more probable value for InAs. The E_1' and $E_1' + \Delta_1'$ transition energies at 6.36 / 7.00 eV are in good agreement with Ehrenreich et al's[158] results. However, the value of Δ_1' which is 0.64 eV is larger than the estimated value, 0.53 eV.[127] From the positions of peaks 5 and 6 the individual values of ΔL_{3V} and ΔL_{3C} are determined as 0.37 and 0.27 eV. On the low energy side of the E_2 peak, the shoulder observed at 4.60 eV is attributed to $E_0' + \Delta_0'$ transition. This transition has not been observed before in either reflectance or modulated reflectance measurements. Taking the E_0' energy value as 4.38 eV from the electroreflectance data given in Table 4.3, the Δ_0' splitting is 0.22 eV which is in very good agreement with the computed value (0.22 eV).[127] The extrapolated value from the electroreflectance measurements on $Ga_xIn_{1-x}As$ alloy system[95] is 0.4 eV which is considerably larger than the value determined presently.

AlSb

From the reflectance spectrum of AlSb given in Fig. 4.2, the E_2, $E_2 + \Delta_2$ and $E_2 + \delta$ transition energies are determined as 4.20, 4.30 and 4.64 eV, respectively. In previous reflectance measurements the corresponding peak for E_2 is seen at 4.36 eV.[185] However, the present reflectance value is in good agreement with electroreflectance data[186] given in Table 4.1. The Δ_2 splitting is 0.1 eV which is very much lower than the estimated value 0.28 eV.[127] In the E_1' complex the peak positions are not without ambiguity. An approximate value of 0.56 eV is obtained for Δ_1' which should be compared with the estimated value of 0.43 eV.[127]

GaSb

In the reflectance spectrum of GaSb shown in Fig. 4.2, the E_2 complex is clearly observed. From the E_2 and $E_2 + \Delta_2$ energy values the splitting Δ_2 is found to be 0.17 eV which is lower than the estimated value 0.29 eV.[127] There is good agreement among the E_2 energy values determined presently from reflectance (4.28 eV), thermoreflectance (4.25 eV) and electroreflectance (4.28 eV) experiments. The E_1' complex is broad in which the E_1' and $E_1' + \Delta_1'$ doublet is found at 5.60 / 6.16(?) eV. The electroreflectance value for E_1' is 5.5 eV which is in good agreement with the present reflectance results. The value of Δ_1' is determined as 0.56 eV with values 0.43 and 0.13 for ΔL_{3_V} and ΔL_{3_C} respectively.[127]

InSb

In the InSb reflectance spectrum shown in Fig. 4.2, the E_2, $E_2 + \Delta_2$ and $E_2 + \delta$ energy values are 4.02, 4.09 and 4.50 eV, respectively. The spin orbit splitting Δ_2 is found to be 0.07 eV which is in good agreement with the calculated value 0.09 eV.[127] From the E_1' and $E_1' + \Delta_1'$ energy values 5.19(?) / 5.93 eV the value of Δ_1' is approximately 0.74 eV which is lower than the predicted value 0.83 eV.[127] The values of ΔL_{3_V} and ΔL_{3_C} are determined as 0.55 and 0.27 eV approximately which compares well with the calculated values 0.50 and 0.33 eV.[127]

From the results given in Table 4.1 it is seen that the E_2 transition energies determined presently are consistent with previous data. With E_2 as reference, the spin orbit splitting Δ_2 is determined knowing the $E_2 + \Delta_2$ energy positions. The Δ_2 values so determined are

compared with computed values. It is seen that fair agreement is obtained except in the cases of InAs, AlSb and GaSb. In the three cases the computed values are larger than the values determined from reflectance spectra. The $X_3 - X_1$ separation δ is found to be 0.4 ± 0.1 eV in all compounds as predicted except in InP. Near the shoulder due to $E_2 + \delta$ transition, structure corresponding to $E_2 + \Delta_2 + \delta$ should also be present.[184] As it is seen in the spectra of InP and InAs (Fig.4.1) the shoulder due to $E_2 + \delta$ is broad and the $E_2 + \Delta_2 + \delta$ is not quite resolved. Perhaps this is the reason for the higher value of δ found for InP. The results on E_1' complex obtained presently are in good agreement with the available previous data.[158] The measured values of Δ_1', ΔL_{3_V} and ΔL_{3_C} compare well with the estimated values.[127] It is found from the values of Δ_1 determined from thermoreflectance data (Table 4.2), electroreflectance data (Table 4.3) and previous data that ΔL_{3V} is of the same order of magnitude as Δ_1, within the limits of experimental uncertainty.

4.3 Results and Discussion of Thermoreflectance Measurements on III - V Compounds

Thermoreflectance spectra of several III - V compounds were determined in the energy range 1.5 to 6.0 eV. Representative spectra, $\Delta R/R$ versus $\hbar\omega$, for samples of GaP, GaAs, GaSb, InP, InAs and InSb are shown in Figs. 4.4 to 4.9. In all compounds except GaP temperature modulation was achieved by heating the sample directly by passing a periodic current pulse through the sample. The GaP sample was heated indirectly with a heater which was a thin layer of silver paint on a sapphire disc. Both direct and indirect heating techniques provided the same type of spectra. Details of the thermoreflectance experiment are given in Section 3.3.

In a thermoreflectance spectrum, structure is expected at critical point energies as is usually the case in a reflectance or an electroreflectance spectrum which has been discussed in Section 2.7. In Fig. 4.3, the reflectance spectra of InSb and GaSb are shown along with their thermoreflectance spectra over the same energy range for comparison. In the neighbourhood of the structure observed as peaks (maxima) in the reflectance spectra due to E_1 and $E_1 + \Delta_1$ transitions, the corresponding structure in the thermoreflectance spectra are seen as asymmetric inverted peaks (minima) for both transitions. A characteristic feature which can be conveniently chosen to determine the transition energies is the position where this minimum occurs in the thermoreflectance spectrum. It is seen immediately that the maxima in the reflectance spectra do not agree with the minima of the corresponding structure in the thermoreflectance spectra. Some of this shift and the breadth of the line shape of

FIGURE 4.3

REFLECTANCE AND THERMOREFLECTANCE SPECTRA

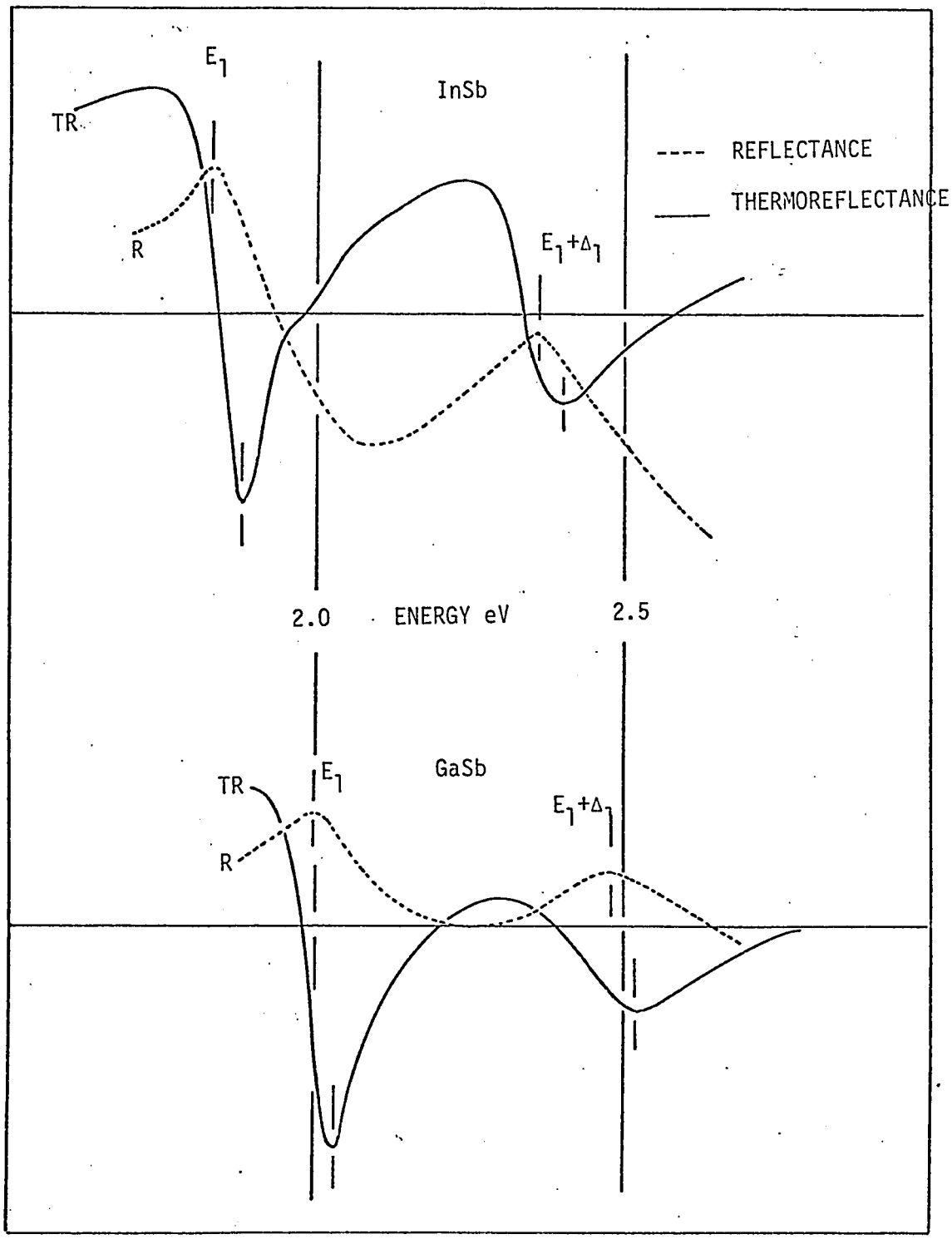

the structure in the thermoreflectance spectra are due to Lorentzian broadening. The effect of Lorentzian broadening on E_1 and $E_1 + \Delta_1$ line shapes has been shown in Fig. 2.9. Sharp structure with a minor shift of its position is observed when the broadening parameter is small. As the magnitude of this parameter is increased the peaks are shifted more as well as broadened. Therefore, the transition energy determined by taking the position of the minimum in the structure of a thermoreflectance spectrum does not represent the true band gap and hence may disagree with the results obtained by other experiments like reflectance and electroreflectance. Before contemplating a rigorous comparison of the critical band gaps determined by various experiments, these band gaps should be determined by careful line shape analysis which is complicated. Other sources which contribute to the shift of the peak and the breadth of the line shape are the quality of the sample surface and the homogeneity of the material. In the thermoreflectance spectra shown in Figs. 4.4 to 4.9, the energy positions corresponding to the negative going peaks (minima) are assumed to represent the critical band gaps. Therefore some disagreements should be expected when the present results are compared with the data obtained from other experiments. Whenever such a discrepancy occurred it is mentioned in the results given in this section.

The locations of interband critical points is fairly well known for zincblende materials over an energy of 0 - 10 eV, shown in Fig. 2.5. The interband transitions responsible for the structure observed in the thermoreflectance spectra in the energy range of the present experiment are the following.

The E_0 and $E_0 + \Delta_0$ peaks are the spin orbit split doublet associated with the transitions between $\Gamma_{15v} - \Gamma_{1c}$ states and Δ_0 gives the spin orbit splitting of the Γ_{15} valence state at $k \simeq 0$, which is shown in Fig. 2.5. The E_1 and $E_1 + \Delta_1$ peaks are due to transitions between $\Lambda_{3v} - \Lambda_{1c}$ levels and Δ_1 is the spin orbit splitting of the valence state. The E_0' and $E_0' + \Delta_0'$ peaks represent transitions between $\Delta_{5v} - \Delta_{1c}$ states which occur very close to the Γ point and hence the energy value obtained for E_0' should be close to the gap between $\Gamma_{15v} - \Gamma_{15c}$ levels. Δ_0' is the spin orbit splitting of the Δ_5 valence level again close to Γ. The E_2 structure has been discussed before and is considered to be due to the $X_{5v} - X_{1c}$ transition. The doublet E_2 and $E_2 + \Delta_2$ is due to the spin orbit splitting of the X_5 valence level. Another transition responsible for the E_2 structure is between $\Sigma_2 - \Sigma_1$ levels. Structure beyond the E_2 peak energies comes from the transitions between $L_{3v} - L_{3c}$ states and the E_1' peaks are beyond the energy range of the present experiment. The structure observed in the thermoreflectance spectra of III - V compounds is identified in terms of the above transitions and discussed for each material.

It should be mentioned that concurrently with this work, thermoreflectance spectra of III - V compounds were also determined by Matatagui et al.[140] The spectra shown in Figs. 4.3 to 4.8 are in good agreement with their spectra. While discussing their results, Matatagui et al[140] did not give the exact locations of the structure found in their spectra. In a few cases where the exact energy values were given they were determined from low temperature spectra. In the present discussion, the locations of structure found in the room temperature spectra are

given and they are compared with the data obtained presently from reflectance (Table 4.1) and electroreflectance (Table 4.3) measurements made on the compounds and previous electroreflectance results of Cardona et al.[127]

GaP

The thermoreflectance spectrum of GaP is given in Fig. 4.4. A doublet structure is observed at 2.73 and 2.90 eV in the fundamental gap energy region. If the doublet is due to E_0 and $E_0 + \Delta_0$ transitions, the corresponding spin orbit splitting Δ_0 is 0.17 eV which is larger than the value (0.10 eV) obtained for Δ_0 from electroreflectance results of Cardona et al.[127] But recently, Kyser et al,[187] while investigating the direct and indirect gap energy region in GaP by electroreflectance and electroabsorption techniques, observed structure due to direct gap transitions at 2.8 eV and three indirect gap transitions in the energy range 2.3 to 2.8 eV. The indirect gap $\Gamma_8 - L_1$ has been determined as 2.701 eV, while the $\Gamma_8 - X_1$ gap is 2.3 eV wide. In the light of these results it seems probable that the 2.90 eV structure is due to E_0 transitions and the peak at 2.73 eV corresponds to the $\Gamma_8 - L_1$ indirect gap. If these assignments were correct, indirect transitions could be observed in thermoreflectance spectra. The large peak at 3.6 eV corresponds to E_1 transition and its close associate, the $E_1 + \Delta_1$ peak, is not resolved. The structure observed at 4.68 eV corresponds to the E_0' transitions. The E_2 peak is seen at 5.28 eV which is in good agreement with electroreflectance results (5.27 eV).[127]

FIGURE 4.4

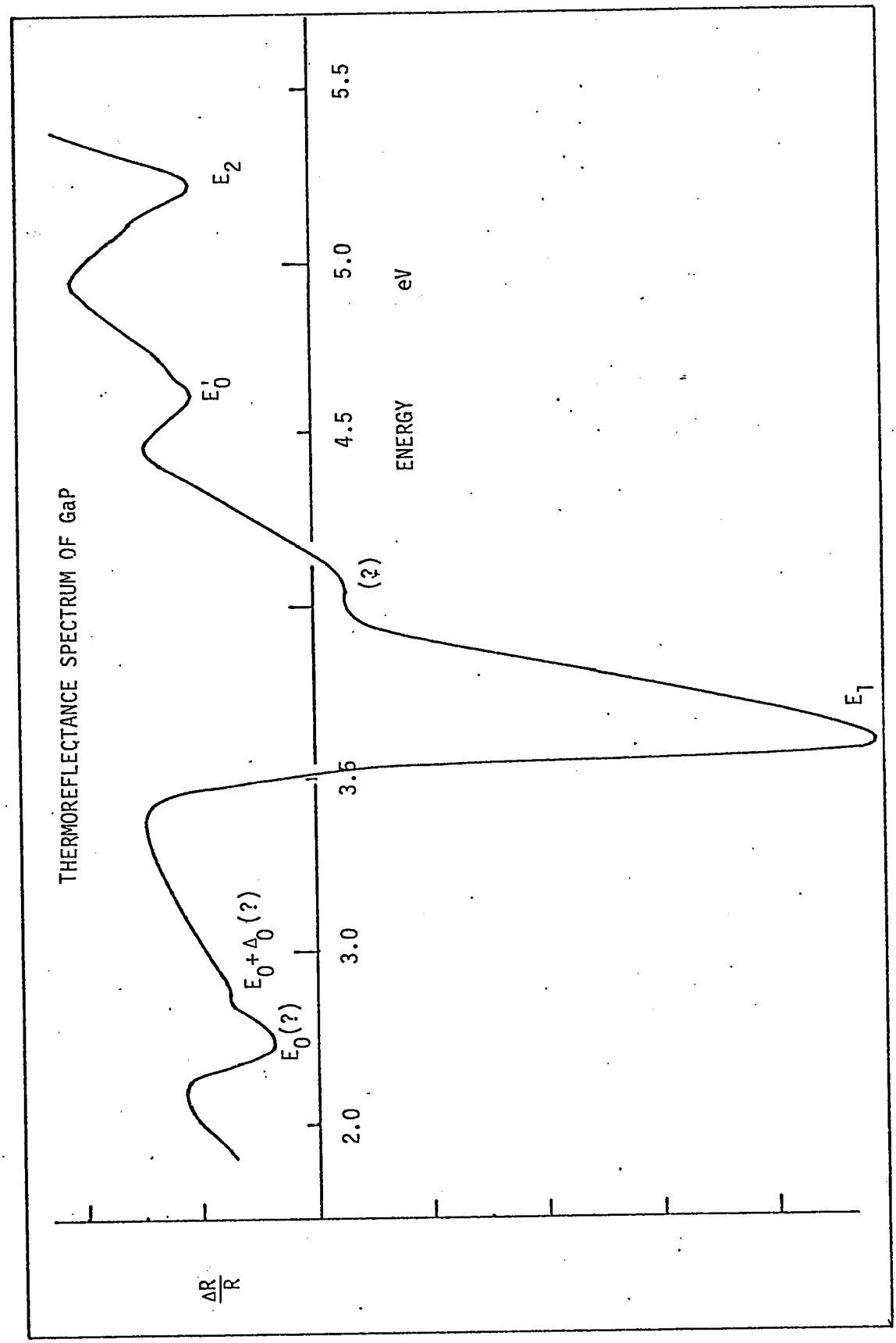
THERMOREFLECTANCE SPECTRUM OF GaP
$\frac{\Delta R}{R}$
$E_0(?)$
$E_0+\Delta_0(?)$
E_1
(?)
E_0'
E_2
2.0
3.0
3.5
4.5
5.0
5.5
ENERGY
eV

GaAs

In Fig. 4.5 the thermoreflectance spectrum of GaAs is shown. The E_0 and $E_0 + \Delta_0$ transition energies are 1.48 and 1.78 eV respectively. The spin orbit splitting Δ_0 is 0.3 eV which is lower than the value determined from electroreflectance data. This is because in the spectrum of GaAs the structure due to E_0 is quite broad compared with other structure. The transition energy determined from this structure (1.48 eV) is larger than the previous value (1.44 eV) determined by electroreflectance technique.[127] The E_1 and $E_1 + \Delta_1$ transitions are responsible for the structures observed at 2.88 and 3.12 eV respectively. These values are in very good agreement with the energies of $E_1(1)$ and $E_1(1) + \Delta_1$ swings in the oscillatory structure observed in the electroreflectance spectrum of GaAs.[127] It should also be mentioned that the E_1 and $E_1 + \Delta_1$ peaks in the reflectance spectrum of GaAs are close to the $E_1(1)$ and $E_1(1) + \Delta_1$ oscillations which implies good agreement of present results also with the reflectance data.[181] The peaks at 4.44 and 5.06 eV correspond to E_0' and E_2 transitions.

GaSb

The thermoreflectance spectrum of GaSb is shown in Fig. 4.6. The energies of the fundamental gap and its spin orbit split component are not in the range of this experimental setup and therefore their structure is not observed. The E_1 and $E_1 + \Delta_1$ transitions are located at 2.04 and 2.52 eV respectively. The spin orbit splitting Δ_1 is 0.48 eV which compares well with the computed value 0.49 eV and the value obtained from the electroreflectance measurements, 0.47 eV (Table 4.3).

FIGURE 4.5

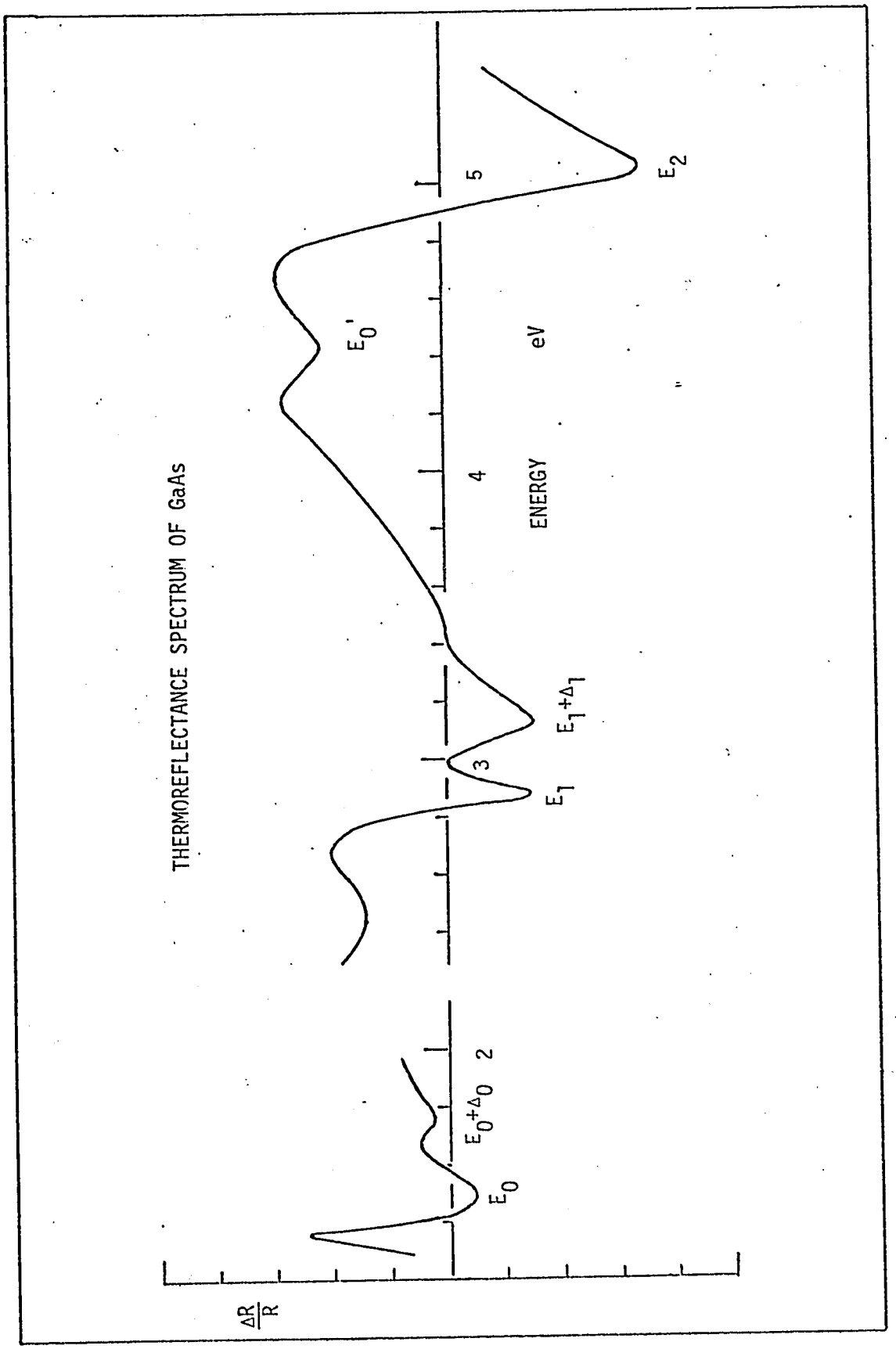
THERMOREFLECTANCE SPECTRUM OF GaAs
$\frac{\Delta R}{R}$
E_0
$E_0+\Delta_0$
E_1
$E_1+\Delta_1$
E_0'
E_2
2
3
4
5
ENERGY eV

FIGURE 4.6

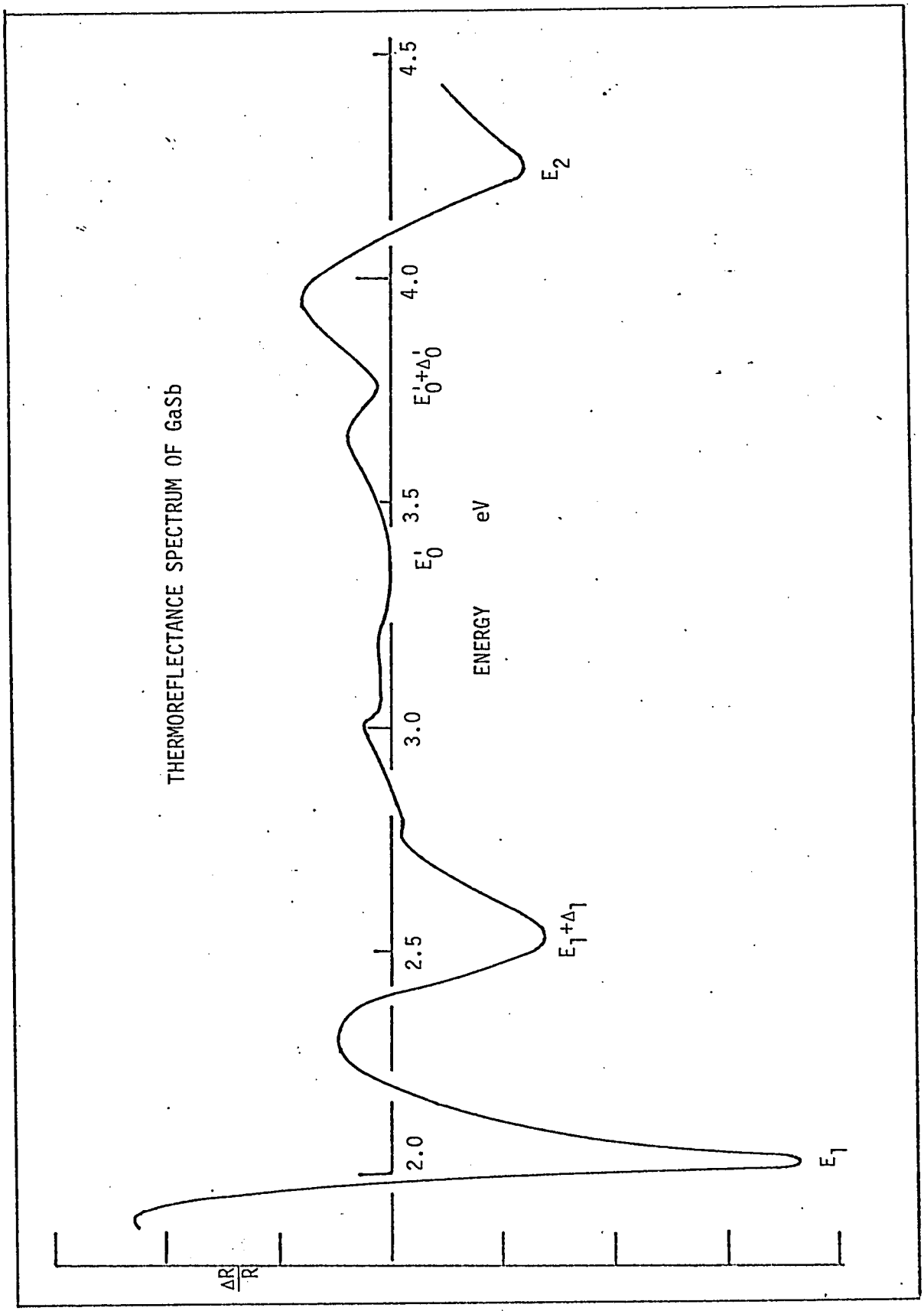
THERMOREFLECTANCE SPECTRUM OF GaSb
ENERGY eV
2.0
2.5
3.0
3.5
4.0
4.5
E_1
$E_1+\Delta_1$
E_0'
$E_0'+\Delta_0'$
E_2
$\frac{\Delta R}{R}$

The E_2 energy gap is 4.25 eV which is in good agreement with the value obtained from reflectance measurements (Table 4.1). The structure observed at 3.75 eV is assigned to transitions in the E_0' complex. While the E_0' and $E_0' + \Delta_0'$ transition energy values are 3.27 and 3.56 eV from electroreflectance data, a triplet was observed by Matatagui et al[140] in the thermoreflectance spectrum at 3.2, 3.65 and 3.8 eV respectively. On this basis the structure seen presently at 3.75 eV is assigned to $E_0' + \Delta_0'$. Also structure is observed around 3.3 eV which is weak for a definite assignment to E_0'. The value of Δ_0' (0.45 eV) is close to the computed value (0.48 eV)[127] and also agrees with the electroreflectance results given in Table 4.3. The previous value for Δ_0' from Cardona et al's[127] electroreflectance results is 0.29 eV.

InP

In the thermoreflectance spectrum of InP shown in Fig. 4.7, the $E_1$and $E_1 + \Delta_1$ doublet is clearly resolved and their respective values are 3.14 and 3.28 eV. The spin orbit splitting Δ_1 is 0.14 eV which is also the value determined from the electroreflectance measurements given in Table 4.3. The value for Δ_1 is in good agreement with 0.15 eV determined by Cardona et al,[127] and the computed value which is 0.11 eV. The structure appearing as a shoulder on the low energy side of the E_2 peak at 4.80 eV corresponds to E_0' transition with the spin orbit split component present at 4.86 eV. The splitting Δ_0' is 0.06 eV which is in good agreement with the value 0.07 eV determined from electroreflectance measurements by Cardona et al.[127] In the reflectance spectrum of InP shown in Fig. 4.1, the $E_0' + \Delta_0'$ is seen

FIGURE 4.7

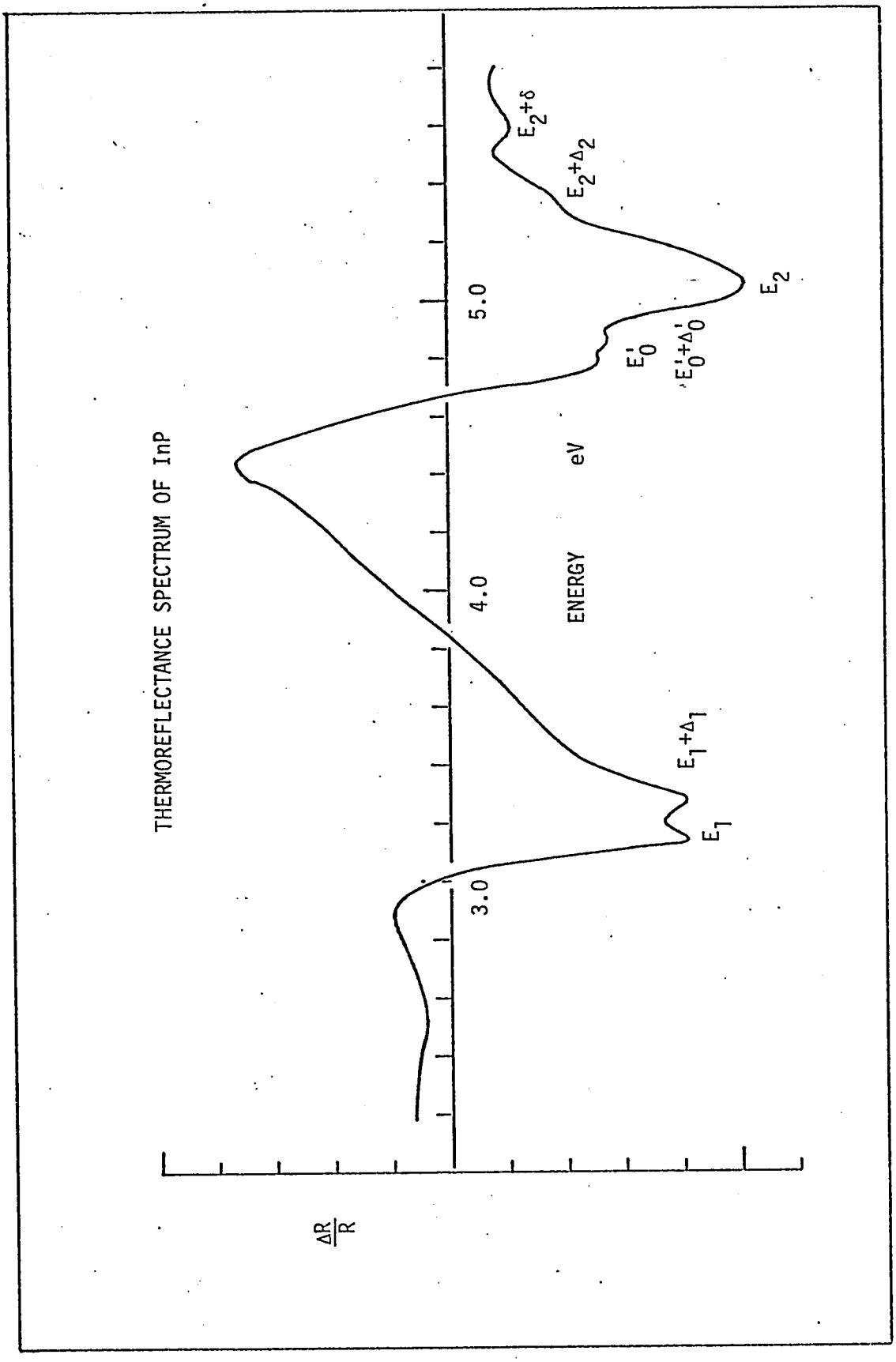
THERMOREFLECTANCE SPECTRUM OF InP
$\frac{\Delta R}{R}$
3.0
4.0
5.0
ENERGY eV
E_1
$E_1+\Delta_1$
E_0'
$E_0'+\Delta_0'$
E_2
$E_2+\Delta_2$
$E_2+\delta$

as a shoulder at 4.9 eV which compares well with the value obtained from the thermoreflectance measurements. The E_2 peak is seen at 5.05 eV. The structure seen beyond the E_2 peak at 5.3 and 5.6 eV represent the $E_2 + \Delta_2$ and $E_2 + \delta$ transitions respectively. The corresponding values to compare are 5.25 and 5.60 eV which are determined from the reflectance spectrum given in Fig. 4.1.

InAs

The thermoreflectance spectrum of InAs is shown in Fig. 4.8. The E_1 and $E_1 + \Delta_1$ transitions correspond to the peaks at 2.56 and 2.86 eV respectively. The value of Δ_1 is 0.3 eV which agrees well with the estimated value, 0.29 eV.[127] The E_0' structure is seen at 4.64 eV as a shoulder on the low energy side of the E_2 peak which is located at 4.83 eV. Both E_0' and E_2 values are larger than the values determined by electroreflectance technique.[127] This discrepancy is suspected to be due to the shift and broadening of the peaks. The shoulder at 4.96 eV corresponds to $E_2 + \Delta_2$ giving a value 0.13 eV for Δ_2 which is in good agreement with the reflectance data given in Table 4.1.

InSb

In Fig. 4.9, the thermoreflectance spectrum of InSb is given. The E_1 and $E_1 + \Delta_1$ gap energies are 1.88 and 2.40 eV respectively. The spin orbit splitting Δ_1 is 0.52 eV which is in good agreement with the computed value, 0.53 eV.[127] There is some disagreement among the values measured for E_1 transition energy by reflectance (1.83 eV), electroreflectance (1.87 eV) and thermoreflectance (1.88 eV) experiments.

FIGURE 4.8

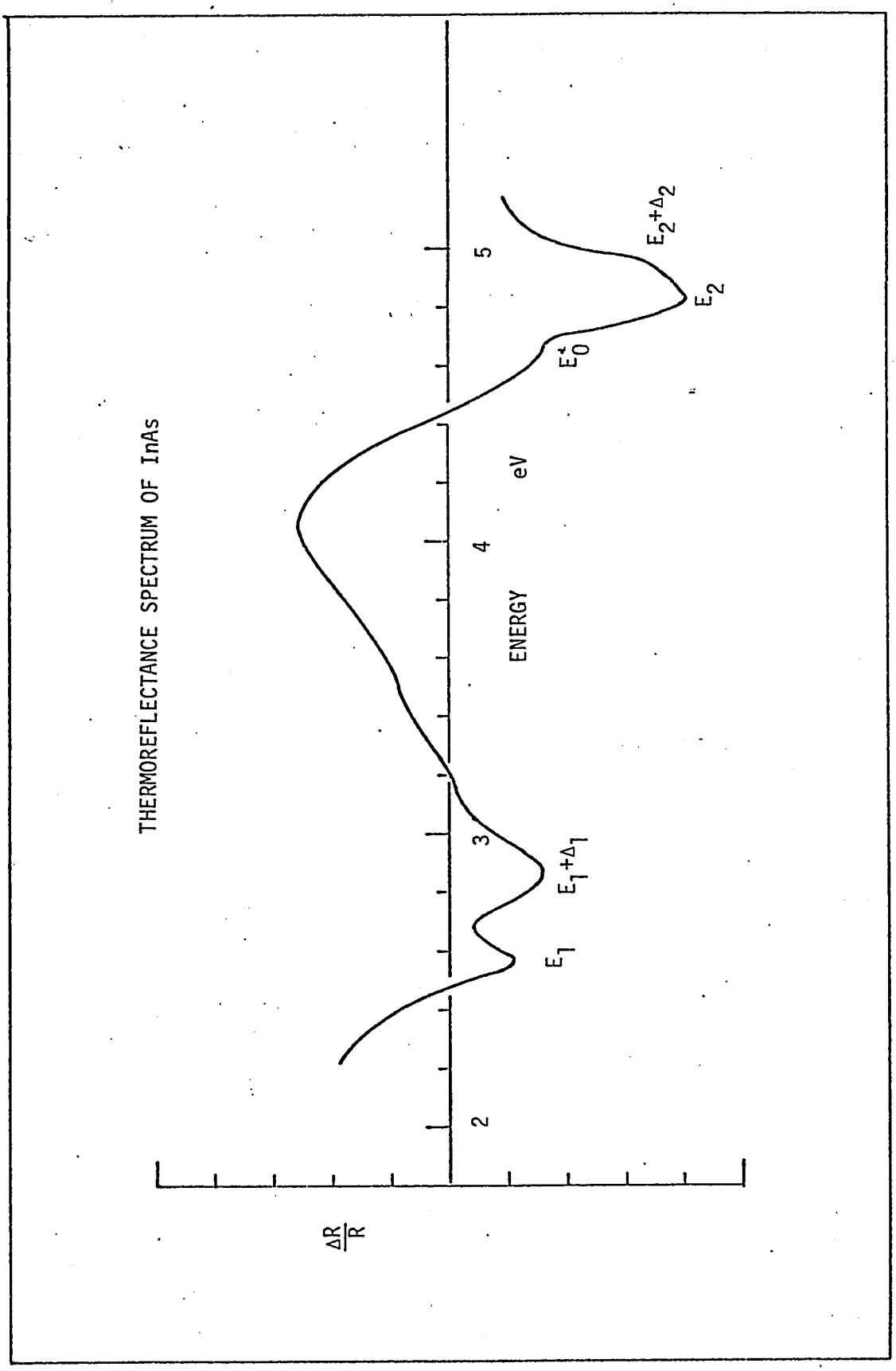
THERMOREFLECTANCE SPECTRUM OF InAs
$\frac{\Delta R}{R}$
2
3
4
5
ENERGY
eV
E_1
$E_1+\Delta_1$
E_0'
E_2
$E_2+\Delta_2$

FIGURE 4.9

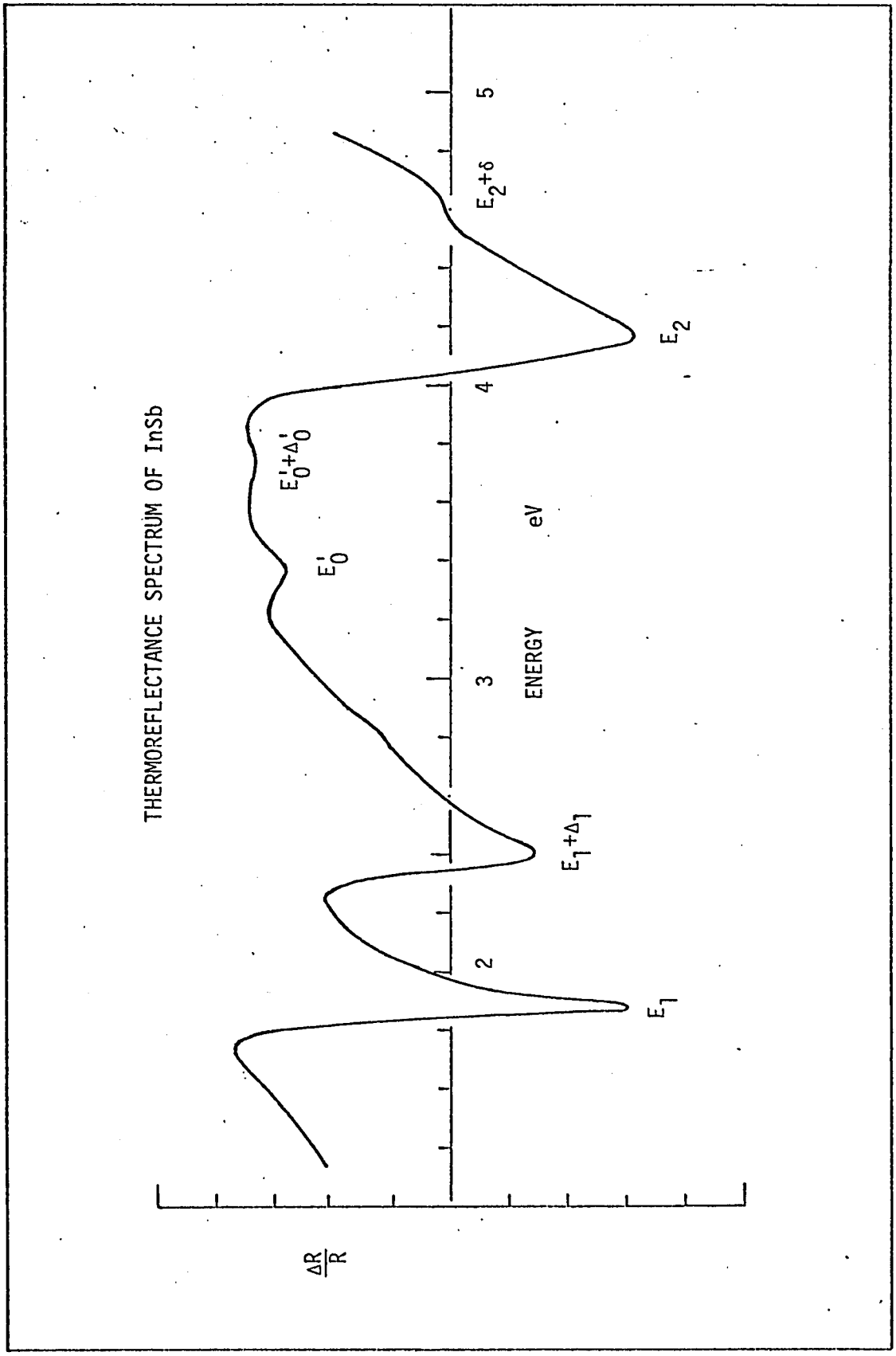
THERMOREFLECTANCE SPECTRUM OF InSb
$\frac{\Delta R}{R}$
2
3
4
5
ENERGY
eV
E_1
$E_1+\Delta_1$
E_0'
$E_0'+\Delta_0'$
E_2
$E_2+\delta$

A pair of weak but clear peaks are observed at 3.36 and 3.74 eV which represent the E_0' and $E_0' + \Delta_0'$ transition giving for Δ_0' a value of 0.38 eV which compares well with the value (0.36 eV) obtained from electroreflectance measurements given in Table 4.3. The structures corresponding to E_2 and $E_2 + \delta$ are found at 4.17 and 4.6 eV respectively. The E_2 transition energy is higher than the values determined by reflectance and electroreflectance measurements as it has been found also in the case of InAs.

The various energy gap values determined from the spectra shown in Figs. 4.4 to 4.9 are listed in Table 4.2. For comparison, the electroreflectance results of Cardona et al[127] are included in the table. Structure due to the fundamental gap is seen only in the spectra of GaP and GaAs. The fundamental gap energies in the other compounds fall below the low energy limit of the present experiment. It seems possible from the structure observed at 2.73 eV which corresponds to the $\Gamma_8 - L_1$ indirect gap in GaP, that structure due to indirect transitions could be observed in thermoreflectance spectra. The doublet structure with its characteristic line shape due to the E_1 and $E_1 + \Delta_1$ transitions is seen clearly in the spectra of all compounds except in GaP because of the small spin orbit splitting for Δ_1 in this material. The values of Δ_1 are in good agreement with previous data. While the E_0' structure is clearly observed in all six compounds, structure due to $E_0' + \Delta_0'$ is seen only in GaSb, InP and InSb. This is because the $E_0' + \Delta_0'$ structure is relatively weak compared with other structures in the spectrum and also it is situated very near to the strong structure due to E_2 transitions. The Δ_0' splittings are in good agreement with the computed values. In

TABLE 4.2

Energies of various transitions determined from thermoreflectance spectra

Values given in ( ) are from electroreflectance results of Cardona et al.[127]

Material	E_0eV	$E_0+\Delta_0$eV	E_1eV	$E_1+\Delta_1$eV	E_0'eV	$E_0'+\Delta_0'$eV	E_2eV	$E_2+\Delta_2$eV	$E_2+\delta$
GaP	2.73 (2.74)	2.9(?) (2.84)	3.6 (3.66)	- -	4.68 (4.78)	- -	5.28 (5.27)	=	=
GaAs	1.48 (1.43)	1.78 (1.77)	2.88 (2.89)	3.12 (3.12)	4.44 (4.44)	=	5.06 (4.99)	=	=
GaSb	=	=	2.04 (2.03)	2.52 (2.49)	3.30 (3.27)	3.75 (3.56)	4.25 (4.20)	=	=
InP	=	=	3.14 (3.12)	3.28 (3.27)	4.8 (4.72)	4.86 (4.79)	5.05 (5.04)	5.3 (5.24)	5.6 (5.6)
InAs	=	=	2.56 (2.50)	2.86 (2.78)	4.64 (4.44)	=	4.83 (4.70)	4.96 -	=
InSb	=	=	1.88 (1.88)	2.40 (2.38)	3.36 (3.16)	3.74 (3.49)	4.17 (4.08)	=	4.6 (4.66)

the E_2 complex, E_2 is observed in all compounds. Unlike in the electroreflectance spectra, the E_2 structure is quite strong in thermoreflectance. The structure due to $E_2 + \Delta_2$ can be identified in the spectra of InP and InAs only. The values of Δ_2 agree with those determined from reflectance spectra, (Table 4.1). In the spectra of InP and InSb structure due to $E_2 + \delta$ is identified and the values of agree with the known ones.

4.4 A Results of Reflectance Measurements on $Ga_xIn_{1-x}Sb$ Alloy

Near normal incidence reflectance measurements were made on samples of $Ga_xIn_{1-x}Sb$ alloy in the low (1.5 to 4.5 eV) and high (3.5 to 6.5 eV) energy regions of the optical spectrum. Reflectance spectra of the compounds InSb and GaSb determined in the low energy region are shown in Fig. 4.10. Two peaks due to E_1 and $E_1 + \Delta_1$ transitions are observed at energies 1.83 and 2.38 eV in InSb and 2.00 and 2.48 eV in GaSb which are in good agreement with earlier reflectance data of Woolley and Blazey,[81] (1.82 and 2.33 eV in InSb and 1.97 and 2.24 eV in GaSb.) Typical reflectance spectra of two alloy specimens, namely the 20 and 50 mole percent of GaSb in InSb ($x = 0.2$ and 0.5) are shown in Fig. 4.10. Again two peaks are noticed as in the spectra of the compounds which are assigned similarly to E_1 and $E_1 + \Delta_1$ transitions. It is seen from the four spectra given in Fig. 4.10 that there is very little shift in the positions of the E_1 and $E_1 + \Delta_1$ structures in the spectra of InSb, $Ga_{.2}In_{.8}Sb$ and $Ga_{.5}In_{.5}Sb$ samples. This is shown more clearly in Fig. 4.11 where the composition dependence of E_1 and $E_1 + \Delta_1$ peak energies are plotted. The energy gap variation as a function of composition is continuous and nonlinear for both E_1 and $E_1 + \Delta_1$ transitions.

The reflectance spectra determined in the high energy range for InSb and GaSb are shown in Fig. 4.2. The structure observed in those spectra has been assigned to the E_2 and E_1' complexes (Section 4.2). Typical reflectance spectra of four alloy samples in this energy region are shown in Figs. 4.12 and 4.13. In these spectra, the structure observed is assigned to E_2 and E_1' transition complexes guided by the

FIGURE 4.10

REFLECTANCE SPECTRA OF $Ga_xIn_{1-x}Sb$

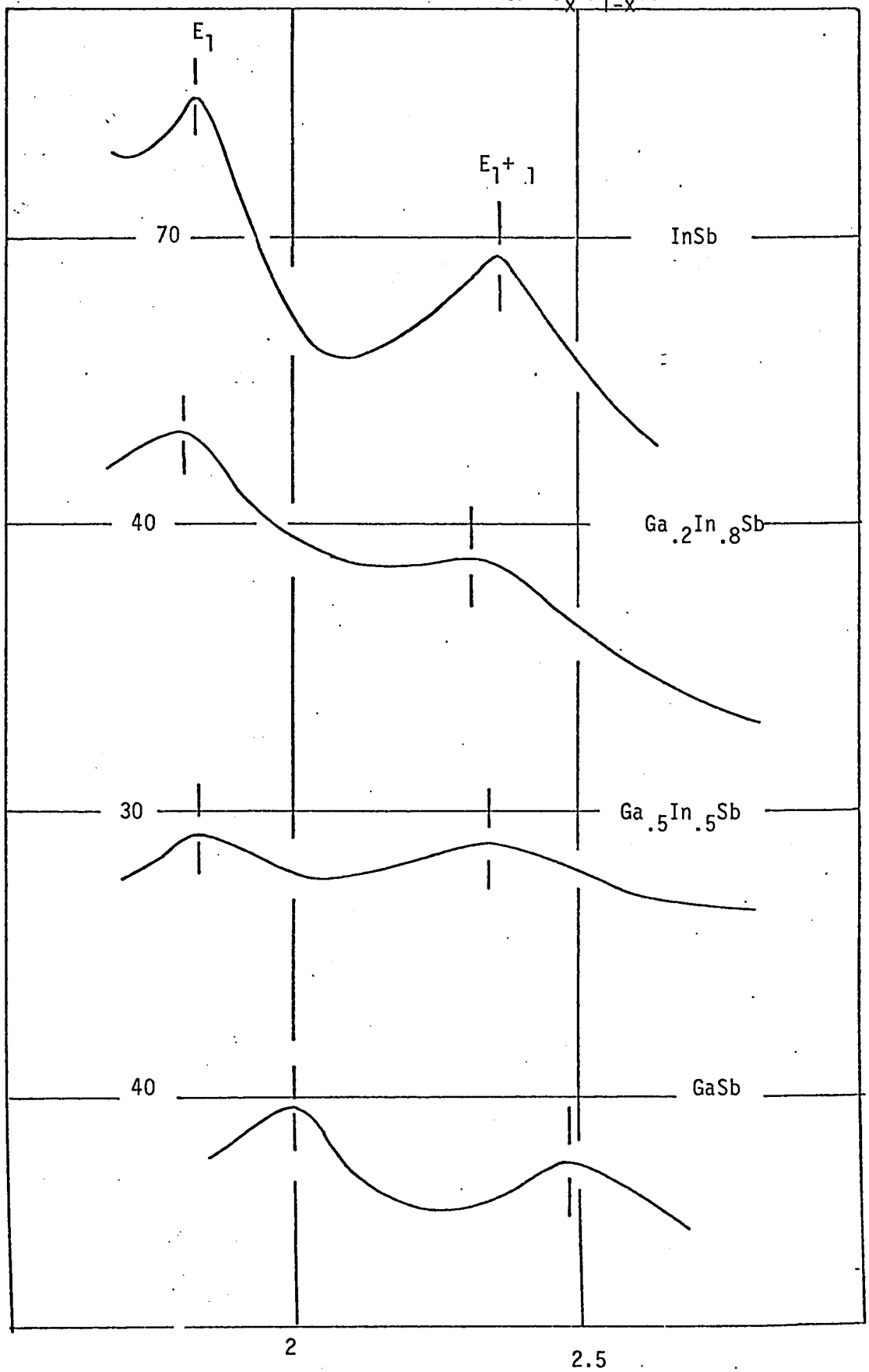

FIGURE 4.11

TRANSITION ENERGIES Versus COMPOSITION

$Ga_xIn_{1-x}Sb$ ALLOYS

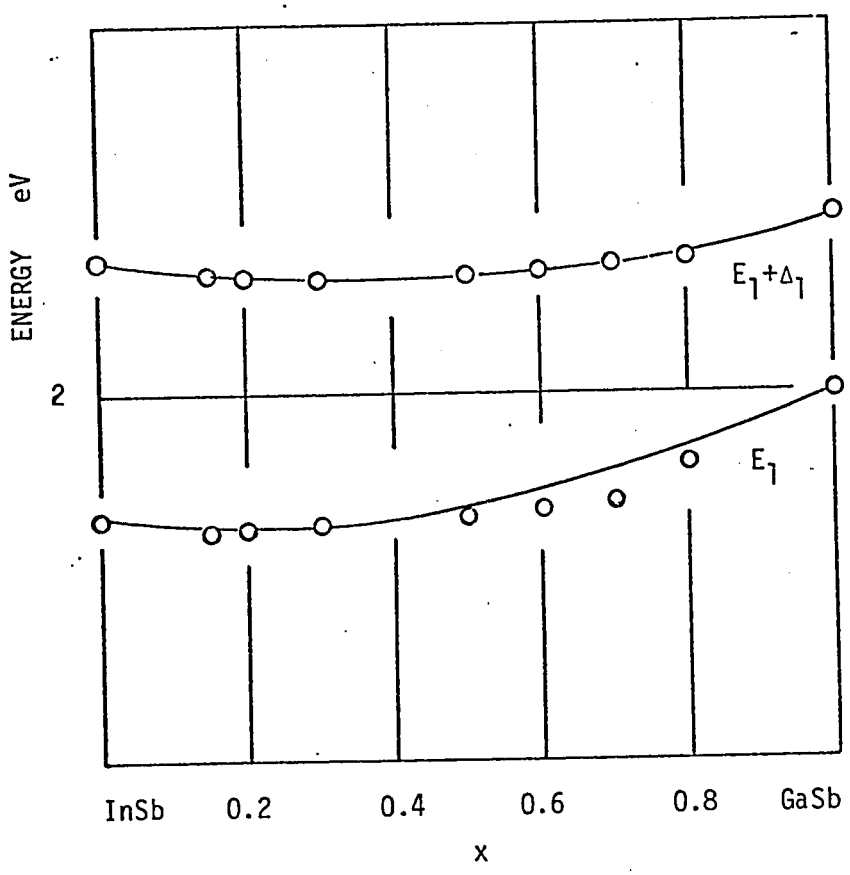

FIGURE 4.12

REFLECTANCE SPECTRA OF $Ga_xIn_{1-x}Sb$ ALLOYS

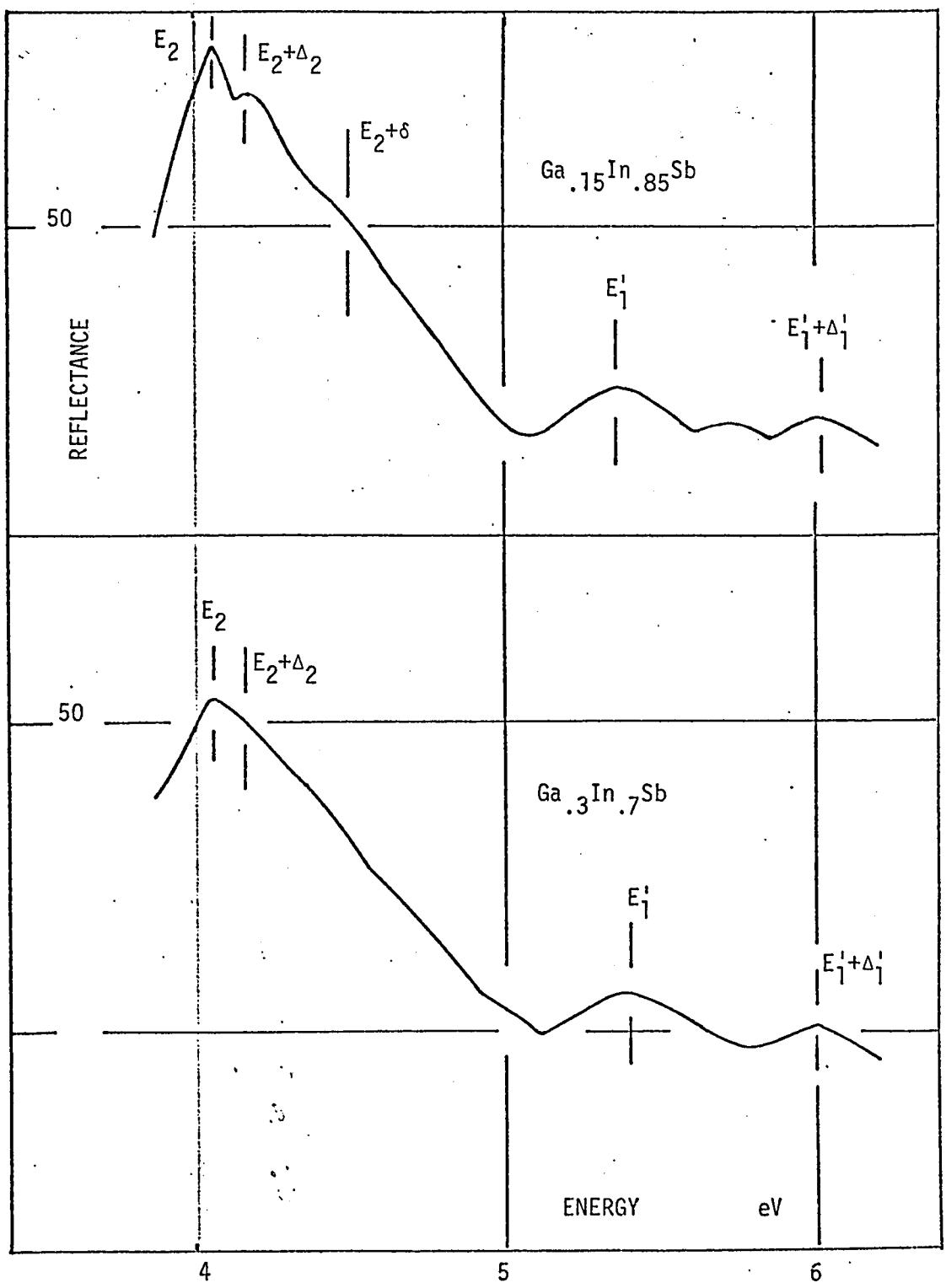

FIGURE 4.13

REFLECTANCE SPECTRA OF $Ga_xIn_{1-x}Sb$ ALLOYS

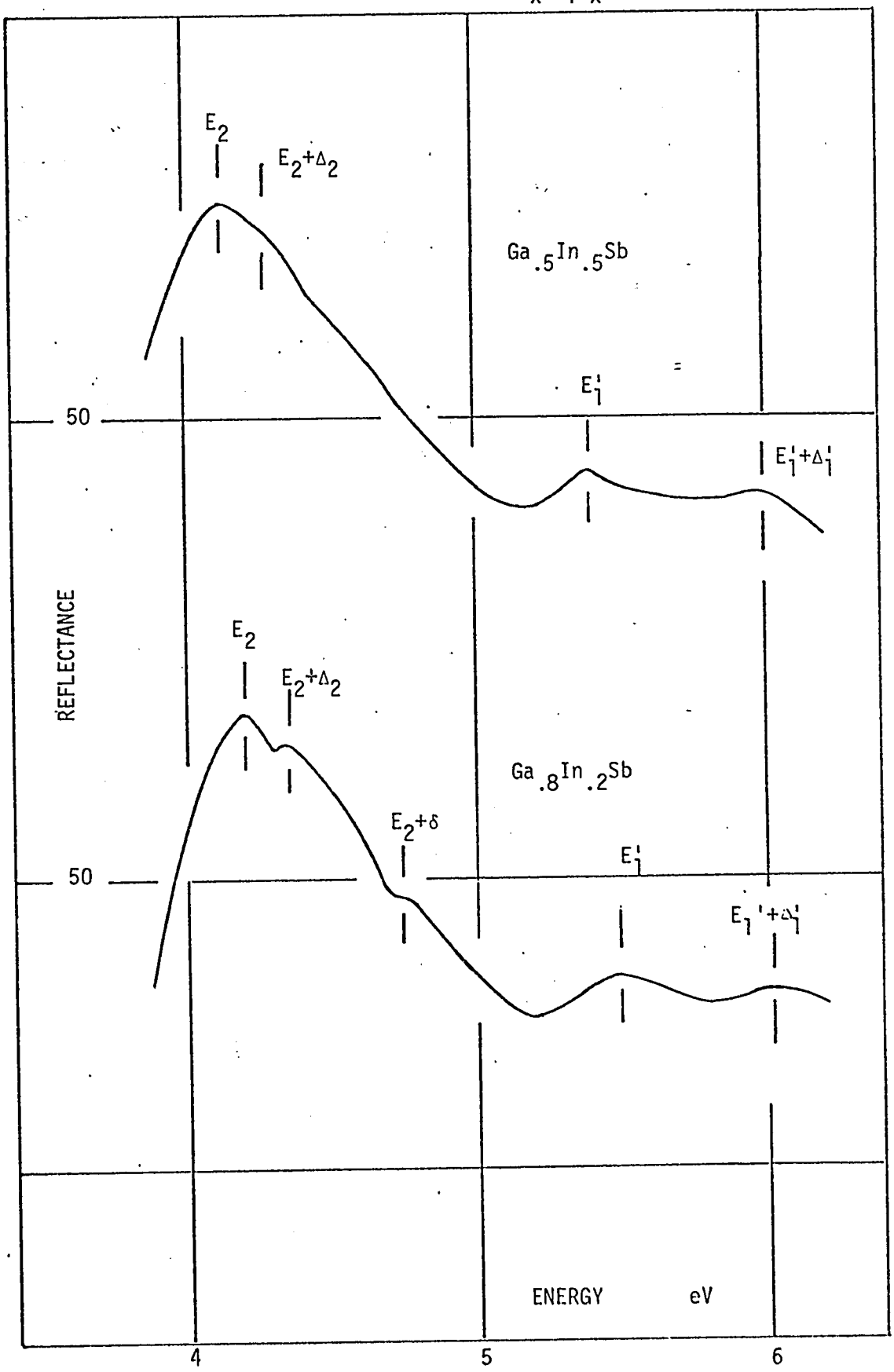

spectra of the compounds (Fig. 4.2). In the order of increasing energy the transitions responsible for the observed structure are E_2, $E_2 + \Delta_2$, $E_2 + \delta$, E_1' and $E_1' + \Delta_1'$. Multiplet structure has been observed in the E_1' complex of a few alloy samples (Fig. 4.12, $x \simeq 0.15$). However, due to large scatter in the experimental data, individual values of ΔL_{3_V} and ΔL_{3_C} are not determined.

The composition dependence of the energies of various transitions observed in the high energy region is shown in Fig. 4.14. It is seen that the E_2 gap variation as a function of composition is nonlinear. The $E_2 + \Delta_2$ versus x curve is shown by a straight line within the limits of experimental uncertainty. The $E_2 + \Delta_2$ gap shift as a function of composition has not been investigated before in III - V alloys. The composition dependence of $E_2 + \delta$ is assumed to be linear. The structures representing $E_2 + \Delta_2$ and $E_2 + \delta$ both appear as shoulders on the main E_2 peak. Therefore, their positions are determined with less accuracy when compared with the precision achieved in determining the position of a peak with a clear maximum. Because the deviation observed from linearity is small in E_2 gap variation with composition, if there is any similar small deviation in $E_2 + \Delta_2$ and $E_2 + \delta$ gap shifts, these may not be observable within the limits of experimental uncertainty. The E_1' and $E_1' + \Delta_1'$ peak positions determined in the alloy spectra are shown to shift linearly as a function of composition. A linear extrapolation of the alloy data shows disagreement of the E_1' and $E_1' + \Delta_1'$ values found in the compounds. This discrepancy is because in the spectra of alloy samples the multiplet structure present in the E_1' complex has not been resolved due to scatter in the experimental values.

FIGURE 4.14

TRANSITION ENERGIES Versus COMPOSITION

$Ga_xIn_{1-x}Sb$ ALLOYS

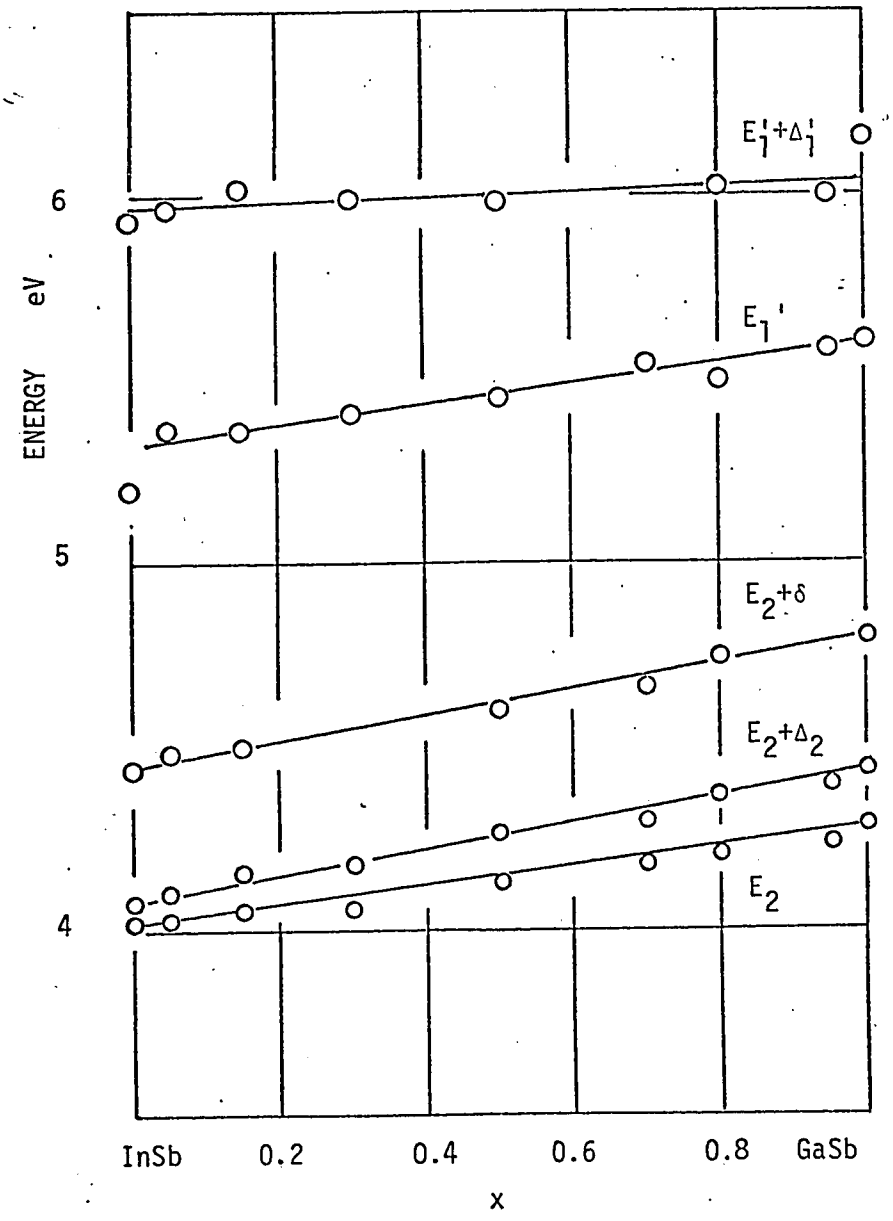

Previous reflectance measurements on this alloy system were made by Woolley and Blazey.[81] The composition dependence of the energy of each peak observed, E_1, $E_1 + \Delta_1$, and E_2 , was shown to be linear within the limits of experimental uncertainty. It is seen from the present results given in Figs. 4.11 and 4.14, the E_1, $E_1 + \Delta_1$ and E_2 gap variation is nonlinear as a function of composition. As there is good agreement between the energy gaps measured in the compounds, the disagreement in the alloy data is probably due to the quality of the alloy material. Further studies using the thermoreflectance and electroreflectance techniques confirmed the nonlinear nature of the E_1, $E_1 + \Delta_1$ and E_2 gap variation with composition. Below, results of the thermoreflectance experiment on the $Ga_xIn_{1-x}Sb$ alloy system are given.

4.4 B Results of Thermoreflectance Measurements on $Ga_xIn_{1-x}Sb$ Alloy

In the present work, thermoreflectance technique has been added to the list of methods available for alloy studies. Thermoreflectance spectra of samples of $Ga_xIn_{1-x}Sb$ alloy were determined in the energy range 1.5 to 6.0 eV. A few typical spectra are shown in Figs. 4.15 to 4.18. They bear a close resemblance to the spectra obtained for the compounds InSb and GaSb which are shown in Figs. 4.9 and 4.6 respectively. The structure found in the spectra of InSb and GaSb has been assigned to E_1, $E_1 + \Delta_1$, E_0', $E_0' + \Delta_0'$, E_2 and $E_2 + \delta$ transitions in the order of increasing energy over the energy range 1.5 to 6.0 eV (Section 4.3). Over the same energy range only part of the structure is seen clearly in the spectra of the alloy samples. The structure due to E_1, $E_1 + \Delta_1$ and E_2 are clearly observed. While the E_1 and $E_1 + \Delta_1$ line shapes are uniformly of the same quality, considerable variation of size and sharpness of E_2 structure is observed in the spectra of the alloy samples. This is found to be a major source of uncertainty in the values determined for E_2 transition energy.

The composition dependence of various transition energies is shown in Fig. 4.19. The E versus x curve for the E_1 and $E_1 + \Delta_1$ energy gaps is found to be nonlinear which is in good agreement with the results obtained from reflectance measurements given in the previous section. However, the E_2 gap variation is shown to be linear within the limits of experimental uncertainty which disagrees with reflectance results. Further information on the energy gap variation with composition on this alloy system is obtained from electroreflectance measurements which are given next.

FIGURE 4.15

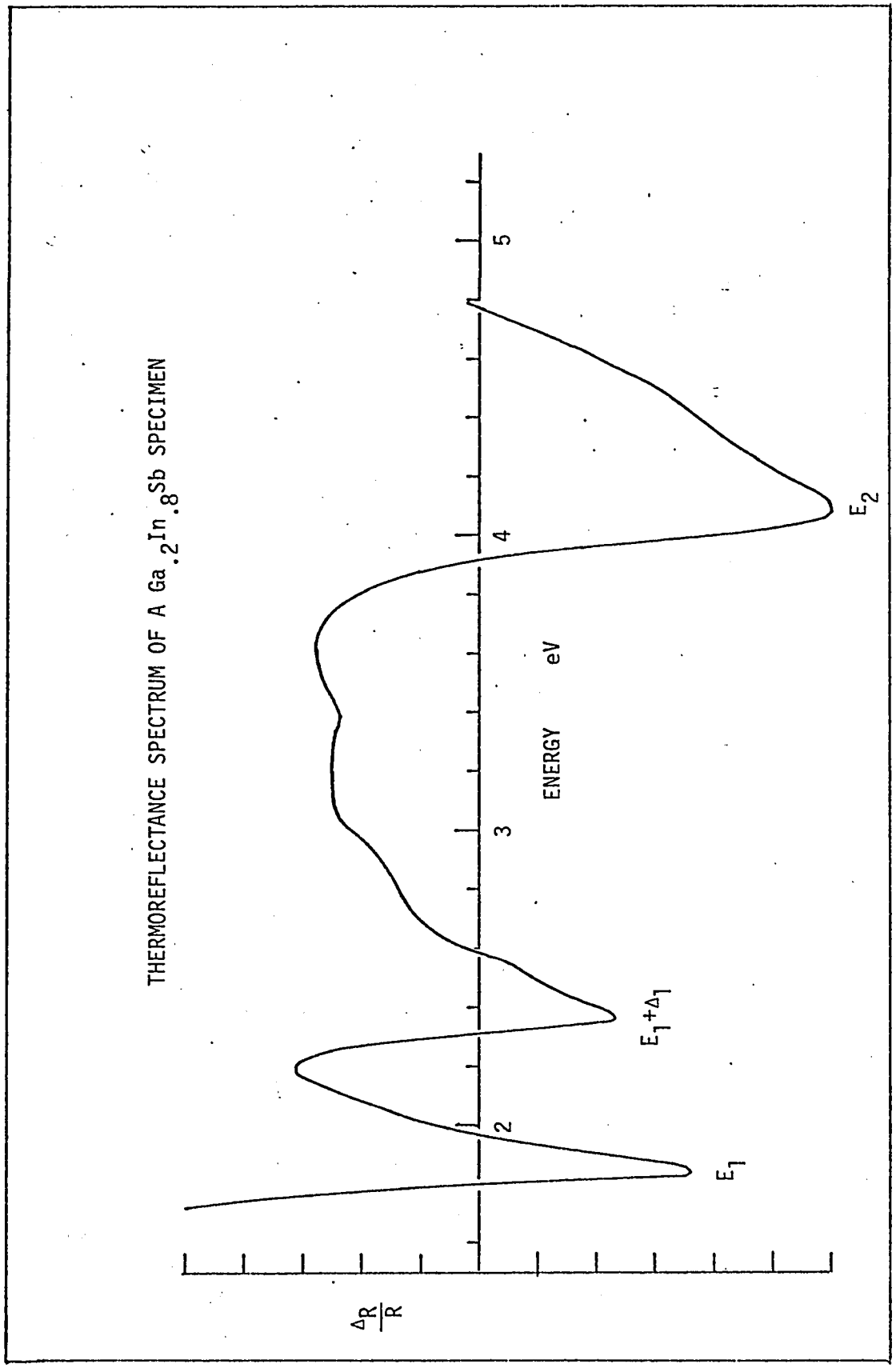
THERMOREFLECTANCE SPECTRUM OF A $Ga_{.2}In_{.8}Sb$ SPECIMEN
$\frac{\Delta R}{R}$
ENERGY eV
1
2
3
4
5
E_1
$E_1+\Delta_1$
E_2

FIGURE 4.16

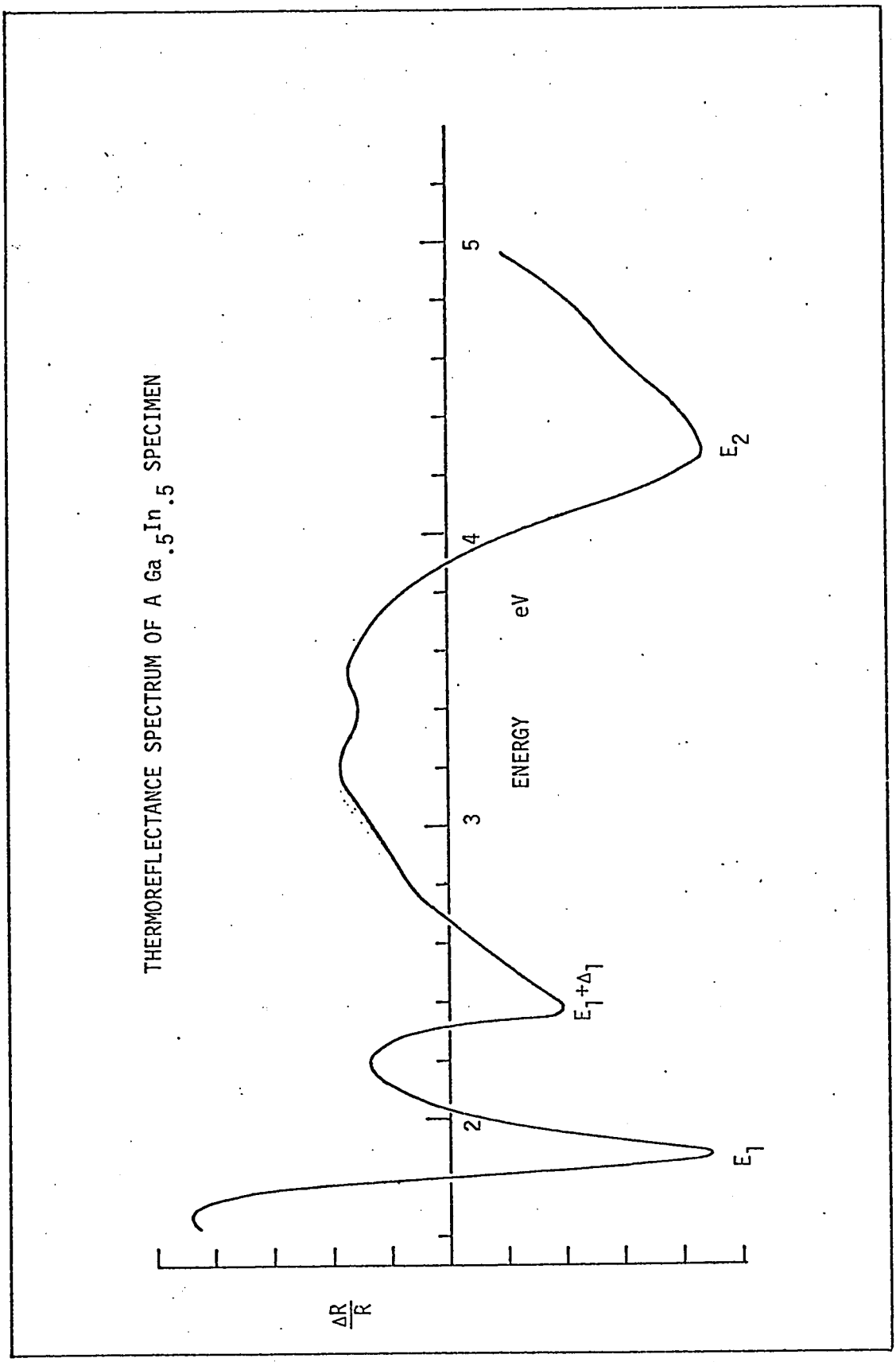
THERMOREFLECTANCE SPECTRUM OF A Ga .5In .5 SPECIMEN
ΔR/R
ENERGY eV
2
3
4
5
E1
E1+Δ1
E2

FIGURE 4.17

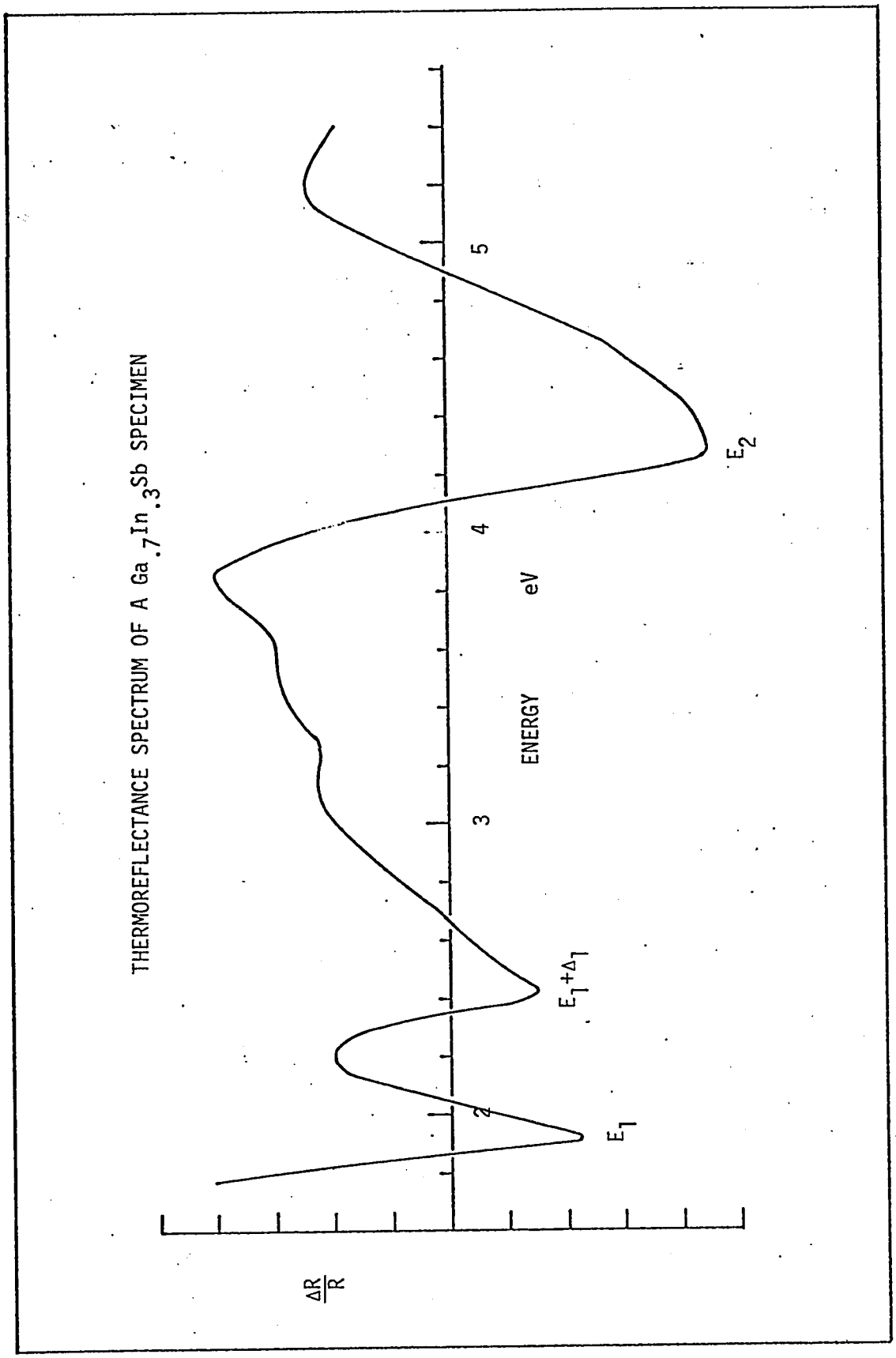
THERMOREFLECTANCE SPECTRUM OF A Ga .7In .3Sb SPECIMEN
ΔR/R
2
3
4
5
ENERGY eV
E1
E1+Δ1
E2

FIGURE 4.18

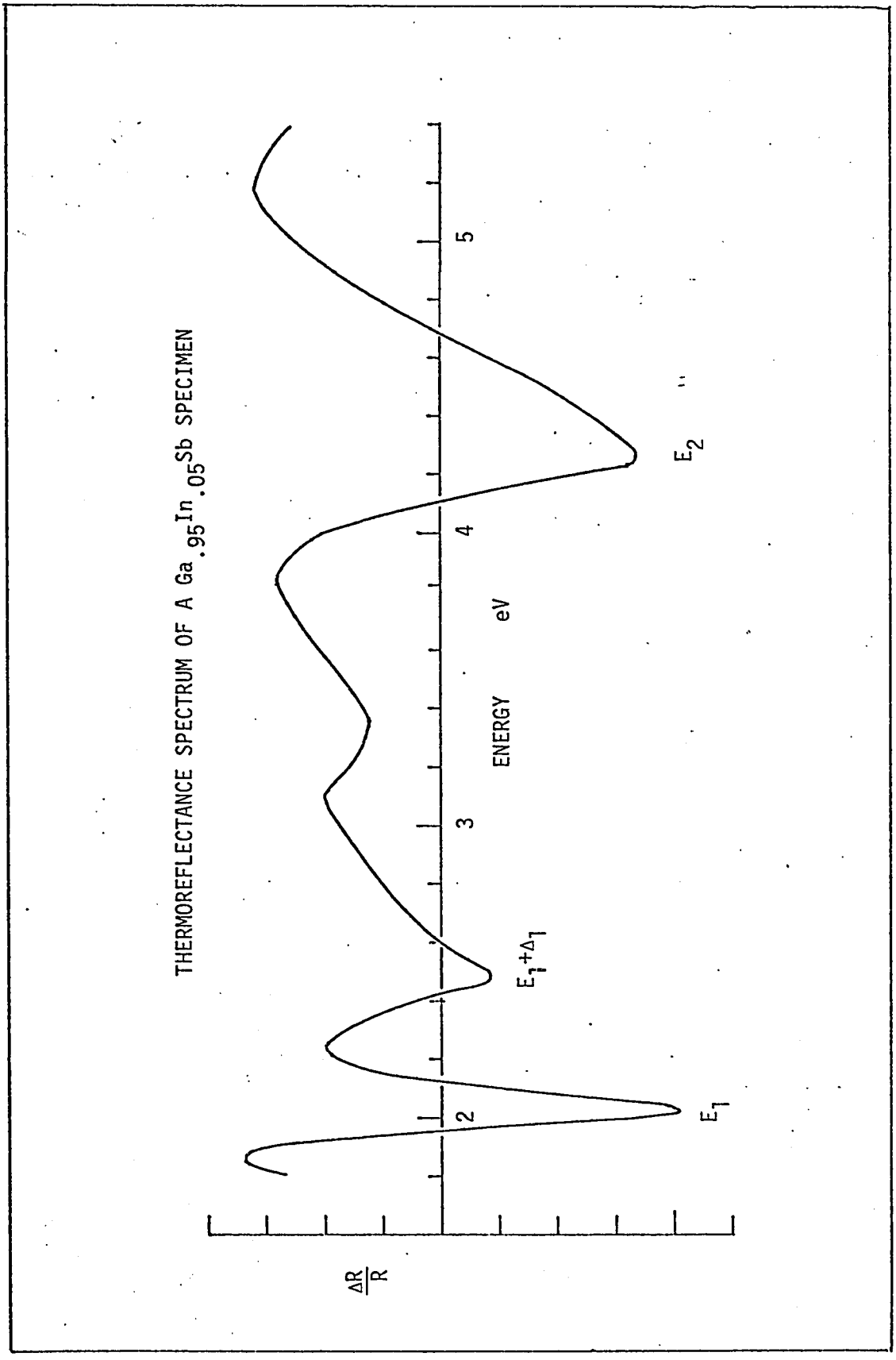
THERMOREFLECTANCE SPECTRUM OF A $Ga_{.95}In_{.05}Sb$ SPECIMEN
$\frac{\Delta R}{R}$
2
3
4
5
ENERGY eV
E_1
$E_1+\Delta_1$
E_2

FIGURE 4.19

TRANSITION ENERGIES Versus COMPOSITION

$Ga_xIn_{1-x}Sb$ ALLOYS

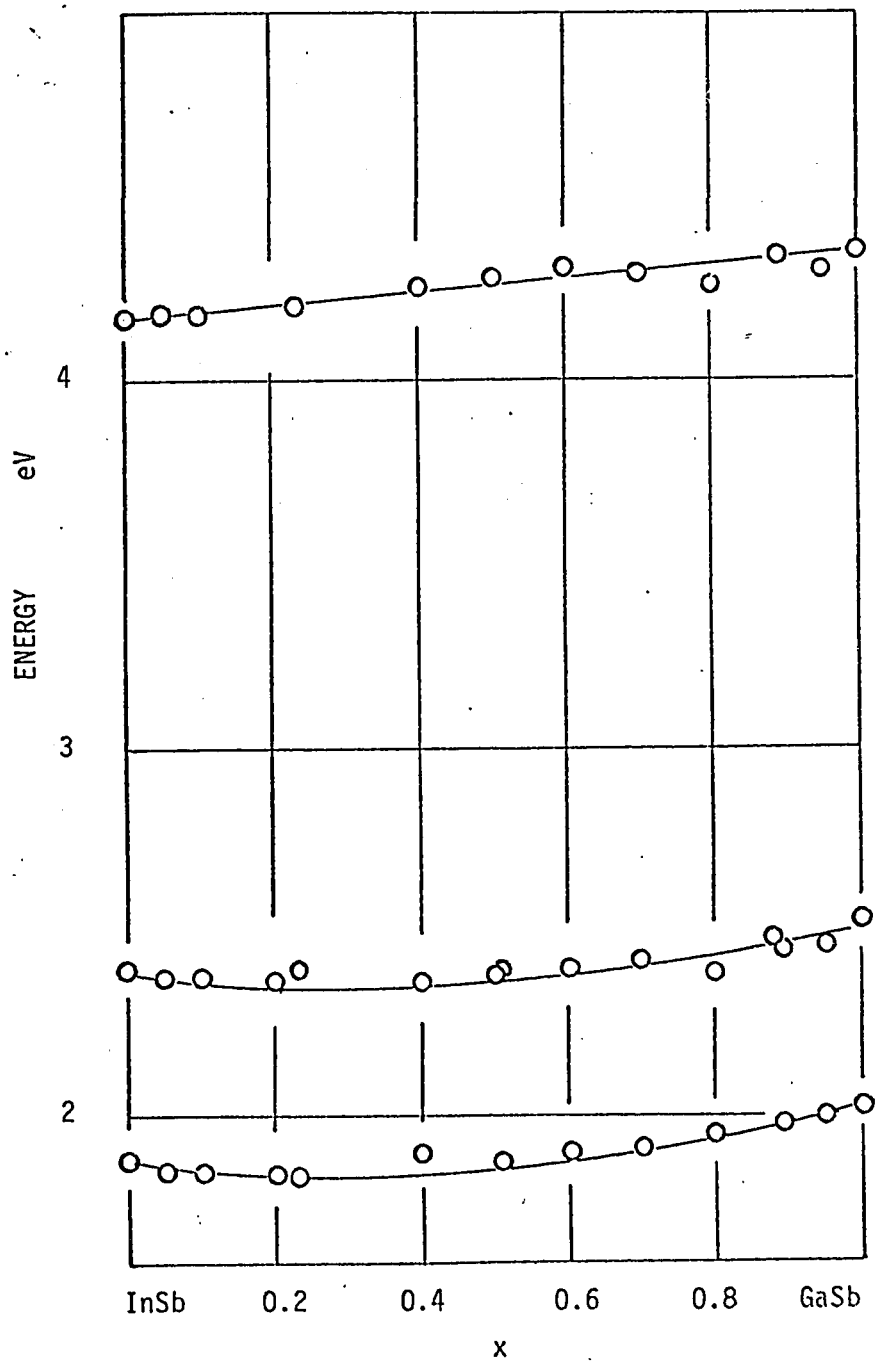

4.4 C Results of Electroreflectance Measurements on $Ga_xIn_{1-x}Sb$ Alloy

Electroreflectance spectra of the samples of $Ga_xIn_{1-x}Sb$ alloy were determined in the spectral range 1.5 to 6.0 eV. The electrolytic electroreflectance technique which was used has been described in Section 3.3. The electroreflectance spectra, $\Delta R/R$ drawn as a function of photon energy, $(\hbar\omega)$, are shown for InSb and GaSb in Figs. 4.20 and 4.21 respectively. In these spectra, the identification of structure corresponding to the interband transitions E_1, $E_1 + \Delta_1$, E_0', $E_0' + \Delta_0'$ and E_2 has been guided by previous work[127] (Section 2.8). The energy values obtained presently for various band gaps in the compounds are given in Table 4.3. For comparison, the results of Cardona et al[127] which were also determined by electrolytic electroreflectance method are included in the table. There is good agreement between the two sets of data except for the energies of E_0', $E_0' + \Delta_0'$ and E_2 transitions in GaSb. Perhaps the discrepancy in determining the energies of E_0' doublet is due to the weak structure observed in the spectra. The E_2 gap energy determined as 4.28 eV is in good agreement with the reflectance value (4.28 eV) given in Table 4.1 for this transition.

Typical electroreflectance spectra of $Ga_xIn_{1-x}Sb$ alloy specimens are given in Figs. 4.22 and 4.23. The spectra are similar to the ones obtained for the compounds InSb and GaSb and therefore there has been no difficulty in identifying the structure in them. The variation of energy gaps as a function of composition is shown in Fig. 4.24. Again, the E_0' and $E_0' + \Delta_0'$ transition energy values are not given because in the spectra of some alloy samples they were not seen while in others where weak structure was found the values determined from them showed large

TABLE 4.3

Energies of various transitions determined from electroreflectance spectra. Values given in ( ) are from electroreflectance results of Cardona et al.[127]

Material	E_1	$E_1+\Delta_1$	E_0	$E_0'+\Delta_0'$	E_2	$E_2+\delta$
InSb	1.87 (1.88)	2.37 (2.38)	3.16 (3.16)	3.52 (3.49)	4.06 (4.08)	4.68 (4.66)
InAs	2.50 (2.50)	2.79 (2.78)	4.38 (4.44)	- -	4.71 (4.70)	- -
InP	3.14 (3.12)	3.28 (3.27)	4.73 (4.72)	 (4.79)	5.02 (5.04)	- -
GaSb	2.00 (2.03)	2.47 (2.49)	3.20 (3.27)	3.65 (3.56)	4.28 (4.20)	4.72 (4.57)

FIGURE 4.20

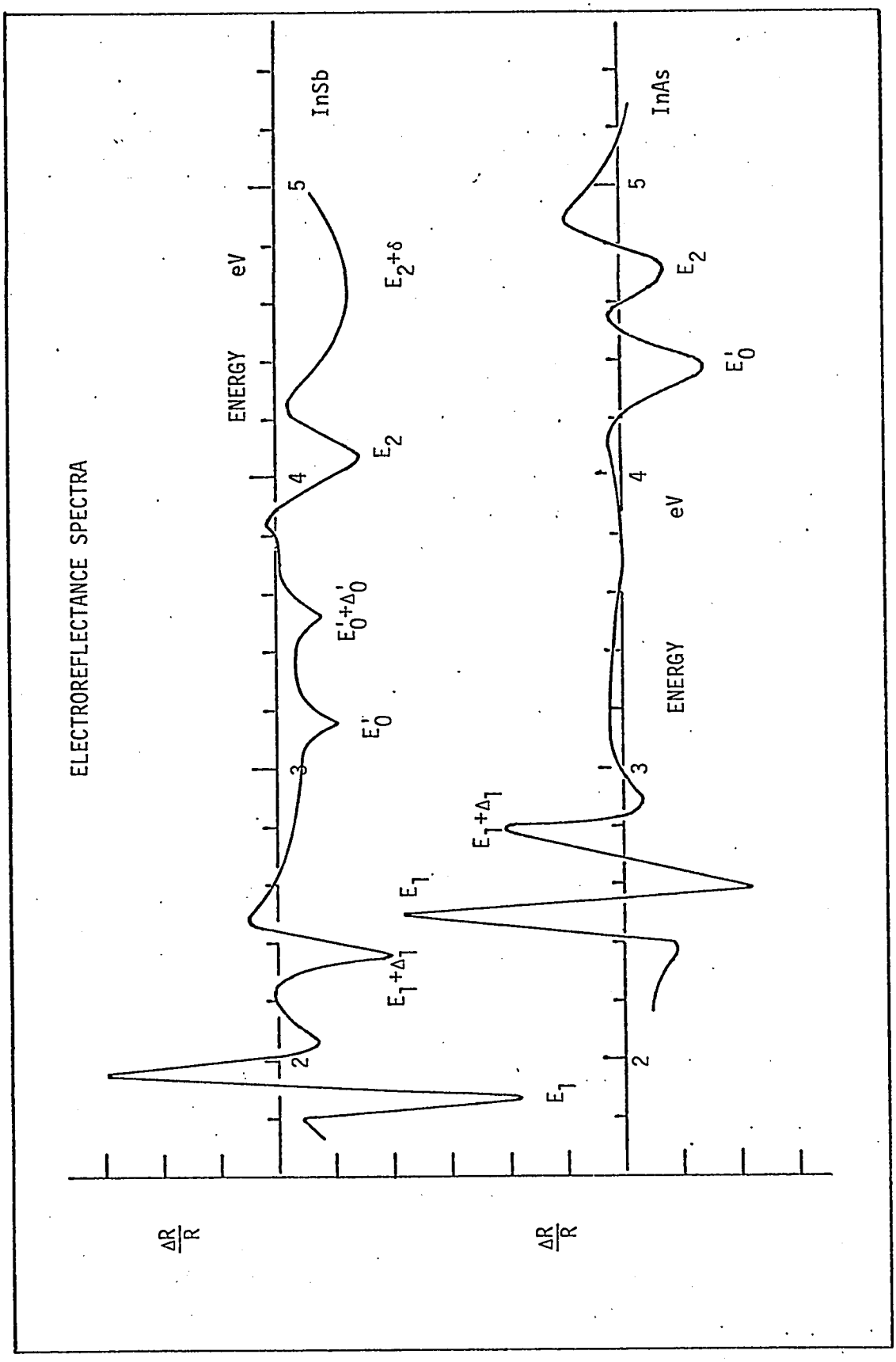
ELECTROREFLECTANCE SPECTRA
InSb
InAs
ENERGY eV
ENERGY eV
$\frac{\Delta R}{R}$
$\frac{\Delta R}{R}$
E_1
$E_1+\Delta_1$
E_0'
$E_0'+\Delta_0'$
E_2
$E_2+\delta$
2
3
4
5

FIGURE 4.21

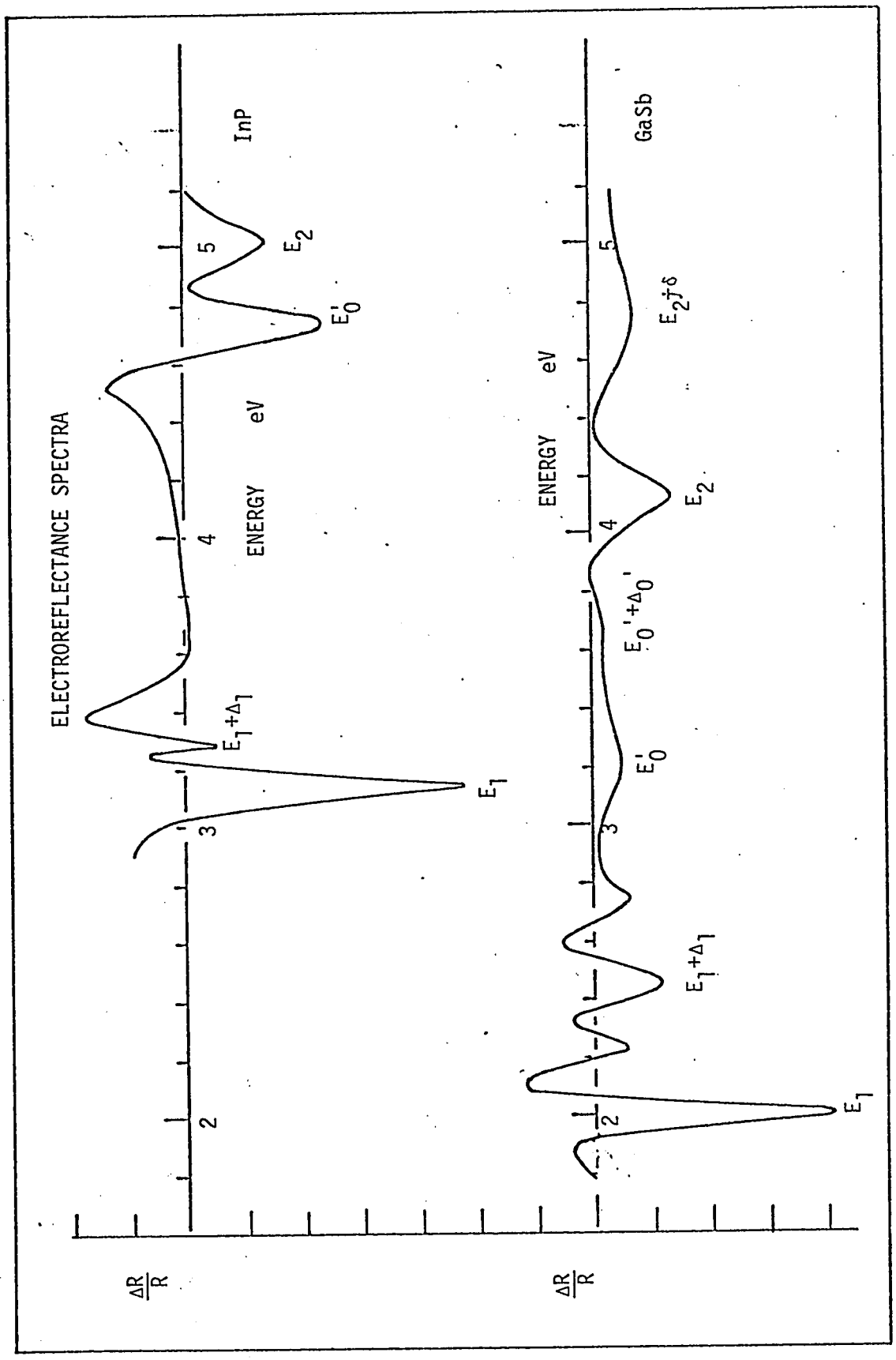
ELECTROREFLECTANCE SPECTRA
InP
GaSb
ENERGY eV
$\frac{\Delta R}{R}$
E_1
$E_1+\Delta_1$
E_0'
E_2
$E_0'+\Delta_0'$
$E_2+\delta$
2
3
4
5

FIGURE 4.22

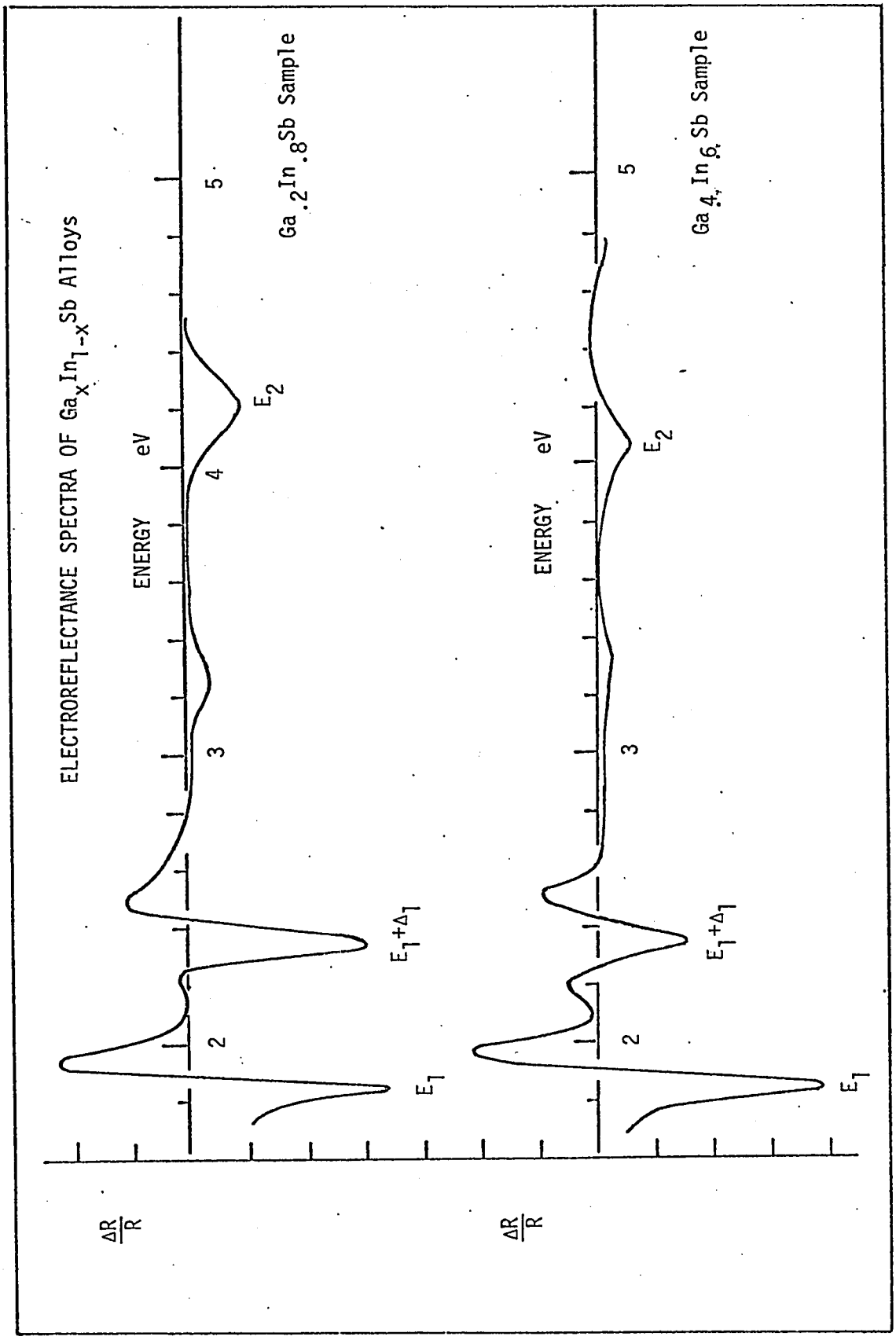
ELECTROREFLECTANCE SPECTRA OF $Ga_xIn_{1-x}Sb$ Alloys
ENERGY eV
2
3
4
5
E_1
$E_1+\Delta_1$
E_2
$Ga_{.2}In_{.8}Sb$ Sample
$Ga_{.4}In_{.6}Sb$ Sample
$\frac{\Delta R}{R}$

FIGURE 4.23

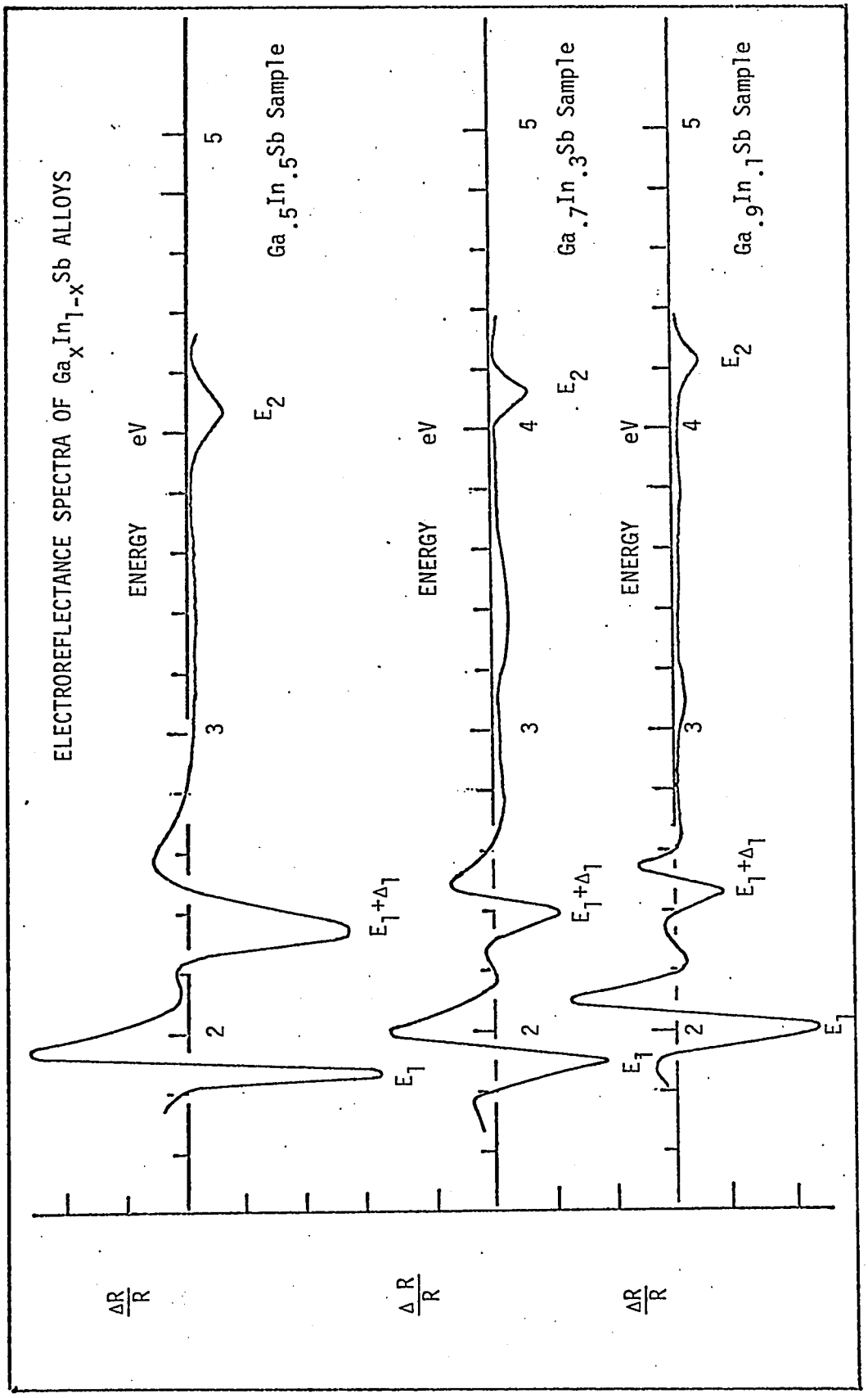
ELECTROREFLECTANCE SPECTRA OF $Ga_xIn_{1-x}Sb$ ALLOYS
ENERGY eV
$Ga_{.5}In_{.5}Sb$ Sample
$Ga_{.7}In_{.3}Sb$ Sample
$Ga_{.9}In_{.1}Sb$ Sample
E_1
$E_1+\Delta_1$
E_2
$\frac{\Delta R}{R}$

FIGURE 4.24

TRANSITION ENERGIES Versus COMPOSITION

$Ga_xIn_{1-x}Sb$ ALLOYS

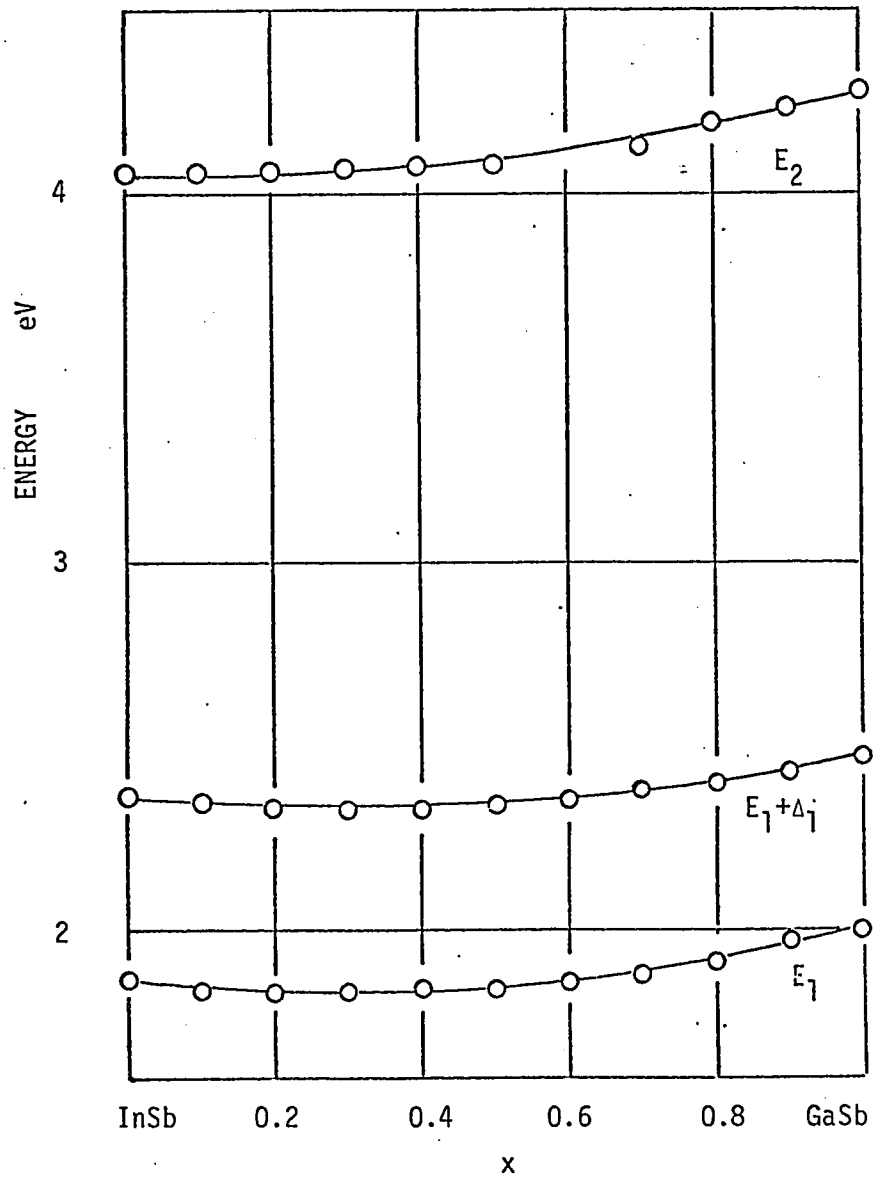

scatter. All the three energy gaps, E_1, $E_1 + \Delta_1$ and E_2 exhibit non-linear dependence on composition. This behaviour is in good agreement with the results of reflectance and thermoreflectance experiments already described on this alloy system. However, the E_2 gap variation with composition determined from thermoreflectance measurements is an exception. Further discussion on the composition dependence of energy gaps will be given in Section 4.8.

4.5 Results of Electroreflectance Measurements on $InAs_{1-x}P_x$ Alloy

The electroreflectance spectra obtained for the compounds InAs and InP are shown in Figs. 4.20 and 4.21. The structure found in these spectra has been assigned to E_1, $E_1 + \Delta_1$, E_0' and E_2 transitions guided by previous work[127] (Section 2.8). The energies of various transitions determined from the spectra of InAs and InP are given in Table 4.3. Good agreement is found between the present results and the results of Cardona et al[127] except perhaps for the E_0' transition energy in InAs.

It is seen from the electroreflectance spectra of the four compounds determined presently, shown in Figs. 4.20 and 4.21, the spectrum of InAs is different from the others with regard to the relative signs of the various peaks. In the spectra of InSb, GaSb and InP, the peaks correspond to E_1, $E_1 + \Delta_1$, E_0' and E_2 are all oriented in the same direction. This behaviour is normally observed for III - V compounds. The phase of the $\Delta R/R$ signal at the fundamental frequency depends upon the nature of the semiconductor material whether it is n or p type. Therefore, the peaks in $\Delta R/R$ spectra should be reversed for n and p type materials. However, for an n type InAs sample it is found that the E_1 and $E_1 + \Delta_1$ peaks are oriented in opposite directions to the E_0' and E_2 peaks. It was shown by Kwan et al[188] that for an n type InAs sample the sign of the E_1 and $E_1 + \Delta_1$ peaks depends upon the carrier, concentration, the dc bias and the type of electrolyte used. It was also observed that the sign of the peaks can be changed by varying the dc bias for a particular sample. The bias value where this change-over occurs is a function of the carrier concentration. It is more important that

at the bias where this change-over occurs, none of the peaks observed in the $\Delta R/R$ spectrum was a true measure of the critical band gaps. The effect of bias variation on the phase of $\Delta R/R$ signal at the E_0 gap in Ge was similarly investigated by Seraphin[170] before. It was observed that by changing the electric field at the reflecting surface of the sample the phase of the $\Delta R/R$ signal and therefore the sign of the peaks could be reversed. On this basis, the reason for spectra with E_1 and $E_1 + \Delta_1$ of opposite sign to E_0' and E_2 is perhaps because the bias voltage required to flip the E_1 and $E_1 + \Delta_1$ peaks is different from that for the E_0' and E_2 peaks. The InAs spectrum presently obtained is such a case.

The anomalous behaviors observed in InAs was also observed in the spectra of InAs rich alloy samples. To illustrate this, the effect of bias variation on the phase of $\Delta R/R$ signal for an alloy specimen ($InAs_{.9}P_{.1}$) which is InAs rich is shown in Fig. 4.25. A normal $\Delta R/R$ spectrum is obtained for - 1.0 V bias setting. Both low (E_1 and $E_1 + \Delta_1$) and high (E_0' and E_2) energy peaks have the same sign. The line shapes do not appear to be distorted. In the spectrum obtained with 0V bias, the low and high energy peaks are oriented in opposite directions. The E_0' peak which was weak when compared with E_2 in the spectrum obtained for - 1.0 V bias became relatively stronger. At a still higher bias voltage + 1.0 V, the E_1 and $E_1 + \Delta_1$ peaks remained as they were before in the 0V bias spectrum except for their size, but the E_0' and E_2 peak line shapes are distorted considerably. However, the bias change was not sufficient to flip the high energy peaks as well. Further increase in voltage resulted in a large current flow through the sample tarnishing

FIGURE 4.25

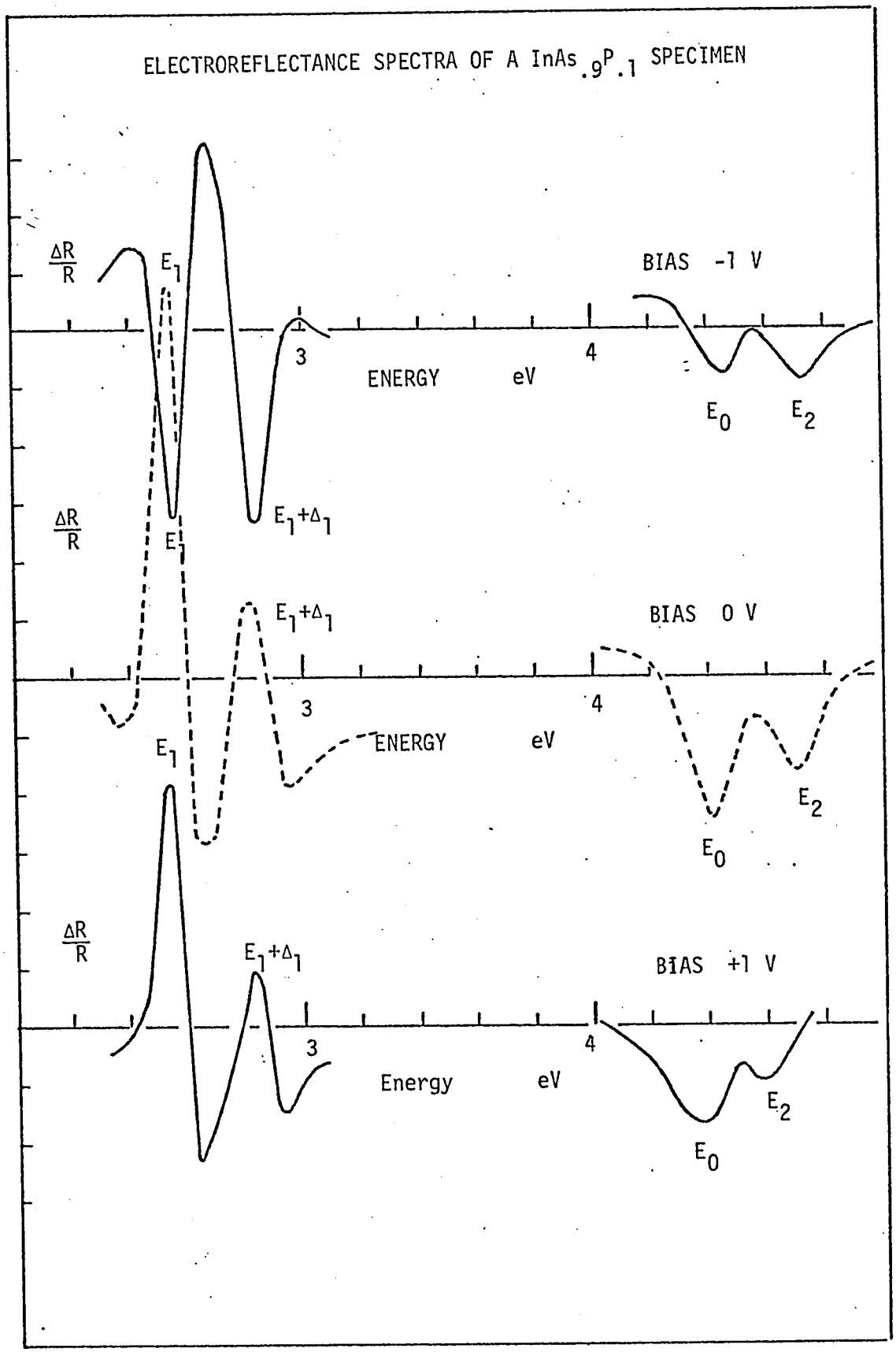
ELECTROREFLECTANCE SPECTRA OF A InAs.9P.1 SPECIMEN
ΔR/R
E1
E1+Δ1
BIAS -1 V
3
4
ENERGY eV
E0
E2
ΔR/R
E1
E1+Δ1
BIAS 0 V
3
4
ENERGY eV
E1
E0
E2
ΔR/R
E1+Δ1
BIAS +1 V
3
4
Energy eV
E0
E2

the reflecting surface. The energy gap values determined for the $InAs_{.9}P_{.1}$ sample for the three bias voltage settings are given in Table 4.4. The effect of bias variation is considerably larger on the E_0' and E_2 gap determination compared with E_1 and $E_1 + \Delta_1$ gaps. This probably is responsible for the disagreement between the E_0' transition energies determined presently and the previous data. Therefore, the important factor in interpreting electroreflectance spectra is first to know whether the spectrum obtained is normal or anomalous. This anomalous behaviour was observed in the InAs rich $InSb_{1-x}As_x$ alloy samples also leading to certain difficulties in interpreting their spectra which will be discussed in the next section.

Typical reflectance spectra of $InAs_{1-x}P_x$ alloy specimens are shown in Figs. 4.26 to 4.28. Over most of the composition range, namely $0.25 < x < 1.0$, the spectra showed normal behaviour and are similar to the one obtained for InP. Only for InAs rich alloy samples, $0 < x < 0.25$, did spectra show behaviour similar to InAs with the sign of the peaks depending on bias. In these cases a careful choice of bias and comparison with the more normally behaved alloys and with well known InAs results allowed a clear determination of the E_0' and E_2 peaks to be made. The variation of E_1, $E_1 + \Delta_1$, E_0' and E_2 gaps with x is shown in Fig. 4.29. All four gaps show nonlinear dependence on composition which will be discussed further in Section 4.8.

Previously, reflectance measurements were made on $InAs_{1-x}P_x$ alloy by Krioturu et al.[88] The energy gap variation as a function of composition was reported to be linear for all transitions observed within the limits of experimental uncertainty. Electroreflectance measurements

TABLE 4.4

Energies of transitions for various bias voltages ($InAs_{.9}P_{.1}$ specimen)

Bias V	E_1 eV	$E_1+\Delta_1$ eV	E_0' eV	E_2 eV
- 1.0	2.55	2.84	4.46	4.73
0	2.53	2.82	4.41	4.71
+ 1.0	2.54	2.82	4.35	4.59

FIGURE 4.26

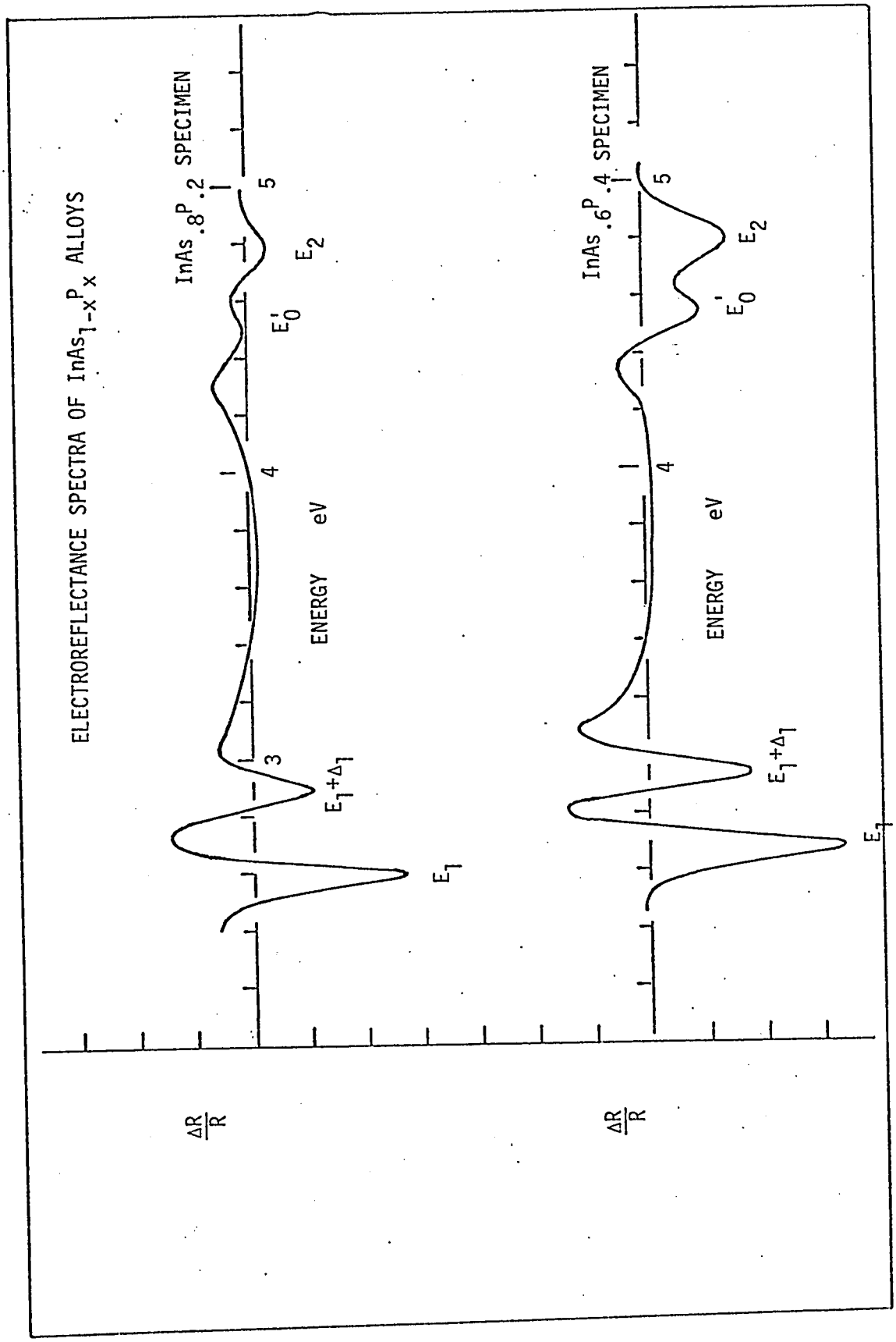
ELECTROREFLECTANCE SPECTRA OF $InAs_{1-x}P_x$ ALLOYS
$InAs_{.8}P_{.2}$ SPECIMEN
$InAs_{.6}P_{.4}$ SPECIMEN
$\frac{\Delta R}{R}$
ENERGY eV
3
4
5
E_1
$E_1+\Delta_1$
E_0'
E_2

FIGURE 4.27

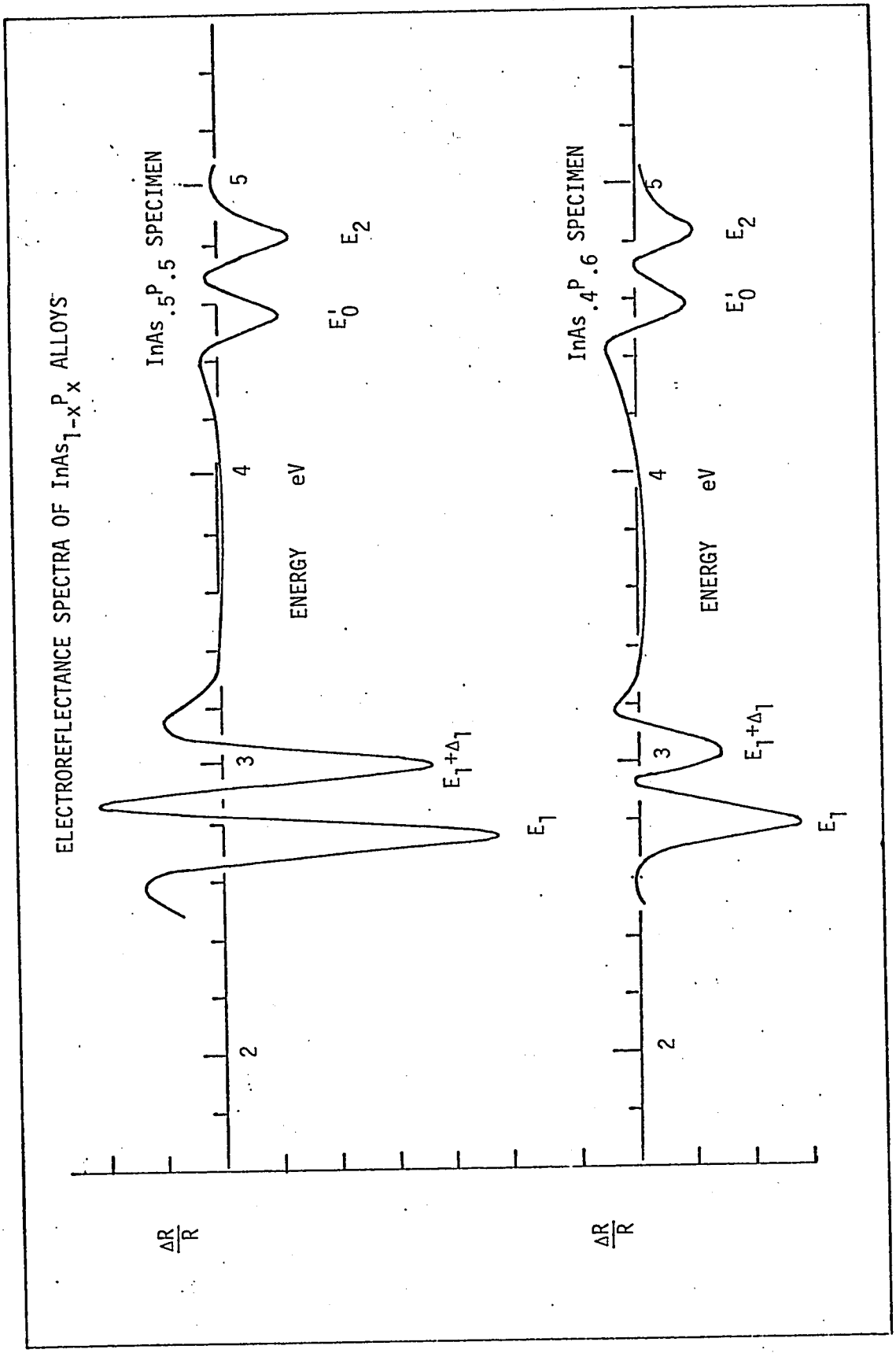
ELECTROREFLECTANCE SPECTRA OF $InAs_{1-x}P_x$ ALLOYS
InAs .5P .5 SPECIMEN
InAs .4P .6 SPECIMEN
ENERGY eV
E_0'
E_2
$E_1+\Delta_1$
E_1
$\frac{\Delta R}{R}$
2
3
4
5

FIGURE 4.28

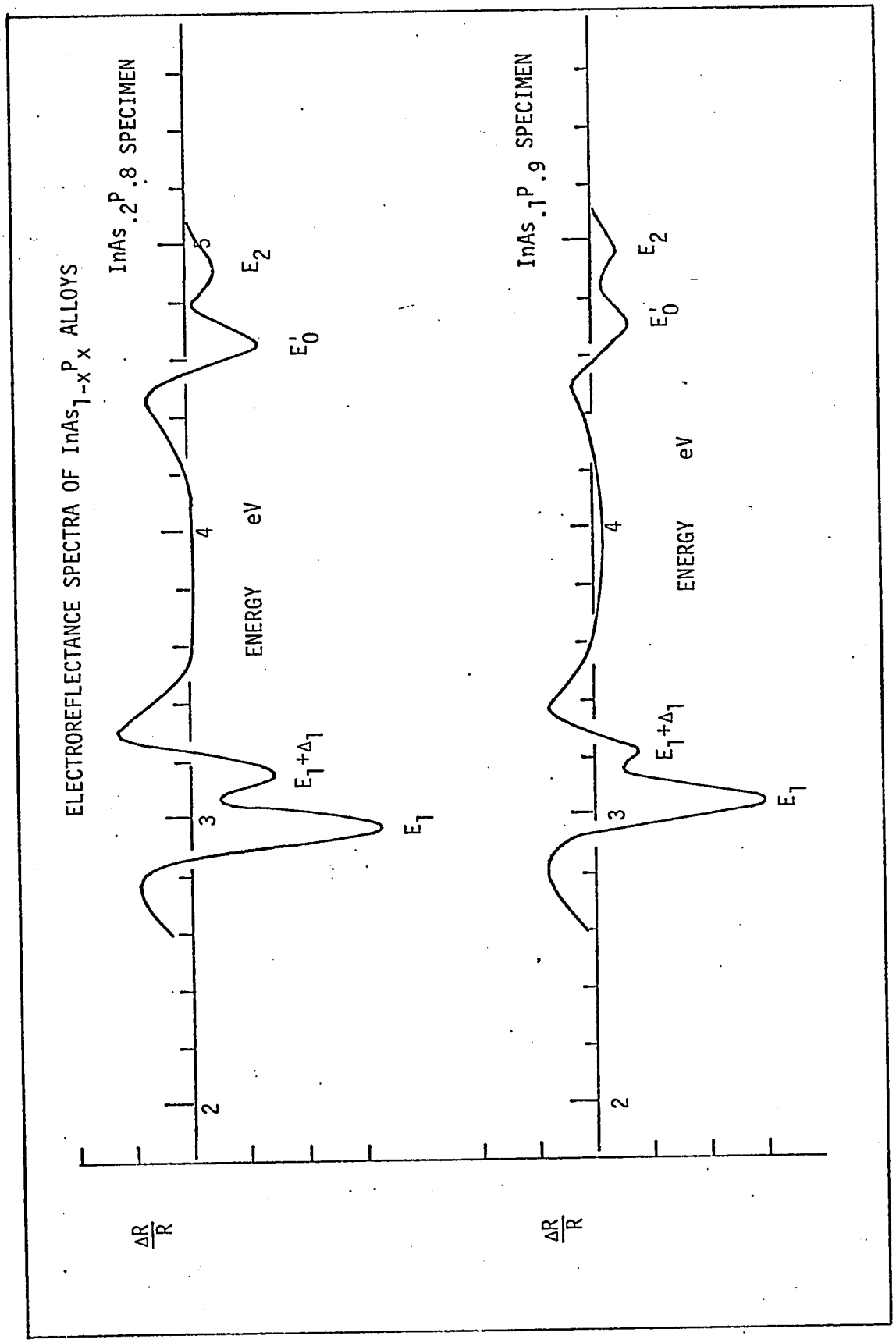
ELECTROREFLECTANCE SPECTRA OF $InAs_{1-x}P_x$ ALLOYS
$InAs_{.2}P_{.8}$ SPECIMEN
$InAs_{.1}P_{.9}$ SPECIMEN
E_1
$E_1+\Delta_1$
E_0'
E_2
ENERGY eV
$\frac{\Delta R}{R}$
2
3
4
5

FIGURE 4.29

TRANSITION ENERGIES Versus COMPOSITION

$InAs_{1-x}P_x$ ALLOYS

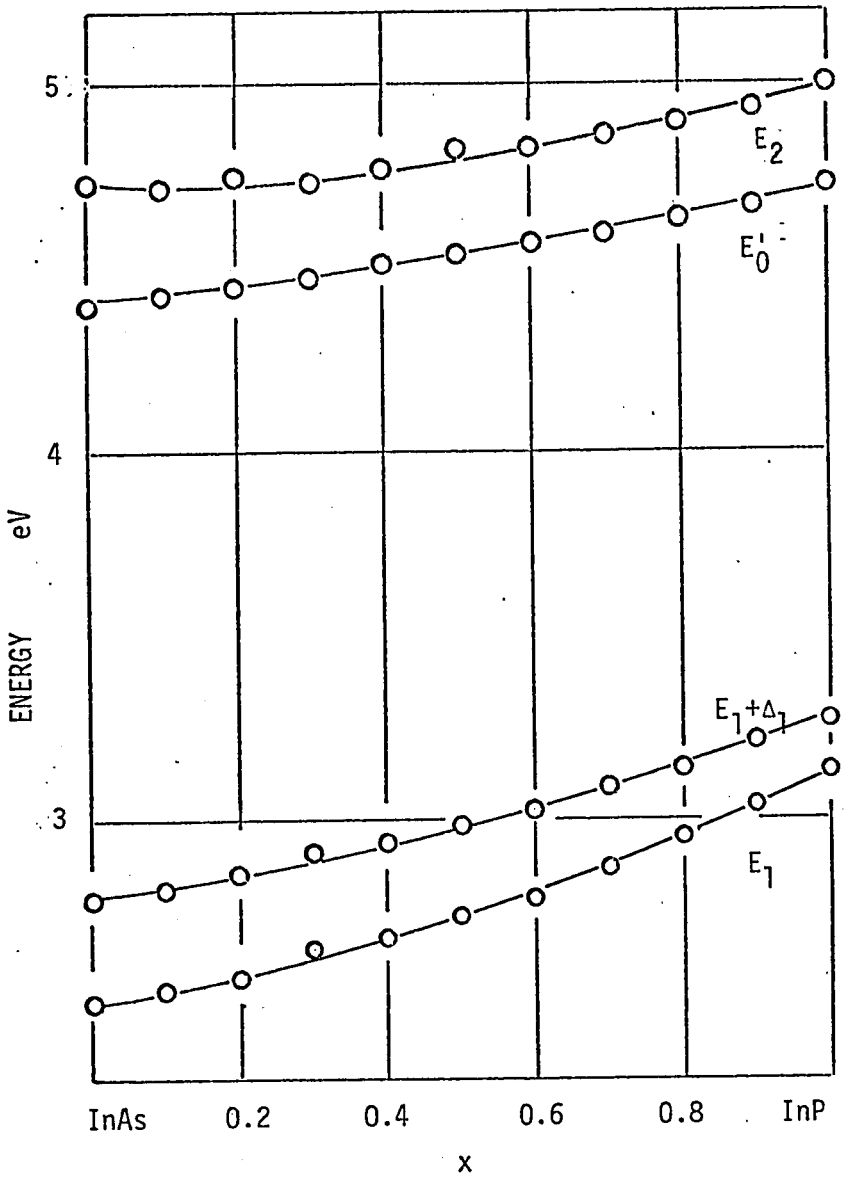

were made on this alloy system by Thompson et al[86] concurrently with the work given in this thesis. Thompson et al[86] found that the E_1 and $E_1 + \Delta_1$ transition energies varied in a concave upwards manner while the E_0', E_2 and $E_2 + \delta$ energies varied linearly with composition. From the present results shown in Fig. 4.29, all four energy gaps E_1, $E_1 + \Delta_1$, E_0' and E_2, are found to vary in a concave upwards manner with composition. The nonlinear variation of E_1 and $E_1 + \Delta_1$ with composition was attributed by Thompson et al to the movement of critical point responsible for E_1 transitions along the <111> direction. Presently it is understood that the nonlinear variation of energy gaps as a function of composition is due to disorder in the alloy lattice and intrinsic bowing. In the case of E_1 and $E_1 + \Delta_1$ transitions there may be a small contribution due to the probable movement of the critical point. This discussion on the composition dependence of band gaps is continued in Section 4.8.

4.6 Results of Electroreflectance Measurements on $InSb_{1-x}As_x$ Alloy

Electroreflectance measurements on samples of $InSb_{1-x}As_x$ alloy provided useful spectra only in two ranges of alloy composition, namely $0 \leq x \leq 0.35$ and $0.05 \leq x \leq 1.0$. In the mid composition range $0.35 < x < 0.65$ only limited number of samples were available. This is because the variation of composition along the length of the $InSb_{1-x}As_x$ ingot is quite rapid in the mid composition range as shown in Fig. 3.8. In particular the composition range of $0.35 < x < 0.65$ falls in an ingot length of about 1 cm. Further, for the few alloy samples cut in this composition range, none of them gave good electroreflectance spectra.

Two typical electroreflectance spectra obtained for the InSb rich samples, $0 < x < .15$ are shown in Fig. 4.30. They exhibit normal behaviour which has been described in the previous section. The structure found in their spectra is identified in terms of E_1, $E_1 + \Delta_1$, E_0', $E_0' + \Delta_0'$ and E_2 transitions. For alloy specimens in the composition range $0.15 < x < 0.35$, while the E_1 and $E_1 + \Delta_1$ peaks could be seen clearly the structure due to E_0', $E_0' + \Delta_0'$ and E_2 transitions could not be observed satisfactorily. Therefore only the E_1 and $E_1 + \Delta_1$ energy gap values are available in this composition range, $0.15 < x < 0.35$.

Typical spectra of samples in the InAs rich composition range $0.65 \leq x \leq 1.0$ are shown in Figs. 4.31 to 4.33. In these spectra the structure due to E_1 and $E_1 + \Delta_1$ transitions could be identified with little ambiguity. However, the fact that the spectra obtained in this composition range are anomalous is understood only when the composition dependence of the high energy transitions is considered. If the spectra shown were to be normal the peaks labelled 2 and 4 in Figs. 4.31 to 4.33

FIGURE 4.30

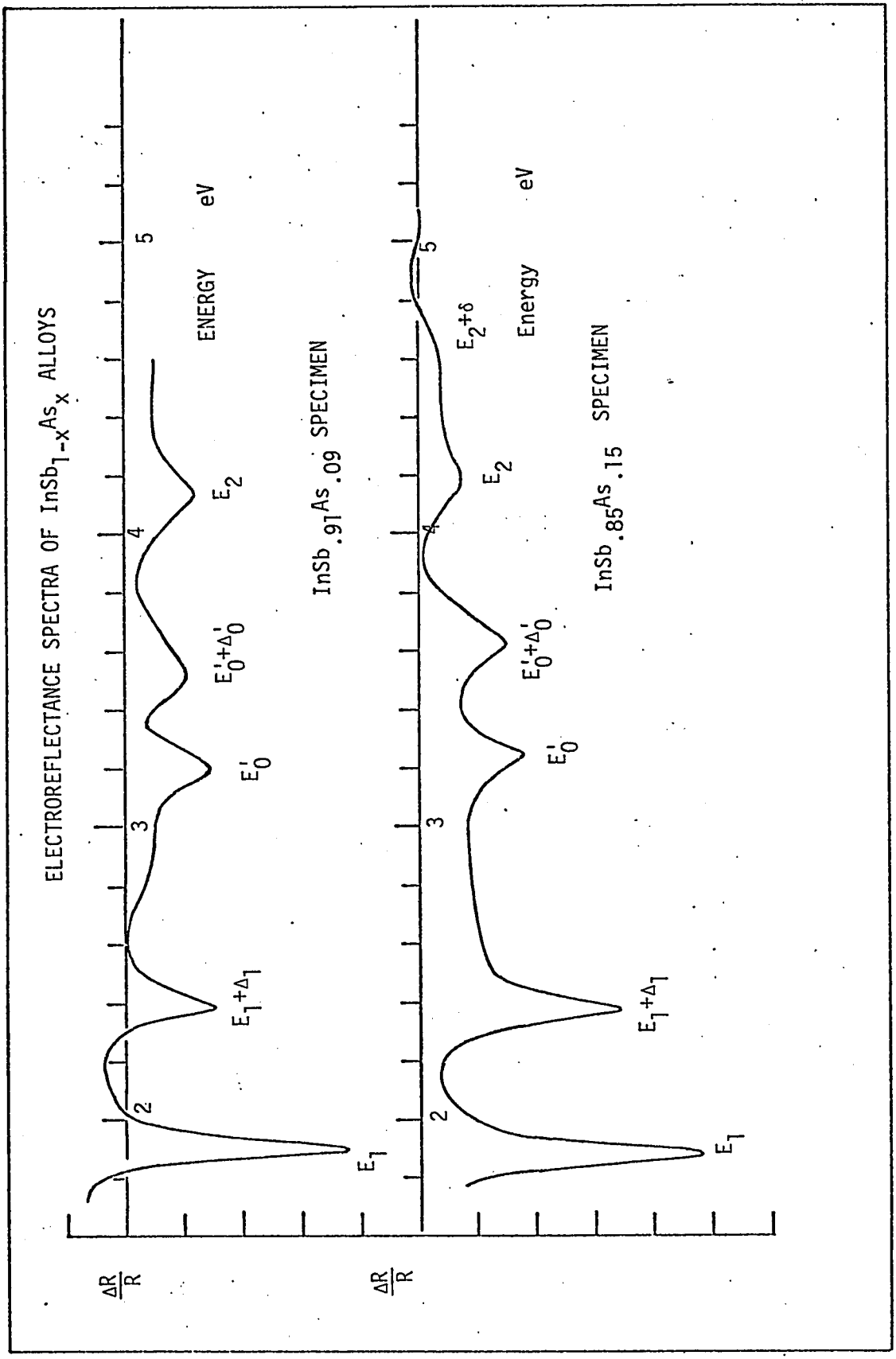
ELECTROREFLECTANCE SPECTRA OF $InSb_{1-x}As_x$ ALLOYS
ENERGY eV
$InSb_{.91}As_{.09}$ SPECIMEN
E_1
$E_1+\Delta_1$
E_0'
$E_0'+\Delta_0'$
E_2
$\frac{\Delta R}{R}$
Energy eV
$InSb_{.85}As_{.15}$ SPECIMEN
$E_2+\delta$

FIGURE 4.31

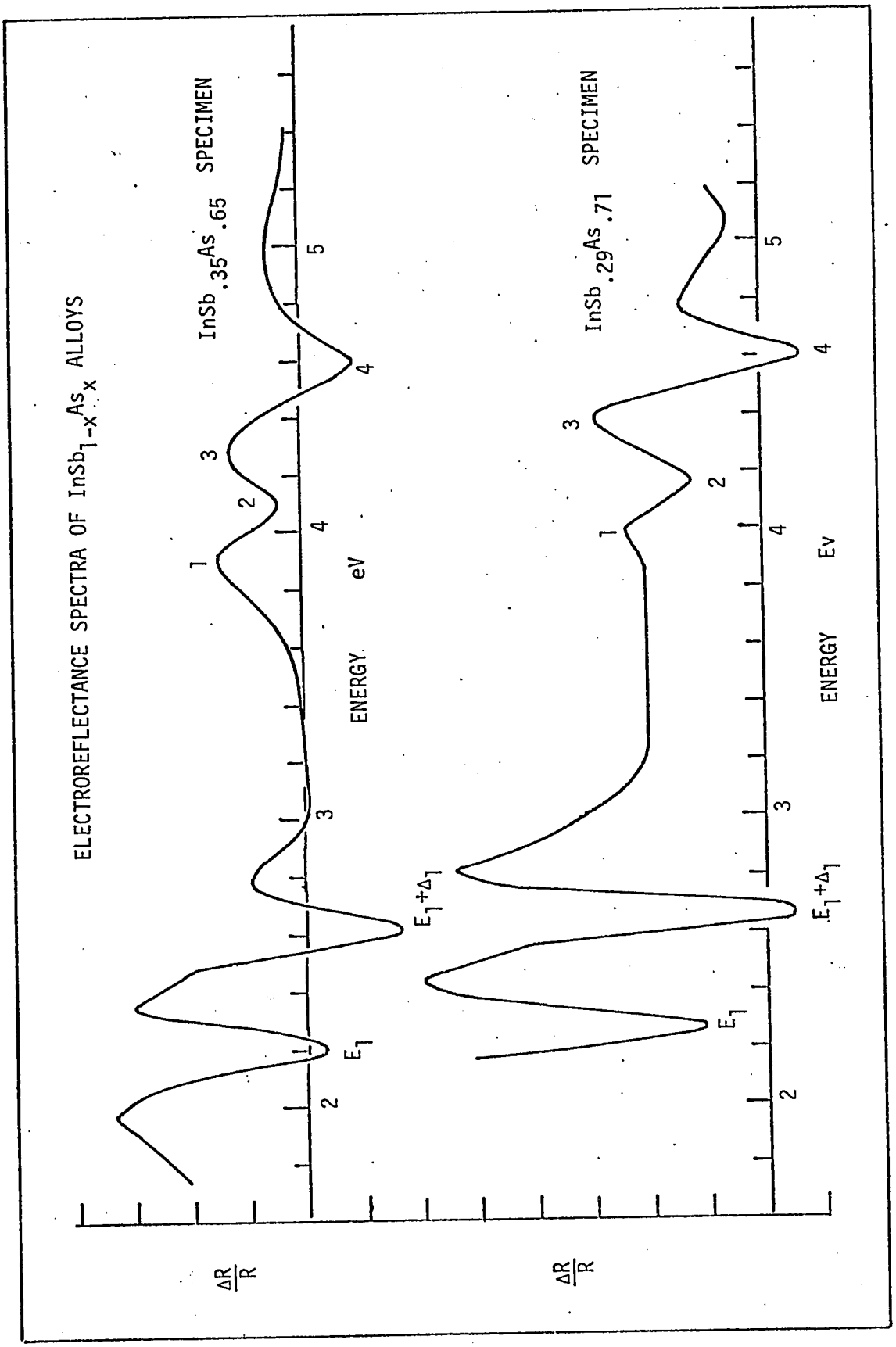
ELECTROREFLECTANCE SPECTRA OF $InSb_{1-x}As_x$ ALLOYS
$InSb_{.35}As_{.65}$ SPECIMEN
$InSb_{.29}As_{.71}$ SPECIMEN
ENERGY eV
ENERGY Ev
$\frac{\Delta R}{R}$
E_1
$E_1+\Delta_1$
1
2
3
4
5

FIGURE 4.32

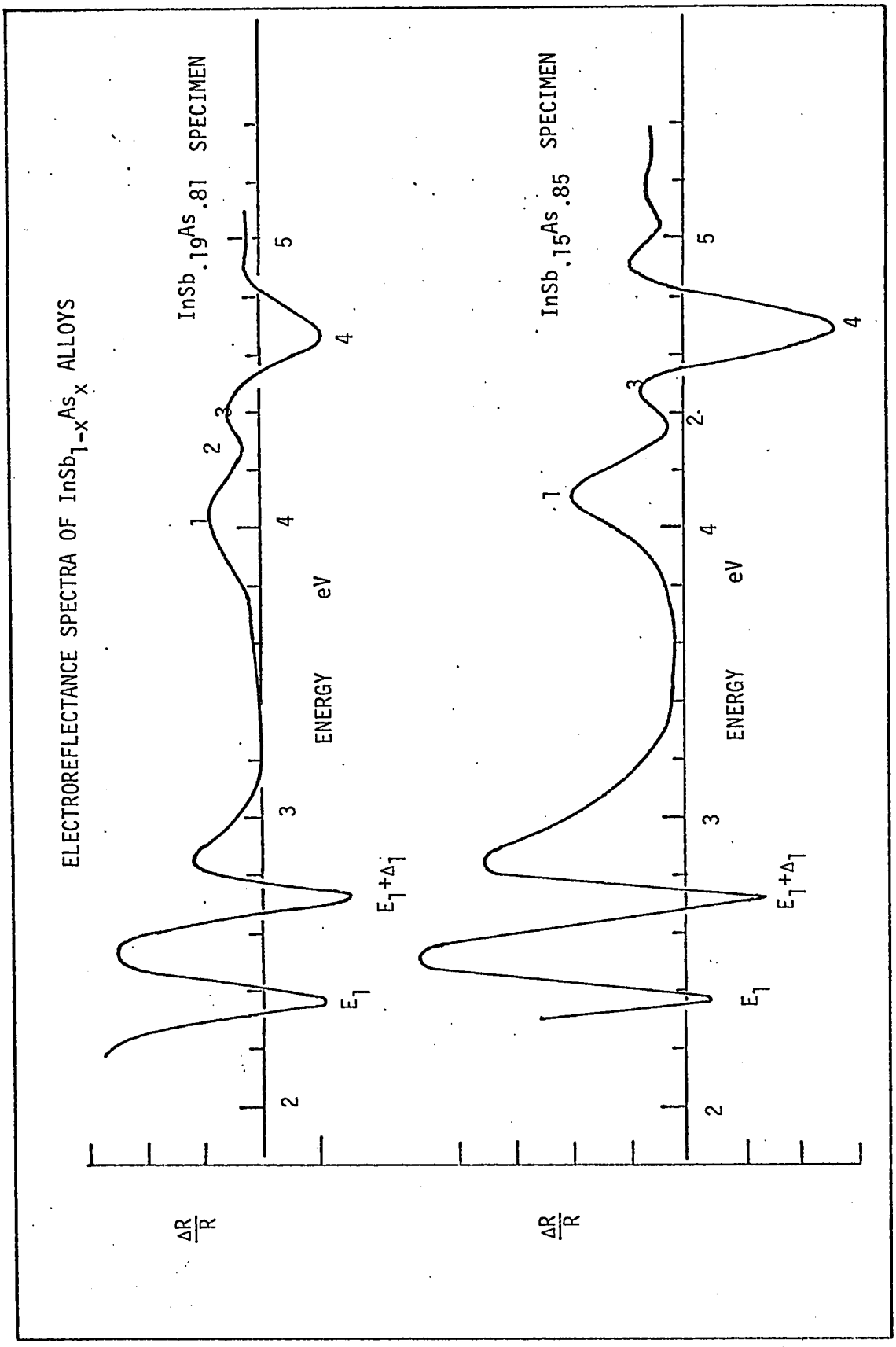
ELECTROREFLECTANCE SPECTRA OF $InSb_{1-x}As_x$ ALLOYS
$InSb_{.19}As_{.81}$ SPECIMEN
$InSb_{.15}As_{.85}$ SPECIMEN
ENERGY eV
E_1
$E_1+\Delta_1$
$\frac{\Delta R}{R}$

FIGURE 4.33

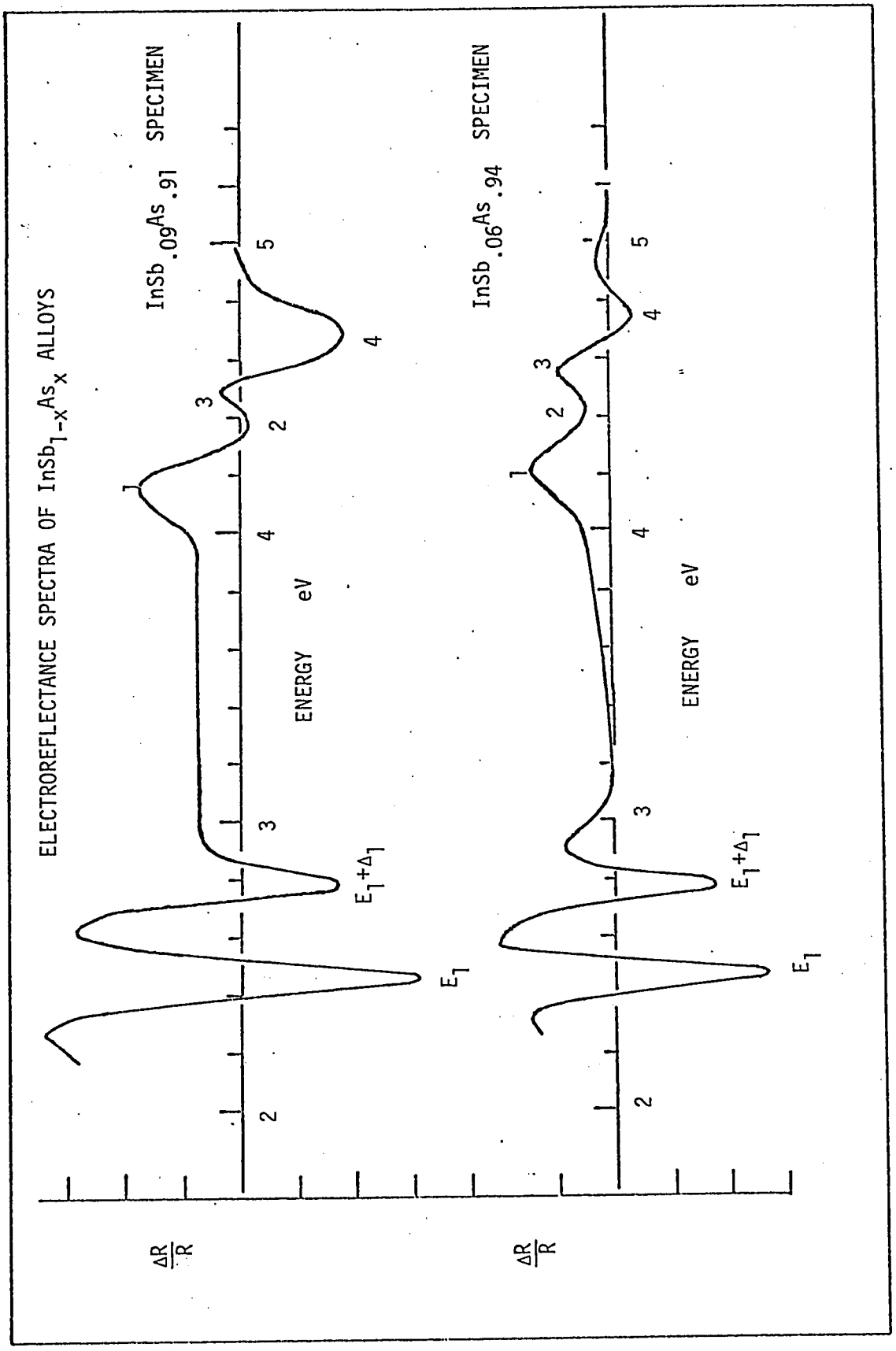
ELECTROREFLECTANCE SPECTRA OF $InSb_{1-x}As_x$ ALLOYS
$InSb_{.09}As_{.91}$ SPECIMEN
$InSb_{.06}As_{.94}$ SPECIMEN
ENERGY eV
E_1
$E_1+\Delta_1$
$\frac{\Delta R}{R}$

should be due to E_0' and E_2 transitions respectively. Here it is assumed that the $E_1' + \Delta_1'$ transition which has not been seen in the spectra of InAs will not be observed in the spectra of InAs rich alloy samples.

From the plot of energy gap versus composition shown in Fig. 4.34, the E_1 and $E_1 + \Delta_1$ gap variation shows the familiar behaviour observed in the $Ga_xIn_{1-x}Sb$ and $InAs_{1-x}P_x$ alloy systems. But it appears that if peaks 2 and 4 were to be chosen as E_0' and E_2 respectively, the E versus x curve would take an unusual convex shape which has never been observed in the III - V alloys studied so far. Further, the extrapolated values from the energies of peaks 2 and 4 in InAs rich alloy samples do not predict correct values for E_0' and E_2 in InAs. In this situation the energy values of all four peaks labelled 1, 2, 3 and 4 are determined and their energies plotted in Fig. 4.34. Studying the variation of these values with composition and correlating with the well known data for InAs and InSb rich alloy range, $0 < x < 0.15$, it appears that the peaks labelled 1 and 3 must be taken as E_0' and E_2 respectively. For further discussion of energy gap variation as a function of composition, given in Section 4.8, the energies of peaks labelled 1 and 3 are chosen as the E_0' and E_2 band gaps.

FIGURE 4.34

TRANSITION ENERGIES Versus COMPOSITION

$InSb_{1-x}As_x$ ALLOYS

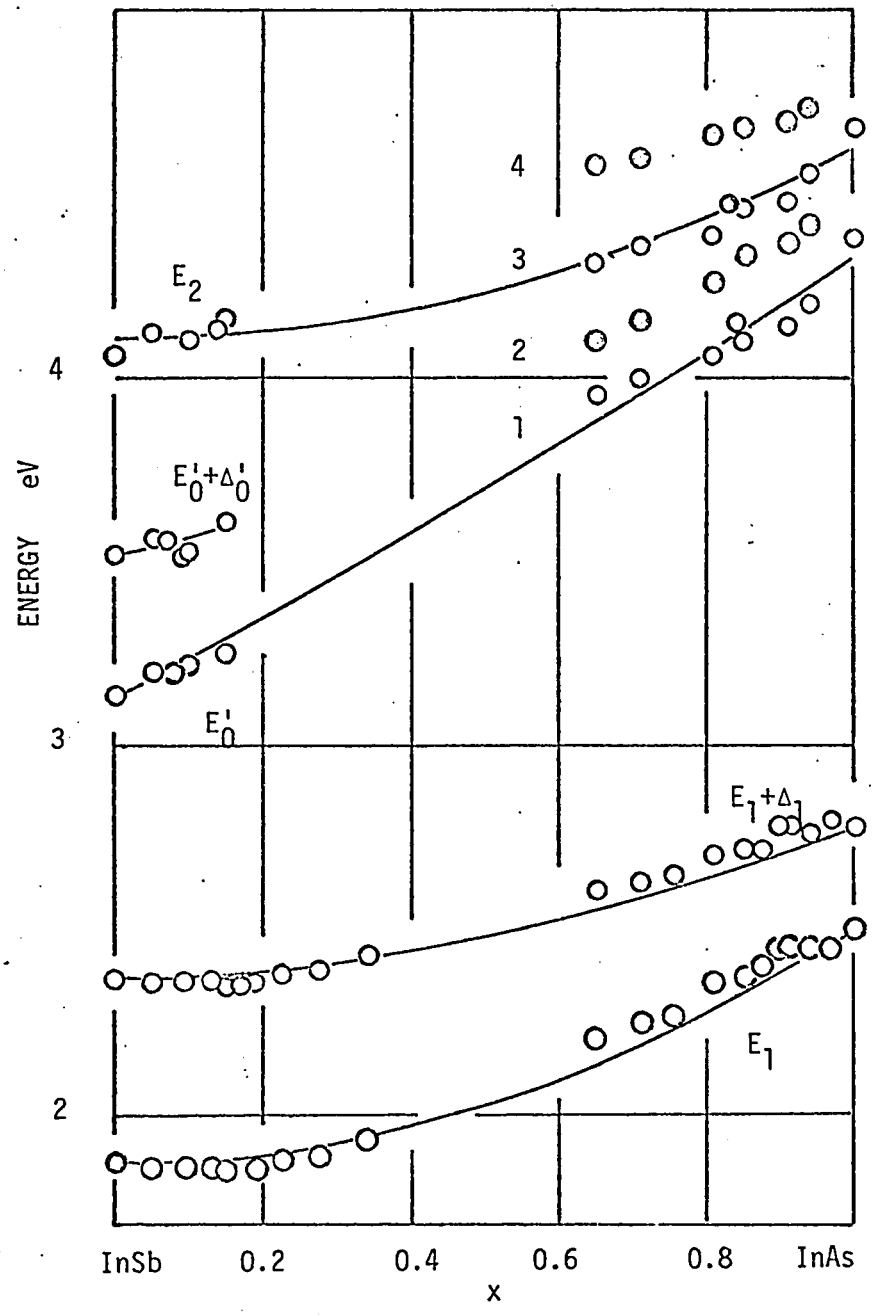

4.7 Summary of Results on III - V Alloys

For the three III - V alloy systems, $Ga_xIn_{1-x}Sb$, $InAs_{1-x}P_x$ and $InSb_{1-x}As_x$, considered presently the variation of energy values of E_1, $E_1 + \Delta_1$, E_0' and E_2 transitions determined from electroreflectance is not a linear function of composition but in every case the E versus x curve takes a concave upwards form.

From reflectance measurements on $Ga_xIn_{1-x}Sb$ alloy, the E_1, $E_1 + \Delta_1$ and E_2 transitions are found to vary nonlinearly as a function of composition in good agreement with electroreflectance results. However, a linear variation may be assumed for $E_2 + \Delta_2$, $E_2 + \delta$, E_1' and $E_1' + \Delta_1'$ transitions within the limits of experimental uncertainty.

While the E_1 and $E_1 + \Delta_1$ energy variation is found to be non-linear as a function of composition in $Ga_xIn_{1-x}Sb$ alloy from the thermo-reflectance measurements also, the composition dependence of E_2 is shown to be linear within the limits of experimental uncertainty.

In analysing the results of the variation of transition energies as a function o f alloy composition in the following section, electro-reflectance data is preferred whenever it is available, assuming that electroreflectance results are more accurate compared with reflectance and thermoreflectance data.

4.8 Discussion of results on III - V Alloys

The correspondence between the structure in the reflectance and modulated reflectance spectra of a material to its energy band structure has been discussed in Chapter 2. In alloy studies using the reflectance and modulated reflectance techniques, variation of band structure can be investigated as a function of composition progressively from one compound to the other.

Two alloy systems, $GaAs_{1-x}P_x$ and $Ga_xIn_{1-x}As$, were studied previously by Thompson and Woolley.[104,95] It was found that the energy gap variation as a function of composition, E versus x, is similar to the results obtained in the present work. However, previously it was assumed that for all transitions at energies higher than the fundamental gap energy the E versus x variation should be linear. Thus the departure of the E_1 and $E_1 + \Delta_1$ gaps from a linear variation as a function of composition was attributed to a movement of the region containing the critical points where $\Lambda_{3v} - \Lambda_{1c}$ transitions take place along the Λ direction. But in the light of the present results on three more alloy systems, the nonlinear variation of E as a function of x seems much more systematic than would be expected from a movement of the critical point in k space. In order to consider the five alloy systems together, the main parts of the previous data on $GaAs_{1-x}P_x$ and $Ga_xIn_{1-x}As$ alloys are given in Figs. 4.35 and 4.36.

The cause of the nonlinear variation of band gaps as a function of composition other than from the movement of critical point in k space can be assumed to come from the effect of disorder in the alloys. From the virtual crystal analysis in disordered alloy lattices given in

FIGURE 4.35

TRANSITION ENERGIES Versus COMPOSITION

$GaAs_{1-x}P_x$ ALLOYS

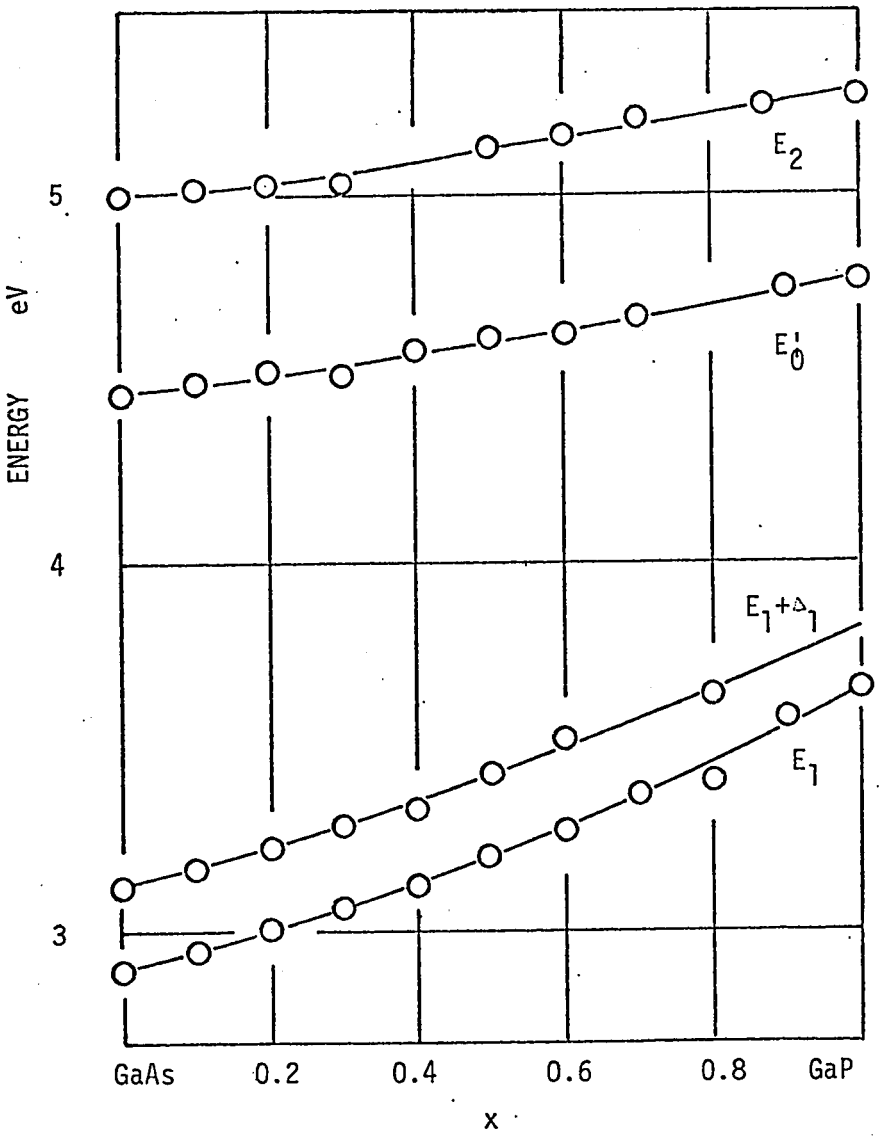

FIGURE 4.36

TRANSITION ENERGIES versus COMPOSITION

$Ga_xIn_{1-x}As$ ALLOYS

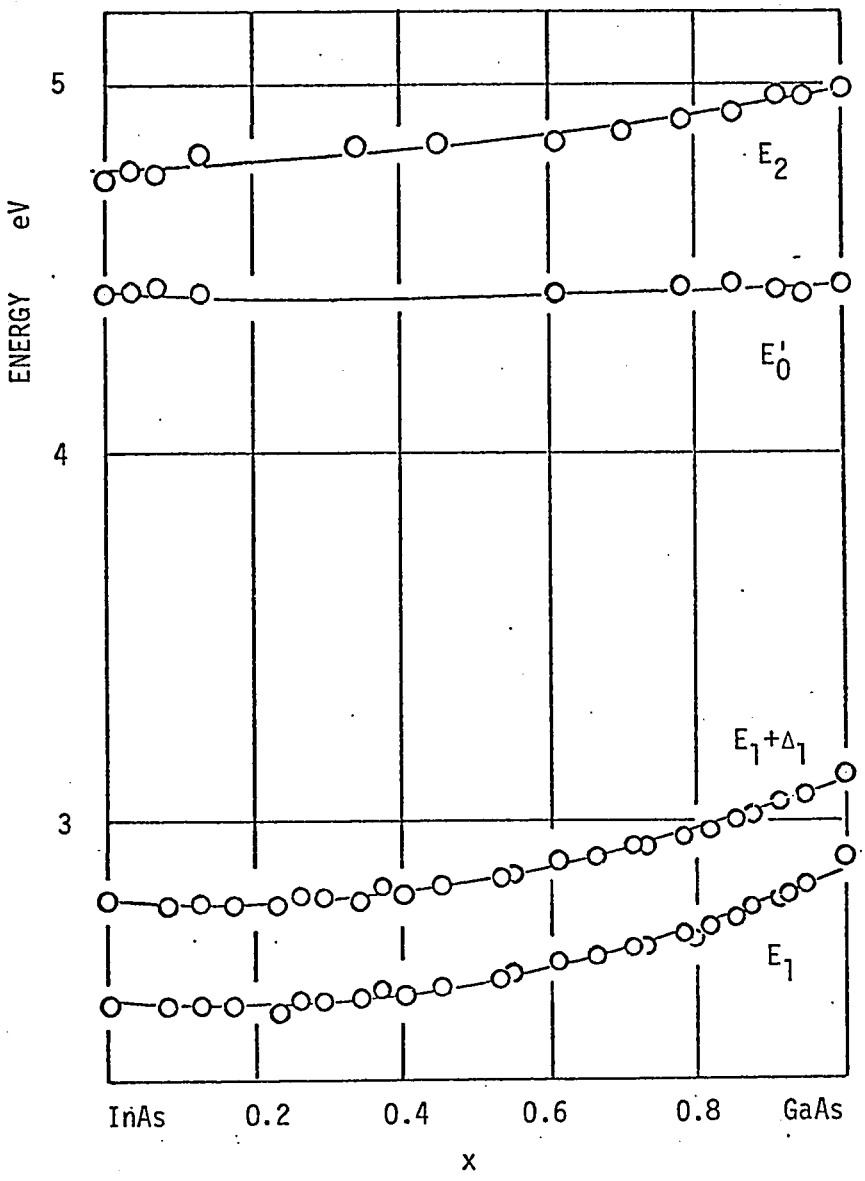

Section 1.7, when V_{per} alone is considered neglecting the V_{aper} term, a smooth variation of band structure is to be expected through an alloy system from one compound to the other. Before the development of the presently available quantitative calculations on the electronic structures of semiconductor alloys by Van Vechten and Bergstresser[55] the energy gap variation as a function of composition determined by virtual crystal method was assumed to be linear. In that case the virtual crystal band gap, E(x) may be written, under linear approximation, as

$$E(x) = a + bx \quad , \tag{4.1}$$

where $E(0) = a$ and $E(1) = a + b$ are the interband gaps in the end compounds of the alloy system. The effect of disorder in an alloy lattice calculated from the second order perturbation theory treating V_{aper} as perturbation is shown to be to adding a term proportional to $x(1 - x)$ to the virtual crystal band gap,[189,105] given in Eq.(4.1)

$$\begin{aligned} E(x) &= a + bx + cx(1-x) \quad , \\ &= a + b^1x + cx^2 \quad , \end{aligned} \tag{4.2}$$

where the coefficient c represents the effect of lattice disorder. The variation of the band gap in a disordered lattice as given by Eq.(4.2) is of a parabolic form. The value of c is a measure of the deviation from linearity.

This modified virtual crystal analysis was applied previously to the fundamental gap variation as a function of composition for five alloy systems by Thompson and Woolley.[105] This gap is known to occur at the Γ point in III - V compounds and hence no movement of the critical point in k space is involved with this transition as a function of alloying. Experimental values of the bowing parameter c obtained for the E_0 transition are summarized in Table 4.5.

TABLE 4.5

Experimental values of total bowing parameters (c) obtained by fitting the various E versus x curves to

$$E(x) = a + bx + cx^2$$

Bowing Parameters	$GaAs_{1-x}P_x$ Alloys	$InAs_{1-x}P_x$ Alloys	$InSb_{1-x}As_x$ Alloys	$Ga_xIn_{1-x}As$ Alloys	$Ga_xIn_{1-x}Sb$ Alloys
$c(E_0)$	0.21	0.27	0.58	0.6	0.43
$c(E_1)$	0.31	0.32	∿0.7	0.52	0.38
$c(E_1+\Delta_1)$	0.19	0.19	∿0.4	0.49	0.28
$c(E_1$ Mean)	0.25	0.26	∿0.55	0.50	0.33
$c(E_0')$	0.02	0.11	∿0.1	0.08	-
$c(E_2)$	0.03	0.27	∿0.6	0.27	0.24

Recently, it has been shown by Van Vechten and Bergstresser,[55] applying the dielectric method for the determination of band structure of alloys, that the energy gap variation as a function of composition is not linear under virtual crystal approximation as it was assumed before. Instead E(x) is shown to obey a quadratic expression

$$E(x) = a + bx + c_i x^2 \quad ,$$

where c_i is known as the intrinsic bowing parameter. The values of c_i calculated for the three band gaps E_0, E_1 and E_2 are given in Table 4.6.

The disorder parameter c, introduced in Eq.(4.2) which is hereafter known as the total bowing parameter is taken as the sum of the intrinsic bowing parameter c_i (Table 4.6) and a disorder bowing parameter c_e which is introduced to account for the effects of lattice disorder in alloys.[55] The value of c_e is determined empirically by knowing the magnitude of the potential fluctuation, C_{FG} in an $MF_{1-x}G_x$ type alloy,

$$c_e = C_{FG}^2 / A \quad ,$$

where A is a constant chosen empirically to fit the experimental data of c_e on one alloy system, namely ZnS - Te which has a large value for C_{FG}. The value of A determined from the above expression is used to determine c_e in all other alloy systems. The values of c_e calculated for the five alloy systems presently considered are given in Table 4.6.

It has been assumed by Van Vechten and Bergstresser[55] that the values of c_e would be the same for all band gaps, namely E_0, E_1 and E_2, considered at present. The total bowing parameters (c values) thus determined theoretically for five alloy systems are listed in Table 4.6.

In the present analysis, the total bowing parameters (c values)

TABLE 4.6

THEORETICAL VALUES OF INTRINSIC BOWING (c_i), DISORDER BOWING (c_e) AND TOTAL BOWING (c) PARAMETERS (Van Vechten and Bergstresser)[55]

Bowing Parameters	$GaAs_{1-x}P_x$ Alloys	$InAs_{1-x}P_x$ Alloys	$InSb_{1-x}As_x$ Alloys	$Ga_xIn_{1-x}As$ Alloys	$Ga_xIn_{1-x}Sb$ Alloys
$c_i(E_0)$	0.21	0.15	0.03	0.28	0.12
$c_i(E_1)$	0.10	0.07	0.02	0.13	0.07
$c_i(E_2)$	0.02	0.02	0.05	0.06	0.05
c_e	0.09	0.08	0.67	0.29	0.24
$c(E_0)$	0.30	0.23	0.70	0.57	0.36
$c(E_1)$	0.19	0.15	0.69	0.42	0.31
$c(E_2)$	0.11	0.10	0.72	0.35	0.29

will be determined for the E_1, $E_1 + \Delta_1$, E_0' and E_2 gaps fitting the experimental results, E versus x, to Eq.(4.2). The experimental values of c will be compared with the available theoretical values given in Table 4.6.

E_1 and $E_1 + \Delta_1$ transitions

The E_1 and $E_1 + \Delta_1$ doublet is due to transitions between the spin orbit split Λ_3 valence and Λ_1 conduction states shown in Fig. 2.5. The composition dependence of these band gaps is nonlinear in all five alloy systems, (Figs. 4.24, 4.29, 4.34 to 4.36). As it is not necessary that the critical point region in the Λ direction remain in one place in all III - V compounds, some nonlinear variation of E_1 gaps with composition could occur in III - V alloys due to this movement. Therefore, the analysis of the E_1 and $E_1 + \Delta_1$ gap variation as a function of composition should take into consideration two effects, namely: 1) the possible movement of the critical point region in k space and 2) the bowing effects. The magnitude of the effect of the movement of the critical point region depends upon the variation of energy of $E(\Lambda_3)$ and $E(\Lambda_1)$ bands as a function of k in the Λ direction. As is seen from Eq.(4.2), the deviation of the experimental results from linear behaviour should be symmetrical if bowing effects only are present and any asymmetry will indicate the presence of some other effect, for example, the movement of critical points in k-space. The difference between the experimental value for E_1 and the value obtained from a linear interpolation between the values for the two compounds, δ when plotted as a function of x for all five alloy systems (Fig. 4.37) showed little deviation from symmetry

FIGURE 4.37

COMPOSITION DEPENDENCE OF δ

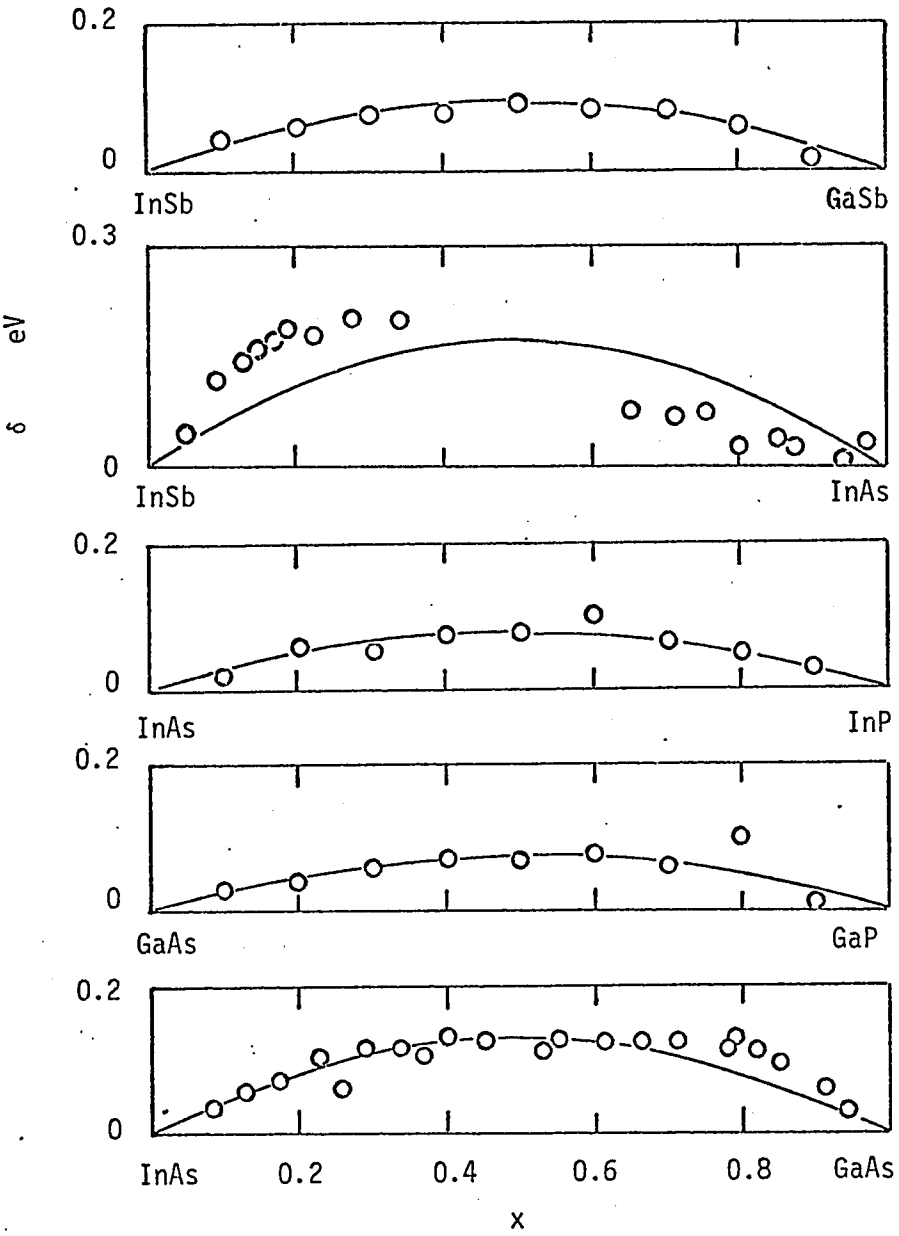

in four alloys except in the case of $InSb_{1-x}As_x$.

A least squares fit to Eq.(4.2) is obtained for the E_1 versus x and $E_1 + \Delta_1$ versus x values for the five alloy systems and the lines representing the best fit are shown in Figs. 4.24, 4.29, 4.34 to 4.36. Obviously, the least squares fit is poor for $InSb_{1-x}As_x$ as is seen already from δ versus x curve, (Fig. 4.37). The parameters have been adjusted to give the best compromise between the results obtained in the two different regions of compositions available. The c values obtained from this fit are listed in Table 4.5. Except in the case of $GaAs_{1-x}P_x$ alloy where the $E_1 + \Delta_1$ data used is from reflectance measurements all the other data is obtained from electroreflectance measurements. However, those electroreflectance data which are available on $E_1 + \Delta_1$ transitions are in good agreement with this reflectance data.

For each alloy specimen, the spin orbit split value of the Λ_3 valence state, Δ_1 is determined as the difference between the experimental values for E_1 and $E_1 + \Delta_1$. The composition dependence of Δ_1 is plotted for each alloy system which is shown in Fig. 4.38. In all five alloy systems the composition dependence of Δ_1 is found to be nonlinear. In the case of Δ_1, it is possible to express the effects of lattice disorder, which are responsible for bowing in the Δ_i versus x curves, in terms of the spin orbit splittings of the constituent atoms in the alloy.

An empirical relation was suggested by Braunstein and Kane[124] for the spin orbit splitting Δ_1 in all III - V compounds,

$$\Delta_1 = \alpha \Delta_{at}^{III} + \beta \Delta_{at}^{V}$$

FIGURE 4.38

COMPOSITION DEPENDENCE OF Δ_1

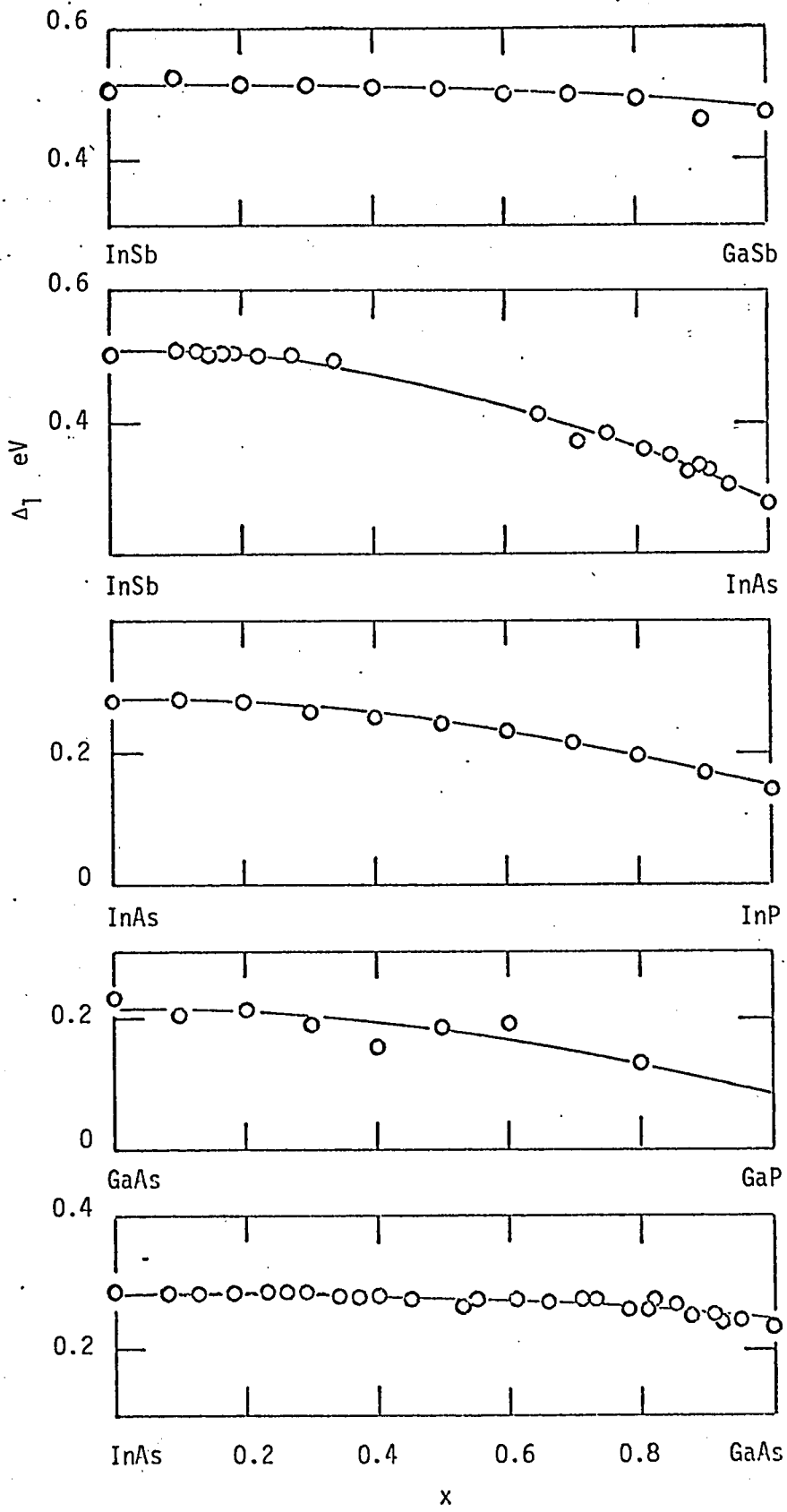

where α and β are the fractional times an electron spends on valence III and V atoms and Δ_{at}^{III} and Δ_{at}^{V} are the spin orbit splittings of the valence III and V atoms respectively. Extension of virtual crystal analysis gives for Δ_1 in an alloy of Mixed V atoms in the form III $V(B)_{1-x}V(A)_x$

$$\Delta_1 = \alpha\, \Delta_{at}^{III} + \beta\{x\, \Delta_{at}^{V}(A) + (1 - x)\ \Delta_{at}^{V}(B)\} \quad . \qquad (4.3)$$

The effect of lattice disorder will add a term $\gamma\, x(1 - x)$ to the virtual crystal value, Eq.(4.3), giving

$$\Delta_1 = \alpha\, \Delta_{at}^{III} + \beta\, \{x\, \Delta_{at}^{V}(A) + (1 - x)\, \Delta_{at}^{V}(B)\ \} + \gamma\, x(1 - x)$$

$$= \{\alpha\, \Delta_{at}^{III} + \beta\, \Delta_{at}^{V}(B)\} + x\big(\beta\{\Delta_{at}^{V}(A) - \Delta_{at}^{V}(B)\} + \gamma\big) - x^2\gamma \qquad (4.4)$$

Eq.(4.4) can be rewritten in the form

$$\Delta_1 = a + bx - cx^2 \quad , \qquad (4.5)$$

with $\quad a = \alpha\, \Delta_{at}^{III} + \beta\, \Delta_{at}^{V}(B) \quad ,$

which is the spin orbit splitting in one of the compounds, III V(B),

$$b = \beta\{\Delta_{at}^{V}(A) - \Delta_{at}^{V}(B)\ \} + \gamma \qquad (4.6)$$

and

$$c = \gamma \ . \qquad (4.7)$$

Similar procedure for an alloy which is of the form $III(A)_x III(B)_{1-x}V$ with mixed valence III atoms leads again to Eq.(4.5) but with

$$b = \alpha\{\Delta_{at}^{III}(A) - \Delta_{at}^{III}(B)\ \} + \gamma \ . \qquad (4.8)$$

A least squares fit to Δ_1 versus x data to Eq.(4.5) gave a very small value for b and a good fit for all five alloys is still obtained when b is chosen to be zero. The condition b = 0 reduces

Eqs. (4.6) and (4.8) to

$$\gamma = \beta \{\Delta_{at}^{V}(B) - \Delta_{at}^{V}(A)\} \quad (4.9)$$

for mixed valence V atoms, and

$$\gamma = \alpha \{\Delta_{at}^{III}(B) - \Delta_{at}^{V}(A)\} \quad (4.10)$$

for mixed valence III atoms. When b = 0, Eq.(4.5) becomes

$$\Delta_1 = a - cx^2 \quad (4.11)$$

where

$$c = \beta \{\Delta_{at}^{V}(B) - \Delta_{at}^{V}(A)\} \quad (4.12)$$

for mixed valence V atoms, and

$$c = \alpha \{\Delta_{at}^{III}(B) - \Delta_{at}^{III}(A)\} \quad (4.13)$$

for mixed valence III atoms, deduced from Eqs.(4.7), (4.9) and (4.10). Eq.(4.11) is fitted to the Δ_1 versus x data for the five alloy systems and the results are shown in Fig. 4.38. It is seen that in all cases including $InSb_{1-x}As_x$ alloy results a good fit is obtained. The resulting experimental values of c are given in Table 4.7. The experimental uncertainty in the c values could be as much as ±20 percent depending upon the scatter of the experimental values.

Table 4.7

Experimental and Theoretical Values of c for Δ_1

	$GaAs_{1-x}P_x$	$InAs_{1-x}P_x$	$InSb_{1-x}As_x$	$Ga_xIn_{1-x}As$	$Ga_xIn_{1-x}Sb$
$c(\Delta_1)$ Exptl.	0.13	0.13	0.23	0.04	0.05
$c(\Delta_1)$ Predicted	0.15	0.15	0.32	0.05	0.05

For comparison, the values of c are calculated for each alloy system

using Eqs.(4.12) and (4.13) and the Δ_{at} values for valence III and V atoms (Table 4.8) suggested by Kane.[24]

Table 4.8

Atomic spin orbit splittings in valence III and V elements

Element	Ga	In	P	As	Sb
Δ_{at} eV	0.12	0.27	0.046	0.29	0.8

The appropriate values for α and β in III - V compounds are $^3/_8$ and $^5/_8$ respectively.[124] The calculated values of c which are given in Table 4.7 are in good agreement with the c values obtained experimentally except again for $InSb_{1-x}As_x$ alloy.

However, this time the probable source of discrepancy could be in the values assumed for α and β. In the case of III - V compounds with heavier atoms as constituents, the values of α and β should probably be more nearly equal and values of $\alpha = \beta = 0.5$ would give the predicted value of 0.25 for c which is in good agreement with the experimental value.

E_0' and $E_0' + \Delta_0'$ transitions

Structure due to E_0' transitions was observed in the spectra of samples of $GaAs_{1-x}P_x$ and $InAs_{1-x}P_x$ alloys over the whole composition range and only in two parts of the composition range, $0 < x < 0.2$ and $0.6 < x < 1.0$ in samples of $Ga_xIn_{1-x}As$ and $InSb_{1-x}As_x$ alloys. In $Ga_xIn_{1-x}Sb$ alloy, the E_0' structure was not clear and the experimental results showed large scatter for which reason they are not included for further discussion. Structure due to $E_0' + \Delta_0'$ was observed only in

$InSb_{1-x}As_x$ alloy samples in the composition range $0 \leq x \leq 0.2$. To the available E_0' versus x data on the four alloy systems, (Figs. 4.29, 4.34 to 4.36), the quadratic equation, Eq.(4.2), is fitted and the c values given in Table 4.5 will be discussed along with the c values of the other transitions. The data available on $E_0' + \Delta_0'$ transitions is not adequate for determining a c value for further discussion.

E_2 transitions

The E_2 transition energies are available over the whole composition range in four alloys. But in the fifth alloy system, $InSb_{1-x}As_x$, the E_2 versus x data is not obtained in the composition range $0.2 < x < 0.6$ because the corresponding structure was not seen in the spectra of the alloy samples. The data available on the five alloy systems (Figs. 4.24, 4.29, 4.34,- 4.36), derived from electroreflectance measurements is fitted to Eq.(4.2) and the resulting values of c are included for further discussion in Table 4.5.

$E_2 + \Delta_2$, $E_2 + \delta$, E_1' and $E_1' + \Delta_1'$ transitions

These transitions are grouped together because they were determined from reflectance measurements in only one alloy system, $Ga_xIn_{1-x}Sb$, and further, the composition dependence of the energies of these transitions is shown to be linear, that is: c is negligible. But it should be expected that the $E_2 + \Delta_2$ energy variation with composition to be nonlinear because it is the spin orbit split associate of the E_2 transition which showed considerable bowing ($c = 0.24$, Table 4.5).

This behaviour is not observed because the accuracy with which $E_2 + \Delta_2$ was determined is 0.05 eV at best and this accuracy is not adequate to see the bowing in the $E_2 + \Delta_2$ versus x curve. As structure due to this transition was not observed in the electroreflectance spectra, $E_2 + \Delta_2$ could not be determined more accurately in order to obtain its c value. Therefore, no bowing parameters are available for these transitions to include them in the following discussion.

Discussion of c values

The bowing parameters determined for various transitions are given in Table 4.5. The c values for the fundamental gap are taken from previous work. It is seen that the values of c for E_1 transition are large when compared with the c values obtained for its spin orbit split associate $E_1 + \Delta_1$. Therefore, to eliminate the spin orbit effect to some extent a mean value for the bowing parameter, c(E_1 Mean) is determined from the c values obtained for E_1 and $E_1 + \Delta_1$ and the values of c(E_1 Mean) are given in Table 4.5. In a similar manner, an average value of c should be calculated for the E_2 transitions from the c values of E_2 and $E_2 + \Delta_2$ transitions. But, at present, data which are sufficiently accurate are not available for $E_2 + \Delta_2$ transitions in III - V alloys. In this situation, the values of c determined for E_2 are used for further discussion.

When the c values for the four transitions E_0, E_1 Mean, E_0' and E_2 are considered in each alloy system they can be divided into two groups, those transitions which showed considerable bowing like E_0, E_1 Mean and E_2 and those whose c values are small, like E_0'. Prior to

the theoretical calculation of c values by Van Vechten and Bergstresser,[55] the large bowing observed in E_0, E_1 and E_2 was attributed to disorder in the alloy lattice.[190] However, the results of Van Vechten and Bergstresser show the presence of some intrinsic bowing due to virtual crystal approximation. The intrinsic bowing is seen to decrease as the energy of the transition increases (Table 4.6). Therefore, when the theoretical values of c_i and c_e are compared for E_2 transitions the main contribution to total bowing is due to lattice disorder in every alloy.

The experimental values of c for E_0, E_1 Mean and E_2 given in Table 4.5 may now be compared with the corresponding theoretical values given in Table 4.6. However, while making this comparison it should be remembered that the theoretical values for the total bowing parameters have been determined empirically. In this calculation the disorder bowing parameter c_e obtained from fitting experimental data on E_0 gap in one alloy system has been assumed to remain the same for E_1 and E_2 gaps as well. In the light of this, any disagreement between the two sets of data could either be due to experimental uncertainty because of scatter in the experimental values or due to uncertainty in the theoretical values. The experimental uncertainty in c values could be as much as $\pm$20 percent for E_1 Mean, E_0' and E_2 transitions. For E_1 transitions, the experimental and the theoretical bowing parameters are in good agreement except in the case of $InAs_{1-x}P_x$ alloy. The calculated and the experimental values of c for E_2 are in good agreement in three alloys while the calculated value is larger than the experimental value in $GaAs_{1-x}P_x$. The situation is reversed in $InAs_{1-x}P_x$ alloy. For the E_0' transition, the experimental bowing parameters are of the same order of magnitude in

three alloys. However, a small value for c is obtained in $GaAs_{1-x}P_x$ alloy. In this case, theoretical values are not available for the bowing parameters of E_0' in order to compare them with the experimental data. Because of this, the E_0' transitions which are between the $\Delta_{5v} - \Delta_{1c}$ states close to the centre of the Brillouin zone are compared with the c values of E_0 transitions, which are located at the centre of the Brillouin zone. But it is seen that the c values of E_0 are considerably larger than those of E_0'. This is probably due to the fact that the conduction bands involved in the two transitions are different. Moving along the Δ direction towards the zone boundary, the E_2 gap energy is of the same order of magnitude as E_0'. When the c values of E_0' are compared with those of E_2 it is seen that the intrinsic bowing of parameters (c_i's) of E_2 are comparable with the total bowing parameters of E_0'. This suggests that in the case of E_0' the contribution from disorder bowing (c_e) to the total bowing parameter is small, indicating that lattice disorder has little effect on the higher conduction band. From this reasoning the bowing parameters should be small for $E_2 + \delta$ and E_1' compared with the c values for E_0, E_1 and E_2 and the bowing in $E_2 + \Delta_2$ should be comparable to the c values of E_2. Therefore it appears that while bowing due to lattice disorder is considerable for the gaps involving the highest valence and the lowest conduction bands, the interband gaps between the same valence band but a higher conduction band seem to be less affected.

CHAPTER 5

SUMMARY AND CONCLUSIONS

In the reflectance spectra of III - V compounds the multiplet structure in E_2 and E_1' complexes were well resolved. From the results on E_2 structure comparing the experimental values of Δ_2 with the corresponding spin orbit splitting of the X_5 valence level $(X_6 - X_7)$from k.p calculations,[127] the agreement is poor in several cases. However, on this basis alone it is not possible to conclude whether this disagreement is due to uncertainty in the computed values or due to an ambiguous assignment of the E_2 complex. The δ splitting is found to be of the order of 0.4 eV agreeing with the computed value for $(X_1 - X_3)$.[111] This means that if $\Sigma_2 - \Sigma_1$ transition is responsible for E_2 instead of $X_5 - X_1$, this transition should be close to the X symmetry point, but situated on the Σ axis. From the results on E_1' complex, as expected from the disagreement of Δ_1' and Δ_1 values, ΔL_{3c} is not negligible. Further, ΔL_{3v} is of the same order of magnitude as Δ_1 within the limits of experimental uncertainty, indicating that the spin orbit splitting of Λ_3 valence level remains the same between the $\Lambda_3 - \Lambda_1$ and $L_{3v} - L_{3c}$ critical points.

The structure found in the thermoreflectance spectra of III - V compounds correlate to the energies where structure is found in reflectance and electroreflectance spectra. The thermoreflectance structure line shapes have a characteristic asymmetric (inverted) peak with the low energy side steeper than the high energy side. Therefore those spin orbit split components which are close to the main peak are not

resolved. The $E_2 + \Delta_2$ is an example. This technique can be extended into infrared and ultraviolet regions as the reflecting surface of the sample is not covered in any way. In the infrared, if the present assignment of the structure found in GaP spectrum were correct, structure due to indirect transitions in Ge and Si can be investigated. In the ultraviolet region the structure due to E_1' transitions would probably lead to the determination of ΔL_{3_V} and ΔL_{3_C} with more accuracy than is presently available from reflectance spectra.

From the results on III - V alloys, the energy gap variation as a function of composition is nonlinear for E_1, $E_1 + \Delta_1$, E_0' and E_2. From the c values determined for the above transitions, E_0, E_1 and E_2 showed considerable bowing while bowing in E_0' is relatively small. This leads to the conclusion that the interband gaps between the highest valence and the lowest conduction bands are affected considerably by lattice disorder in addition to some virtual crystal effects. On this basis, bowing in $E_2 + \Delta_2$ should be comparable to what is seen for E_2. In the case of E_0', comparison of its c values with those of E_0 and E_2 indicate that the contribution from bowing due to lattice disorder to the total bowing parameter is small. Similarly, very little bowing due to lattice disorder can be expected for other transitions like $E_2 + \delta$ and E_1' which take place between the same pair of bands responsible in E_0' transition.

References

1. H. Welker, Z. Naturforsch. 7A, 744 (1952).
2. O. G. Folberth, Z. Naturforsch. 10A, 502 (1955).
3. F. Herman and J. Callaway, Phys.Rev. 89, 518 (1953).
4. P. Drude, Ann. der Physik 1, 566 (1900).
5. H. A. Lorentz, Proc. Amsterdam Acad. 7, 684 (1905).
6. A. Sommerfeld, Zeit. Phys. 47, 1 (1928).
7. A. H. Wilson, Proc. Phys. Soc. A133, 458 (1931).
8. A. H. Wilson, Proc. Phys. Soc. A134, 277 (1931).
9. F. Bloch, Zeit. Phys. 52, 555 (1928).
10. L. Brillouin, J. Phys. Radium 1, 377 (1930).
11. L. P. Bouckaert, R. Smoluchowski and E. Wigner Phys. Rev. 50, 58 (1936).
12. H. Jones, " The Theory of Brillouin Zones and Electronic States in Crystals ", Interscience Publishers Inc. (1960) New York.
13. J. Callaway, " Energy Band Theory ", Academic Press (1964) New York.
14. J. C. Slater, " Quantum Theory of Molecules and Solids ", Vol.2 McGraw - Hill Book Company (1965) New York.
15. F. Herman, Rev. Mod. Phys. 30, 1 (1958).
16. F. Herman, Proc. Intern. Conf. Phys. Semicond. (1964) Paris.
17. J. C. Slater, " Methods in Computational Physics. Advances in Research and Applications-Energy Bands of Solids, Volume 8, Academic Press (1969) New York.
18. C. Herring, Phys. Rev. 57, 1169 (1940).
19. F. Herman, " Methods in Computational Physics, Energy Bands of Solids " Volume 8, Academic Press (1969) New York.

20. G. Dresselhaus, A.F.Kip and C. Kittel, Phys. Rev. 98, 368 (1955).

21. E. O. Kane, " Semiconductors and Semimetals " Volume 1 Academic Press (1966) New York.

22. F. H. Pollak and M. Cardona, Phys. Rev. 142, 530 (1966).

23. E. O. Kane, J. Phys. Chem. Solids 1, 83 (1956).

24. E. O. Kane J. Phys. Chem. Solids 1, 249 (1957).

25. M. Cardona J. Phys. Chem. Solids 24, 1543 (1963).

26. F. H. Pollak, C.W. Higginbotham and M. Cardona Proc. Intern. Conf. Phys. Semicond. (1966) Kyoto. J. Phys. Soc. Japan 21S, 20 (1966).

27 F. H. Pollak, C. W. Higginbotham and M. Cardona Proc. Intern. Conf. Phys. Semicond. (1968) Moscow.

28 J. C. Phillips and L. Kleinman Phys. Rev. 116, 287 (1959).

29 J. C. Phillips Phys. Rev. 112, 685 (1958).

30 J. C. Phillips Proc. Intern. Conf. Phys. Semicond. (1966) Kyoto. J. Phys. Soc. Japan 21S, 3 (1966).

31 M. L. Cohen and T. K. Bergstresser Phys. Rev. 141, 789 (1966).

32 J. C. Phillips and J. A. Van Vechten Phys. Rev. Letters 22, 705 (1966).

33 J. C. Phillips Phys. Rev. Letters 20, 550 (1968).

34 S. Grooves and W. Paul Phys. Rev. Letters 11, 194 (1963).

35 M. Cardona, P. McElroy, F. H. Pollak and K. L. Shaklee Solid State Commun. 4, 319 (1966).

36 R. Robertson, J. J. Fox and A. E. Martin Phil. Trans. A232, 463 (1934).

37 F. Herman, R. L. Kortum, C. D. Kuglin, R. A. Short " Quantum Theory of Atoms, Molecules and the Solid State " , Academic Press (1966) New York.

38 C. Herring J. Franklin Inst. 233, 525 (1942).

39 R. J. Elliott Phys. Rev. 96, 280 (1954).

40 R. A. Smith " Semiconductors " Cambridge University Press (1959).

41 D. Long, " Energy Bands in Semiconductors ", Interscience Publishers (1968) New York.

42 F. Herman, Phys. Rev. 95, 847 (1954).

43 O. Madelung, " Physics of III - V Compounds ", John Wiley and Sons Inc. (1964) New York.

44 R. H. Parmenter, Phys. Rev. 100, 573 (1955).

45 G. Dresselhaus, Phys. Rev. 100, 580 (1955).

46 F. Herman, J. Electron. 1, 103 (1955).

47 W. Hume-Rothery and G. V. Raynor, "The Structure of Metals and Alloys" Institute of Metals (1962) London.

48 H. Stohr and W. Klemm, Z. Anorg. Allgem. Chem. 241, 305 (1939).

49. E. R. Johnson and S. M. Christian, Phys. Rev. 95, 560 (1954).

50 J. C. Woolley, " Compound Semiconductors ", Volume 1, Reinhold (1962).

51 O. G. Folberth, Z. Naturforsch. 13A, 856 (1958).

52 E. K. Muller and J. L. Richards, J. Appl. Phys. 35, 1233 (1964).

53 F. Bassani and D. Brust, Phys. Rev. 131, 1524 (1963).

54 D. Jonesand A. H. Lettington, Bull. Am. Phys. Soc. 14, 329 (1969).

55 J, A. Van Vechten and T. K. Bergstresser, (To be published).

56 L. Nordheim, Ann. Phys. Leipzig, 9, 607 (1931).

57 T. Muto, Sci. Papers Inst. Phys. Chem. Res. Tokyo, 34, 377 (1938).

58 R. H. Parmenter, Phys. Rev. 97, 587 (1955).

59 R. H. Parmenter, Phys. Rev. 99, 1759 (1955).

60 R. H. Parmenter, J. Phys. Chem. Solids, 6, 6 (1958).

61 F. Herman, Phys. Rev. 93, 1214 (1954).

62 C. S. Smith, Phys. Rev. 94, 42 (1954).

63 G. L. Pearson and C. Herring, Am. Phys. Soc. (1953) Stanford.

64 B. Lax and Dexter (Ref. given in F. Herman, Phys. Rev. 95,847(1954).

65 J. Tauc and A. Abraham, Proc. Intern. Conf. Phys. Semicond. (1960) Prague.

66 J. Tauc and A. Abraham, J. Phys. Chem. Solids, 20, 190 (1961).

67 J. S. Kline, F. H. Pollak and M. Cardona, Helv. Phys. Acta, 172, 816 (1968).

68 H. Weiss, Z. Naturforsch. 11A, 430 (1956).

69 N. A. Goryunova and N. N. Fedorova, Zhur. Tekh. Fiz. 25, 1339 (1955).

70 J. C. Woolley and B. A. Smith, Proc. Phys. Soc. 72, 214 (1958).

71 J. C. Woolley and B. A. Smith, Proc. Phys. Soc. B70, 153 (1957).

72 J. C. Woolley and B. A. Smith and D. Lees, Proc. Phys. Soc. B69, 1339(1956).

73 V. I. Ivanov - Omskii, B. T. Kolomiets, Fiz. Tv. Tela, 1, 913 (1959).

74 M. S. Abrahams, R. Braunstein and F. D. Rossi
J. Phys. Chem. Solids, 10, 204 (1959).

75 W. M. Coderre, Ph. D. Thesis (1969) U of Ottawa, Ottawa.

76 J. C. Woolley, J. A. Evans and C. M. Gillet
Proc. Phys. Soc. (London) 74, 244 (1959).

77 J. C. Woolley and S. A. Evans, Proc. Phys. Soc. 78, 354 (1961).

78 J. C. Woolley and C. M. Gillett, J. Phys. Chem. Solids, 17, 34 (1960).

79 J. C. Woolley, Can. J. Phys. 44, 2709 (1966).

80 W. M. Coderre and J. C. Woolley, Can. J. Phys. 47, 2553 (1969).

81 J. C. Woolley and K. W. Blazey, J. Phys. Chem. Solids, 25, 713 (1964).

82 J. C. Woolley and J. Warner, Can. J. Phys. 42, 1879 (1964).

83 W. M. Coderre and J. C. Woolley, Low Band Gap Semicond. Conf. (1970)Dallas.

84 A. G. Thompson and J. C. Woolley, Bull. Am. Phys. Soc. 12, 639 (1967).

85 W. Koster and W. Ulrich, Z. Metallk. 49, 365 (1958).

86 A. G. Thompson, J. E. Rowe and M. Rubenstein
J. Appl. Phys. 40, 3280 (1969).

87 F. Oswald, Z. Naturforsch. 14A, 374 (1959).

88 S. G. Krioturu, V. V. Sobolov and S. D. Shutov, Inorg. Mat. 2, 687 (1966).

89 B. Ross, Bull. Am. Phys. Soc. 13, 1640 (1968).

90 J. C. Woolley, C. M. Gillett and J. A. Evans
Intern. Conf. Phys. Semicond. (1960) Prague.

91 E. F. Hokongs, I. Kudman, T. Seidel, C. M. Schmeltz and E. M. Steigmeier
J. Appl. Phys. 37, 2879 (1966).

92 J. C. Woolley, M. B. Thomas and A. G. Thompson
Can. J. Phys. 46, 157 (1968).

93 W. M. Coderre and J. C. Woolley, Can. J. Phys. 48, 463 (1970).

94 R. W. Conrad, C. E. Jones and E. W. Williams
J. Electrochem. Soc. 113, 287 (1966).

95 A. G. Thompson and J. C. Woolley, Can. J. Phys. 45, 2597 (1967).

96 E. W. Williams and V. Rehn, Phys. Rev. 172, 798 (1968).

97 M. Rubenstein, J. Electrochem. Soc. 112, 426 (1965).

98 J. J. Tietjen and J. A. Amick, J. Electrochem. Soc. 113, 724 (1966).

99 S. A. Abagyan, Sov. Phys. Sol. State, 6, 2266 (1965).

100 T. K. Bergstresser, Phys. Rev. Letters, 15, 662 (1965).

101 A. G. Thompson, J. C. Woolley and M. Rubenstein
Can. J. Phys. 44, 2927 (1966).

102 J. C. Woolley, A. G. Thompson and M. Rubenstein
Phys. Rev. Letters, 15, 670 (1965).

103 E. W. Williams and C. E. Jones, Solid State Commun. 3, 195 (1965).

104 A. G. Thompson, M. Cardona, K. L. Shaklee and J. C. Woolley
Phys. Rev. 146, 601 (1966).

105 A. G. Thompson and J. C. Woolley, Can. J. Phys. 45, 255 (1967).

106 J. A. Stratton, "Electromagnetic Theory", McGraw-Hill Book Company(1941).

107 F. Stern, Elementary Theory of the Optical Properties of Solids,
Solid State Physics, 15, 299 (1963).

108 L. I. Schiff, " Quantum Mechanics ", McGraw-Hill Book Company (1955).

109 G. F. Bassani, " The optical properties of solids", Course 34, Proc. Intern. School of Physics, Academic Press (1966).

110 F. Seitz, " The Modern Theory of Solids ", McGraw-Hill Book Company (1940) New York.

111 J. C. Phillips, Solid State Physics, Volume 18, Academic Press (1966).

112 L. van Hove, Phys. Rev. 89, 1189 (1953).

113 J. C. Phillips, Phys. Chem. Solids, 12, 208 (1960).

114 D. Brust, J. C. Phillips and F. Bassani Phys. Rev. Letters, 9, 94 (1962).

115 D. Brust, M. L. Cohen and J. C. Phillips Phys. Rev. Letters, 9, 389 (1962).

116 D. Brust, Phys. Rev. 134, A1337 (1964).

117 E. O. Kane, Phys. Rev. 146, 558 (1966).

118 C. W. Higginbotham, F. H. Pollak and M. Cardona Solid State Commun. 5, 513 (1967).

119 M. Cardona, " Semiconductors and Semimetals ", Volume 3, Academic Press (1967) New York.

120 M. Cardona and D. L. Greenaway, Phys. Rev. 133, A1685 (1964).

121 H. R. Phillip and E. A. Taft, Phys. Rev. 129, 1002 (1959).

122 D. M. Roessler, Brit. J. Appl. Phys. 16, 1119 (1965).

123 M. Cardona and D. L. Greenaway, Phys. Rev. 131, 98 (1963).

124 R. Braunstein and E. O. Kane, J. Phys. Chem. Solids, 23, 1423 (1962).

125 M. Cardona, J. Appl Phys. 32, 2151 (1961).

126 J. Tauc and E. Antoncik, Phys. Rev. Letters 5, 253 (1960).

127 M. Cardona, K. L. Shaklee and F. H. Pollak Phys. Rev. 154, 696 (1967).

128 M. Cardona, Solid State Physics, Supplement 11, Academic Press(1969).

129 B. O. Seraphin, Optical Properties of Solids, North- Holland Publishing Company, Amsterdam.

130 B. O. Seraphin and N. Botka, Phys. Rev. 139, A560 (1965).

131 B. O. Seraphin and N. Botka, Phys. Rev. 145, 628 (1966).

132 H. R. Philipp and E. A. Taft, Phys. Rev. 120, 37 (1960).

133 H. Ehrenreich and H. R. Philipp
Proc. Intern. Conf. Phys. Semicond. (1962) Exeter.

134 W. E. Engler, H. Fritzsche, H. Garfinkel and J. J. Tiemann
Phys. Rev. Letters 14, 1069 (1965).

135 G. W. Gobeli and E. O. Kane, Phys. Rev. Letters 15, 142 (1965).

136 M. Garfinkel, J.J. Tiemann and W. E. Engler
Phys. Rev. 148, 695 (1966).

137 B. Batz, Solid State Commun. 4, 241 (1966).

138 B. O. Seraphin, Proc. Intern. Conf. Phys. Semicond. (1964) Paris.

139 K. L. Shaklee, F. H. Pollak and M. Cardona
Phys. Rev. Letters 15, 883 (1965).

140 E. Matatagui, A. G. Thompson and M. Cardona
Phys. Rev. 176, 950 (1968).

141 B. Batz, Solid State Commun. 5, 985 (1967).

142 W. Franz, Z. Naturforsch. 13A, 484 (1958).

143 L. V. Keldysh, Sov. Phys. JETP, 7, 788 (1958).

144 T. S. Moss, J. Appl. Phys. 32, 2136 (1962).

145 J. Callaway, Phys. Rev. 130, 549 (1963).

146 K. Tharmalingam, Phys. Rev. 130, 2204 (1963).

147 J. Bardeen, F. J. Blatt and L. H. Hall, Photoconductivity Conference, John Wiely and Sons Inc. (1956) New York.

148 J. C. Phillips, Proc. Intern. School of Physics, Academic Press(1966).

149 D. E. Aspnes, Phys. Rev. 147, 554 (1966).

150 D. E. Aspnes, Phys. Rev. 153, 972 (1967).

151 D. E. Aspnes, P. Handler and D. F. Blossey
Phys. Rev. 166, 921 (1968).

152 N. Botka, U. Rossler, Solid State Commun. 5, 939 (1967).

153 Y. Hamakawa, P. Handler and F. A. Germano
Phys. Rev. 167, 709 (1968).

154 T. Nishino, Y. Hashimoto, M. Okuyama and Y. Hamakawa
J. Phys. Soc. Japan 26, 1555 (1969).

155 C. R. Pidgeon and S. H, Grooves, " II - VI Semiconducting Compounds"
W. A. Benjamin Inc. (1967) New York.

156 B. O. Seraphin, Phys. Rev. 140, A1716 (1965).

157 J. C. Phillips, Phys. Rev. 125, 1931 (1962).

158 H. Ehrenreich, H. R. Philipp and J. C. Phillips
Phys. Rev. Letters 8, 59 (1962).

159 H. R. Philipp and H. Ehrenreich, Phys. Rev. 129, 1550 (1963).

160 M. Cardona, Z. Physik, 161, 99 (1961).

161 M. Cardona, J. Appl. Phys. 32, 958 (1961).

162 D. L. Greenaway, Phys. Rev. Letters 9, 97 (1962).

164 R. Zallen and W. Paul, Phys. Rev. 134, A1628 (1964).

163 D. L. Greenaway and M. Cardona, Proc. Intern. Conf. Phys. Semicond.
(1962) Exter.

165 A. K. Ghosh, Solid State Commun. 4, 565 (1966).

166 R. F. Potter, Phys. Rev. 150, 562 (1966).

167 B. O. Seraphin, R. B. Hess, Phys. Rev. Letters 14, 138 (1965).

168 B. O. Seraphin and N. Botka, Appl. Phys. Letters 6, 134 (1965).